

THESIS
2

LIBRARY
Michigan State
University

# PLACE IN RETURN BOX to remove this checkout from your record. TO AVOID FINES return on or before date due. MAY BE RECALLED with earlier due date if requested.

DATE DUE	DATE DUE	DATE DUE
OCTO16 702000	MAR & 2 2805	
·		

11/00 c:/CIRC/DateDue.p65-p.14

# OUTPUT FEEDBACK SAMPLED-DATA CONTROL OF NONLINEAR SYSTEMS USING HIGH-GAIN OBSERVERS

 $\mathbf{B}\mathbf{y}$ 

#### AHMED MOHAMED DABROOM

#### A DISSERTATION

Submitted to

Michigan State University
in partial fulfillment of the requirements
for the degree of

DOCTOR OF PHILOSOPHY

Department of Electrical and Computer Engineering

2000

#### **ABSTRACT**

# OUTPUT FEEDBACK SAMPLED-DATA CONTROL OF NONLINEAR SYSTEMS USING HIGH-GAIN OBSERVERS

By

#### AHMED MOHAMED DABROOM

This thesis presents a separation principle for sampled-data control of a class of nonlinear systems. The basic ingredients of this technique are: a continuous-time high-gain observer that robustly estimates the derivatives of the output, a global bounded state feedback control, and a discrete-time implementation of the high-gain observer. For sufficiently small sampling period and sufficiently high observer gain, the sampled-data controller recovers the performance of the continuous-time state feedback controller. The high-gain observer is discretized using different discretization methods to achieve the best discretization algorithm and parameters choice.

Analysis of the discretized high-gain observer as a numerical differentiator provides answers to a number of important questions such as: what is the best discretization method? what are the best choices for the observer parameters and how do they relate to the sampling period? and what is the effect of the order of the observer on the estimation of the output derivatives. This is done for noisy as well as noise-free measurements. We also show how other numerical differentiators are special cases of the high-gain observer discretized by the bilinear discretization

method. The closed-loop analysis shows that the sampled-data output feedback controller recovers the performance of the continuous-time state feedback controller as the sampling frequency and the observer gain become sufficiently large. Performance recovery is shown in two steps. First we show boundedness of trajectories which come arbitrarily close to the desired equilibrium point as time progress. Second, we show convergence to the equilibrium point.

Finally, we experimentally test the use of the discretized high-gain observer in controlling an electromechanical system of (the pendubot). We show how saturation is used to overcome peaking and the effect of increasing the observer gain on the steady-state error. The experimental results confirm our analysis and show that the discretized high-gain observer outperforms the Euler formula as a means for calculating velocities from optical encoder.

To the memory of my father, Mohamed, and to the great women in my life my mother, Saidah, and my wife, Ferdous.

#### **ACKNOWLEDGMENTS**

In the name of Allah, the most merciful and the most beneficent

All praise and thanks are due to Allah, Lord of the Universe, for His merciful and divine direction throughout my study. I am indebted to Professor Hassan Khalil, my advisor and committee chairman, for his valuable time, assistance, and encouragement. His kind consideration and understanding have been an incentive for the completion of this dissertation. Dr. Khalil taught and showed me how I can be professional and well organized in my thoughts and work.

Sincere appreciation and gratitude are extended to the other members of my guidance committee: Professors Fathi Salam, Sheldon Newhouse, Steven Shaw, and Robert Schlueter, for their contributions, advice, and constructive comments to the study. The author would like to thank Jeddah College of Technology in Jeddah, Saudi Arabia, for supporting this study.

I would like to extend my deepest thank to my sisters: Fatima, Zahra, Maryam, and Halima, my brother Fuad, my father in law, and my mother in law for their support and prayers. Last but not least my greatest thanks are for my most valuable treasure in the world my children Weaam, Mohammed, and Albara for their patience, love, and for learning sacrifice at an early eage.

# TABLE OF CONTENTS

L	LIST OF TABLES		ix
L	IST (	OF FIGURES	x
1	IN	TRODUCTION	1
	1.1	The Class of systems and Observer Design	2
	1.2	The Peaking Phenomenon and Bounded Control	7
	1.3	Separation Principle Results	8
	1.4	Other High-Gain Observer Designs	9
	1.5	Sampled-Data Control	11
	1.6	Overview Of The Thesis	12
2	Dis	crete-Time Implementation of High-Gain Observers for Numer-	
	ical	Differentiation	19
	2.1	Introduction	19
	2.2	High-Gain Observers	21
	2.3	Digital Implementation	26
		2.3.1 Discretization Methods	27
		2.3.2 Comparison of the Five Methods	29
	2.4	Bilinear Implementation	38
	2.5	Numerical Differentiators	46
		2.5.1 Comparison with the Bilinear High-Gain Observer	49
		2.5.2 Spline Method Initialization of The High-Gain Observer	<b>52</b>
	2.6	Further Considerations	<b>52</b>
		2.6.1 Modified Observers	55
	•	2.6.2 Additional Examples	<b>58</b>
	2.7	Conclusions	67
3	Out	tput Feedback Sampled-Data Control of Nonlinear Systems Us-	
		High-Gain Observers	77

	3.1	Introduction	77
	3.2	Continuous-time Design	78
		3.2.1 The Class of Nonlinear Systems	78
		3.2.2 Partial State Feedback Control	79
		3.2.3 High-Gain Observer (HGO)	80
	3.3	Sampled-Data Control	81
		3.3.1 Discretization of the HGO	82
		3.3.2 Discrete-Time Closed-Loop Model	84
		3.3.3 The Discrete-time Singularly Perturbed Form	87
	3.4	Performance Recovery	89
		3.4.1 Boundedness and Ultimate Boundedness	91
		3.4.2 Exponential Stability of The Origin and Trajectory Convergence 1	01
	3.5	Example on the Recovery of the Region of Attraction	.09
	3.6	Conclusion	11
4	A	oplication to the Pendubot 1	12
-32	4.1	Introduction	
	4.2	What Is The Pendubot?	
	4.3	Mathematical Model	
	4.4	The Equilibrium Manifold	
	4.5	Controlling The Pendubot	
	4.6	Hardware Description	
	4.7	Experimental Results	
	7.1	4.7.1 Confirmation of the Open-Loop Study	
		4.7.2 Confirmation of the Closed-Loop Study	
	4.8	Conclusion	
	4.0	Conclusion	נט
5	Con	clusions and Future Work	55
	5.1	Conclusions	55
	<b>5.2</b>	Future Work	56
		5.2.1 Extending the Scope of the Sampled-Data Observer-Based	
		Control	<b>5</b> 6
		5.2.2 Sampled-Data Control	57
A	Ар	pendix 1	59
	_	Developing The Singularly Perturbed Form For The Forward Differ-	
			59

<b>A.2</b>	The Transformation Steps To The Singularly perturbed Form For The		
	Other	Discretization methods	167
	A.2.1	Using Backward Difference Method	167
	A.2.2	Using Bilinear Transformation	169
BIBLIOGRAPHY			172

## LIST OF TABLES

2.1	Guidelines for choosing $T/\epsilon$ for different $\omega_s/\omega_{max}$ and SNR	45
3.1	Coefficient of the discrete time implementation of the linear HGO	83
4.1	The values of $\alpha = T/\epsilon$ for the different discretization methods	127

### LIST OF FIGURES

1.1	The closed-loop system a) under state feedback b) under output feedback	10
1.2	The closed-loop system a) under state feedback b) under output feed-	
	back c) sampled-data output feedback	13
2.1	The output signal and its first and second derivatives	<b>3</b> 0
2.2	The maximum steady state absolute error in estimating $\dot{y}$ and $\ddot{y}$ for	
	all five discretization methods for the full-order observer; $T=0.01$	32
2.3	The error in $\dot{y}$ and $\ddot{y}$ for all five methods; $T=0.01$ and $\epsilon=0.00667$	33
2.4	Error in $\ddot{y}$ for the bilinear and FOH methods for the full, reduced, and	
	extended observers	35
2.5	The maximum steady state absolute error in estimating $\dot{y}$ and $\ddot{y}$ for all	
	five discretization methods for the full-order observer in the presence	
	of noise; $T=0.01$ and $\sigma=0.0316$	36
2.6	Calculating $\dot{y}$ and $\ddot{y}$ in the presence of noise; $T=0.01,\epsilon=0.033,$ and	
	$\sigma = 0.0316 \ldots \ldots \ldots \ldots \ldots$	37
2.7	Effect of the ratio of $\frac{T}{\epsilon}$ on the full-order high-gain observer with real	
	poles at $s = -1/\epsilon$ and T=0.01	41
2.8	The transient response for different choices of poles: real and complex,	
	T=0.01	42
2.9	Comparing the maximum absolute steady-state error for the full, re-	
	duced and extended-order observers with noise; $T=0.01,\sigma=0.1$	<b>43</b>
2.10	Comparing the signal to noise ratio with $T/\epsilon$ and root mean square	
	error $r.m.s.$ for the full-order observer for $T = 0.01 \dots \dots$	44
2.11	Comparing full-order observer and spline interpolant methods; $T =$	
	$0.001, \epsilon = 0.0154, \sigma^2 = 0.001, \text{ and } W = 70$	51
2.12	The effect of initializing the high-gain observer by spline interpolant	
	methods; $T/\epsilon = 10$ , $T = 0.001$ , $W = 2$ , and $N = 2$	<b>53</b>
2.13	The effect of initializing the high-gain observer by spline interpolant	
	methods in the presence of noise; $T/\epsilon = 0.065$ , $T = 0.001$ , $\sigma = 0.01$	
	$W = 40 , N = 2 \text{ and } \sigma = 0.0316 \dots$	54

2.14	The comparison between the regular, the modified, and the extended	
	HGO where $T = 0.01 \dots \dots \dots \dots \dots$	57
2.15	The output signal and its first and second derivatives	59
2.16	The maximum steady state absolute error in estimating $\dot{y}$ and $\ddot{y}$ for	
	all five discretization methods for the full-order observer; $T=0.01$	60
2.17	The error in $\dot{y}$ and $\ddot{y}$ for all five methods; $T=0.01$ and $\epsilon=0.00667$	61
2.18	Error in $\ddot{y}$ for the bilinear and FOH methods for the full, reduced, and	
	extended observers	62
2.19	The maximum steady state absolute error in estimating $\dot{y}$ and $\ddot{y}$ for all	
	five discretization methods for the full-order observer in the presence	
	of noise; $T = 0.01$ and $\sigma = 0.0316$	63
2.20	Calculating $\dot{y}$ and $\ddot{y}$ in the presence of noise; $T=0.1,T/\epsilon=0.28,$ and	
	$\sigma = 0.0707 \ldots \ldots \ldots \ldots \ldots \ldots$	64
2.21	Effect of the ratio of $\frac{T}{\epsilon}$ on the full-order high-gain observer with real	
	poles at $s = -1/\epsilon$ and T=0.1	65
2.22	The transient response for different choices of poles: real and complex,	
	T=0.1	66
2.23	The output signal and its first and second derivatives	68
	The maximum steady state absolute error in estimating $\dot{y}$ and $\ddot{y}$ for	
	all five discretization methods for the full-order observer; $T=0.1$	69
2.25	The error in $\dot{y}$ and $\ddot{y}$ for all five methods; $T=0.1$ and $\epsilon=0.0667$	70
	Error in $\ddot{y}$ for the bilinear and FOH methods for the full, reduced, and	
	extended observers	71
2.27	The maximum steady state absolute error in estimating $\dot{y}$ and $\ddot{y}$ for all	
	five discretization methods for the full-order observer in the presence	
	of noise; $T=0.1$ and $\sigma=0.0707\ldots$	72
2 28	Calculating $\dot{y}$ and $\ddot{y}$ in the presence of noise; $T = 0.01$ , $T/\epsilon = 0.4$ , and	. ~
2.20	$\sigma = 0.1414 \dots \dots$	73
2 29	Effect of the ratio of $\frac{T}{\epsilon}$ on the full-order high-gain observer with real	
2.20	poles at $s = -1/\epsilon$ and T=0.1	74
2 3N	The transient response for different choices of poles: real and complex,	1-2
2.00	T=0.1	75
3.1		75
J.I	Recovery of region of attraction: $\epsilon^* = 0$ (solid), $\epsilon^* = 0.007$ (dotted), $\epsilon^* = 0.057$ (dotted) and $\epsilon^* = 0.082$ (dotted)	110
<i>A</i> 1		110
4.1	• -	114
4.2	The Pendubot model parameters are shown on a pendubot schematic.	
4.3	The pendubot arm at a: controllable position, b: uncontrollable position	119

4.4	Pictorial description of the Pendubot's interface with its controller	123
4.5	The output signals for both links and their derivatives, $T = 0.003$ and	
	$\alpha = 2.5$	128
4.6	Using the bilinear transformation to calculate the steady state track-	
	ing error $e_{ss} = x_1 + x_3 - \pi/2$ , where $T = 0.003sec$ . and $\alpha =$	
	1.0, 1.5, 2.0, 2.5 respectively	130
4.7	Using the backward difference method to calculate the steady state	
	tracking error $e_{ss}$ , where $T = 0.003sec$ . and $\alpha = 1.2$ , 1.5, 2.0, 2.5	
	respectively	131
4.8	Using the forward difference method to calculate the steady state	
	tracking error $e_{ss}$ , where $T = 0.003sec$ . and $\alpha = 0.8, 0.9, 1.0, 1.1$	
	respectively	132
4.9	The effect of different choices of poles real and complex on the tran-	
	sient response, $T=0.005$ and $\alpha=3.0$ discretized by the bilinear	
	transformation	133
4.10	Tracking error e and control signal for the full, reduced and extended	
	order HGO using the bilinear transformation, $T = 0.01$ and $\alpha = 2.1$ .	134
4.11	Effect of increasing the ratio $\alpha = T/\epsilon$ on the full order HGO with real	
	poles at $s=-1/\epsilon, T=0.01$ and $\alpha=2.1,3.0,5.0,,6.0$ respectively.	136
4.12	The transient of estimating speed of the first link as $\alpha$ increases while	
	T=0.01	138
4.13	The control during the transient period as $\alpha$ increases while $T=0.01$	139
4.14	The transient speed of link one while $T$ decreases $\ldots \ldots \ldots$	140
4.15	The control during the transient period as $T$ decreases $\ldots \ldots$	141
4.16	Peaking in the transient of estimating speed of the first link as $\alpha$	
	increases while $T=0.01$	142
4.17	The effect of the peaking on the control during the transient period	
	as $\alpha$ increases while $T=0.01$	143
4.18	Peaking in the transient speed of link one while $T$ decreases $\dots$	144
4.19	The effect of the peaking on the control during the transient period	
	as $T$ decreases	145
4.20	The sampling time $T=0.003$ is fixed while $\alpha$ is increased $\dots \dots$	147
4.21	Fixing $\alpha=3.0$ and decreasing the sampling time $T$	148
4.22	Tracking error at steady-state using linear and nonlinear HGO	149
4.23	Tracking error at the steady-state using the linear and nonlinear in	
	another run	150

4.24	Comparison of the different discretization methods of the full order	
	(FOHG) and reduced order (ROHG) with the Euler formula with and	
	without averaging	<b>152</b>
4.25	Comparing the performance of the reduced order HGO discretized by	
	bilinear method for $\alpha=2$ and $T=0.04$ and $\alpha=6.5$ and $T=0.06$	
	with the Euler method when $T = 0.04$ sec	153

# CHAPTER 1

### INTRODUCTION

The use of high-gain observers in continuous-time has evolved as an important technique for the design of output feedback control of nonlinear systems. The basic ingredients of this technique are

- 1. a high-gain observer that robustly estimates the derivatives of the output;
- 2. a global bounded state feedback control, usually obtained by saturating a continuous state feedback function outside a compact region of interest, that meets the design objectives. The global boundedness of control protects the state of the plant from peaking when the high-gain observer estimates are used instead of the true states.

The technique was first introduced by Esfandiari and Khalil [16] and since then has been used by many other researchers. It was used in [16] and [36] to achieve stabilization and semiglobal stabilization of fully-linearizable systems, in [32, 42, 43] to design robust servomechanisms for nonlinear systems, in [49] to design variable structure control, and in [31] to control the speed of induction motors. Teel and Praly [62, 63] and Lin and Saberi [40] used it in a few papers to achieve semiglobal stabilization. Jankovic [29] used it in adaptive control problem. Isidori [27] used it to unify his pioneering work on servomechanisms [28] with Khalil's work [32]. Jiang,

Hill and Guo [30] used a reduced-order high-gain observer to achieve semiglobal stabilization for a nonlinear benchmark problem.

In most of these papers the controller is designed in two steps. First, a globally bounded state feedback control is designed to meet the design objective. Second, a high-gain observer, designed to be fast enough, recovers the performance achieved under state feedback. This recovery is shown using asymptotic analysis of a singularly perturbed closed-loop system. The combination of these two steps of design allows for a separation approach. This separation approach is used in most of the papers that utilize high-gain observers. It is proved in a generic form in the work of Teel and Praly [62], where it is shown that global stabilizability by state feedback and uniform observability imply semiglobal stabilizability by output feedback. A more comprehensive separation principle is proved by Atassi and Khalil [8].

#### 1.1 The Class of systems and Observer Design

We consider a multivariable nonlinear system represented by

$$\dot{x} = Ax + B\phi(x, z, u) \tag{1.1}$$

$$\dot{z} = \psi(x, z, u) \tag{1.2}$$

$$y = Cx ag{1.3}$$

$$\zeta = \Theta(x, z) \tag{1.4}$$

where  $u \in \mathcal{U} \subseteq R^m$  is the control input,  $y \in \mathcal{Y} \subseteq R^p$  and  $\zeta \in R^s$  are measured outputs, and  $x \in \mathcal{X} \subseteq R^r$  and  $z \in \mathcal{Z} \subseteq R^l$  constitute the state vector. The  $r \times r$  matrix A, the  $r \times 1$  matrix B, and  $p \times r$  matrix C, given by

$$A = block \ diag[A_1, \ldots, A_p]$$

$$B = block \ diag [B_1, \dots, B_p]$$
 $C = block \ diag [C_1, \dots, C_p]$ 
 $A_i = \begin{bmatrix} 0 & 1 & \dots & 0 \\ 0 & 0 & 1 & \dots & 0 \\ \vdots & & & \vdots & & \vdots \\ 0 & \dots & \dots & 0 & 1 \\ 0 & \dots & \dots & 0 \end{bmatrix}_{r_i \times r_i}; B_i = \begin{bmatrix} 0 & 0 & 0 \\ 0 & \vdots & \vdots & \vdots \\ 0 & 0 &$ 

where  $1 \le i \le p$  and  $r = r_1 + \ldots + r_p$ , represent p chains of integrators. The functions  $\phi$ ,  $\psi$  and  $\Theta$  satisfy the following assumption.

Assumption 1.1 The functions  $\phi$  and  $\psi$  are locally Lipschitz and  $\Theta$  is continuous over the domain of interest. In addition,  $\phi(0,0,0) = 0$ ,  $\psi(0,0,0) = 0$  and q(0,0) = 0.

This assumption guarantees that the origin is an equilibrium point of the open-loop system. The main source of the system (1.1)-(1.4) is the normal form of a nonlinear system having a vector relative degree  $(r_1, \ldots, r_p)$  [16]. It is well known that if the nonlinear system

$$\dot{\chi} = f(\chi) + g(\chi)u$$

$$y = h(\chi)$$

has a vector relative degree  $(r_1, \ldots, r_p)$ , then it can transformed into the form

$$\dot{\xi} = A\xi + B [f_1(\xi, z) + g_1(\xi, z)u]$$

$$\dot{z} = f_2(\xi, z, u)$$

$$y = C\xi$$

In this case  $g_1(\cdot, \cdot)$  is nonsingular in the domain of interest, y is the only measured output, and (1.4) is dropped. Another source where (1.4) is relevant arises when the dynamics are extended by augmenting a series of integrators at the input side [33, 62, 66]. Khalil in [33] considers a single-input single-output system modeled by the  $n^{th}$  – order differential equation

$$y^n = f_o(\cdot) + g_o(\cdot)\mu^{(n-\rho)}$$

where  $\mu$  is the input, y is the output,  $f_o$  and  $g_o$  are functions of  $y, y^{(1)}, \ldots, y^{(n-1)}, \mu, \ldots, \mu^{(n-\rho-1)}$ . Augmenting  $(n-\rho)$  integrators at the input side, denoting their states by  $z_i = \mu^{(i-1)}$ , setting  $u = \mu^{(n-\rho)}$  as the control input of the augmented system, and taking  $x_i = y^{(i-1)}$ , results in a system of the form (1.1)-(1.4) with r = n. In this case all the components of z are measured; hence  $\Theta(x,z) = z$  in (1.4). Another example of the use of extended dynamics can be found in [62]. Reference [62] considers a single-input single-output nonlinear system where complete uniform observability guarantees that the state  $\chi$  can be expressed as  $\chi = h(y, \ldots, y^{(n_y)}, \mu, \ldots, \mu^{(n_u)})$  where  $\mu$  is the input, y is the output, and  $h(\cdot)$  is a known function. Furthermore,  $y^{(n_y+1)} = \alpha(\chi, u, \ldots, u^{(m_u)})$  where  $\alpha$  is known function. The dynamics are extended by adding  $l_u = \max\{n_u, m_u\}$  integrators at the input side. Taking  $x_i = y^{(i)}$ , for  $1 \le i \le n_y$ ,  $z_i = \mu^{(i)}$ , for  $1 \le i \le l_u$ , and  $u = \mu^{(l_u+1)}$ , the system can be represented as

$$\dot{x} = Ax + B\alpha(h(x, z), z)$$
 $\dot{z} = A_o z + B_o u$ 
 $y = Cx$ 

where (A, B, C) and  $(A_o, B_o)$  represent chains of  $n_y$  and  $l_u$  integrators, respectively. In this case  $\phi$  is independent of u and all the components of z are measured; hence  $\Theta(x, z) = z$  in (1.4).

The model (1.1)-(1.4) may also arise in models of mechanical and electromechanical systems where displacement variables are measured while their derivatives (velocities, accelerations, etc.) are not measured. Examples of such models can be found in [31, 24, 41, 25, 64, 30]. A model of induction motor [31] can be represented in the form (1.1)-(1.4) with  $x = [\delta, \dot{\delta}, \ddot{\delta}]^T$  where  $\delta = \theta - \theta_{ref}$  is the rotor position error, and z constitutes the rotor flux and stator current. The measured variables y and C are the rotor position error and stator current, respectively. Examples of models that can be put in the normal form are the models given in [24] and [41] for the inverted pendulum-on-a-cart system. These models, taking the cart displacement as the measured output, have relative degree two but are non-minimum phase. In [25] and [64], the models given of the ball and beam system fit in the form of (1.1)-(1.4). These systems can not be represented in the normal form because, taking the ball's position as one of the measured outputs, the relative degree is not well defined. A last example of systems fitting the model (1.1)-(1.4) is the model of the benchmark rotational/translational actuator given in [30] where the system has well defined relative degree with respect to the cart's position but only locally. The design of the globally stabilizing state feedback controller of [30] does not transform the system into the normal form.

The bounded state feedback control u takes the form<sup>1</sup>

$$u = \gamma(x, \zeta) \tag{1.5}$$

<sup>&</sup>lt;sup>1</sup>Reference [8] deals with the more general case of dynamic state feedback controllers.

and is implemented by

$$u = \gamma(\hat{x}, \zeta) \tag{1.6}$$

where the state estimate  $\hat{x}$  is generated by the high-gain observer (for demonstration we take p=1)

$$\dot{\hat{x}} = A\hat{x} + B\phi_o(\hat{x}, \zeta, u) + H(y - C\hat{x})$$
(1.7)

where  $\phi_o$  is a known nominal model of  $\phi$ . The estimation error  $e = x - \hat{x}$  satisfies the differential equation

$$\dot{e} = (A - HC)e + B\Delta(x, e)$$

where  $\Delta(x,e)$  is due to uncertainty in the state equation and the imperfect cancellation of the nonlinearities due to the use of states estimates. The observer gain H is designed to render (A - HC) a Hurwitz matrix, as in linear observer theory. In the presence of  $\Delta$ , H needs to stabilize (A - HC) while rejecting the effect of the perturbation  $\Delta$ . Rejection of  $\Delta$  is approximately achieved if the transfer function  $(SI - A + HC)^{-1}B$  approaches zero asymptotically as a design parameter  $\epsilon$  tends to zero. This can be achieved via the singular perturbation approach described in [16]. For the case where (A, B, C) represents a chain of integrators, the observer gain is given by

$$H = \begin{bmatrix} \frac{\alpha_1}{\epsilon} & \frac{\alpha_2}{\epsilon^2} & \dots & \frac{\alpha_r}{\epsilon^r} \end{bmatrix}^T$$

where  $\epsilon$  is a positive constant to be specified and the positive constants  $\alpha_i$  are chosen such that the roots of

$$s^r + \alpha_1 s^{r-1} + \ldots + \alpha_{r-1} s + \alpha_r = 0$$

are in the open left-half plane.

For the purpose of analysis, the observer dynamics are replaced by the equivalent dynamics of the scaled estimation error

$$\eta_j = \frac{x_j - \hat{x_j}}{\epsilon^{r-j}}, \quad j = 1, \ldots, r$$

Hence,  $\hat{x} = x - D(\epsilon)\eta$  where

$$D(\epsilon) = diag\left[\epsilon^{r-1}, \dots, 1\right]_{r \times r}$$

The closed-loop system is represented by

$$\dot{x} = Ax + B\phi(x, z, \gamma(x - D(\epsilon)\eta, \zeta))$$

$$\dot{z} = \psi(x, z, \gamma(x - D(\epsilon)\eta, \zeta))$$

$$\epsilon \dot{\eta} = A_{\sigma}\eta + \epsilon B\delta(x, z, D(\epsilon)\eta)$$

where

$$\delta(x, z, D(\epsilon)\eta) = \phi(x, z, \gamma(\hat{x}, \zeta)) - \phi_o(\hat{x}, \zeta, \gamma(\hat{x}, \zeta))$$

and

$$\frac{1}{\epsilon}A_o = D^{-1}(\epsilon)\left[A - HC\right]D(\epsilon)$$

is an  $r \times r$  Hurwitz matrix.

# 1.2 The Peaking Phenomenon and Bounded Control

The high-gain observer design places the observer poles far in the left-half plane. In particular, they are located at  $O(1/\epsilon)$  values that approach infinity as  $\epsilon \to 0$ . This is

a typical feature of all high-gain observer designs which attempt to reduce the error transfer function to zero asymptotically. This feature can cause an impulsive like behaviour known as the peaking phenomena. Designing the state feedback control u to be globally bounded eliminates the undesirable features of peaking as shown in [16]. During a short period of time, the excessively large overshot due to peaking decays to an  $O(\epsilon)$  value. This short period of time tends to zero as  $\epsilon \to 0$ . During the same interval the control saturates and the state of the plant x remains close to its initial values. After that period, the controller starts to function in a normal way as if the initial conditions for the fast error equation were of order O(1). The only place where peaking could be observed is in the estimates  $\hat{x}$  (observer states), which are internal variables of the controller. The physical variables of the plant x and u will be free of peaking.

#### 1.3 Separation Principle Results

It is shown in [8] that output feedback controller (1.6) recovers the performance of the state feedback controller (1.5) for sufficiently small  $\epsilon$ . The performance recovery manifests itself in three points. First, the origin  $(x=0,z=0,\hat{x}=0)$  of the closed-loop system under output feedback is asymptotically stable. Second, the output feedback controller recovers the region of attraction of the state feedback controller in the sense that if  $\mathcal{R}$  is the region of attraction under state feedback, then for any compact set  $\mathcal{S}$  in the interior of  $\mathcal{R}$  and any compact set  $\mathcal{Q} \subseteq \mathcal{R}^r$ , the set  $\mathcal{S} \times \mathcal{Q}$  is included in the region of attraction under output feedback control. Third, the trajectory of (x,z) under output feedback approaches the trajectory under state feedback as  $\epsilon \to 0$ .

Performance recovery is shown in three steps. First, boundedness of trajectories starting in the specified compact set is established by regulating the parameter  $\epsilon$ 

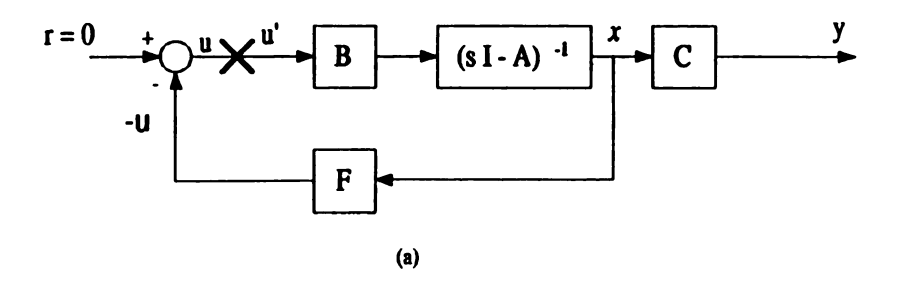
such that state estimation is fast enough. The global boundedness of the control function is of paramount importance at this stage. Then, these trajectories are shown to be arbitrarily close to the origin after a finite time interval; thus a property of ultimate boundedness is established. Finally, local asymptotic stability of the origin is argued in three cases: the case where perfect knowledge of the system's nonlinearity is available ( $\phi_o = \phi$ ), the case where the origin under state feedback control is exponentially stable, and the case where the origin under state feedback control is asymptotically but not exponentially stable combined with an imperfect knowledge of the system's nonlinearity. In the last case, certain conditions were imposed on the growth of the modeling error due to the imperfect knowledge of the system's nonlinearity.

In [6] Atassi and Khalil proved the separation principle for a more general case where the state feedback control renders a certain compact set positively invariant and asymptotically attractive. This more general result allows the separation principle to be applied to a number of control tasks beyond the stabilization of an equilibrium point. Examples include finite time convergence to a set [14], ultimate boundedness [63], servomechanisms [32, 42, 43, 27, 35], and adaptive control [33, 4, 5].

#### 1.4 Other High-Gain Observer Designs

Building a controller to stabilize any system needs good measurements of the states or their estimates. If an observer is used in the implementation, no guaranteed robustness properties hold. Doyle and Stein 1979 [13] showed that the robustness guaranteed by state feedback can be recovered by the use of a robust observer as in the following example.

**Example 1.1** Consider an *n*th order linear system that is observable, controllable and has all the zeros in the left half plane (*minimum phase*). The closed-loop system



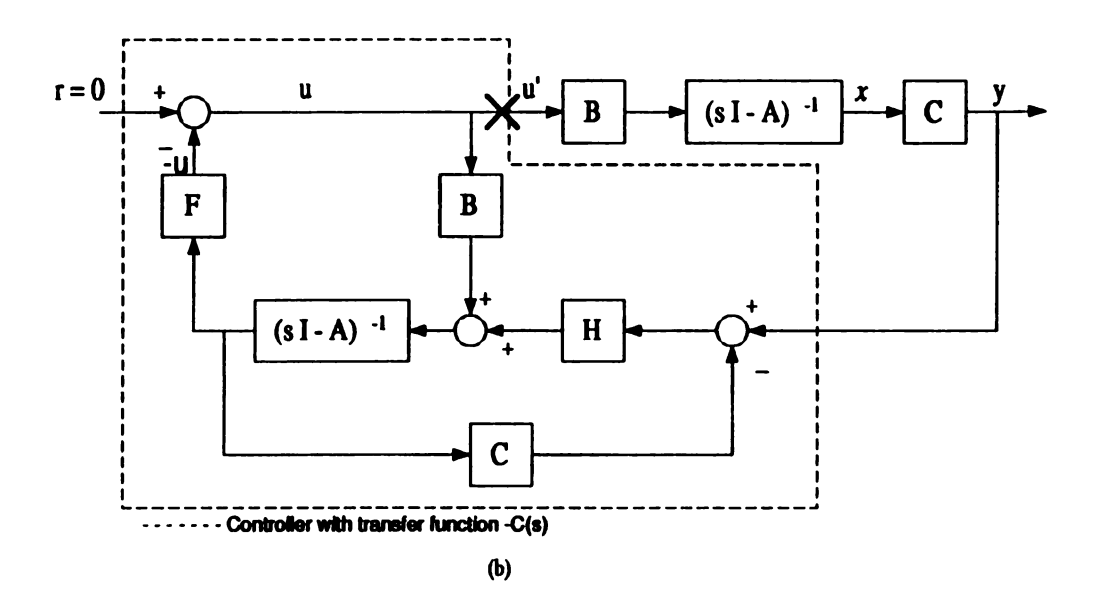


Figure 1.1. The closed-loop system a) under state feedback b) under output feedback

in Figure (1.1a) uses full-state feedback, while the one in Figure (1.1b) uses output feedback (states estimates). Examining robustness of the two closed-loop systems at the breaking point  $\times$ , the loop transfer functions from the control signal u' to the control signal u are generally different in the two implementations. They are identical if the observer dynamics satisfy

$$H\left[I+C(sI-A)^{-1}H\right]^{-1}=B\left[C(sI-A)^{-1}B\right]^{-1}$$
 (1.8)

where A, B and C are plant matrices and H is the observer gain. Satisfaction of (1.8) offers a way to adjust observers so that full-state loop transfer characteristics are recovered at point  $\times$ . In particular, if the observer gain is parameterized as a function of a scalar variable q, H(q), such that

$$\frac{H(q)}{q} \to BW \text{ as } q \to \infty$$

for any nonsingular matrix W, then (1.8) will be satisfied asymptotically as  $q \to \infty$ .

Atassi and Khalil [7] reviewed various techniques for the design of high-gain observers and classified them into three groups. First, pole-placement algorithms which lead to either a two-time scale structure as in [16] or a multiple time-scale structure as in [54]. Second, Riccati equation-based algorithms which lead to either an  $H_2$  Riccati equation as in [13] and [53, Section 4.4.1] or to an  $H_{\infty}$  Riccati equation as in [50] and [53, Section 4.4.2]. Third, Lyapunov equation-based algorithm as in [23]. They showed that separation result similar to those of [8] can be obtained for any one of the other high-gain observer designs provided the state feedback control is globally bounded.

#### 1.5 Sampled-Data Control

Due to the advancement in computer technology, the controller is typically implemented using digital computers. Moreover, in most of today's applications, measurements are available only at sampling points. In recent years there has been some progress in the analysis and design of sampled-data control of nonlinear systems. The closed-loop system consists of a continuous-time plant, a digital controller, a digital-to-analog converter (D/A), and an analog-to-digital (A/D) converter. In sampled-data systems, the plant output y(t) is sampled as y(kT) where T and k

are the sampling period and sample number, respectively. The output y(kT) is used to calculate the state estimate  $\hat{x}(kT)$  via a high-gain observer. The observer is implemented in discrete-time and u(k) is calculated using a microcontroller or a DSP board. Then, u(kT) is fed to the continuous-time plant through a zero-order hold device.

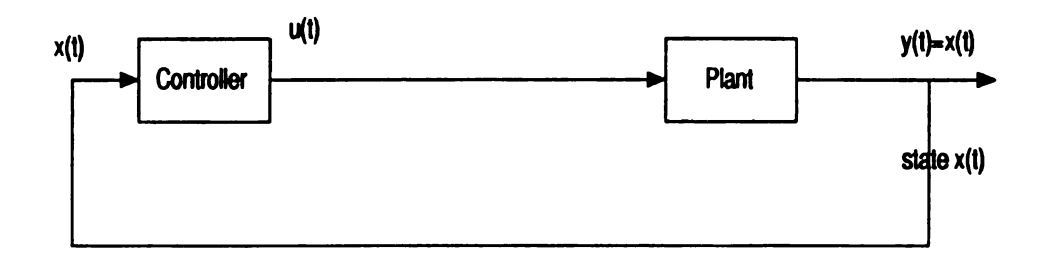
The sampled-data control design is carried out in three steps; see Figure 1.2. First the control is designed assuming that all states are available for measurements. Second, a high-gain observer is designed to estimate the states using the measured outputs. Finally, the observer and the controller are implemented in discrete-time.

Most of the literature on sampled-data control of nonlinear systems assumes state feedback. The work of Monaco and Normand-Cyrot [45] enables a first parallel between the continuous-time and discrete-time state space representations. Some properties of the state equations are not preserved under sampling as studied in [57] for certain accessibility properties. Also it is shown in [12] that certain properties, like observer error linearizability [37], are not inherited from the underlying continuous-time system.

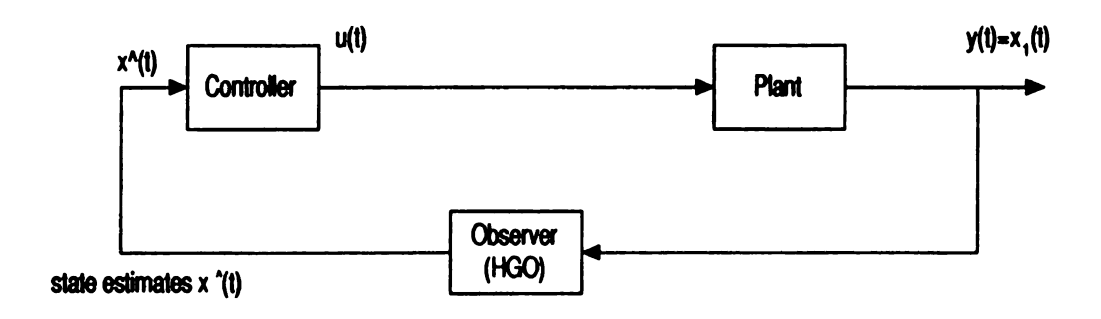
#### 1.6 Overview Of The Thesis

Up to this point, all studies of the closed-loop nonlinear system using high-gain observers have been limited to continuous-time analysis, despite the fact that such a system is a combination of a continuous-time system (plant) and a discrete-time system (high-gain observer and controller). The main goal of this thesis is to analyze the performance of the closed-loop system when the discrete-time implementation of the observer and controller is taken into consideration. This will complicate the analysis compared with the continuous-time case.

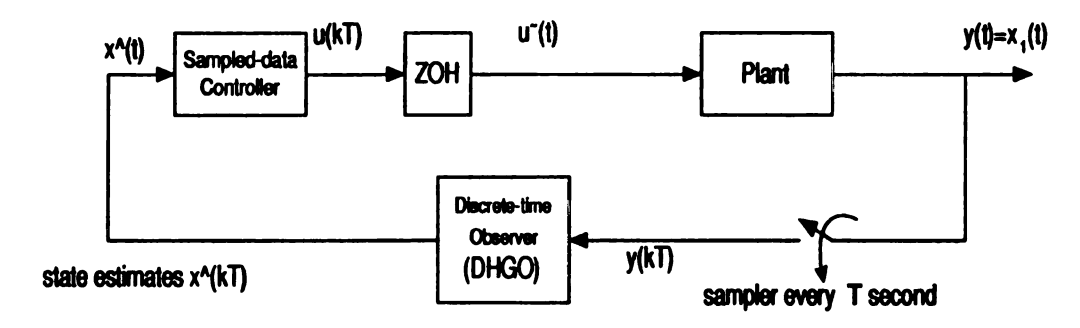
We are going to investigate the sampled-data output feedback controller in three



#### a: Closed-loop for state feedback continuous-time control system



#### b: Closed-loop for output feedback continuous time control system



c: Closed-loop for output feedback sampled-data control system

Figure 1.2. The closed-loop system a) under state feedback b) under output feedback c) sampled-data output feedback

steps. First, we study the discretization of the high-gain observer by looking at the problem as a numerical differentiator design problem (open-loop system) and investigate many discretization methods and their effect on reducing the approximation error. Second, we study the closed-loop system when we apply discrete-time high-gain observer. Third, we implement the discrete-time via simulation and an experimental setup.

The fact that the high-gain observer, especially its linear version, is an approximate differentiator can be seen by examining the transfer function from y to  $\hat{x}$ , given by

$$G(s) = (sI - A + HC)^{-1}H$$

The following two transfer functions give G(s) for second and third-order systems, respectively, in the limit when the observer gain  $1/\epsilon \to \infty$ .

$$\lim_{\epsilon \to 0} G(s) = \lim_{\epsilon \to 0} \frac{1}{\epsilon^2 s^2 + \alpha_1 \epsilon s + \alpha_2} \left[ \begin{array}{c} \epsilon s \alpha_1 + \alpha_2 \\ \alpha_2 s \end{array} \right] = \left[ \begin{array}{c} 1 \\ s \end{array} \right]$$

$$\lim_{\epsilon \to 0} G(s) = \lim_{\epsilon \to 0} \frac{1}{d(\epsilon s)} \begin{bmatrix} \alpha_1 \epsilon^2 s^2 + \alpha_2 \epsilon s + \alpha_3 \\ \epsilon s^2 \alpha_2 + \alpha_3 s \\ \alpha_3 s^2 \end{bmatrix} = \begin{bmatrix} 1 \\ s \\ s^2 \end{bmatrix}$$

where  $d(\epsilon s) = \epsilon^3 s^3 + \alpha_1 \epsilon^2 s^2 + \alpha_2 \epsilon s + \alpha_3$ . The linear high-gain observer can be used to approximate the derivatives of any smooth signal y(t) by representing the signal as the output of a normal form driven by the *n*th derivative of the signal, i.e.,

$$\dot{x} = Ax + By^{(n)}(t),$$

$$v = Cx$$

For any bounded  $y^{(n)}(t)$ , the singular perturbation argument used in [16] shows that

the estimation error will be of order  $O(\epsilon)$  after a short transient period.

Implementing the linear high-gain observer in discrete time amounts to numerical differentiation. In Chapter 2 we concentrate on this issue. There has been a lot of literature on numerical differentiation, both in digital signal processing and in numerical analysis. We compare the discrete-time linear high-gain observer with them. The study explores the degrees of freedom we have in choosing the discretization method, the relationship between the observer bandwidth (observer gain)  $1/\epsilon$  and the sampling frequency  $f_{\bullet} = 1/T$ , pole locations, and the dimension of the observer. The study covers noise-free as well as noisy measurements. The noise is modeled as white Gaussian noise. We investigate five different discretization methods: forward difference, backward difference, zero-order-hold, first-order-hold and bilinear transformation methods. For the bilinear transformation method, we investigate the design of the observer parameters and the choice of the observer order (full, reduced and extended-order observer). We explore the freedom of choosing real poles verses complex poles distributed in a butterworth pattern and the effect of that choice on the transient and steady state errors. Furthermore, using the extended-order observer gives less error than the other observers. Comparison of the bilinear high-gain observer with several existing numerical differentiators from the literature shows two interesting findings. First, most of those differentiators are special cases of the bilinear reduced-order high-gain observer for certain choices of the observer parameters. Exploiting the freedom to choose these parameters, the bilinear high-gain observer outperforms those numerical differentiators, especially when measurement noise is taken into consideration. Second, the bilinear high-gain observer is compared to a causal spline interpolant method. It is shown that the high-gain observer compares favorably even though it uses less computation time and memory requirements than the spline method. The chapter ends with a novel idea of using the spline interpolant method to initialize the high-gain observer, which significantly improves

the observer's transient behavior and eliminate the peaking phenomena. Additional examples are presented to confirm the chapter's findings.

After we know how to discretize the high-gain observer we proceed to the analvsis of the interconnected hybrid system. There is no study of the behavior of the closed-loop system in the presence of the digitally implemented high-gain observer. References [10] and [20] studied the problem where the high-gain observer was implemented digitally in closed-loop control. However, their analysis concentrated only on studying the error equation without using a complete model of the closed-loop system. In Chapter 3 we study the coupled closed loop-system (the plant dynamics and the error dynamics). Our study of the discrete-time system is guided by the corresponding study of the continuous-time case. The main tool in the continuoustime case [8, 16] is the representation of the system in a singularly perturbed form that shows the slow dynamics (the plant under control) and the fast dynamics (the observer). The main tool in our analysis is to develop a discrete-time version by representing the closed-loop system in a singularly perturbed form. In the continuous-time case, the singularly perturbed form is derived by scaling the estimation errors. In the discrete-time case, however, scaling by itself is not sufficient and we have to perform additional changes of variables to weaken the slow input into the fast equation.

Moreover, we approximate the continuous-time system (the plant under control) up to the order of  $O(T^r)$ ). This approximation complicates the analysis but makes it more accurate. A lot of mathematical manipulation will be included in the analysis as it can be seen in Chapter 3 and the Appendices. The closed-loop analysis is performed at the sampling points and in between samples. The closed-loop analysis shows that the sampled data controller using the digitally implemented high-gain observer recovers the performance of the continuous-time controller as the sampling frequency and the observer gain become sufficiently large. Performance recovery is shown in two steps. First we show boundedness of trajectories which comes arbitrarily close

to the origin as time progress. Second, we assume that the origin of the continuoustime system is exponentially stable and show that trajectories enter some ball in the neighborhood of the origin in finite time and stay thereafter.

The theoretical results developed in Chapter 3 need to be complimented by either simulation or experimental results to study various factors which the theory may not reveal, learn how to tune various parameters, or confirm the various observations we have seen. Also, one of the usual concerns with high-gain observers is their performance in the presence of noise. This can be addressed either by performing additional analysis to study the effect of noise or by studying that by simulation and experiments. In Chapter 2 we use simulations to study the effect of noise. In Chapter 4, we use high-gain observers in the control of the Pendubot, an electromechanical system consisting of two rigid links interconnected by revolute joints. The first joint is actuated by a DC-motor while the second joint is unactuated as a simple pendulum. The pendulum motion is controlled by actuation of the first link. The experimental results confirm the conclusions of Chapter 2. Moreover, the experiment confirms the closed-loop analysis of Chapter 3. We compare the use of high-gain observers with the more common engineering practice of using the Euler formula (difference method) to calculate speed from position measurements; this actually is the algorithm provided by the pendubot manufacturer. To compare the performance of the high-gain observer with the simple Euler method, we determine what we exactly we gain by using the digital high-gain observer. Our experimental results show that there is a definite advantage for approaching the problem as a digital high-gain observer design. This advantage can be seen in two ways. First, high-gain observers can work for a larger range of sampling periods (or sampling frequencies) compared to the Euler method. Second, for the same frequency, especially for the large sampling periods, the high-gain observer produces good performance with less oscillation in the steady state compared with the Euler method.

Finally, Chapter 5 contains our conclusions and directions of future research.

# CHAPTER 2

# Discrete-Time Implementation of High-Gain Observers for

## **Numerical Differentiation**

#### 2.1 Introduction

In the past few years, high-gain observers played an important role in the design of nonlinear output feedback control of nonlinear systems. They are mainly used to estimate the derivatives of the output. All studies of high-gain observers, however, have been limited to continuous-time analysis, despite the fact that such high-gain observers are almost always implemented digitally. In this chapter we try to overcome this deficiency by investigating discrete-time implementation of high-gain observers. We limit our study to linear high-gain observers so that we can make use of the rich literature on discretization of linear filters. Our study covers reduced-order, full-order and extended-order high-gain observers. We emphasize the use of (discrete-time) high-gain observers as numerical differentiators.

The chapter is organized as follows: Section 2.2 gives background on high-gain observers and their use as approximate differentiators. Section 2.3 investigates digital

implementation of high-gain observers. Five discretization methods are considered: bilinear transformation (BT), zero-order hold (ZOH), first-order hold (FOH), backward difference (BD) and forward difference (FD). The comparison is carried out for noise free as well as noisy measurements. Several numerical examples were examined. but only a few representative cases are included in the chapter. The comparative study shows that the bilinear transformation method outperforms the other methods. Section 2.4 concentrates on the Bilinear Transformation method and investigates the choice of different design parameters. Section 2.5 reviews various numerical differentiators from the signal processing and numerical analysis literature, including the backward difference method (Euler's formula), the spline interpolant method and several digital filters. It is shown that, except for the spline interpolant, all these methods are special cases of the bilinear implementation of full-order or reducedorder high-gain observers. Optimization of the design parameters, as discussed in Section 2.4, allows the bilinear high-gain observer to outperform all these methods. With noisy measurements and under a causality constraint, the bilinear high-gain observer uses less computation time and less memory compared with the spline interpolant method and results in comparable performance. The section ends with a novel idea to initialize the high-gain observer by the spline interpolant method, eliminating the peaking phenomena associated with high-gain observers. In Section 2.6 we discuss a modified high-gain observer by showing via an example how it has less error than the full order high-gain observer. The section includes also two other examples to show that the concluded results are common. The conclusions are given in Section 2.7.

# 2.2 High-Gain Observers

To illustrate the role of high-gain observers as numerical differentiators, let us consider the special case of a single-input-single-output nonlinear system which has a uniform relative degree equal to the dimension of the state vector. Such a system has no zero dynamics and can be transformed into the normal form [26]

$$\dot{x} = Ax + B[a(x)u + b(x)] \tag{2.1}$$

$$y = Cx (2.2)$$

where

$$A = \begin{bmatrix} 0 & 1 & \dots & 0 \\ 0 & 0 & 1 & \dots & 0 \\ \vdots & & & \vdots \\ 0 & \dots & \dots & 0 & 1 \\ 0 & \dots & \dots & 0 \end{bmatrix}_{n \times n}, \quad B = \begin{bmatrix} 0 \\ 0 \\ \vdots \\ 0 \\ 1 \end{bmatrix}_{n \times 1}$$

$$C = \begin{bmatrix} 1 & 0 & \dots & \dots & 0 \end{bmatrix}_{1 \times n}$$

and  $a(x) \neq 0$ . To estimate the state x, we use the observer

$$\dot{\hat{x}} = A\hat{x} + B[a_o(\hat{x})\psi(\hat{x},t) + b_o(\hat{x})] + H(y - C\hat{x})$$
 (2.3)

where  $a_o(x)$  and  $b_o(x)$  are nominal models of the nonlinear functions a(x) and b(x), respectively, and the  $n \times 1$  matrix H is the observer gain. The estimation error  $e = x - \hat{x}$  satisfies the equation

$$\dot{e} = (A - HC)e + B\Delta(x, e, t) \tag{2.4}$$

where

$$\Delta(\cdot) = [a(x) - a_o(\hat{x})]\psi(\hat{x}, t) + b(x) - b_o(\hat{x})$$

The observer gain H is taken as

$$H^T = \left[\begin{array}{cccc} \underline{\alpha_1} & \underline{\alpha_2} & \dots & \underline{\alpha_n} \\ \epsilon^{n} & & \end{array}\right] \tag{2.5}$$

where  $\epsilon$  is a small positive parameter and the positive constants  $\alpha_i$  are chosen such that the roots of

$$s^{n} + \alpha_{1}s^{n-1} + \dots + \alpha_{n-1}s + \alpha_{n} = 0$$
 (2.6)

have negative real parts. This choice of H assigns the eigenvalues of (A - HC) at  $1/\epsilon$  times the roots of (2.6). Using singular perturbation analysis, it is shown in [16] that the estimation error will decay to  $O(\epsilon)$  values after a short transient period of the form  $[0, T_1(\epsilon)]$  where  $\lim_{\epsilon \to 0} T_1(\epsilon) = 0$ . During this transient period, the estimate  $\hat{x}$  may exhibit peaking behavior where the transient response takes the impulsive-like form  $(a/\epsilon^r)e^{-\alpha t/\epsilon}$  for some positive constants r and  $\alpha$ . It is shown in [16] that this peaking phenomenon can be overcome by saturating the control or the state estimates outside a compact region of interest.

The observer equation (2.3) is nonlinear due to the terms  $a_o\psi$  and  $b_o$ . Choosing the nominal functions  $a_o$  and  $b_o$  to be zero results in the linear observer

$$\dot{\hat{x}} = A\hat{x} + H(y - C\hat{x}) \tag{2.7}$$

In this chapter, we limit our discussion to the linear high-gain observer (2.7). It is important to notice that this high-gain observer is essentially an approximate differentiator. This can be seen by examining the transfer function from y to  $\hat{x}$ , given by

$$G(s) = (sI - A + HC)^{-1}H (2.8)$$

The following two examples give G(s) for n=2 and n=3.

**Example 2.1** For n = 2, G(s) is given by

$$G(s) = \frac{1}{\epsilon^2 s^2 + \alpha_1 \epsilon s + \alpha_2} \begin{bmatrix} \epsilon s \alpha_1 + \alpha_2 \\ \alpha_2 s \end{bmatrix}$$

It is clear that  $G_2(s)$ , the transfer function from y to  $\hat{x}_2$ , approaches s as  $\epsilon$  tends to zero, which shows that, on a frequency band much smaller than  $\sqrt{\alpha_2}/\epsilon$ ,  $\hat{x}_2$  approximates the derivative  $\dot{y}$ .

**Example 2.2** For n = 3, G(s) is given by

$$G(s) = rac{1}{d(\epsilon s)} \left[ egin{array}{c} lpha_1 \epsilon^2 s^2 + lpha_2 \epsilon s + lpha_3 \ & \epsilon s^2 lpha_2 + lpha_3 s \ & lpha_3 s^2 \end{array} 
ight]$$

where  $d(\epsilon s) = \epsilon^3 s^3 + \alpha_1 \epsilon^2 s^2 + \alpha_2 \epsilon s + \alpha_3$ . From the limit

$$\lim_{\epsilon o 0} G(s) = \left[ egin{array}{c} 1 \\ s \\ s^2 \end{array} 
ight]$$

we see that  $\hat{x}_2$  and  $\hat{x}_3$  approximate  $\dot{y}$  and  $\ddot{y}$ , respectively.

The high-gain observer (2.7) can be used to approximate the derivatives of any smooth signal y(t) by representing the signal as the output of a normal form driven by the nth derivative of the signal, i.e.,

$$\dot{x} = Ax + By^{(n)}(t),$$

$$y = Cx$$

For any bounded  $y^{(n)}(t)$ , the singular perturbation argument used in [16] shows that the estimation error will be of order  $O(\epsilon)$  after a short transient period.

The high-gain observers (2.3) and (2.7) are full-order ones. It is also possible to design reduced-order high-gain observer of order (n-1) [54]. Partitioning the state vector x as

$$x = \begin{bmatrix} y \\ z \end{bmatrix}$$
, where  $z = \begin{bmatrix} x_2 \\ \vdots \\ x_n \end{bmatrix}$ 

we can rewrite equation (2.1) as

$$\dot{y} = A_{12}z \tag{2.9}$$

$$\dot{z} = A_{22}z + B_2[a(x)u + b(x)] \tag{2.10}$$

where the triple  $(A_{22}, B_2, A_{12})$  has the same canonical form structure of the triple (A, B, C), except that its dimension is (n - 1) instead of n. The reduced-order observer

$$\dot{v} = (A_{22} - LA_{12})(v + Ly) \tag{2.11}$$

$$\hat{z} = v + Ly \tag{2.12}$$

results in the estimation error equation

$$\dot{e}_2 = (A_{22} - LA_{12})e_2 + B_2\Delta(\cdot) \tag{2.13}$$

where  $e_2 = z - \hat{z}$ . The similarity between equations (2.4) and (2.13) is clear. Therefore, the observer gain L takes the same form as H, namely,

$$L^{T} = \left[\begin{array}{cccc} \underline{\alpha_{1}} & \underline{\alpha_{2}} & \dots & \underline{\alpha_{n-1}} \\ \epsilon^{2} & & & \end{array}\right]. \tag{2.14}$$

where  $\epsilon$  is a small positive parameter and the positive constants  $\alpha_i$  are chosen such that the roots of

$$s^{n-1} + \alpha_1 s^{n-2} + \dots + \alpha_{n-2} s + \alpha_{n-1} = 0$$
 (2.15)

have negative real parts. The transfer function from y to  $\hat{z}$  is given by

$$G_R(s) = L + (sI - A_{22} + LA_{12})^{-1}(A_{22} - LA_{12})L$$
  
=  $s(sI - A_{22} + LA_{12})^{-1}L$  (2.16)

Examination of  $G_R(s)$  shows that the reduced-order high-gain observer (2.11) is an approximate differentiator. The following two examples give  $G_R(s)$  for n=2 and n=3.

**Example 2.3** For n = 2,  $G_R(s)$  is given by

$$G_R(s) = \frac{\alpha_1 s}{\epsilon s + \alpha_1}$$

It is clear that  $\lim_{\epsilon\to 0} G_R(s) = s$ ; hence,  $\hat{x}_2 = \hat{z}$  approximates the derivative  $\dot{y}$ . Compared with  $G_2(s)$  of Example 2.1, we note that  $G_2(s)$  is strictly proper while  $G_R(s)$  is only proper. This shows that in the presence of wide-band measurement noise, the full-order observer should perform better than the reduced-order observer because its frequency response rolls off at high frequency.

**Example 2.4** For n = 3,  $G_R(s)$  is given by

$$G_R(s) = \begin{bmatrix} \frac{\alpha_1 \epsilon s^2 + \alpha_2 s}{\epsilon^2 s^2 + \alpha_1 \epsilon s + \alpha_2} \\ \frac{\alpha_2 s^2}{\epsilon^2 s^2 + \alpha_1 \epsilon s + \alpha_2} \end{bmatrix}$$

and

$$\lim_{\epsilon \to 0} G_R(s) = \left[ \begin{array}{c} s \\ s^2 \end{array} \right]$$

Therefore,  $\hat{x}_2$  and  $\hat{x}_3$  approximate  $\dot{y}$  and  $\ddot{y}$ , respectively.

# 2.3 Digital Implementation

In this section, we investigate different discretization methods for high-gain observers. We start by scaling the observer variables to avoid inherent ill-conditioning of the realizations (2.7), or (2.11)–(2.12) when  $\epsilon$  is very small. For the full-order observer (2.7), let

$$q_i = \epsilon^{i-1} \hat{x}_i, \quad i = 1, \dots, n \tag{2.17}$$

Then

$$\epsilon \dot{q} = (A - \bar{H}C)q + \bar{H}y \tag{2.18}$$

$$\hat{x} = D^{-1}(\epsilon)q \tag{2.19}$$

where

$$\bar{H}^T = \begin{bmatrix} \alpha_1 & \alpha_2 & \dots & \alpha_n \end{bmatrix}, D(\epsilon) = \text{diag } [1, \epsilon, \dots, \epsilon^{n-1}]$$

The characteristic equation of  $(A-\bar{H}C)$  is (2.6); hence it is Hurwitz. Equation (2.18) is a standard singularly perturbed system, whose coefficients are of order  $O(1/\epsilon)$  irrespective of the order n of the system. Note that in equation (2.7) some right-hand side coefficients are of order  $O(1/\epsilon^{n-1})$ . The solution of (2.18) does not exhibit peaking for small  $\epsilon$ , which makes it easier to discretize the equation. The effect of peaking is now contained in the output equation (2.19), and it can be overcome be saturating the estimates  $\hat{x}$  outside a compact region of interest.

A similar scaling is applied to the reduced-order observer (2.11)-(2.12) by using

$$p_i = \epsilon^i \hat{v}_i, \quad i = 1, \dots, n - 1 \tag{2.20}$$

Then

$$\epsilon \dot{p} = (A_{22} - \bar{L}A_{12})(p + \bar{L}y)$$
 (2.21)

$$\hat{z} = \Gamma^{-1}(\epsilon)(p + \bar{L}y) \tag{2.22}$$

where

$$\bar{L}^T = \begin{bmatrix} \alpha_1 & \alpha_2 & \dots & \alpha_{n-1} \end{bmatrix}, \quad \Gamma(\epsilon) = \operatorname{diag}\left[\epsilon, & \dots, \epsilon^{n-1}\right]$$

### 2.3.1 Discretization Methods

Discrete-time equivalents of the continuous-time system (2.18) or (2.21) can be found by standard methods which are well documented in the literature, e.g., [21]. We consider here five of these methods: the bilinear transformation (BT), the zero-order hold (ZOH), the first-order hold (FOH), the backward difference (BD), and the forward difference (FD) methods. Formulas for discrete-equivalents of state-space models, for the first three methods, are given in [21, Chapter 4], and they are available in the control toolbox of Matlab. It is important to remember that all these methods are approximations; there is no exact solution for all possible inputs because the continuous-time system responds to the complete time history of y(t), whereas the discrete-time equivalent has access only to the samples y(kT). In a sense, the various discretization methods make different assumptions about what happens to y(t) in between the sample points. A brief description of each of the five methods is given below.

#### Forward Difference

The discrete-time equivalent is obtained by the forward rule of numerical integration. The discrete-time transfer function G(z) is obtained from the continuous-time transfer function G(s) via the mapping s = (z - 1)/T, where T is the sampling period. This mapping does not preserve stability of the continuous-time model, except when T is sufficiently small.

#### **Backward Difference**

The discrete-time equivalent is obtained by the backward rule of numerical integration. The discrete-time transfer function G(z) is obtained from the continuous-time transfer function G(s) via the mapping  $s = (1 - z^{-1})/T$ . This mapping does not preserve stability of the continuous-time model, except when T is sufficiently small.

#### **Bilinear Transformation**

The discrete-time equivalent is obtained by the trapezoidal rule of numerical integration. The discrete-time transfer function G(z) is obtained from the continuous-time transfer function G(s) via the mapping  $s = \frac{2}{T} \left( \frac{z-1}{z+1} \right)$ . This mapping preserves stability of the continuous-time model for any T > 0.

#### Zero Order Hold

The input signal y(t) is approximated by a stair-case function where the input is kept constant throughout the sampling period. The output of the discrete-time equivalent would give the precise values of the state estimates at the sample points, had the input been a stair-case function. The discrete-time transfer function G(z) is the z-transform of the continuous-time transfer function  $G(s)G_{oh}(s)$ , where  $G_{0h}(s) = (1 - e^{-Ts})/s$ . The discrete-time poles map the continuous-time poles according to  $z = e^{sT}$ ; hence stability of the continuous-time model is preserved.

#### First Order Hold

This method is similar to the previous one, except that the input y(t) is approximated

The z-transform of a function F(s) is interpreted as  $\mathcal{Z}\{f(kT)\}$  where  $f(t) = \mathcal{L}^{-1}\{(F(s))\}$ ; see [21]

between two sampling points by connecting a straight line from sample to sample. The discrete-time transfer function G(z) is the z-transform of continuous-time transfer function  $G(s)G_{1h}(s)$ , where  $G_{1h}(s) = T[(1 - e^{-Ts})/Ts]^2$ . The discrete-time poles map the continuous-time poles according to  $z = e^{sT}$ .

## 2.3.2 Comparison of the Five Methods

Let us consider a third-order nonlinear system in the normal form (2.1), with u = 0 and

$$b(x) = \alpha(x)g_s(x) + (1 - \alpha(x)g_u(x))$$

$$\alpha(x) = 2\frac{x'x}{1 + x'x}$$

$$g_s(x) = -54x_1 - 36x_2 - 9x_3$$

$$g_u(x) = 54x_1 - 36x_2 + 9x_3$$

This system was used in [17] to test a numerical differentiator. Figure 2.1 shows the output and its exact first and second derivatives. We design three high-gain observers for this system. The poles of all three observers are at  $s=-1/\epsilon$ ; we will justify this choice of poles later on. The first observer is a third-order full-order observer with  $\alpha_1=3$ ,  $\alpha_2=3$ , and  $\alpha_3=1$ . The second one is a second-order reduced-order observer with  $\alpha_1=2$ , and  $\alpha_2=1$ . The third one is a fourth-order full-order observer with  $\alpha_1=4$ ,  $\alpha_2=6$ ,  $\alpha_3=4$ , and  $\alpha_4=1$ . We will refer to this observer as the extended-order observer. It corresponds to modeling y(t) as the output of a fourth-order system driven by  $y^{(4)}(t)$ . All three observers are discretized using each of the five methods described in the previous section. In all cases, T=0.01. We did not specify the value of  $\epsilon$  to examine the effect of the ratio  $T/\epsilon$  on the performance of the five methods. The ratio  $T/\epsilon$  determines the bandwidth of the high gain observer,

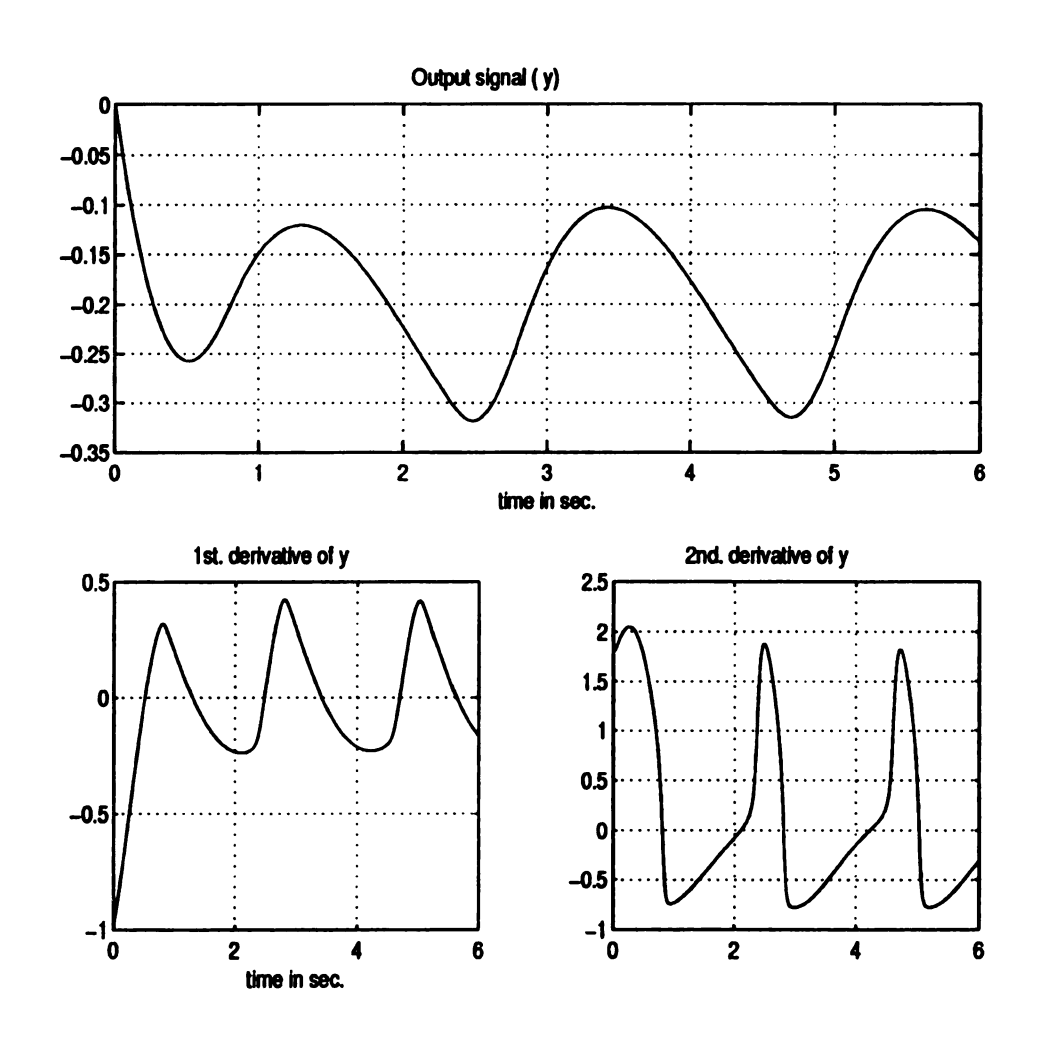


Figure 2.1. The output signal and its first and second derivatives.

so increasing or decreasing it will affect the error in calculating the derivatives.

Figure 2.2 shows the steady-state root mean square error  $^2$  in estimating  $\dot{y}$  and  $\ddot{y}$  for all five discretization methods in the case of the third-order observer. From the figure it is clear that, for the BD and BT methods, the errors in estimating the derivatives decrease with increasing  $T/\epsilon$ . The first derivative error reaches a plateau at  $T/\epsilon = 2$ , while the second derivative decreases all the way as we increase  $T/\epsilon$ . The figure shows also that increasing  $T/\epsilon$  hurts the ZOH and FD methods for both derivatives. As for the FOH method, the errors decrease with  $T/\epsilon$  until about  $T/\epsilon = 2$ ; then they increase. At  $T/\epsilon = 2$  both the FOH and BT have the same error. It appears from the figure that to reduce the steady-state error in the BT method we should increase  $T/\epsilon$ . However, as  $T/\epsilon \to \infty$ , the poles approach -1; thus, increasing  $T/\epsilon$  leads to oscillatory transient behavior. We found that a good compromise is to take  $T/\epsilon = 2$ .

From the previous figure, its looks like the FD method has less steady-state error for the higher derivative. To investigate this point further, we look at the error for both derivatives at  $T/\epsilon = 1.5$ . Figure 2.3 displays the error in estimating  $\dot{y}$  and  $\ddot{y}$  for the five discretization methods in the case of the third-order observer, with T = 0.01 and  $T/\epsilon = 1.5$ .

It shows that the transient behavior of the FD method is more oscillatory compared with the other methods, while the BT and FOH methods give less errors with relatively shorter transient periods. Figure 2.4 compares the BT and FOH methods for the three observers when  $T/\epsilon = 2$  by looking at the error in estimating  $\ddot{y}$ . It shows that the extended-order high-gain observer gives less error in calculating the second derivative. Moreover, the figure shows that the BT method outperforms the

<sup>&</sup>lt;sup>2</sup>The steady-state root mean square (r.m.s) error is taken as  $\sqrt{\frac{1}{N}\sum_{i=0}^{N-1}e(t_1+iT)^2}$  where N is the number of samples in an interval  $[t_1, t_2]$ , which starts beyond the transient period and lasts long enough to capture the steady-state behavior.

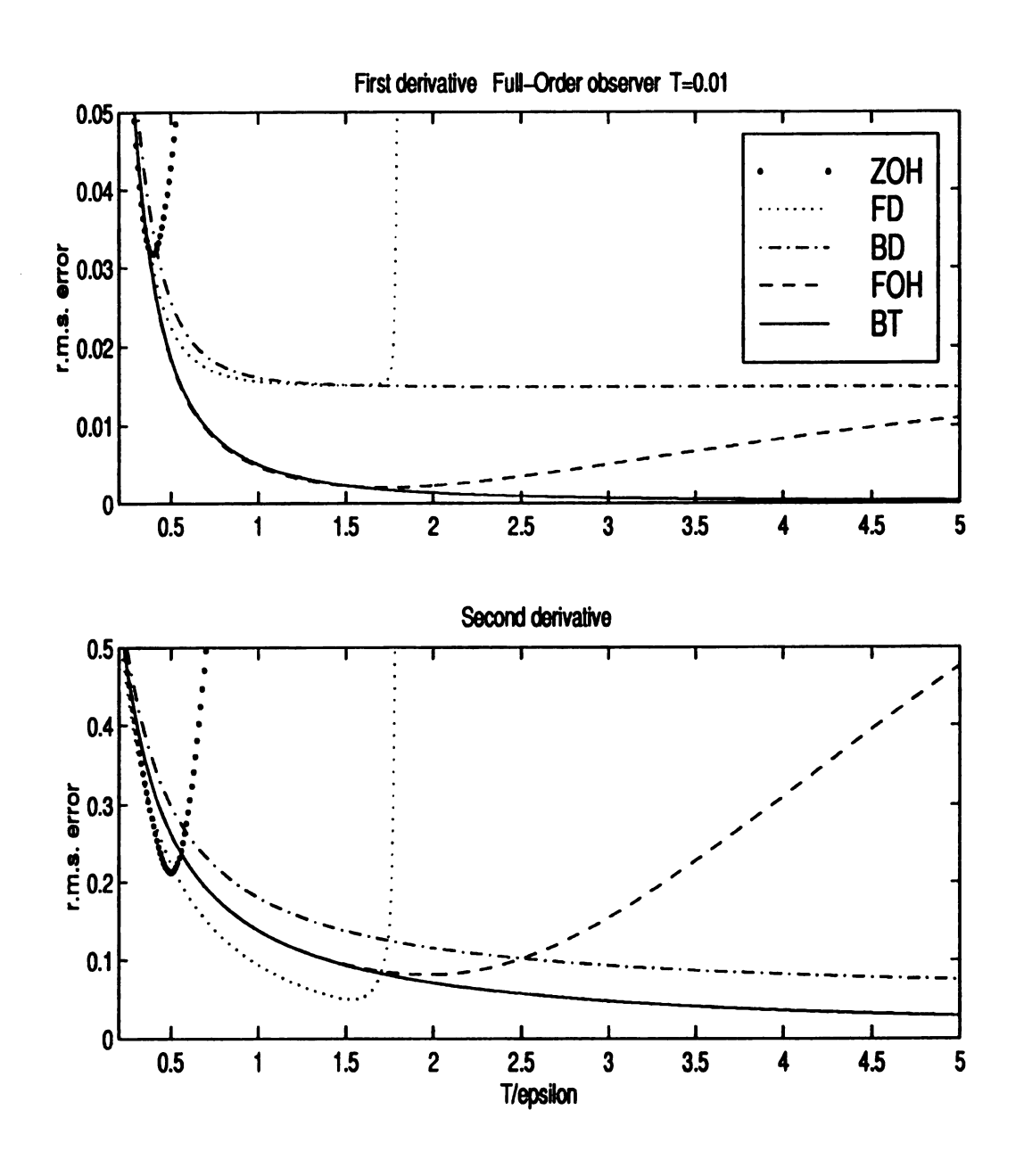


Figure 2.2. The maximum steady state absolute error in estimating  $\dot{y}$  and  $\ddot{y}$  for all five discretization methods for the full-order observer; T=0.01

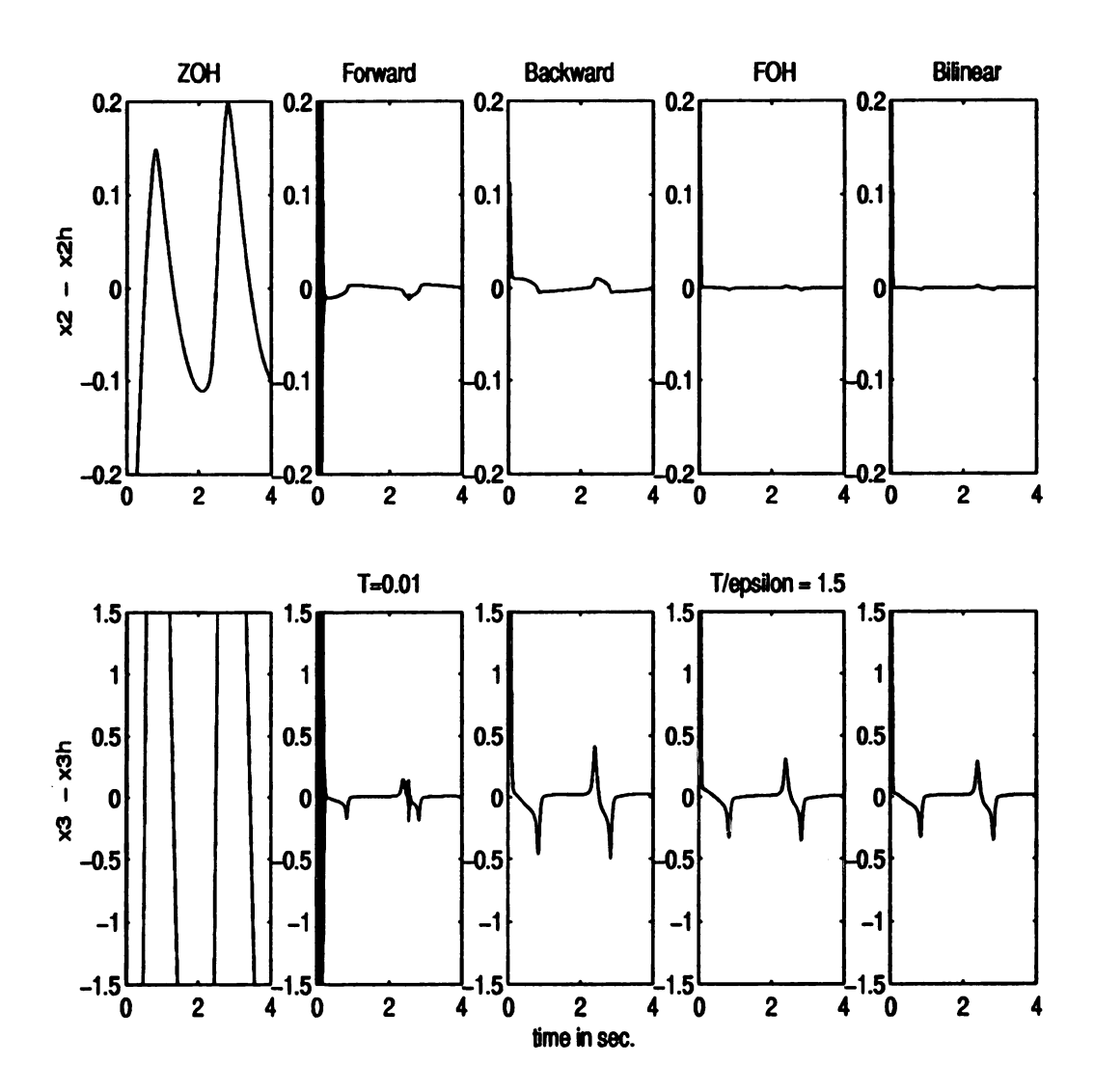


Figure 2.3. The error in  $\dot{y}$  and  $\ddot{y}$  for all five methods; T=0.01 and  $\epsilon=0.00667$ 

FOH method in estimating  $\ddot{y}$ , and the extended-order high-gain observer gives less error than the other two observers.

Taking both the transient and steady state behavior into consideration, we see that the bilinear transformation method provides the best performance among the five discretization methods. In fact, it provides the best performance for all three observers. This conclusion is typical of numerical testing of several other examples.

The parameter  $T/\epsilon$  determines the bandwidth of the discrete-time observer. The bandwidth increases with  $T/\epsilon$ . It is clear that in the presence of measurement noise the observer bandwidth will have to be limited. To study the effect of noise, consider the noisy measurement  $y_m = y + v$ , where  $y_m$  is the measured output, y is the exact output, and v is white Gaussian noise of variance  $\sigma^2$ . We studied the effect of the noise for different noise level and a representative case is given in Figure 2.5. It shows the steady-state r.m.s. error in estimating  $\dot{y}$  and  $\ddot{y}$ , for all five discretization methods with  $\sigma = 0.0316$ . Increasing  $T/\epsilon$ , the steady-state r.m.s. error decreases to a minimum; then it increase with  $T/\epsilon$ . The same behavior has been observed for different examples and different noise levels. This is reasonable because there is a certain bandwidth that allows the high-gain observer to achieve the best trade-off between filtering the noise and estimating the derivative. On the other hand, decreasing  $T/\epsilon$  increases the transient period. Thus, the choice of  $T/\epsilon$  is a trade-off between reducing the transient period and minimizing the steady-state error. Taking both the transient and steady-state behaviors into consideration, we observed, as in the noise-free case, that the bilinear transformation method outperforms other methods for large signal to noise ratio. But for small signal to noise ratio, all discretization methods have the same minimum steady-state error which occurs at almost the same value of  $T/\epsilon$ . Figure 2.6 shows this result for a low signal to noise ratio. It is clear from the figure that almost all methods behave equally and, by the help of Figure 2.5, we see that the minimum steady-state error for the various methods occurs at about  $T/\epsilon = 0.3$ .

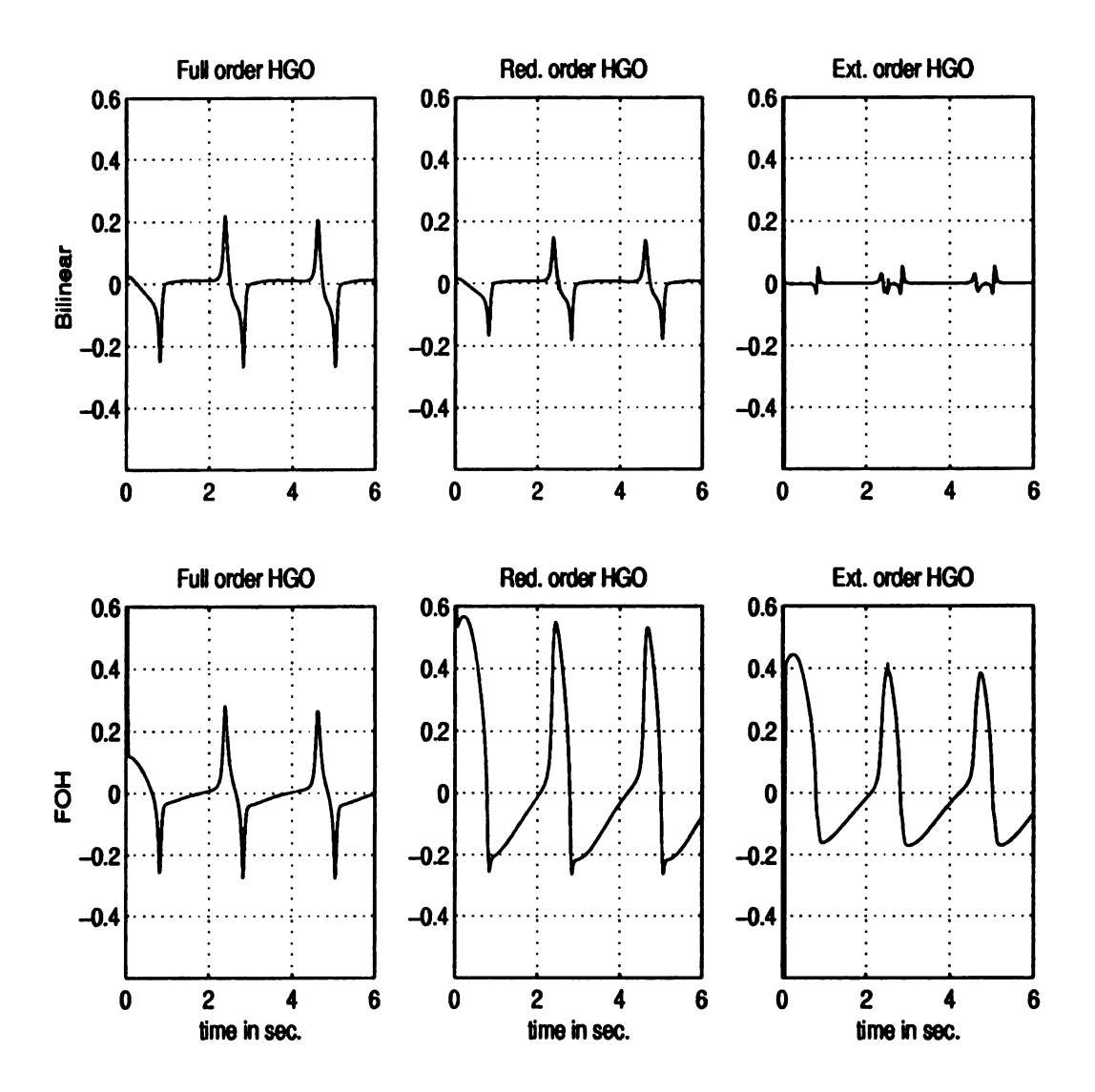


Figure 2.4. Error in  $\ddot{y}$  for the bilinear and FOH methods for the full, reduced, and extended observers.

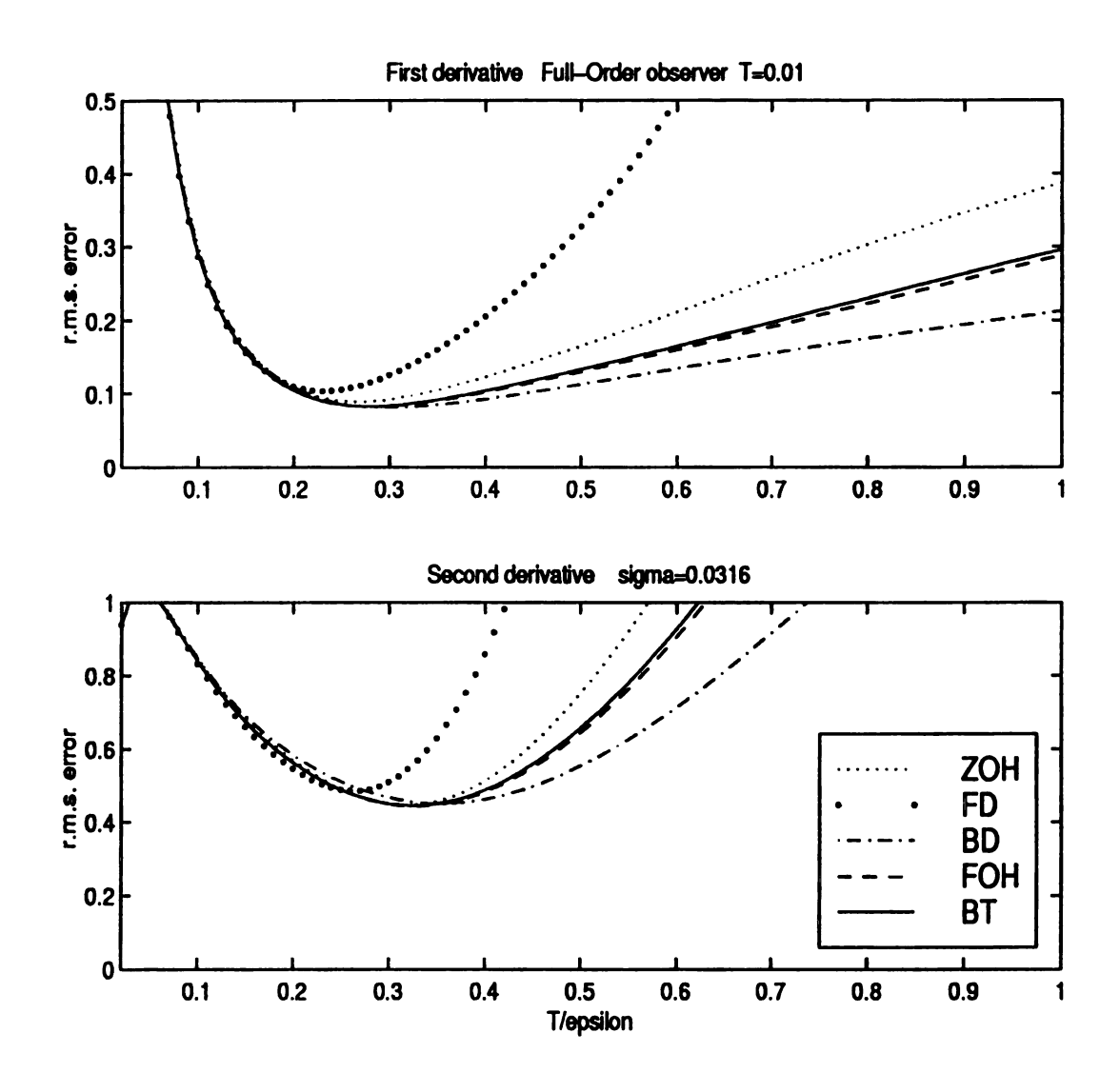


Figure 2.5. The maximum steady state absolute error in estimating  $\dot{y}$  and  $\ddot{y}$  for all five discretization methods for the full-order observer in the presence of noise; T=0.01 and  $\sigma=0.0316$ 

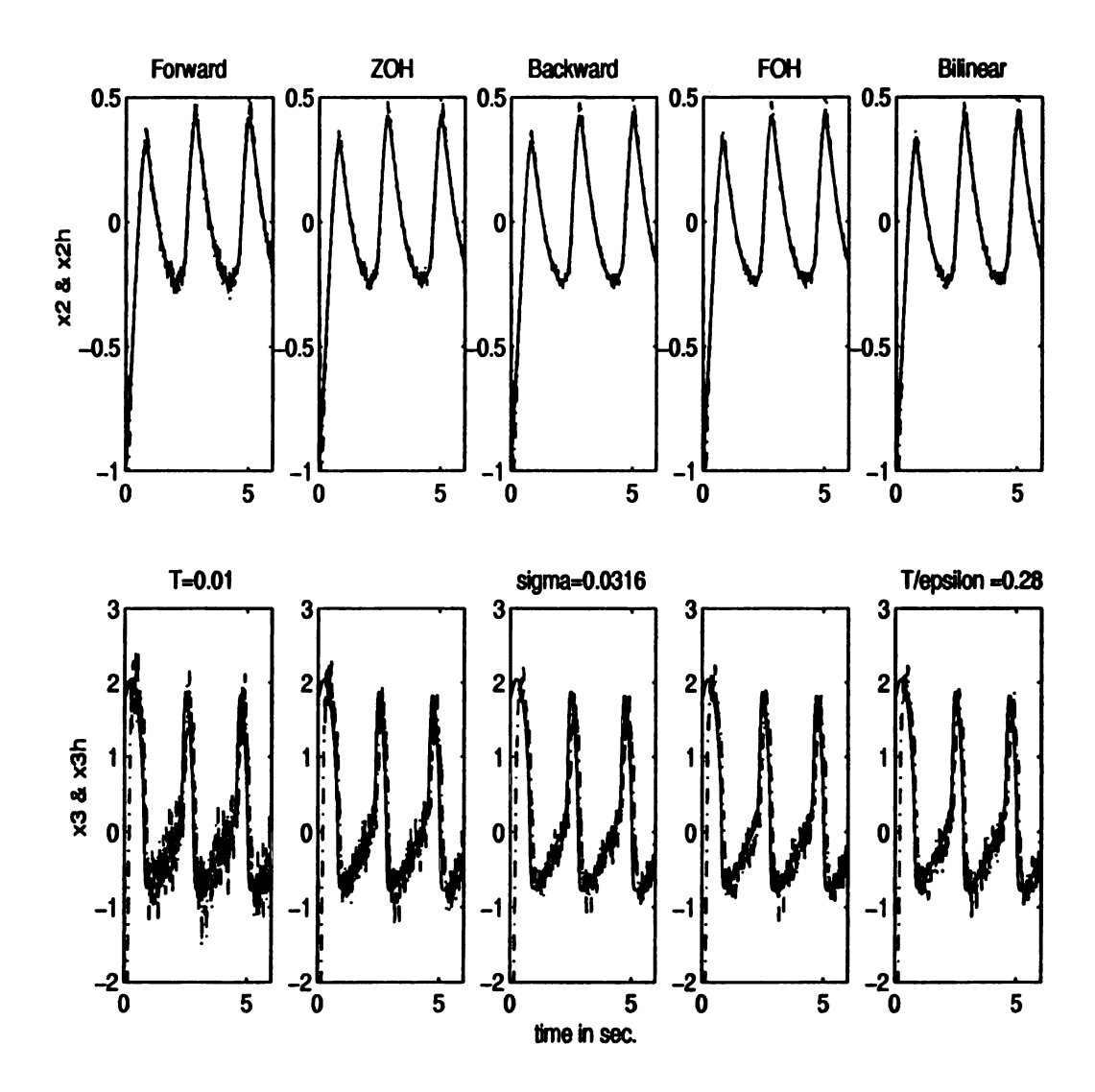


Figure 2.6. Calculating  $\dot{y}$  and  $\ddot{y}$  in the presence of noise;  $T=0.01,\,\epsilon=0.033,$  and  $\sigma=0.0316$ 

# 2.4 Bilinear Implementation

Based on the comparative study of the previous section, we adopt the bilinear transformation as our discretization method. Let us study the design of high-gain observers with bilinear discrete implementation. The design parameters are the sampling period T, the observer parameter  $\epsilon$  and the  $\alpha_i$  coefficients which assign the roots of the characteristic equation (2.6) or (2.15). The questions that should be addressed are: How should we choose the observer poles? Should they be all real, or should we have complex poles? How small should  $\epsilon$  be? What is the proper ratio of  $T/\epsilon$ ?

Regarding the choice of poles, we note that the bilinear high-gain observer can be made an FIR (Finite Impulse Response) filter or an IIR (Infinite Impulse Response) filter. An FIR filter has all its poles at the origin z = 0. This can be achieved by assigning all roots of (2.6) or (2.15) at s = -1, which assigns the observer poles at  $s = -1/\epsilon$ , and then choosing  $T = 2\epsilon$ . The pole mapping  $z = \frac{1+Ts/2}{1-Ts/2}$  shows that all poles map into the origin point z = 0. The only design freedom left in this case is the choice of the sampling period T (or equivalently the choice of  $\epsilon$ ). If T is given, all design parameters would have been determined by the FIR requirement. The FIR filters corresponding to Examples 2.1 to 2.4 are given, respectively, by

$$G(z) = \begin{bmatrix} \frac{1}{2}(1+z^{-1}) \\ \frac{1}{2T}(1-z^{-1}) \end{bmatrix}$$
 (2.23)

$$G(z) = \begin{bmatrix} \frac{1}{8}(7+3z^{-1}-3z^{-2}+z^{-3}) \\ \frac{1}{2T}(2-z^{-1}-2z^{-2}+z^{-3}) \\ \frac{1}{2T^{2}}(1-z^{-1}-z^{-2}+z^{-3}) \end{bmatrix}$$
(2.24)

$$G_R(z) = \frac{1}{2T}(1 - z^{-1}) \tag{2.25}$$

and

$$G_R(z) = \begin{bmatrix} \frac{1}{2T}(3 - 4z^{-1} + z^{-2}) \\ \\ \frac{1}{T^2}(1 - 2z^{-1} + z^{-2}) \end{bmatrix}$$
 (2.26)

In the case of an IIR filter, there is more freedom in choosing the observer poles and the ratio  $T/\epsilon$ . Let us consider first the case where all poles are real. A real pole  $s=-a/\epsilon$  maps into  $z=\left(1-\frac{Ta}{2\epsilon}\right)/\left(1+\frac{Ta}{2\epsilon}\right)$  which lies on the real axis in the z-plane. The ratio  $T/\epsilon$  determines the exact location of the pole. Notice that the limiting cases when T is much smaller than  $\epsilon$  or vice versa drive the pole towards instability, since

$$\lim_{T/\epsilon \to 0} \frac{\left(1 - \frac{Ta}{2\epsilon}\right)}{\left(1 + \frac{Ta}{2\epsilon}\right)} = 1$$

and

$$\lim_{T/\epsilon \to \infty} \frac{\left(1 - \frac{Ta}{2\epsilon}\right)}{\left(1 + \frac{Ta}{2\epsilon}\right)} = -1$$

Moreover, if  $T/\epsilon > 2a$ , the pole will be negative, resulting in oscillatory transient behavior which is clear from Figure 2.7. For good transient behavior, the pole should be restricted to  $|z| \leq \frac{1}{5}$ . This corresponds to the constraint  $(4/3a) \leq T/\epsilon \leq (3/a)$ . If the roots of (2.6) or (2.15) are real and satisfy  $-a_2 \leq s \leq -a_1$  for some positive constants  $a_1$  and  $a_2$ , then the ratio  $T/\epsilon$  should satisfy  $(4/3a_2) \leq T/\epsilon \leq (3/a_1)$ . The limiting case when all roots are assigned at -1 and  $T=2\epsilon$  yields the FIR filter as

seen before.

In the case of complex poles, we investigated distributing the poles on a semi-circle of radius  $r = 1/\epsilon$ . For n = 3, the poles are taken as  $-1/\epsilon$  and  $-(1/\epsilon)e^{\pm j\theta}$ . For this case, the results of Figure 2.8 show that with complex poles the transient response is oscillatory and the transient period is longer than with real poles. As for steady-state errors, complex poles result in less errors, but such reduction is insignificant. Therefore, for IIR filters we limit the choice of poles to real ones.

Another degree of freedom in designing high-gain observers is the choice of the order of the observer. For example, in Section 2.3 we used a second (reduced), third (full) and forth (extended)-order observers to estimate the first and second derivatives of a signal y. Let us use the same example to shed some light on the choice of the observer order. Figure 2.4 shows that the extended-order observer outperforms both the full and the reduced-order observer in the case of no noise. This result is expected because the extended-order observer uses more information to estimate the derivatives.

For the case of measurement noise, both the reduced-order and extended-order observers have wider bandwidth compared with the full-order observer. This is clear from the transfer functions in Examples 2.3 and 2.4. This allows more high-frequency noise to pass. Figure 2.9 shows this result with T=0.01 and  $\sigma=0.1$ . Notice from the figure that the minimum steady-state error occurs at different values of  $T/\epsilon$ , but the observer which gives the least steady-state error is the full-order observer. We observed also from different examples that changing the noise level will change the value of  $T/\epsilon$  at which the steady-state error is minimum. In general  $T/\epsilon < 2$ , but it is important for implementation to find the minimizing values of  $T/\epsilon$ . In conclusion, we see that, without noise, the extended-order high-gain observer with  $T/\epsilon=2$  outperforms the other two observers. With noise, the full-order observer gives the best performance.

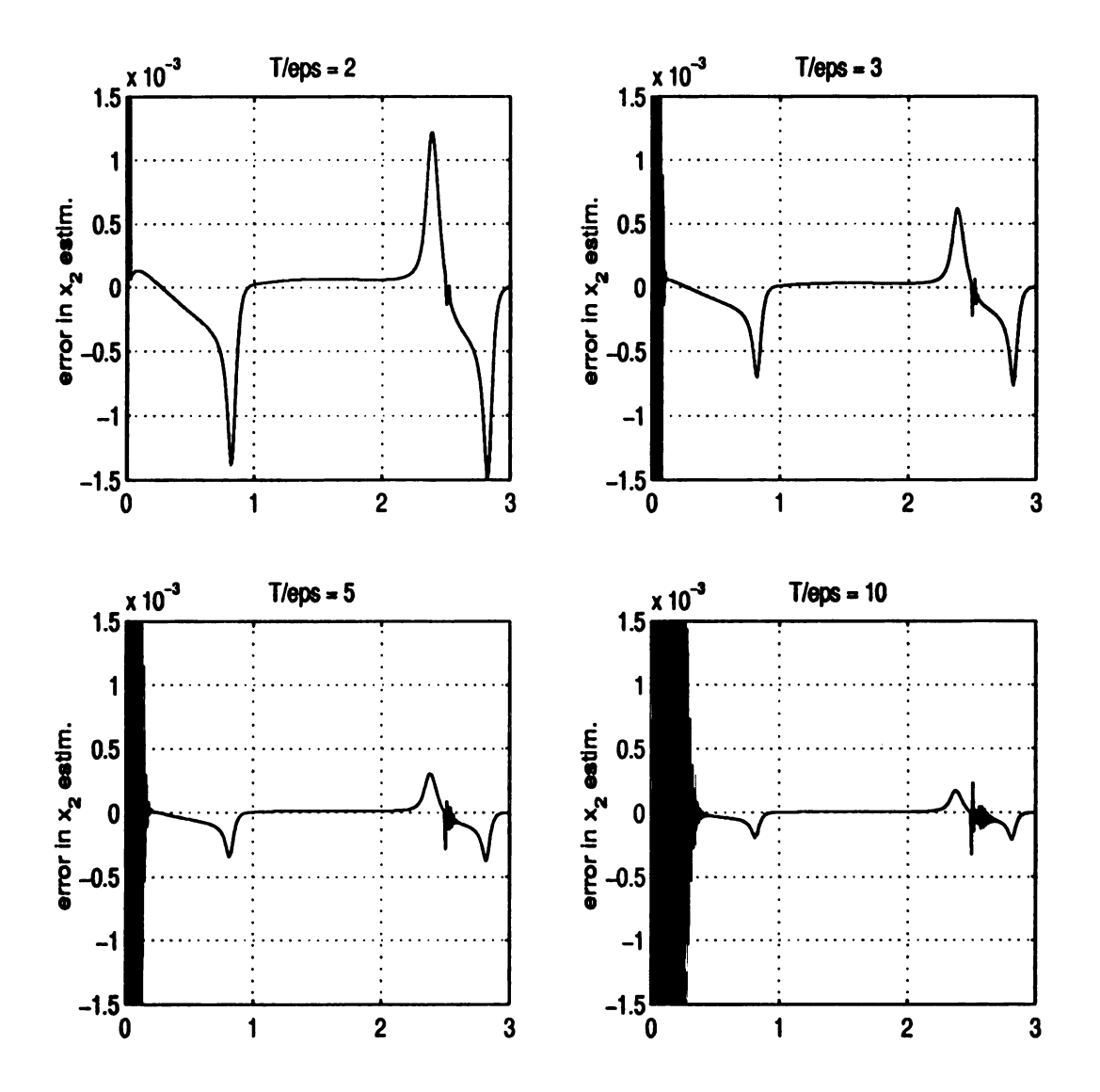


Figure 2.7. Effect of the ratio of  $\frac{T}{\epsilon}$  on the full-order high-gain observer with real poles at  $s=-1/\epsilon$  and T=0.01

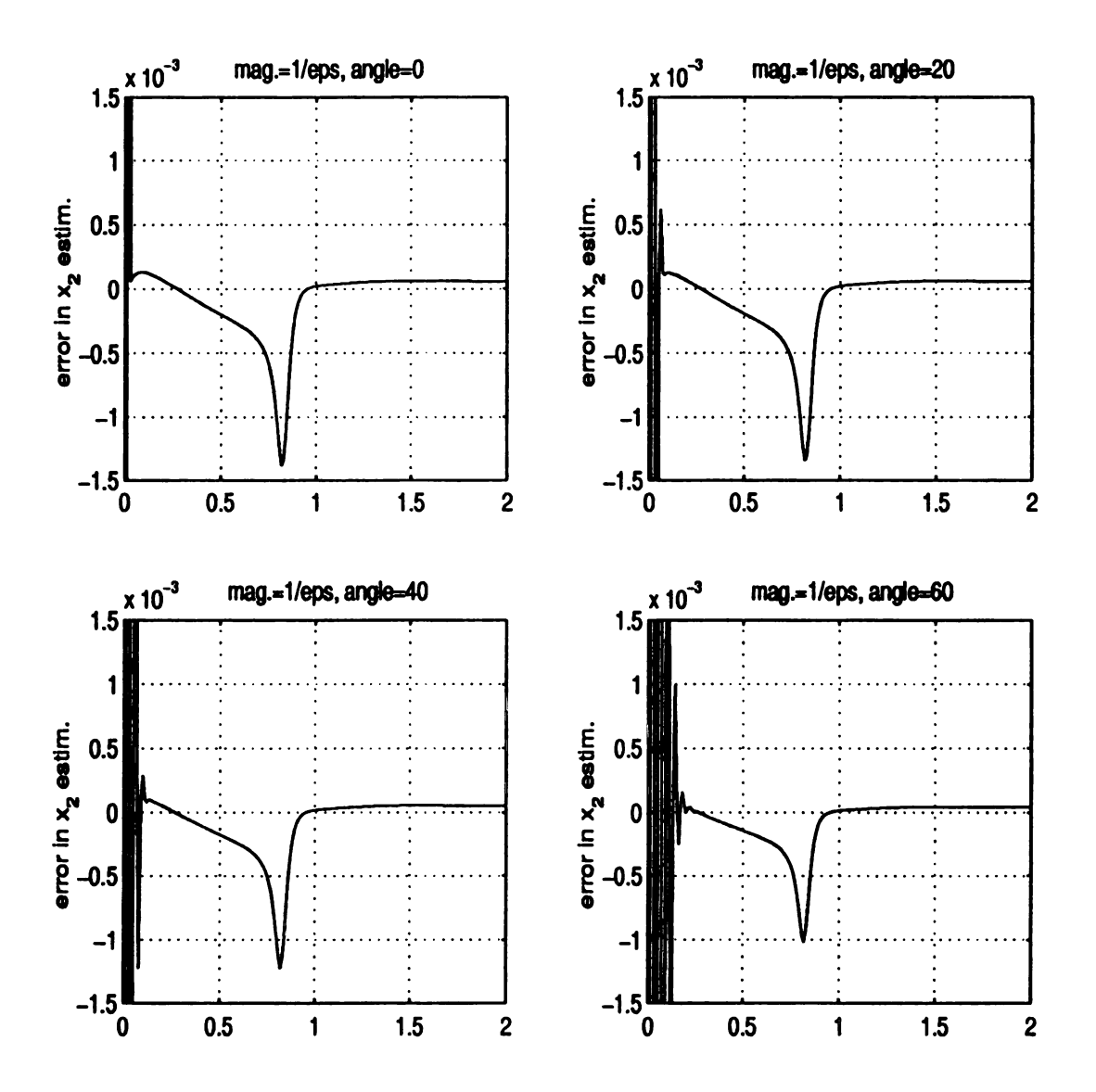


Figure 2.8. The transient response for different choices of poles: real and complex, T=0.01

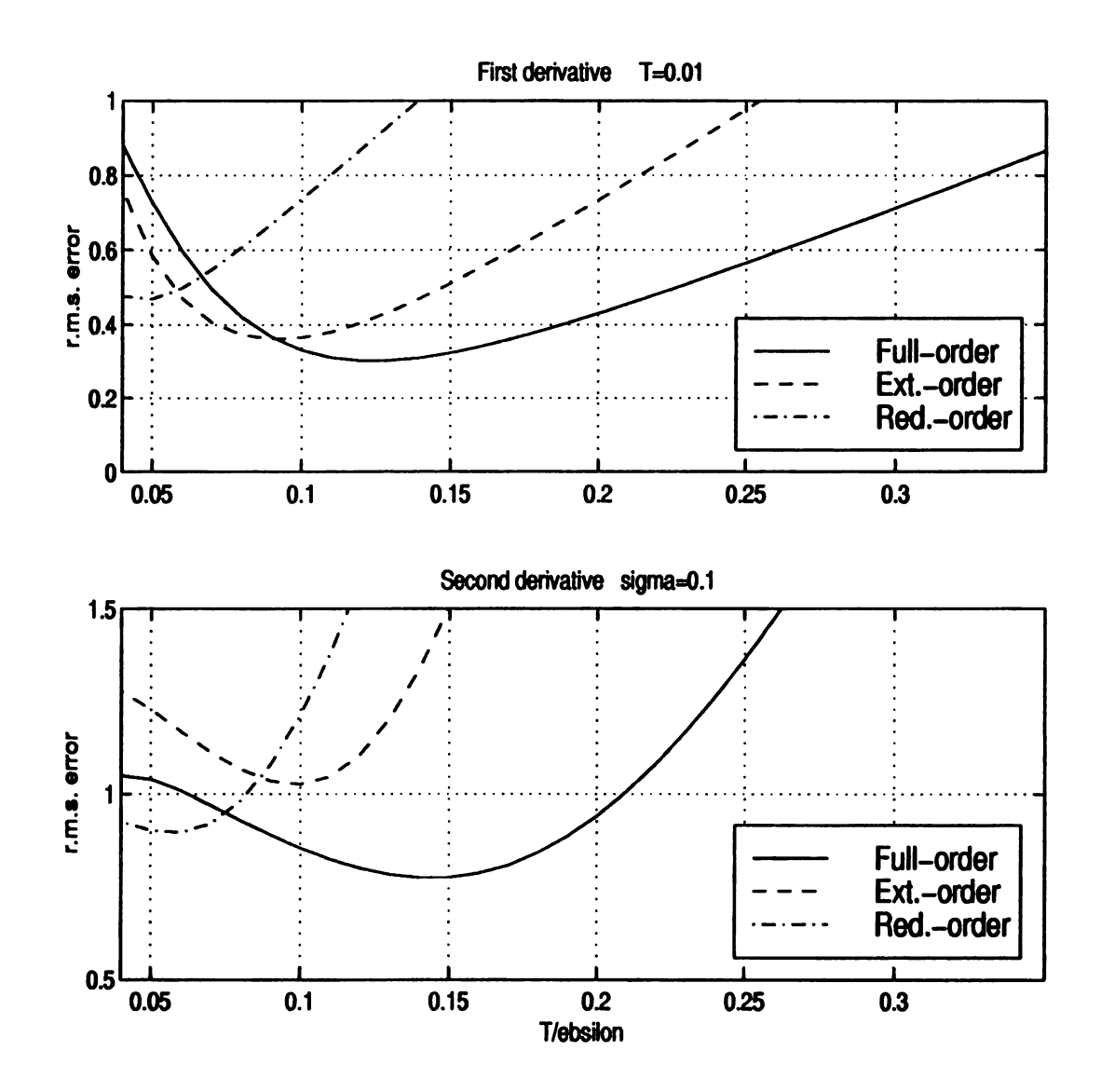


Figure 2.9. Comparing the maximum absolute steady-state error for the full, reduced and extended-order observers with noise;  $T=0.01,\,\sigma=0.1$ 

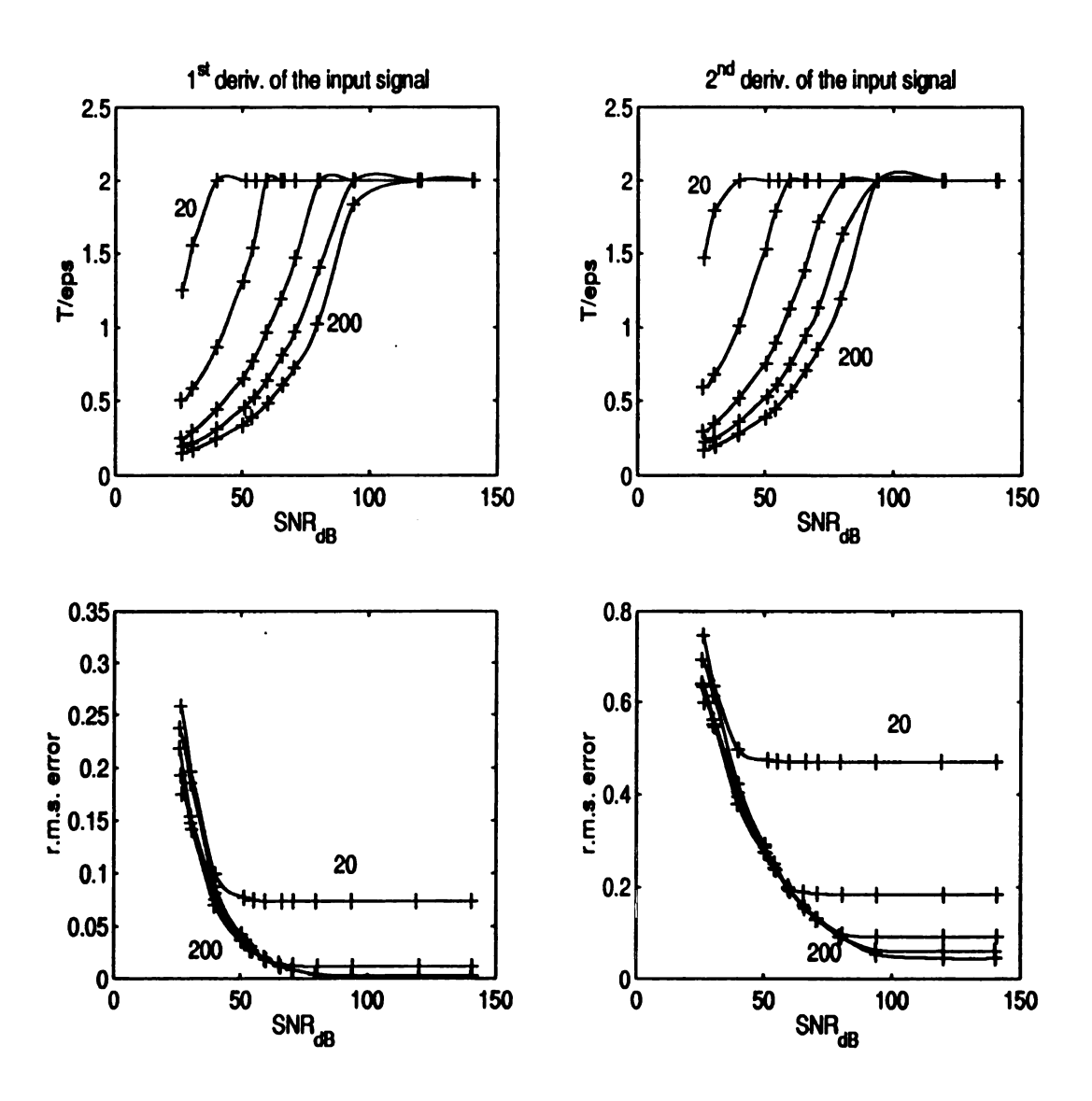


Figure 2.10. Comparing the signal to noise ratio with  $T/\epsilon$  and root mean square error r.m.s. for the full-order observer for T=0.01

$\omega_s/\omega_{max}$	SNR = 80 dB	SNR = 60 dB	SNR = 40 dB	SNR = 30 dB
20	2	2	2	1.55
50	2	2	0.88	0.6
100	2	0.98	0.45	0.3

Table 2.1. Guidelines for choosing  $T/\epsilon$  for different  $\omega_s/\omega_{max}$  and SNR.

The foregoing conclusions depend on the choice of  $T/\epsilon$ , so we need to give some guidelines on the proper choice of  $T/\epsilon$  in the presence of noise. We studied different examples where the output signals had different frequencies and magnitudes, to determine the minimizing value of  $T/\epsilon$  and how it changes with the noise level. We found out that if the ratio of the sampling frequency to the maximum frequency of the input signal  $(\omega_s/\omega_{max})$  is fixed, we get the same curves that describe the relation between the signal to noise ratio and  $T/\epsilon$ . Figure 2.10 shows that these curves change with  $\omega_s/\omega_{max}$ . The curves are shown for both the first and second derivatives, for  $\omega_s/\omega_{max} = 20, 50, 100, 150,$  and 200. The rationale behind choosing these numbers is how fast we can sample the input signal. It is clear from the figure that increasing  $\omega_s/\omega_{max}$  more than 100 does not result in a large reduction in the error, especially in the presence of noise. We note from Figure 2.5 that the convexity of the curve where the minimum occurs is not sharp, so using a tolerance of  $\pm 10\%$  or 20% for choosing  $(T/\epsilon)$  will be reasonable. Also, as the signal to noise ratio decreases, the change of the value of  $T/\epsilon$  gets smaller. From these curves we propose the guidelines shown in Table 2.1

## 2.5 Numerical Differentiators

Numerical calculation of the derivatives of a signal is an old problem in numerical analysis and digital signal processing. The backward difference method (Euler's formula) gives one of the earliest and simplest numerical differentiators. Although it is very crude, its use is quite common in engineering applications. One can also use formulas from other numerical integration techniques. A different approach to numerical differentiation is to use interpolation techniques, like the spline interpolant method [17]. In the digital signal processing literature, this problem goes back to the work of Rabiner and Steiglitz [52] who used digital filters for wide-band digital differentiators. They used filters of order 16 to 256 (in powers of two). Various other types of digital differentiators have been designed to minimize both the filter order and the relative error in the frequency range of interest. Kumar and Dutta Roy [38] proposed digital differentiators from maximally flat nonrecursive low-pass digital filters for the narrow frequency band of 0 to 0.2  $\pi$  radians, using filters of order ranging from 9 to 21. Al-Alaoui [1] introduced a new approach that makes use of the idea that the ideal integrator response lies between the response of the rectangular and trapezoidal rules. Interpolating these two rules, he gave better approximations of the ideal differentiator.

In this section, we describe the backward difference method, the spline interpolant method, and several formulas from the digital signal processing literature. Then, we study their connection with the bilinear high-gain observer of the previous section.

Euler's formula for finding the first derivative of a signal y is

$$\hat{\dot{y}}(k) = \frac{1}{T}[y(k) - y(k-1)] \tag{2.27}$$

In the spline interpolant method [17], we start with a window of data  $\{y_{k-W}, \ldots, y_k\}$ .

Let the interpolating polynomial be denoted by

$$\hat{y}_k(t) = a_0 + a_1(t - (k - W)T) + \ldots + a_N(t - (k - W)T)^N$$

where the coefficients  $\{a_0, a_1, \ldots, a_N\}$  are determined from the least squares solution of

$$\begin{bmatrix} 1 & 0 & \dots & 0 \\ 1 & T & \dots & (T)^{N} \\ \vdots & & \vdots \\ 1 & WT & \dots & (WT)^{N} \end{bmatrix} \begin{bmatrix} a_{0} \\ a_{1} \\ \vdots \\ a_{N} \end{bmatrix} = \begin{bmatrix} y_{k-W} \\ y_{k-W+1} \\ \vdots \\ y_{k} \end{bmatrix}$$
(2.28)

N is the order of the interpolating polynomial, and  $W \times T$  is the length of the moving window in time. The estimated derivatives of the polynomial y at time  $\tau$  are calculated by

$$\widehat{\frac{d^j}{dt^j}y_k}(\tau) = \widehat{\frac{d^j}{dt^j}}\hat{y_k}(\tau)$$

For real time applications we have to use causal differentiators. Therefore, we estimate the derivatives at the end of the window. To compare with other methods, let us consider a third order system which gives first and second derivatives, i.e., N=2, and W=2. Solving for the coefficients  $\{a_0,a_1,a_2\}$  from equation (2.28) and substituting in the derivative of  $\hat{y}$ , we obtain

$$\dot{\hat{y_k}} = T^{-1}(0.5y_{k-2} - 2y_{k-1} + 1.5y_k) \tag{2.29}$$

$$\ddot{\hat{y_k}} = T^{-2}(y_{k-2} - 2y_{k-1} + y_k) \tag{2.30}$$

Various types of Digital Differentiators have been designed using the min max criterion, which amounts to minimization of the relative error over the frequency range of interest. It is shown by Al-Alaoui in [1] that these nonrecursive differentiators are outperformed by a digital differentiator which is obtained by interpolating two pop-

ular digital integration techniques, the rectangular and trapezoidal rules. The new differentiator is obtained by taking the inverse of the transfer function of the integrator. The effective range of the differentiator is about 0.8 of the Nyquist frequency. The resulting transfer function of the new digital differentiator is

$$G(z) = \frac{8(z-1)}{7T(z+\frac{1}{7})} \tag{2.31}$$

This filter was generalized by Bihan [9] to a class of first-order differentiators. The filter parameters are calculated to satisfy various defined criteria. The minimum phase digital differentiator is

$$G(z) = \frac{2}{T} \frac{(z-1)}{(1+\chi)z + (1-\chi)}$$
 (2.32)

where  $0 \le \chi \le 1$ . Al-Alaoui [2] proposed a stable second-order recursive differentiator

$$G(z) = \frac{3(z^2 - 1)}{T(3.7321)(z^2 + 0.5358z + 0.0718)}$$
(2.33)

suitable for applications that require fast differentiation methods. It is obtained from the Simpson integration rule. The accuracy and the range of the amplitude response of the proposed differentiator is the same as that of the Simpson integrator. Thus, it is comparable to that obtained by higher order algorithms.

In [3], a new class of stable second-order low-pass differentiators was considered. These second-order differentiators are obtained by interpolating the traditional Simpson and trapezoidal integrators, inverting the resultant transfer function to obtain the proposed differentiator

$$G(z) = \frac{6(z^2 - 1)}{Tr_1(3 - a)(z + r_2)^2}$$
 (2.34)

where  $0 \le a \le 1$ ,  $r_1 = (3 + a + 2\sqrt{3a})/(3 - a)$ , and  $r_2 = 1/r_1$ .

## 2.5.1 Comparison with the Bilinear High-Gain Observer

It is interesting that all the numerical differentiators described in this section can be viewed as special cases of the high-gain observer. We show this fact for each one of them.

The bilinear discrete equivalent of the transfer function of Example 2.3 is given by

$$G_R(z) = \frac{2\alpha_1}{2\epsilon + \alpha_1 T} \times \frac{z - 1}{z + \frac{1 - \frac{2\epsilon}{\alpha_1 T}}{1 + \frac{2\epsilon}{\alpha_1 T}}}$$

Taking  $\alpha_1 = 1$  and  $\epsilon/T = 3/8$  results in the filter (2.31). Taking  $\alpha_1 = 1$ , and  $T/\epsilon = 2$ gives the backward difference method, while the choice  $\alpha_1=1,\,T/\epsilon=2/\chi$  yields the filter (2.32). The bilinear discrete equivalent of the transfer function of Example 2.1 with  $\alpha_1 = 2$ ,  $\alpha_2 = 1$  and  $\epsilon/T = 1/\sqrt{12}$  yields (2.33). Furthermore, with  $\alpha_1 = 2$ ,  $\alpha_2 = 1$ 1, and  $\epsilon/T = \sqrt{a/12}$  for  $0 \le a \le 1$ , we obtain (2.34). All the foregoing numerical differentiators are special cases of high-gain observers with certain choices of the observer parameters. Such choices are not necessarily the best choices for an observer design, in view of the results of the previous section on how to choose the observer parameters. This is particularly so in the presence of noise. Let us elaborate on this point by considering specific numerical differentiators. In the backward difference method, the sampling period T is the only design parameter. To calculate (n-1)derivatives, we end up with a filter whose bandwidth is proportional to  $1/T^{n-1}$ . If T is very small, the backward difference filter will have a large bandwidth. The same observation holds for the digital filters described by Al-Alaoui and Bihan. They are special cases of bilinear high-gain observers. All of them have  $T/\epsilon > 2$ , and for a small T,  $\epsilon$  must be small too. Consequently these filters have wide bandwidth. With such filters, it will be necessary to use low pass filters to filter out the high-frequency noise, which will add delay to the estimates of the derivative. We saw in the previous section that high-gain observers can be designed to have a smaller bandwidth by

taking  $T/\epsilon < 2$ .

For the special case of the spline interpolant method with N=2 and W=2, it can be seen that the FIR filter of (2.26), corresponding to the high-gain observer of Example 2.3, coincides with (2.29)-(2.30). This relationship does not hold for higher values of N and W. Therefore, by optimizing the choices of N and W, it is conceivable that the spline interpolant method may outperform the bilinear high-gain observer. As for the choice of N, it was observed in [17] that the order of the interpolating polynomial should be selected as low as possible in order to smooth the noise in the estimates of the derivatives. Hence, for estimating the first and second derivatives, we should use N=2. For a fixed T, this leaves us with the window size W as the only design parameter that can be adjusted to filter out the noise. For T = 0.001,  $\epsilon = 0.0154$ ,  $\sigma^2 = 0.001$ , and W = 70, Figure 2.11 shows that the bilinear high-gain observer and the spline interpolant method have the same error for both derivatives. It shows also that the spline interpolant method has a shorter transient period. Decreasing the window size allows more high-frequency noise to pass. For very small T, the window size should be increased to capture more information about the input signal y in order to smooth the calculated derivatives. For higher noise levels, we need to increase the window size in order to filter out most of the noise. This will work up to a certain limit, after which the error becomes independent of the window size. Increasing the window size increases the computation time and the memory requirements of the spline interpolant method. For W = 70, the computation time for the spline interpolant method is about four times that of the full-order high-gain observer (the CPU average time for using the full-order high-gain observer is 7.44 sec., and the CPU average time for the spline interpolant is 29.79 sec.). Increasing the window size requires more memory in each loop for calculation, while the fullorder high-gain observer requires only n memory locations. Therefore, we can see that the high-gain observer can achieve results comparable to the spline interpolant

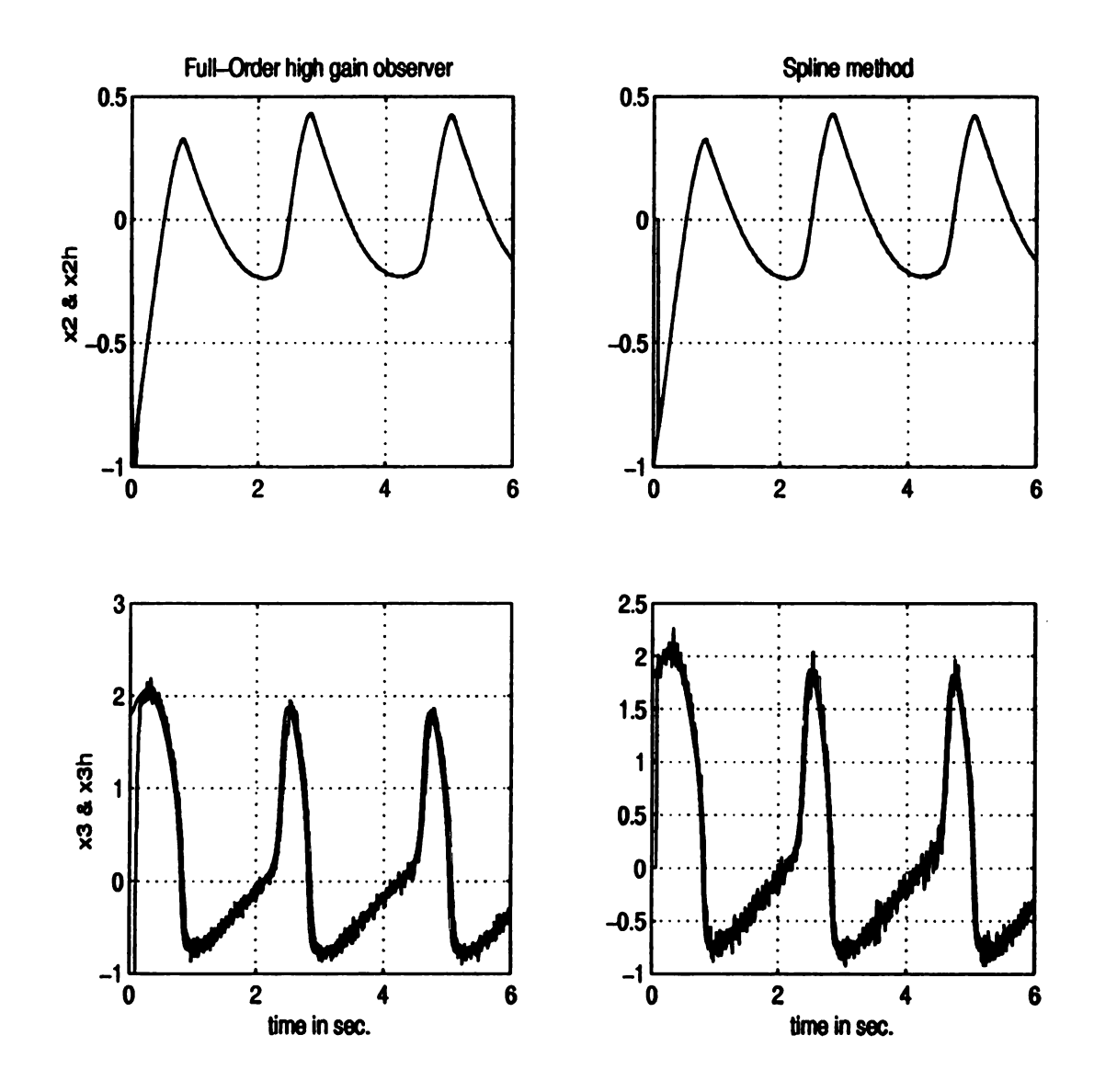


Figure 2.11. Comparing full-order observer and spline interpolant methods;  $T=0.001,\,\epsilon=0.0154,\,\sigma^2=0.001,$  and W=70.

method, with less computation time and memory requirements.

# 2.5.2 Spline Method Initialization of The High-Gain Observer

One advantage of the spline interpolant method over the high-gain observer is its nice transient behavior. Starting from zero, it usually approaches its estimates in a fast monotonic motion. The transient behavior of the high-gain observer, on the other hand, could be oscillatory and accompanied with the peaking phenomena. We may use saturation to overcome peaking [16], but the estimates will be degraded during the saturation period. This drawback of the high-gain observer can be eliminated by using the spline interpolant method to initialize the the high-gain observer. Even though in the presence of noise the window size needs to be large enough to filter out the noise, the window width is usually much less than the transient period of the high-gain observer. Figure 2.12 shows the difference between initializing the high-gain observer by the spline interpolant method and without it in the noise-free case, with  $T/\epsilon = 10$ , T = 0.001, W = 2, and N = 2.

It is clear from the figure that initializing the high-gain observer from a spline interpolant methods has reduced the transient period oscillations, especially in the estimates of the second derivative. Figure 2.13 shows a similar comparison in the presence of noise, with  $T/\epsilon = 0.065$ , T = 0.001, W = 40, N = 2, and  $\sigma = 0.0316$ . Notice that the size of the window has been increased in the presence of noise to give a good start. Both Figures 2.12 and 2.13 are for the extended-order observer.

# 2.6 Further Considerations

In this section we study a modified HGO and compare it with the regular HGO. We also give two more examples to show that the conclusions drawn from the simulation

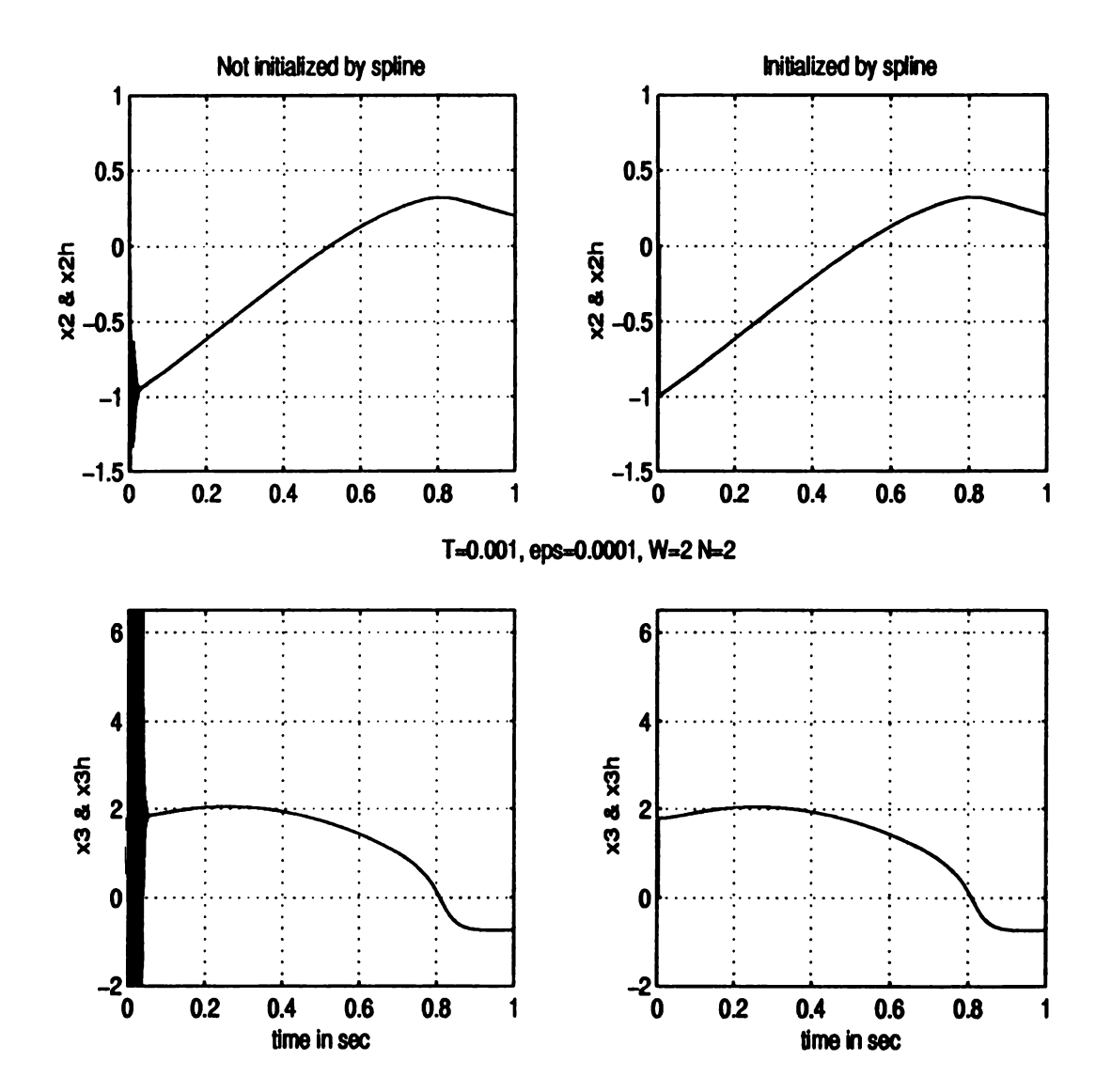


Figure 2.12. The effect of initializing the high-gain observer by spline interpolant methods;  $T/\epsilon=10,\,T=0.001,\,W=2,$  and N=2.

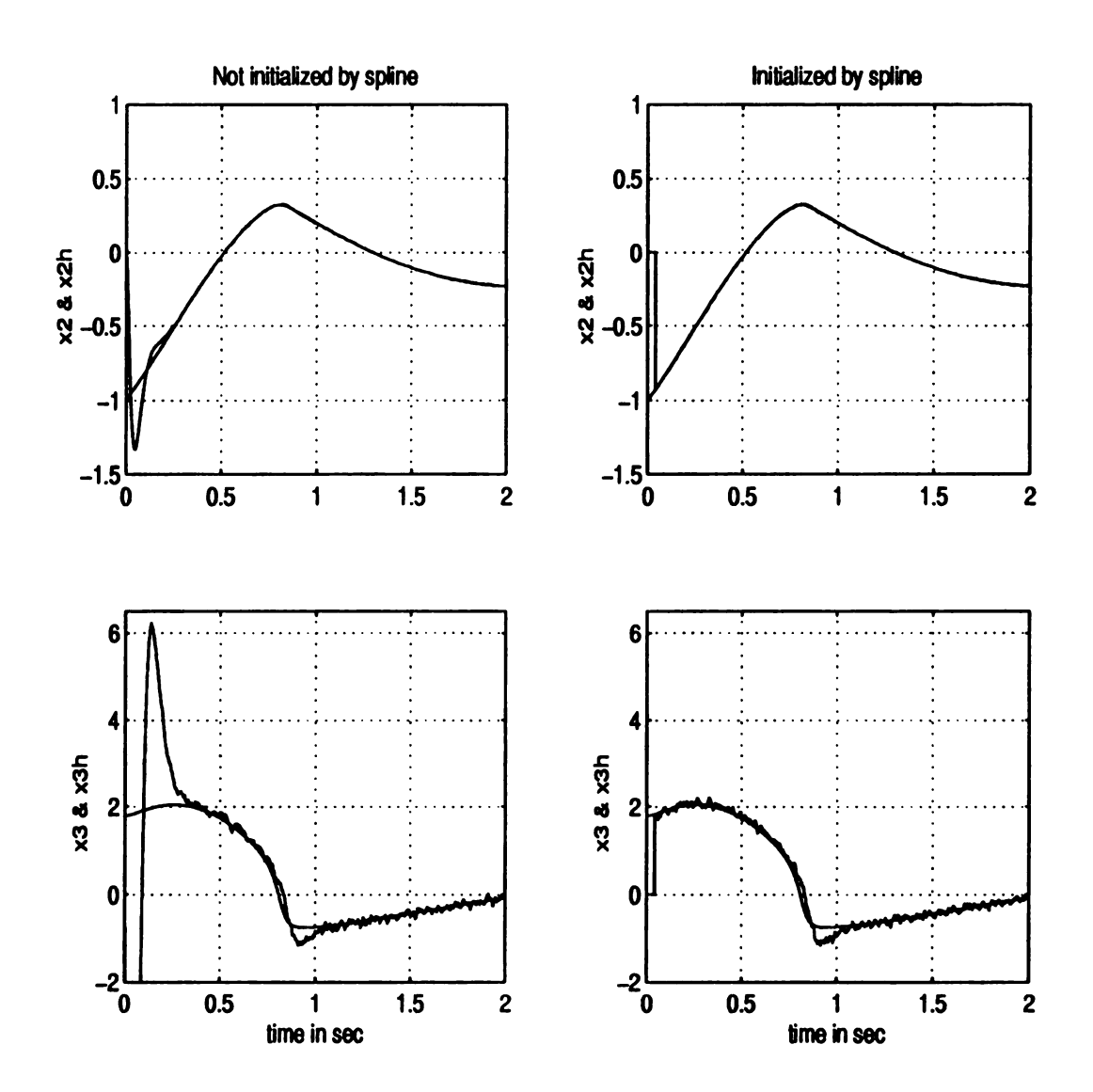


Figure 2.13. The effect of initializing the high-gain observer by spline interpolant methods in the presence of noise;  $T/\epsilon=0.065,\,T=0.001,\,\sigma=0.01\,W=40$ , N=2 and  $\sigma=0.0316$ 

of the third-order example of Section 2.3.2 are common in other examples. Notice that the main example is the most difficult one because the output signal is fast, which requires a smaller sampling period. The simulation results will be repetitions of Figures 2.1-2.8.

## 2.6.1 Modified Observers

Modified observers were discussed in the literature for both HGO and SMO (sliding mode observer). In [48], [18] the modification was done only for second-order systems to estimate  $x_2$ , while in [19] it was done for the SMO for higher-order systems to estimate n derivatives.

For a second order system the modified HGO is given by

$$\tilde{x}_1 = \hat{x}_1$$

$$\tilde{x}_2 = \hat{x}_2 + k_1 (x_1 - \hat{x}_1)$$

In this work we are going to extend the modified HGO observer to dimension n as it was done for the SMO in [19].

Changing the observer output from  $\hat{x}$  to  $\tilde{x}$  results in different output equations

$$ilde{x}_1 = \hat{x}_1$$
 $ilde{x}_i = \hat{x}_i + rac{lpha_{i-1}}{\epsilon^{i-1}} (x_1 - \hat{x}_1), \qquad 2 \leq i \leq n$ 

which can be written in the vector form

$$\tilde{x} = C_m \ \hat{x} + D_m \ y$$

where  $C_m$  is  $n \times n$  and  $D_m$  is  $n \times 1$ . The transfer function for the modified linear

HGO is

$$G_m(s) = (sI - A + H C_m)^{-1}H + D_m$$

**Example 2.5** For n = 3,  $G_m(s)$  is given by

$$G_m(s) = rac{1}{d(\epsilon s)} \left[ egin{array}{l} lpha_1 \epsilon^2 s^2 + lpha_2 \epsilon s + lpha_3 \ lpha_1 \epsilon^2 s^3 + lpha_2 \epsilon s^2 + lpha_3 s \ lpha_2 \epsilon s^3 + lpha_3 s^2 \end{array} 
ight]$$

where  $d(\epsilon s) = \epsilon^3 s^3 + \alpha_1 \epsilon^2 s^2 + \alpha_2 \epsilon s + \alpha_3$ . Comparing the error in estimating the derivative for both  $\hat{x}$  in Example 2.2 and  $\tilde{x}$  in this example we get the following:

$$e_{regular} = \begin{bmatrix} \frac{\hat{x}_2 - sy}{sy} \\ \frac{\hat{x}_3 - s^2y}{s^2y} \end{bmatrix} = \frac{1}{d(s)} \begin{bmatrix} -\epsilon^3 s^3 - \alpha_1 \epsilon^2 s^2 \\ -\epsilon^3 s^3 - \alpha_1 \epsilon^2 s^2 - \alpha_2 \epsilon s \end{bmatrix} = O(\epsilon)$$

and

$$e_{modified} = \begin{bmatrix} \frac{\bar{x}_2 - sy}{sy} \\ \frac{\bar{x}_3 - s^2y}{s^2y} \end{bmatrix} = \frac{1}{d(s)} \begin{bmatrix} -\epsilon^3 s^3 \\ -\epsilon^3 s^3 - \alpha_1 \epsilon^2 s^2 \end{bmatrix} = O(\epsilon^2)$$

This preliminary investigation shows that the error for the linear modified HGO is of order  $O(\epsilon^2)$  where as for the regular observer it is of order  $O(\epsilon)$ . Studying the error equations  $e_{regular} = x - \hat{x}$  and  $e_{modified} = x - \tilde{x}$  in simulation we can see easily how the modified is better than regular. Including in this comparison the extended order HGO we can see that the extended order HGO outperforms both the regular and modified observers. Figure 2.14 shows the error in the highest derivative. The extended observer has the least error, followed by the modified observer, followed by the regular observer.

The modified high-gain observer has a larger bandwidth than the regular high-gain observer. This can be seen from the transfer functions in example 2.5. Therefore, the modified observer passes more noise than the regular observer, which makes the

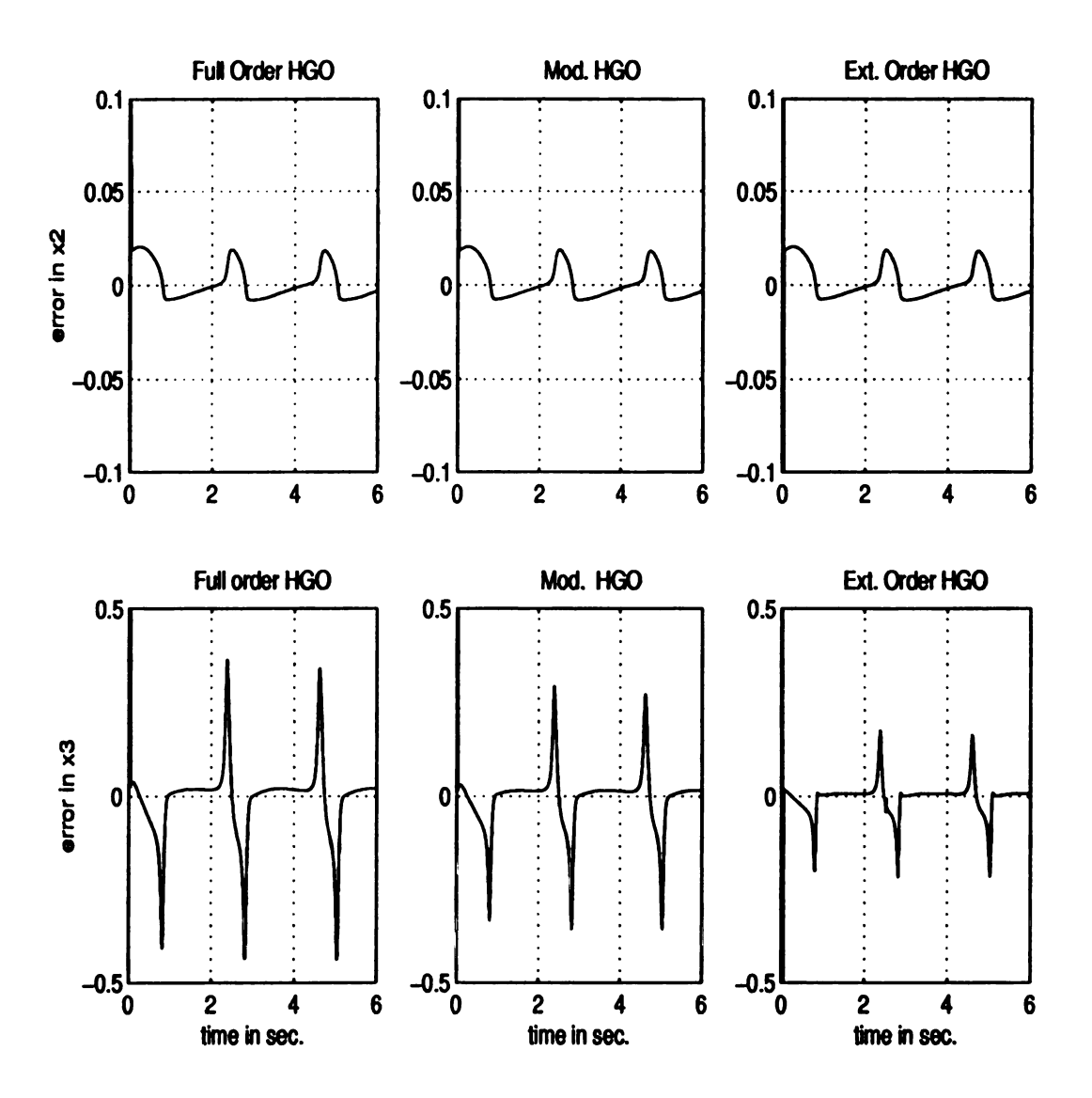


Figure 2.14. The comparison between the regular, the modified, and the extended HGO where  $T=0.01\,$ 

modified observer less desirable in the presence of noise.

## 2.6.2 Additional Examples

We will consider two more examples to support the conclusions of this chapter.

Example 2.6 Consider third-order nonlinear system in the normal form as follow

$$\dot{x}_1 = x_2$$
 $\dot{x}_2 = x_3$ 
 $\dot{x}_3 = -x_2 \cos(x_1) - 4\mu x_1 x_2^2 - 2\mu x_3 x_1^2 + u$ 
 $y = x_1$ 

where the control  $u=-\omega \ k \sin(\omega t)$ . The parameters are  $\mu=2, \ k=0.5$ , and  $\omega=0.25$ . We would like to estimate the states  $x_2$  and  $x_3$  from the measured output  $x_1$ . We use the discrete-time high-gain observer. From the output signal shown in Figure 2.15 we see that the signal period is about 25 sec; this system is slower than the system of Section 2.3.2. In particular, comparison of Figures 2.1 and 2.15 shows that the output of the main example has frequency almost 10 times higher than the current output. Using three different high-gain observers, described in Section 2.2, we compare the different discretization methods. Figures 2.16 to 2.22 show the same trends which were observed from Figures 2.2 to 2.8, respectively. It is important to notice that for slower systems, in the presence of noise, it is better to use larger sampling periods.

**Example 2.7** Consider the third-order nonlinear system

$$\dot{x}_1 = x_2$$

$$\dot{x}_2 = x_3$$

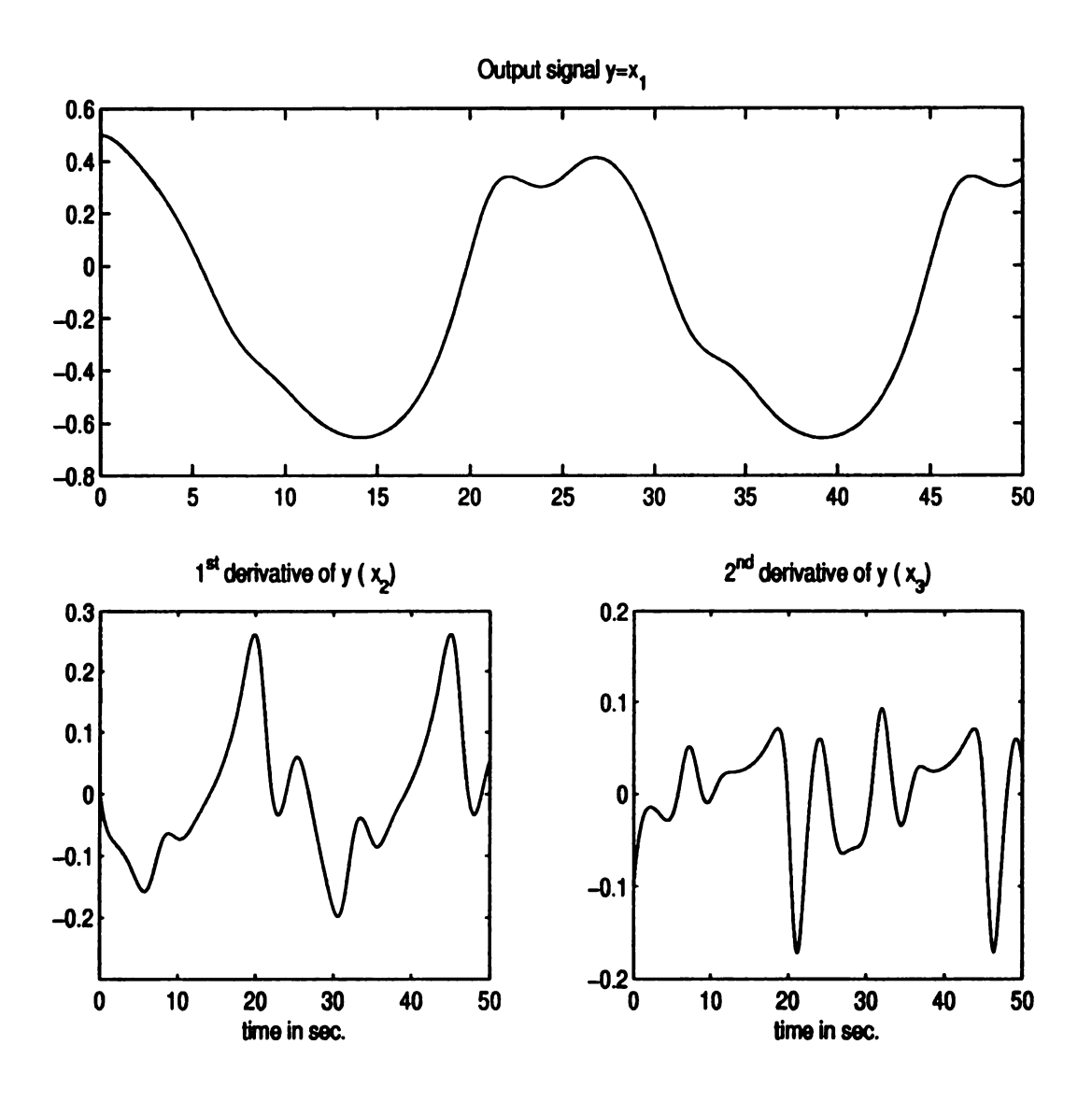


Figure 2.15. The output signal and its first and second derivatives.

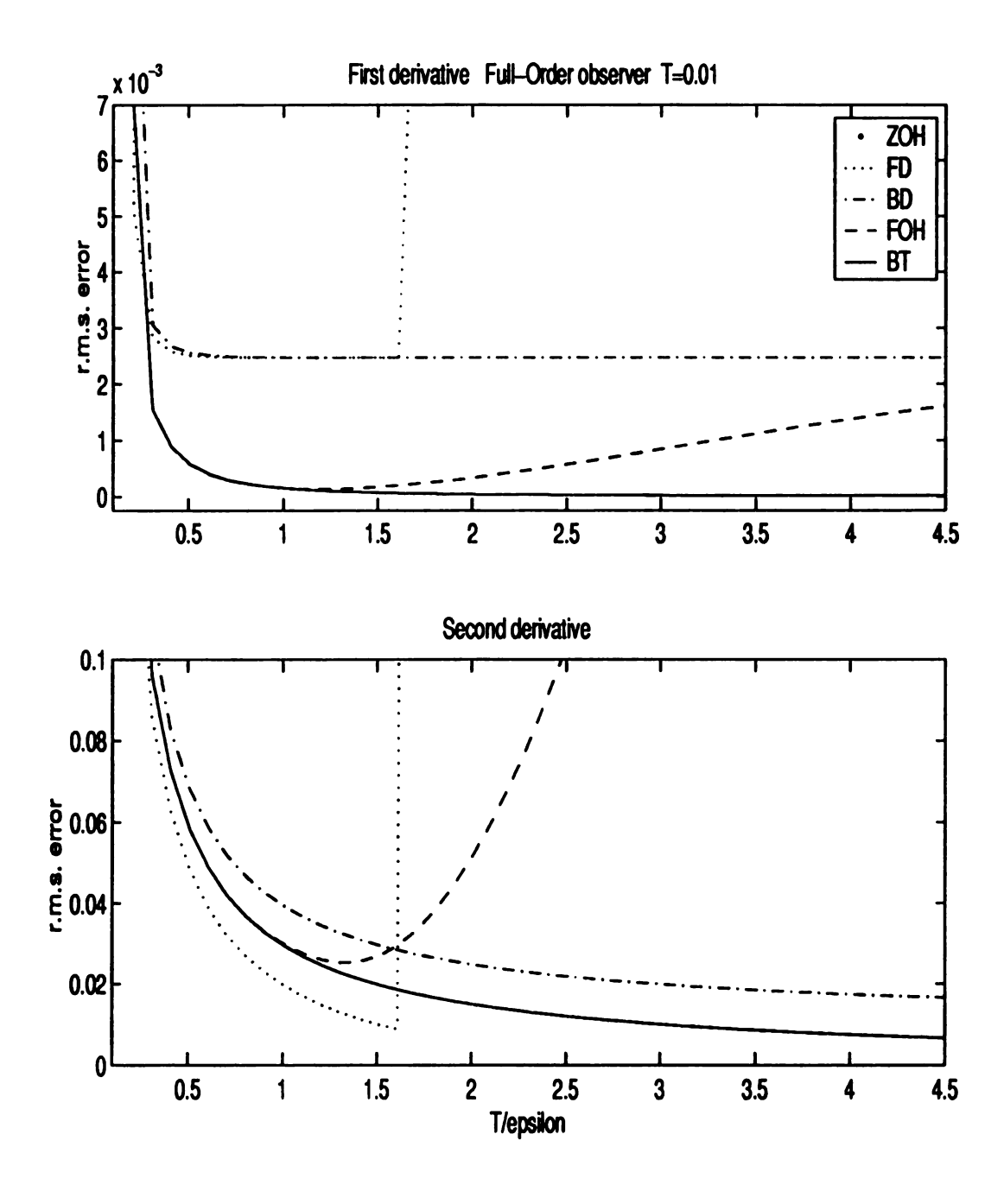


Figure 2.16. The maximum steady state absolute error in estimating  $\dot{y}$  and  $\ddot{y}$  for all five discretization methods for the full-order observer; T = 0.01

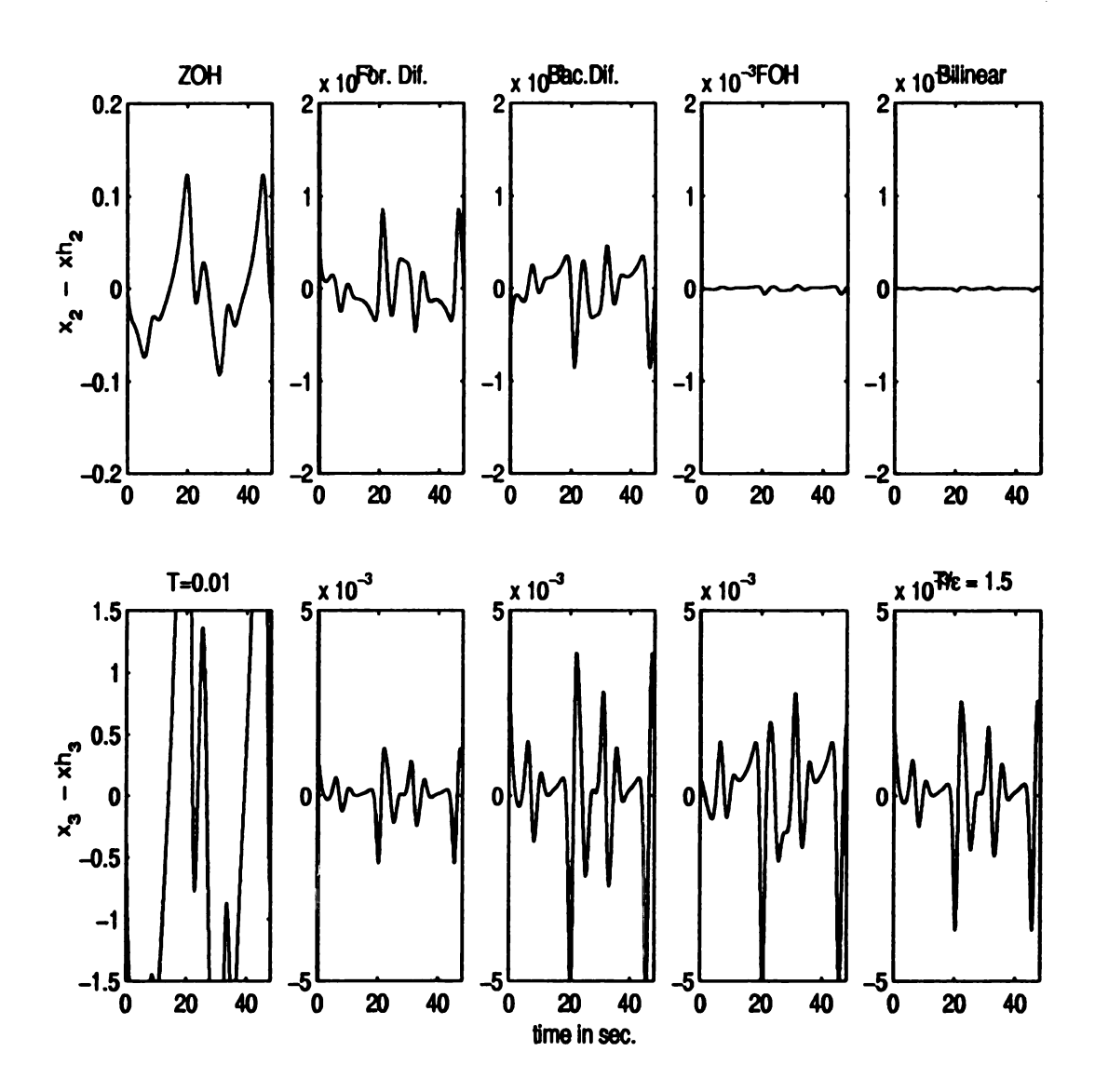


Figure 2.17. The error in  $\dot{y}$  and  $\ddot{y}$  for all five methods; T=0.01 and  $\epsilon=0.00667$ 

Fi ex

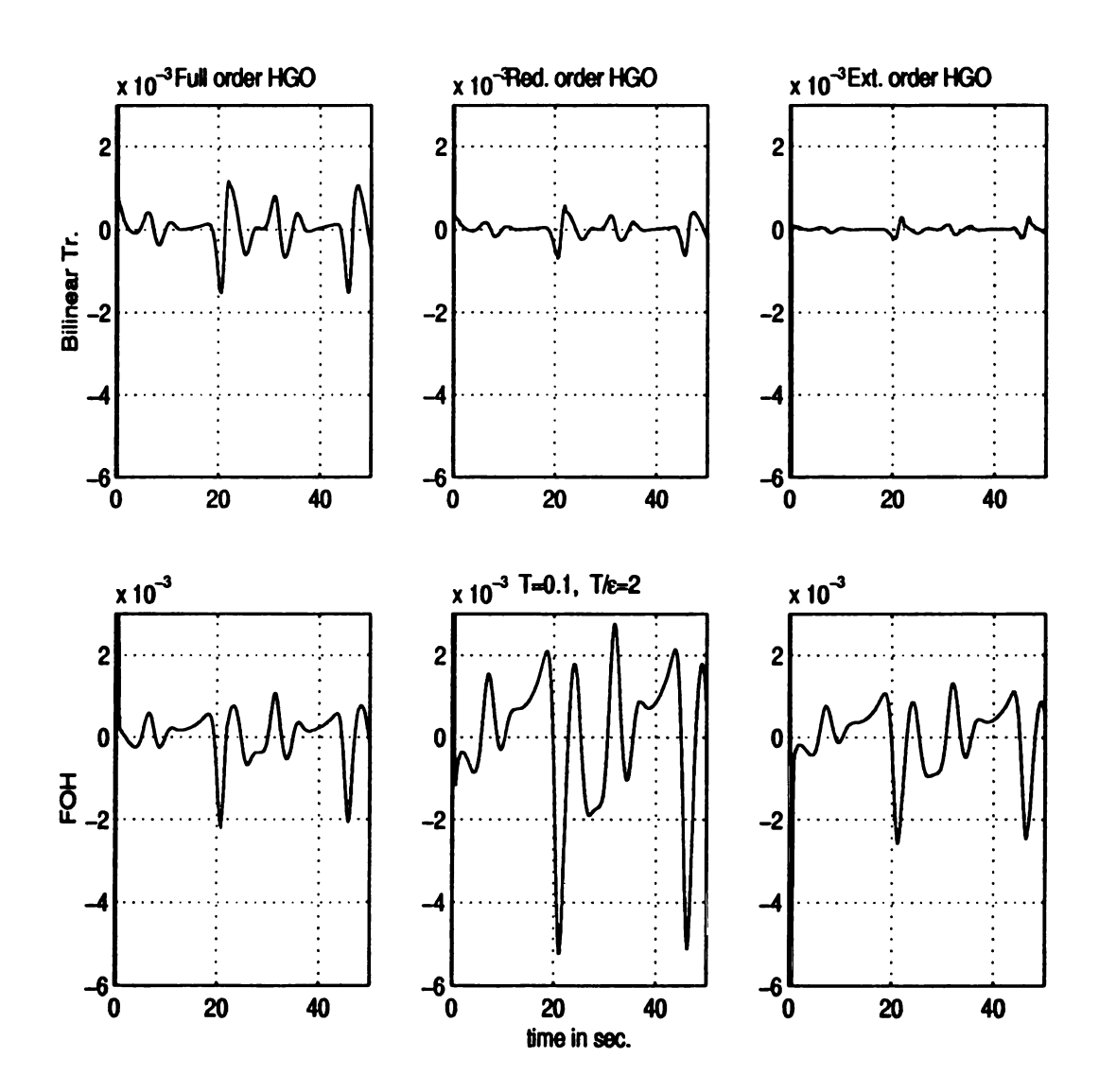


Figure 2.18. Error in  $\ddot{y}$  for the bilinear and FOH methods for the full, reduced, and extended observers.

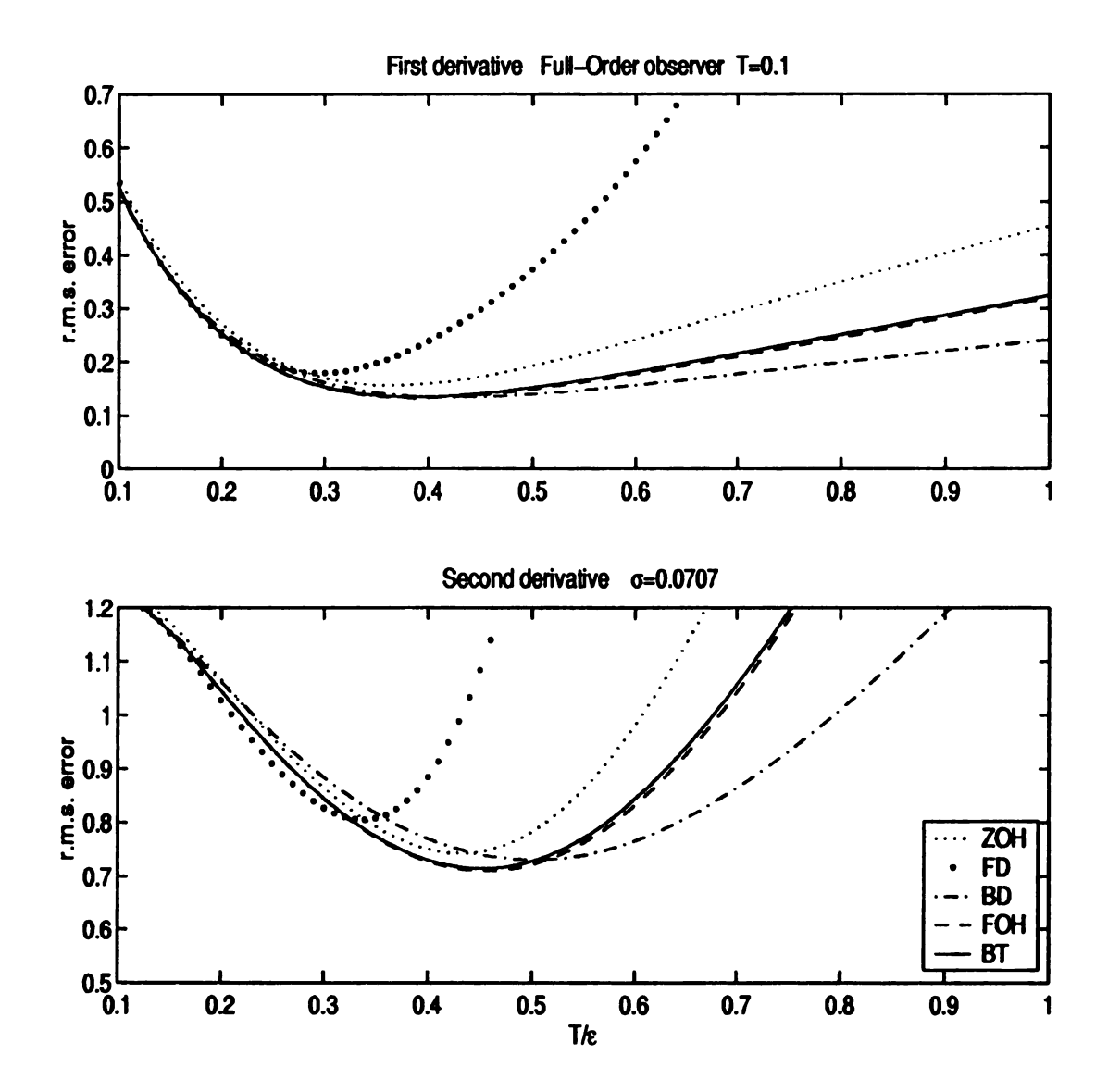


Figure 2.19. The maximum steady state absolute error in estimating  $\dot{y}$  and  $\ddot{y}$  for all five discretization methods for the full-order observer in the presence of noise; T = 0.01 and  $\sigma = 0.0316$ 

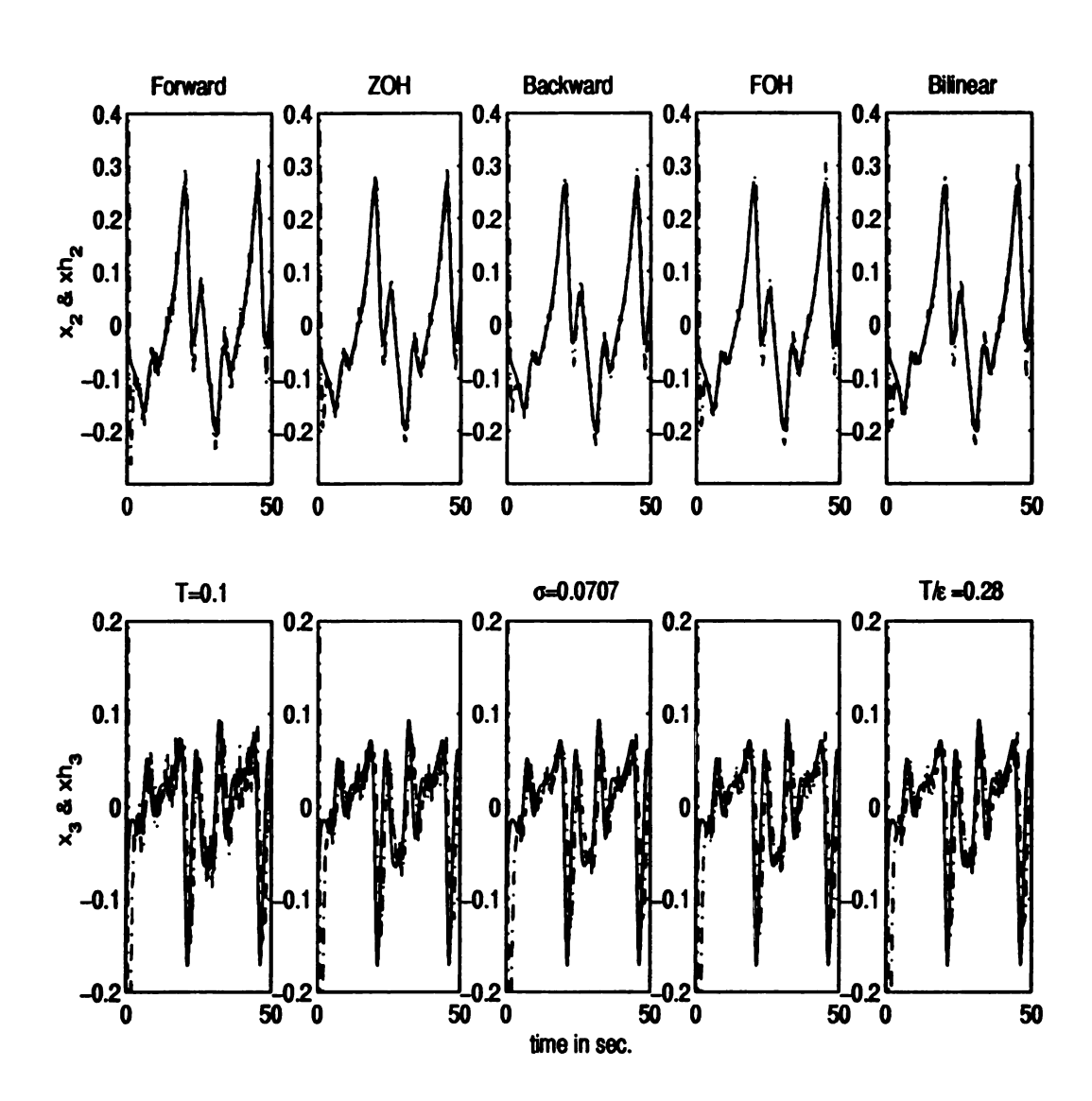


Figure 2.20. Calculating  $\dot{y}$  and  $\ddot{y}$  in the presence of noise;  $T=0.1,\,T/\epsilon=0.28,$  and  $\sigma=0.0707$ 

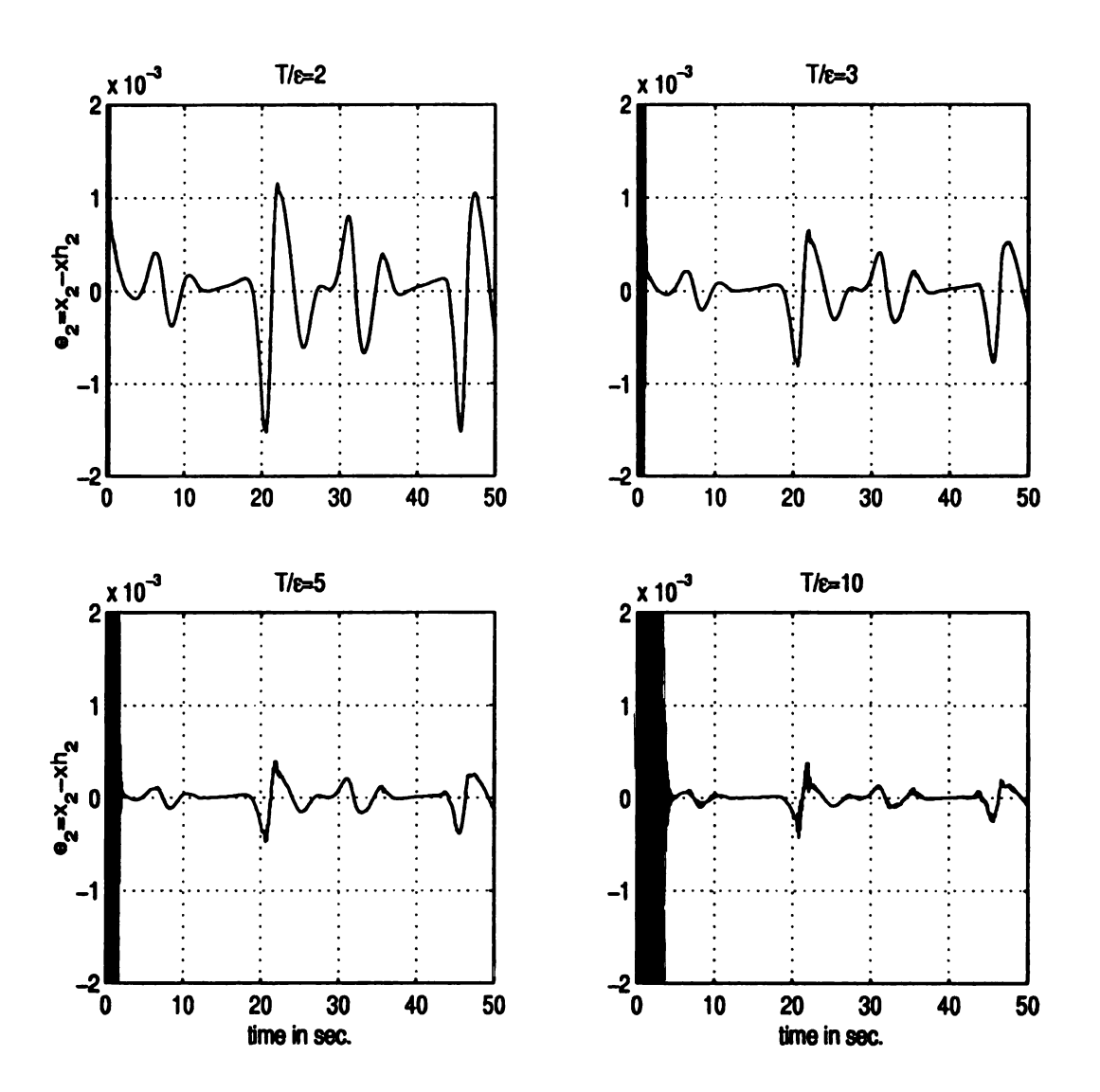


Figure 2.21. Effect of the ratio of  $\frac{T}{\epsilon}$  on the full-order high-gain observer with real poles at  $s=-1/\epsilon$  and T=0.1

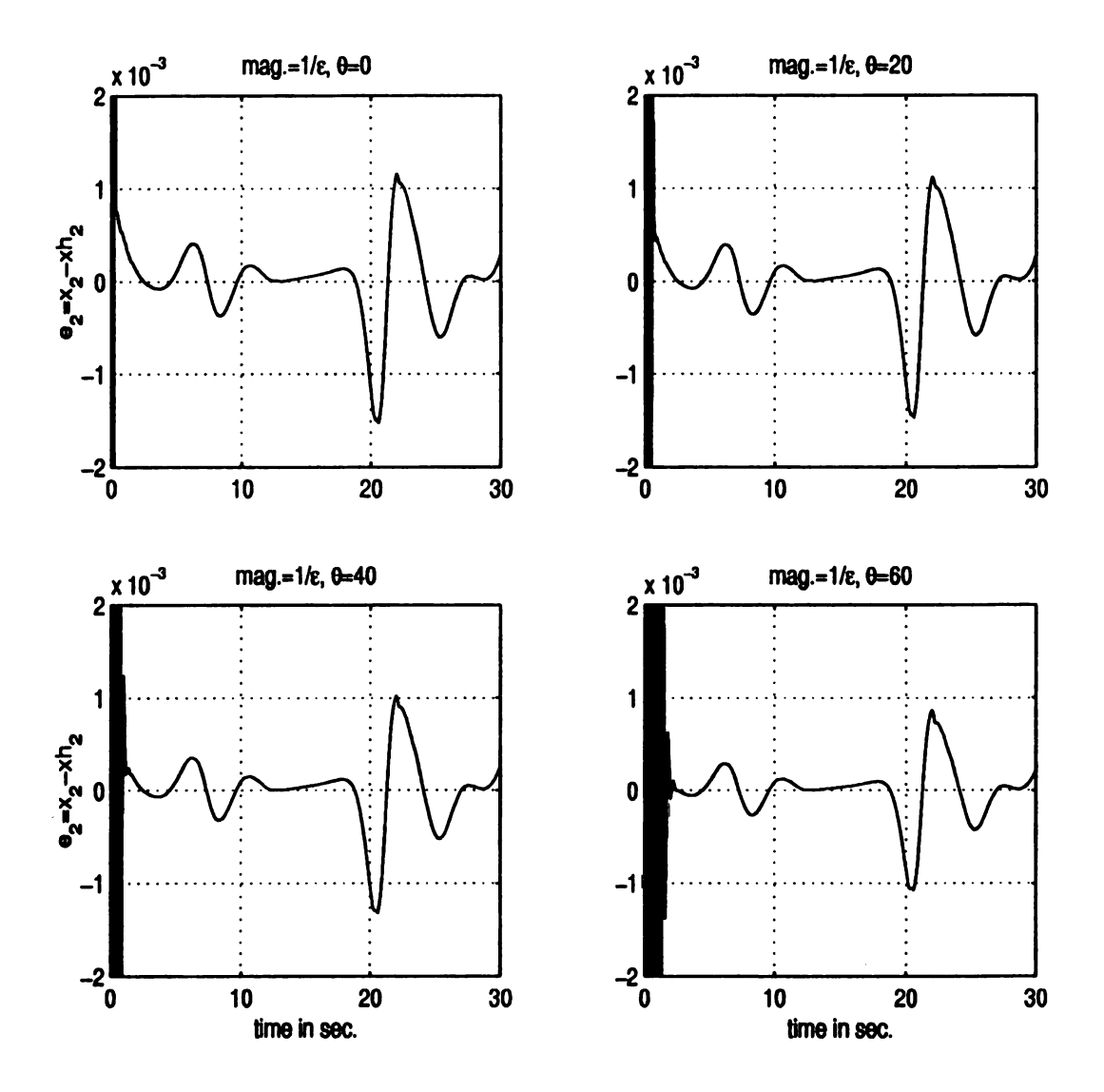


Figure 2.22. The transient response for different choices of poles: real and complex, T=0.1

$$\dot{x}_3 = -x_1 - 3x_3 - x_2^3$$

$$y = x_1$$

We use discrete-time high-gain observers to estimate  $x_2$  and  $x_3$  from the measured output  $x_1$ . The exact states of the system are shown as in Figure 2.23. Using three different high-gain observers, described in section 2.2, we compare the different discretization methods. Figure 2.24 to 2.30 show the same trends which were observed from Figures 2.2 to 2.8, respectively.

# 2.7 Conclusions

We studied discrete-time implementation of high-gain observers and their use as numerical differentiators. The study covered noise-free as well as noisy measurements. The noise was modeled as white Gaussian noise. After investigating five different discretization methods, we concluded that the bilinear transformation method gives the best performance. This conclusion was also based on numerical testing of several examples. After adopting the bilinear transformation method, we investigated the design of the observer parameters and the choice of the observer order (full, reduced and extended-order observer). We found out that it is preferable to assign the poles as real ones. In noise-free measurements, we found it advantageous to take  $T/\epsilon=2$  for two reasons: first, it gives an FIR filter when all observer poles are located at  $-1/\epsilon$ ; second, it produces the shortest transient period. Furthermore, using the extendedorder observer gives less error than the other observers. In noisy measurements, we found out that the ratio  $T/\epsilon$  should be reduced, depending on the noise level. This reduction of  $T/\epsilon$  allows the high-gain observer to play a dual role. On one hand, it acts as a numerical differentiator, and on the other hand, it acts as a low pass filter that filters out high-frequency noise. In this case the observer which gives the

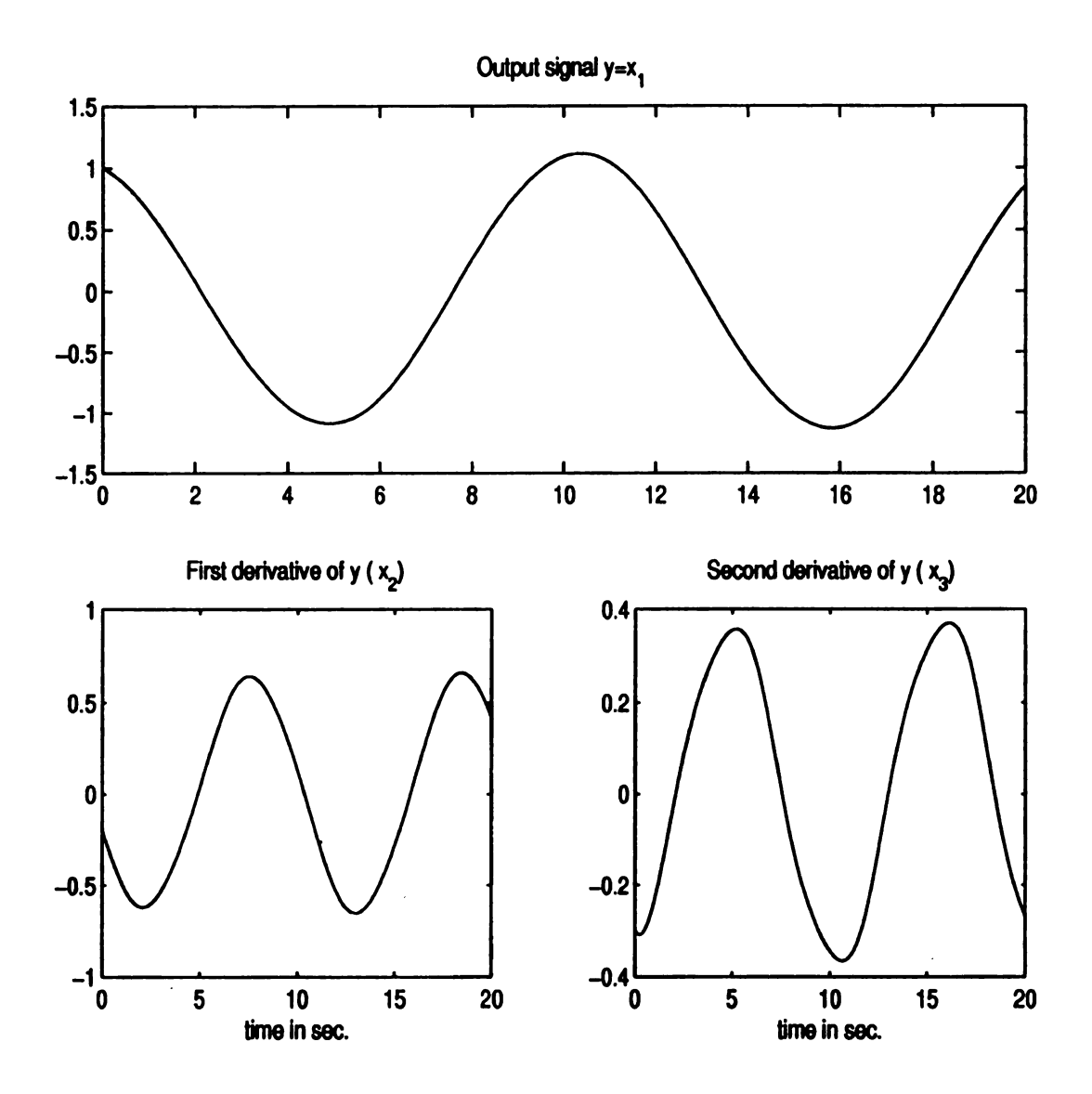


Figure 2.23. The output signal and its first and second derivatives.

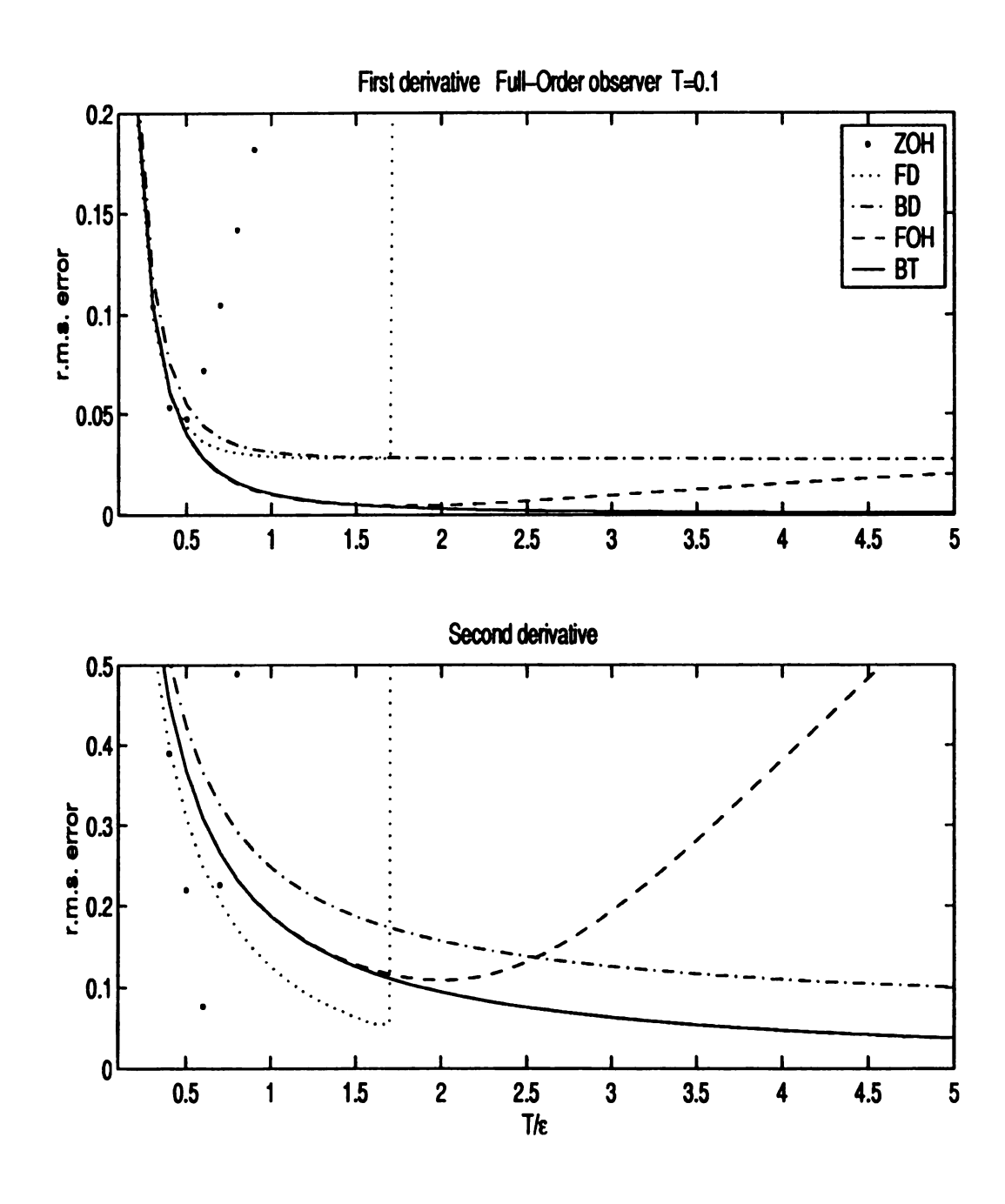


Figure 2.24. The maximum steady state absolute error in estimating  $\dot{y}$  and  $\ddot{y}$  for all five discretization methods for the full-order observer; T=0.1

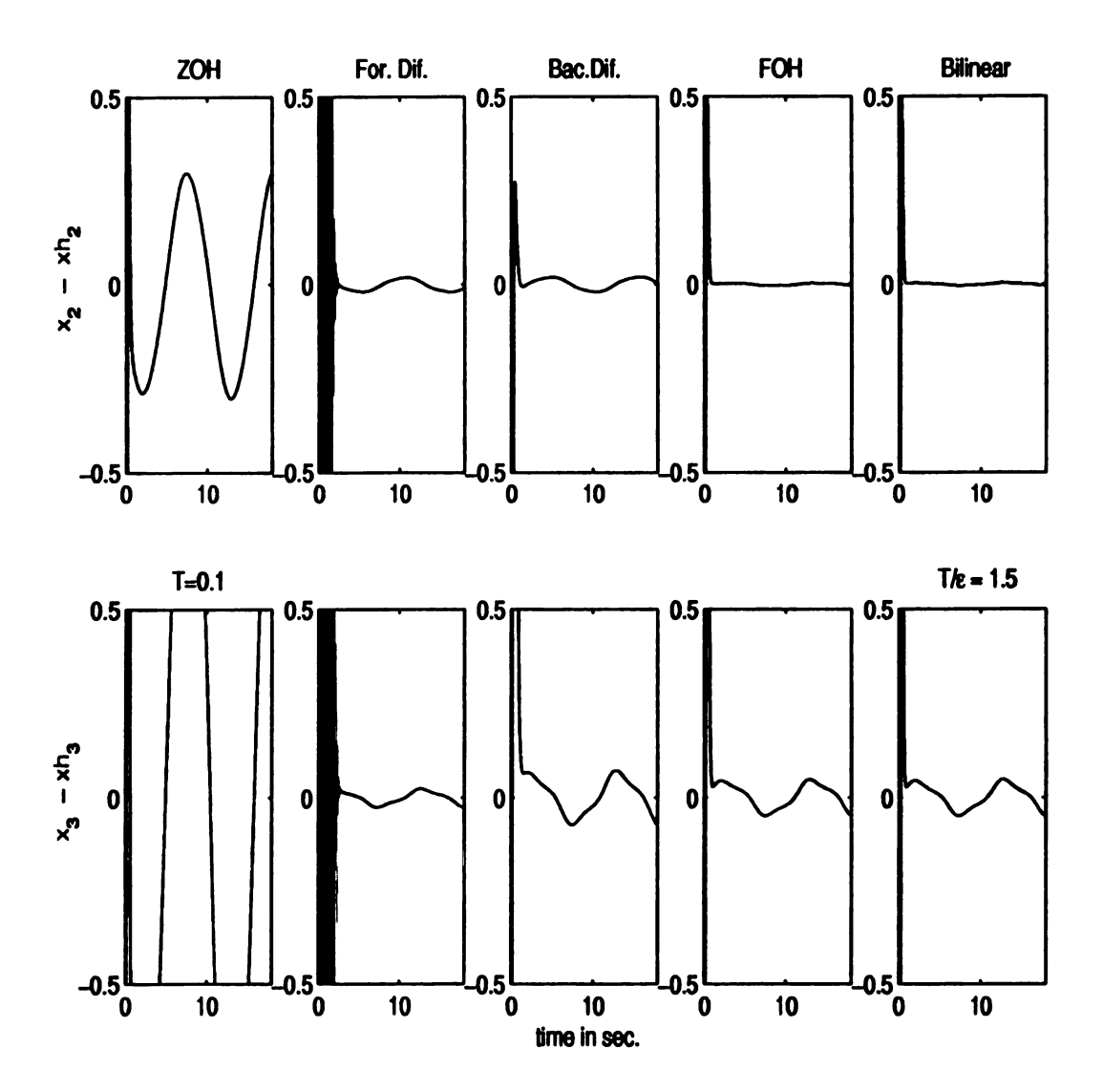


Figure 2.25. The error in  $\dot{y}$  and  $\ddot{y}$  for all five methods;T=0.1 and  $\epsilon=0.0667$ 

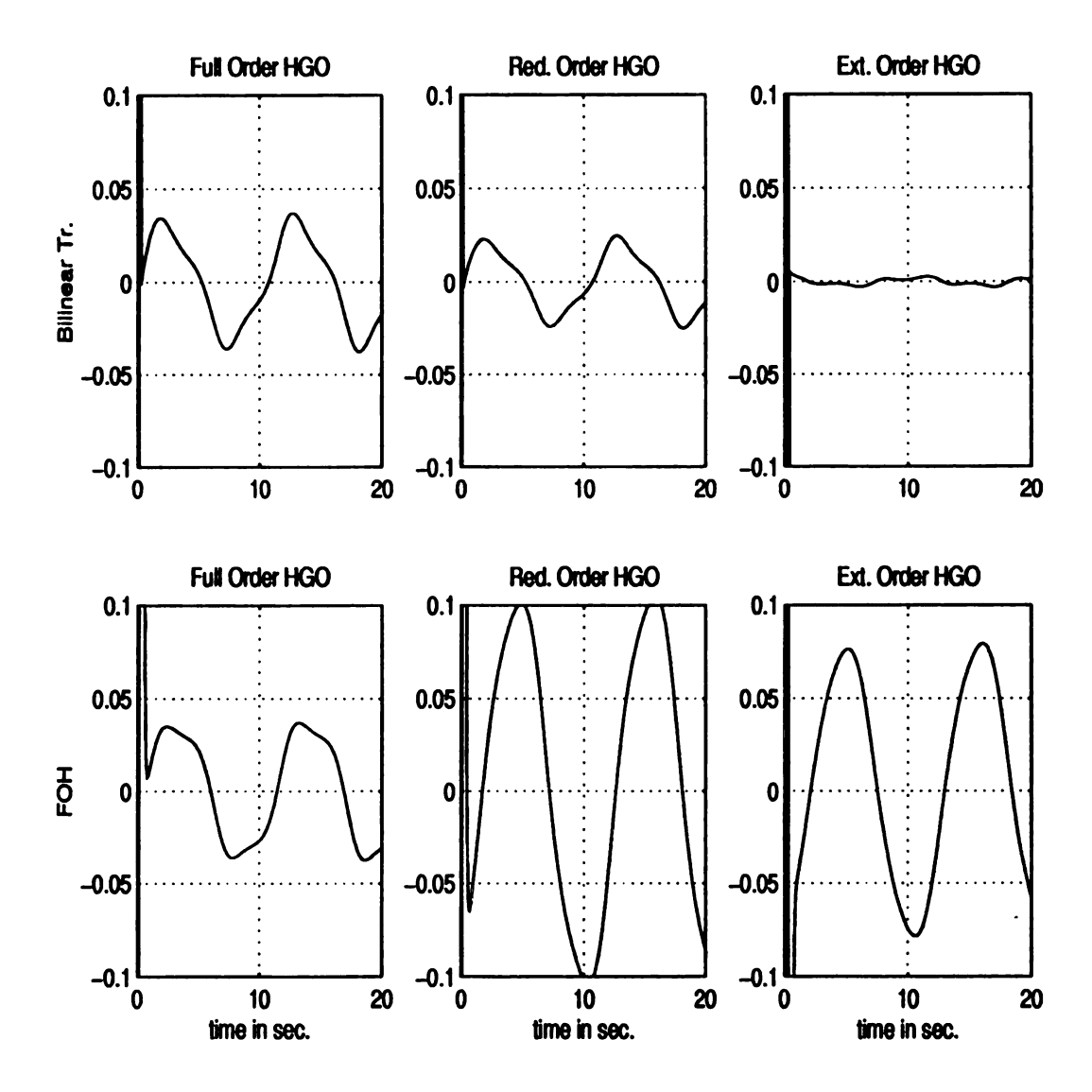


Figure 2.26. Error in  $\ddot{y}$  for the bilinear and FOH methods for the full, reduced, and extended observers.

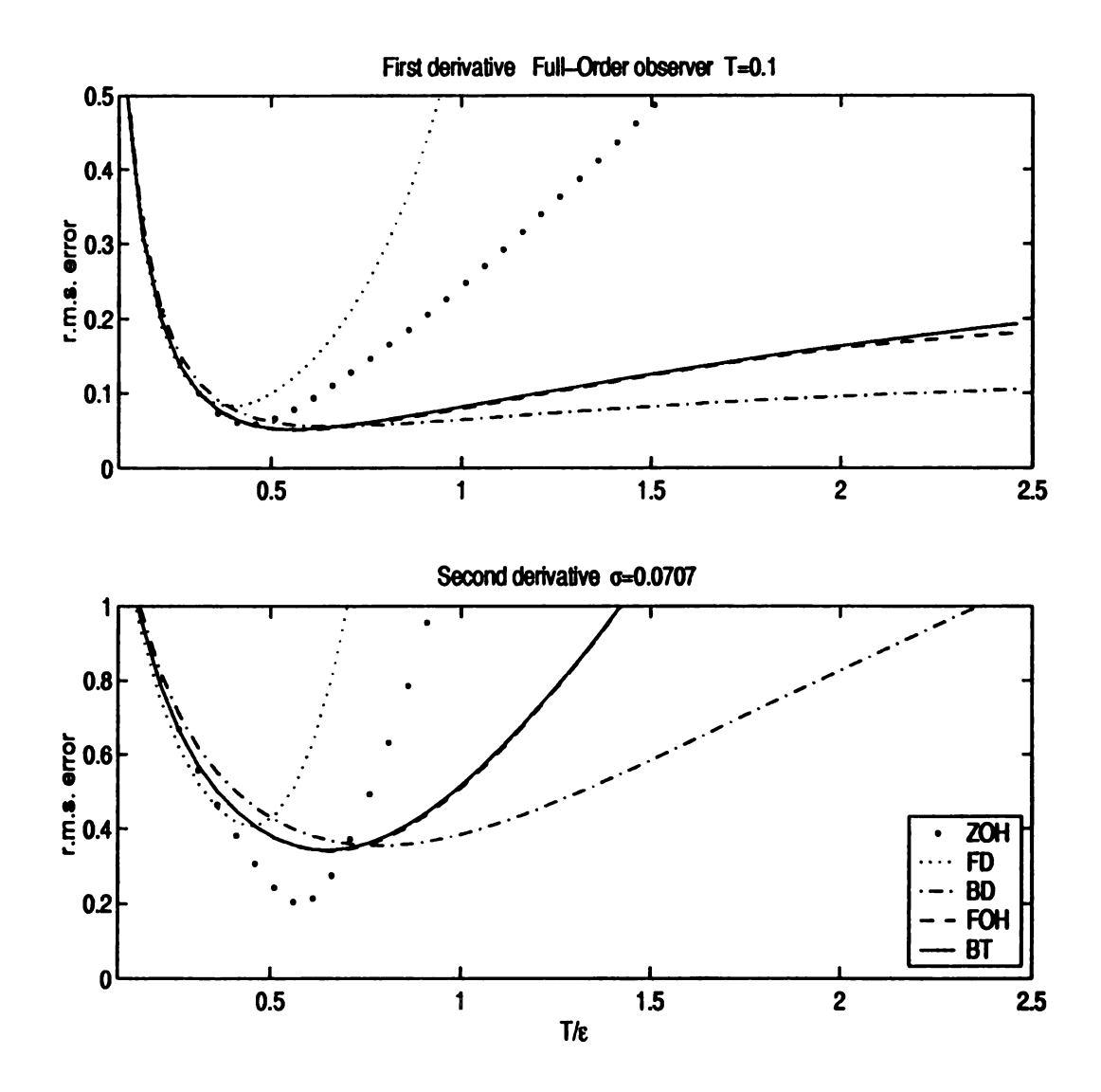


Figure 2.27. The maximum steady state absolute error in estimating  $\dot{y}$  and  $\ddot{y}$  for all five discretization methods for the full-order observer in the presence of noise; T=0.1 and  $\sigma=0.0707$ 

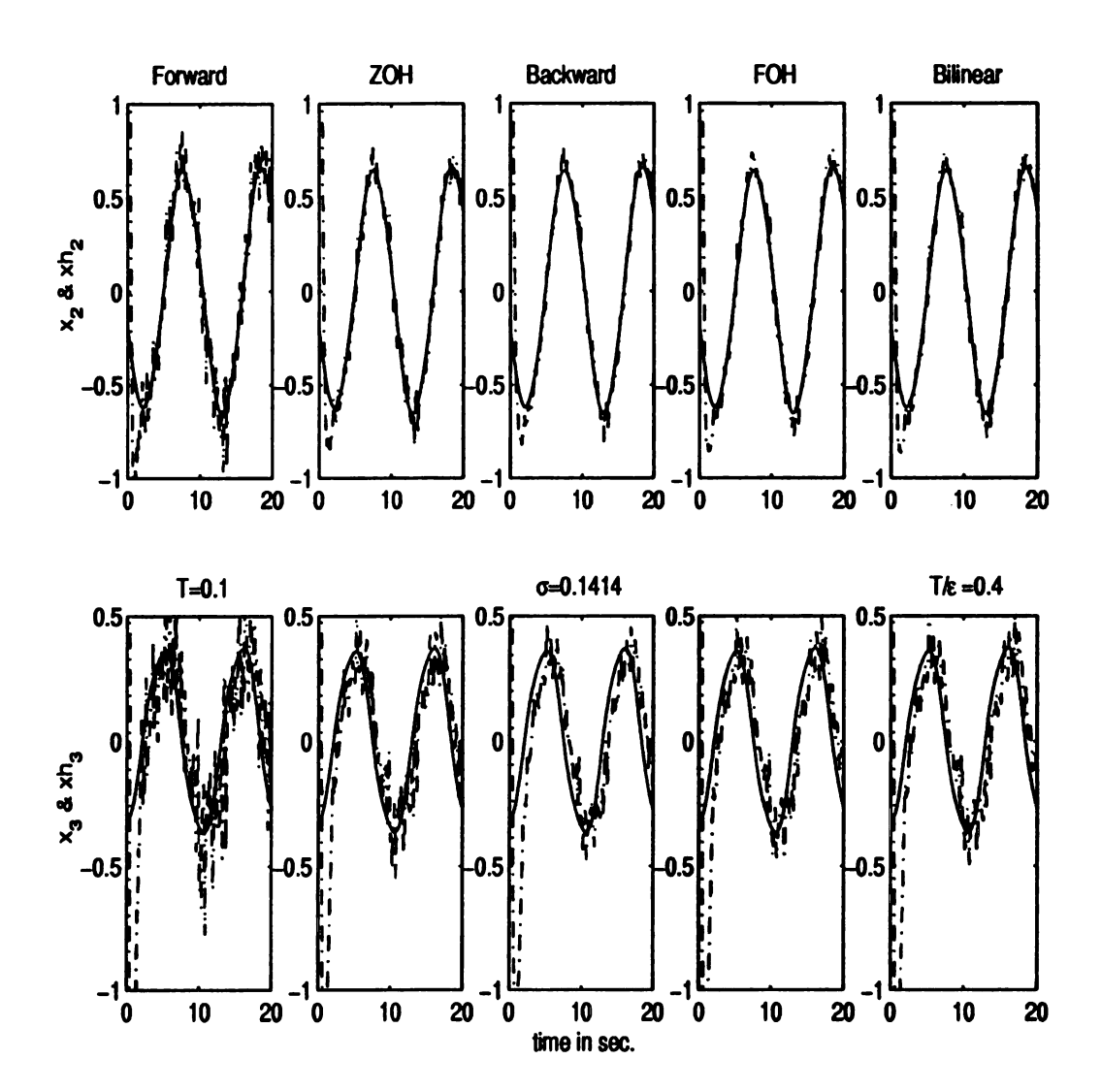


Figure 2.28. Calculating  $\dot{y}$  and  $\ddot{y}$  in the presence of noise;  $T=0.01,\,T/\epsilon=0.4,$  and  $\sigma=0.1414$ 

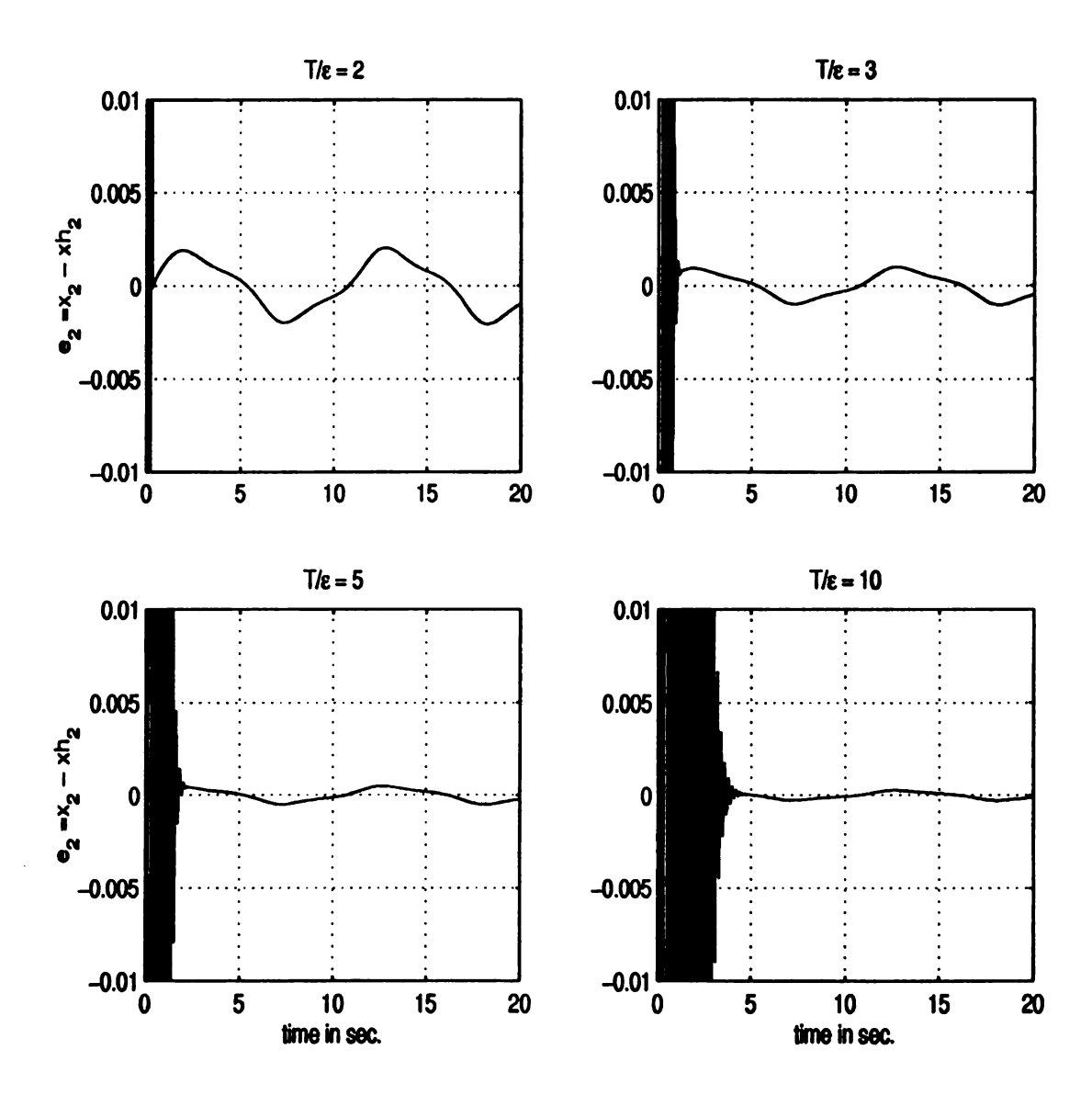


Figure 2.29. Effect of the ratio of  $\frac{T}{\epsilon}$  on the full-order high-gain observer with real poles at  $s=-1/\epsilon$  and T=0.1

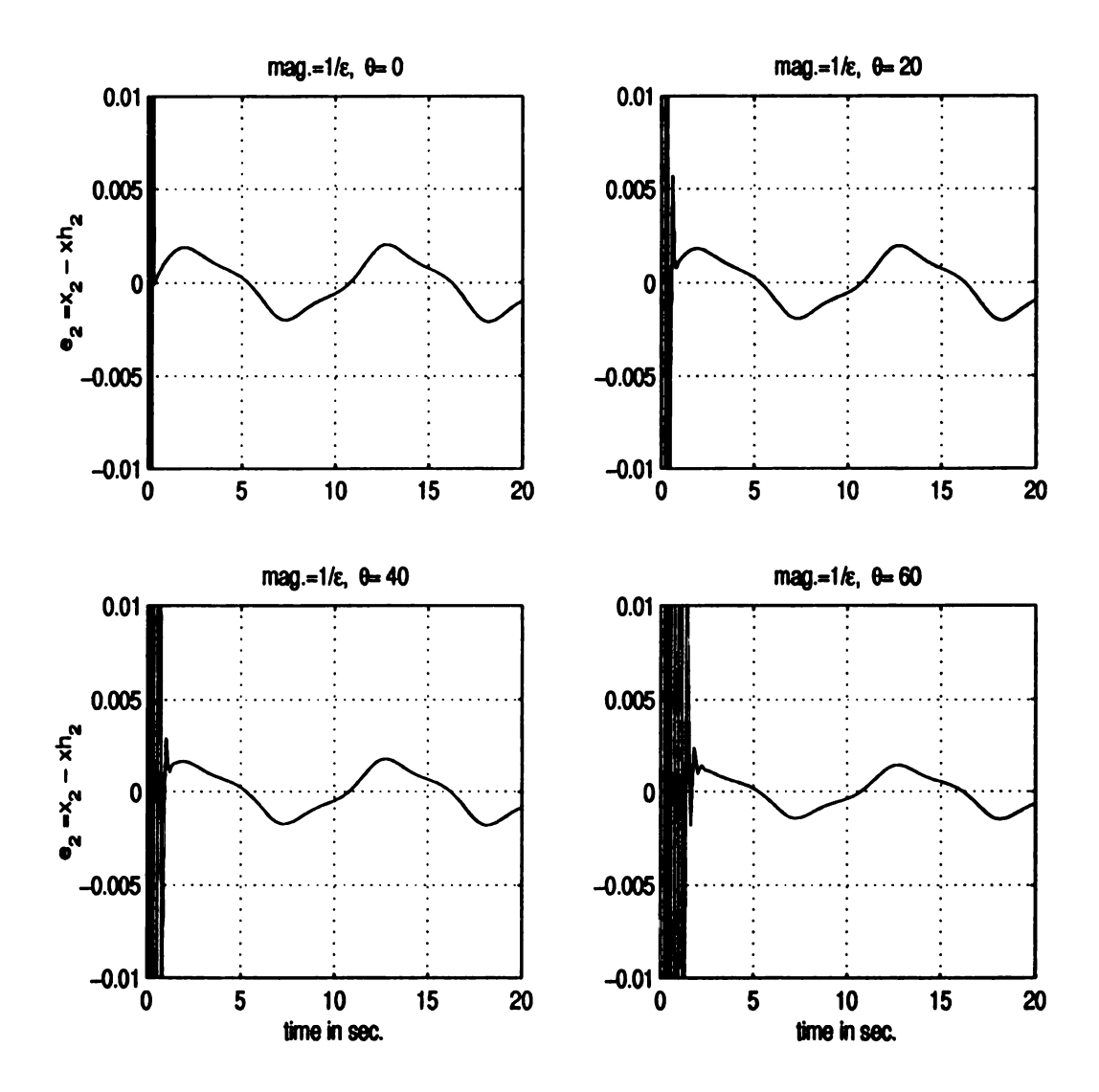


Figure 2.30. The transient response for different choices of poles: real and complex, T=0.1

least error is the full-order observer because it has smaller bandwidth compared with other observers.

Comparison of the bilinear high-gain observer with several numerical differentiators from the literature showed two interesting findings. First, most of those differentiators are special cases of the bilinear reduced-order high-gain observer for certain choices of the observer parameters. We found out also that by exploiting the freedom to choose these parameters, the bilinear high-gain observer outperforms those numerical differentiators, especially when measurement noise is taken into consideration. Second, the bilinear high-gain observer gives results comparable to a causal spline interpolant method, especially in the presence of noise. The high-gain observer uses less computation time and memory requirements than the spline method. Finally, we proposed a novel idea of using the spline interpolant method to initialize the high-gain observer, which significantly improves the observer's transient behavior.

# CHAPTER 3

# Output Feedback Sampled-Data Control of Nonlinear Systems Using High-Gain Observers

## 3.1 Introduction

In Chapter 2, we studied different discretization methods of the high-gain observer as a numerical differentiator. That study was based on simulation. In this chapter, we study the performance of a closed-loop nonlinear system under a sampled-data, high-gain, observed-based controller.

Sampled-data control of nonlinear systems was investigated by several researchers. A topic of particular interest is how certain continuous-time properties are affected by sampling [51]. Considerable work was done by Sontag in [56] to study the preservation of controllability and observability under sampling. Monaco and Normand-Cyrot [44, 46] gave an explicit power series representation of sampled systems in terms of the vector fields of the original continuous-time-data system. Grizzle at el. in [12, 55, 47] showed that certain properties, like observer error linearizability, are not inherited from continuous-time systems.

The Chapter is organized as follows: Section 3.2 describes the continuous-time design. Section 3.3 describes the sampled-data system, where we discuss the discretization of the high-gain observer, the discrete-time closed-loop model, and the development of the discrete-time singularly perturbed form. Section 3.4 shows performance recovery by the output feedback sampled-data controller. Section 3.5 shows example of recovery of the region of attraction. Finally, the conclusions are given in Section 3.6.

# 3.2 Continuous-time Design

## 3.2.1 The Class of Nonlinear Systems

We consider a single-input-single-output nonlinear system represented by

$$\dot{x} = A_c x + B_c \phi(x, z, u) \stackrel{\Delta}{=} f(x, z, u)$$
 (3.1)

$$\dot{z} = \psi(x, z, u) \tag{3.2}$$

$$y = C_c x \tag{3.3}$$

$$\zeta = \Theta(x,z) \tag{3.4}$$

where  $u \in \mathcal{U} \subseteq R^m$  is the control input,  $y \in \mathcal{Y} \subseteq R^p$  and  $\zeta \in R^s$  are measured outputs, and  $x \in \mathcal{X} \subseteq R^r$  and  $z \in \mathcal{Z} \subseteq R^l$  constitute the state vector. The  $r \times r$  matrix  $A_c$ , the  $r \times 1$  matrix  $B_c$ , and  $1 \times r$  matrix  $C_c$ , given by

$$C_c = \begin{bmatrix} 1 & 0 & \dots & 0 \end{bmatrix}$$

represent a chain of r integrators.

**Assumption 3.1** The functions  $\phi : \mathcal{X} \times \mathcal{Z} \times \mathcal{U} \to R$  and  $\psi : \mathcal{X} \times \mathcal{Z} \times \mathcal{U} \to R^l$  are locally Lipschitz in their arguments over the domain of interest. In addition,  $\phi(0,0,0) = 0$ ,  $\psi(0,0,0) = 0$  and  $\Theta(0,0) = 0$ .

### 3.2.2 Partial State Feedback Control

The task of feedback control is to stabilize the origin of the closed loop system using only the measured outputs y and  $\zeta$ . We follow a two-step approach to this problem. First, we design a partial state feedback control that uses measurements of x and  $\zeta$ . Then we use a high-gain observer to estimate x from y. The state feedback control takes the form

$$u = \gamma(x, \zeta) \tag{3.5}$$

We allow any state feedback design that holds the following four properties.

#### Assumption 3.2

- 1.  $\gamma(0,0)=0$ ;
- 2.  $\gamma$  is a locally Lipschitz function in its argument over the domain of interest;
- 3.  $\gamma$  is a globally bounded function of x;
- 4. The origin (x = 0, z = 0) is an asymptotically stable equilibrium point of the closed-loop system.

For some of our results, the forth property will be strengthened to exponential stability. The global boundedness requirement is typically achieved by saturation of  $\gamma(\cdot)$ , or its x-input, outside a compact region of interest. The boundedness of  $\gamma(\cdot)$  may also follow from design constrains.

## 3.2.3 High-Gain Observer (HGO)

To implement the control (3.5) using output feedback, we design the high-gain observer

$$\dot{\hat{x}} = A_c \hat{x} + B_c \phi_o(\hat{x}, \zeta, u) + H(y - C_c \hat{x}) \tag{3.6}$$

where  $\phi_o(\hat{x}, \zeta, u)$  is a nominal model of the nonlinear function  $\phi(x, z, u)$ . If  $\phi$  is a known function of x,  $\zeta$  and u, we can take  $\phi_o = \phi$ . On the other hand, if such nominal model is not available, we can take  $\phi_o = 0$ , which results in a linear observer. The function  $\phi_o$  is required to satisfy the following assumption.

Assumption 3.3  $\phi_o(x,\zeta,\gamma(x,\zeta))$  is locally Lipschitz in its argument over the domain of interest and globally bounded in x. Moreover,  $\phi_o(0,0,0) = 0$ .

The output feedback controller is taken as

$$u=\gamma(\hat{x},\zeta)$$

The estimation error  $e = x - \hat{x}$  satisfies the equation

$$\dot{e} = (A_c - HC_c)e + B_c\Delta(x, z, e, t)$$

where

$$\Delta(\cdot) = [\phi(x,z,u) - \phi_o(\hat{x},\zeta,u)]$$

It is shown in [54, 16] that the output feedback controller recovers the performance achieved under state feedback if the observer gain H is chosen as

$$H^T = \left[\begin{array}{cccc} \underline{\alpha_1} & \underline{\alpha_2} & \dots & \underline{\alpha_r} \\ \frac{\alpha_r}{\epsilon} & \frac{\alpha_r}{\epsilon^2} & \dots & \dots & \frac{\alpha_r}{\epsilon^r} \end{array}\right]$$

where  $\epsilon$  is a small positive parameter and the positive constants  $\alpha_i$  are chosen such that the roots of

$$s^{r} + \alpha_{1}s^{r-1} + \dots + \alpha_{r-1}s + \alpha_{r} = 0$$
 (3.7)

have negative real parts. This choice of H assigns the eigenvalues of  $(A_c - HC_c)$  at  $1/\epsilon$  times the roots of (3.7). Using singular perturbation analysis, it is shown in [16] that the estimation error decays to  $O(\epsilon)$  values after a short transient period of the form  $[0, T_1(\epsilon)]$  where  $T_1(\epsilon)$  tends to zero as  $\epsilon$  tends to zero. During this transient period, the estimate  $\hat{x}$  may exhibit peaking behavior where the transient response takes the impulsive-like form  $(a/\epsilon^{\delta})e^{-\alpha t/\epsilon}$  for some positive constants  $\delta$  and  $\alpha$ . It is shown in [16] that this peaking phenomenon can be overcome by saturating the control or the state estimates outside a compact region of interest.

# 3.3 Sampled-Data Control

In sampled-data control, the output variables y and  $\zeta$  are sampled and the control input u is applied at the sampling points. Let T denote the sampling period. We assume that the control is implemented through a zero-order hold. Hence, u is constant over the sampling period. The continuous-time observer is discretized and implemented in discrete-time as a difference equation. Since the observer dynamics, parameterized by  $\epsilon$ , are fast for small  $\epsilon$ , we choose  $T = \alpha \epsilon$  for some  $\alpha > 0$ . For convenience we denote the signals at the kth sampling point by x(k),  $\hat{x}(k)$ , u(k), etc. The control is implemented by

$$u(k) = \gamma(\hat{x}(k), \zeta(k))$$

## 3.3.1 Discretization of the HGO

In this section, we investigate discrete-time implementation of the observer (3.6). We start by scaling the observer variables to avoid inherent ill-conditioning of the realization (3.6) when  $\epsilon$  is very small. Let

$$q_i = \epsilon^{i-1} \hat{x}_i, \quad i = 1, \ldots, r$$

to obtain

$$\dot{q} = D(A_c - HC_c)D^{-1}q + DHy + DB_c\phi_o(D^{-1}q, \zeta, u)$$
 (3.8)

$$\hat{x} = D^{-1}(\epsilon)q \tag{3.9}$$

where

$$D(\epsilon) = \text{diag} [1, \epsilon, \ldots, \epsilon^{r-1}]$$

The characteristic equation of  $\epsilon D(A_c - HC_c)D^{-1}$  is (3.7); hence it is Hurwitz. The scaled observer is

$$\dot{q} = \frac{1}{\epsilon} [A_o q + B_o y + \epsilon^r B_c \phi_o(D^{-1} q, \zeta, u)] \tag{3.10}$$

where  $A_o = \epsilon D(A_c - HC_c)D^{-1}$ ,  $B_o = \epsilon DH$ , and  $DB_c = \epsilon^{r-1}B_c$ . Equation (3.10) is a standard singularly perturbed system whose coefficients are of order  $O(1/\epsilon)$  irrespective of the order of the system. Note that in equation (3.6) some right-hand side coefficients are of order  $O(1/\epsilon^{r-1})$ . The solution of (3.8) does not exhibit peaking for small  $\epsilon$ , which makes it easier to discretize the equation. The effect of peaking is now contained in the output equation (3.9), and can be overcome by saturating the estimates  $\hat{x}$  outside a compact region of interest.

Depending on whether or not the nominal function  $\phi_o$  is zero, the HGO (3.8) can be linear or nonlinear. Linear observers can be discretized using different methods.

	Forward Diff.	Backward Diff.	Bilinear Transformation
A <sub>do</sub>	$(I + \frac{T}{\epsilon}A_o)$	$(I - \frac{T}{\epsilon}A_o)^{-1} \stackrel{def}{=} M_1$	$(I + \frac{T}{2\epsilon}A_o)(I - \frac{T}{2\epsilon}A_o)^{-1} \stackrel{\text{def}}{=} N_2M_2$
$B_{do}$	$rac{T}{\epsilon}B_o$	$rac{T}{\epsilon}M_1B_o$	$rac{T}{\epsilon}M_2B_o$
Cdo	$C_o = D^{-1}$	$D^{-1}M_1$	$D^{-1}M_2$
$D_{do}$	0	$rac{T}{\epsilon}C_{oldsymbol{do}}B_{oldsymbol{o}}$	$rac{T}{2\epsilon}C_{f do}B_{m o}$

Table 3.1. Coefficient of the discrete time implementation of the linear HGO.

We consider three methods: Forward Difference, Backward Difference and Bilinear Transformation. For the nonlinear case, we use the Forward Difference method.

Linear HGO The linear high-gain observer is a special case of the general form (3.8) when  $\phi_o(\cdot) = 0$ . It is implemented in discrete-time by

$$q(k+1) = A_{do}q(k) + B_{do}y(k)$$

$$\hat{x}(k) = C_{do}q(k) + D_{do}y(k)$$

where  $A_{do}$ ,  $B_{do}$ ,  $C_{do}$  and  $D_{do}$  depend on the discretization methods, as shown in Table 3.1.

Nonlinear HGO When  $\phi_o \neq 0$ , the observer (3.8) is nonlinear. We discretize it using the Forward Difference method, to obtain

$$q(k+1) = A_{do}q(k) + B_{do}y(k) + T\epsilon^{r-1}B_c\phi_o(D^{-1}q(k),\zeta(k),u(k))$$

$$\hat{x}(k) = C_{do}q(k)$$

where  $A_{do}$ ,  $B_{do}$ , and  $C_{do}$  are given in the first column of Table 3.1

## 3.3.2 Discrete-Time Closed-Loop Model

To analyze the closed-loop system, we derive a discrete-time model that describes the state variables at the sampling points. We start by discretizeing the plant dynamics. A key step in deriving our closed-loop model is the representation of the system in a singularly perturbed form that reflects the fact that the observer dynamics are faster than the plant dynamics. As in continuous-time analysis [8], arriving at the desired singularly perturbed form requires replacing the observer states by scaled estimation errors. Unlike the continuous-time case, however, this change of variable by itself may not be sufficient and we may have to perform additional changes of variables to weaken the slow input into the fast equation. To keep track of this slow input, our discretization of the plant must have  $O(T^{r+1})$  accuracy.

**Assumption 3.4** The nonlinear functions f(x, z, u) and  $\psi(x, z, u)$  are  $C^{r+1}$  in the domain of interest.

#### **Plant Dynamics**

An equidistant grid on the time axis with a fixed step size  $T = t_{k+1} - t_k > 0$  (sampling period) is considered and  $u(t_k) = constant$  over the time interval  $[t_k, t_{k+1})$  (zero-order hold). For convenience, let us rewrite (3.1) and (3.2) as

$$\dot{\chi} = F(\chi, u) \tag{3.11}$$

where

$$\chi = \left[ egin{array}{c} x \\ z \end{array} 
ight], \quad F(\chi,u) = \left[ egin{array}{c} f(x,z,u) \\ \psi(x,z,u) \end{array} 
ight]$$

By expanding the solution of (3.11) in a Taylor series about  $\chi(k)$  and using the fact that u(k) is constant during the sampling interval, the plant dynamics are described

in discrete-time by

$$\chi(k+1) = \chi(k) + \sum_{l=1}^{r} \frac{T^{l}}{l!} F_{l}(\chi(k), u(k)) + T^{r+1} R(\chi(k), u(k), T)$$
 (3.12)

where  $F_l(\chi, u)$ , for  $1 \le l \le r$ , are determined recursively by

$$F_1(\chi, u) = F(\chi, u) \tag{3.13}$$

$$F_{l+1}(\chi, u) = \frac{\partial F_l(\chi, u)}{\partial \chi} F(\chi, u)$$
 (3.14)

and the remainder term  $R(\chi, u, T)$  is bounded on compact sets of  $(\chi, u)$ , uniformly in T for all  $T \leq T^*$  for any given  $T^* > 0$ . Using (3.13)-(3.14), it can be verified that

$$F_{\ell}(\chi, u) = \begin{bmatrix} A_c^{\ell} x + \sum_{i=1}^{\ell} A_c^{\ell-i} B_c h_i(\chi, u) \\ g_{\ell}(\chi, u) \end{bmatrix}$$
(3.15)

where  $h_{\ell}$  and  $g_{\ell}$ , for  $1 \leq \ell \leq r$ , are determined recursively by

$$h_1(\chi, u) = \phi(x, z, u), \qquad h_{\ell}(\chi, u) = \frac{\partial h_{\ell-1}}{\partial \chi}(\chi, u) F(\chi, u)$$
 $g_1(\chi, u) = \psi(x, z, u), \qquad g_{\ell}(\chi, u) = \frac{\partial g_{\ell-1}}{\partial \chi}(\chi, u) F(\chi, u)$ 

Using (3.15) in (3.12), the equation for x can be written as

$$x(k+1) = x(k) + \sum_{\ell=1}^{r} \frac{T^{\ell}}{\ell!} A_{c}^{\ell} x(k) + \sum_{\ell=1}^{r} \frac{T^{\ell}}{\ell!} \sum_{i=1}^{\ell} A_{c}^{\ell-i} B_{c} h_{i}(\chi(k), u(k)) + T^{r+1} R_{x}(\chi(k), u(k), T)$$
(3.16)

where  $R_x(\cdot)$  is formed of the first r components of  $R(\cdot)$ . The double summation term of (3.16) can be written as

$$\sum_{j=1}^{r} \frac{T^j}{j!} A_c^{j-1} B_c G_j$$

where

$$G_j = \sum_{i=1}^{r-j+1} \frac{(j!)T^{i-1}}{(j+i-1)!} h_i$$

Hence, (3.16) can be rewritten as

$$x(k+1) = x(k) + \sum_{\ell=1}^{r-1} \frac{T^{\ell}}{\ell!} A_c^{\ell} x(k) + \sum_{\ell=1}^{r} \frac{T^{\ell}}{\ell!} A_c^{\ell-1} B_c G_{\ell}(\chi(k), u(k)) + T^{r+1} R_x(\chi(k), u(k), T)$$
(3.17)

where we used the fact that  $A_c^r = 0$ . Note that, because of the property  $A_c^r = 0$ , the Taylor series (3.12) is written with only r terms.

#### **Observer Dynamics**

To represent the observer dynamics, we perform the change of variables

$$\eta_i(k) = \frac{1}{\epsilon^{r-i}} \left[ x_i(k) - \hat{x}_i(k) \right] \qquad 1 \leq i \leq r$$

For the linear HGO,  $\eta(k)$  satisfies the equation

$$\eta(k+1) = \frac{1}{\epsilon^{r-1}} D(I - D_{do}C_c)x(k+1) + DC_{do}A_{do}C_{do}^{-1}D^{-1}\eta(k) 
- \frac{1}{\epsilon^{r-1}} DC_{do}[B_{do}C_c + A_{do}C_{do}^{-1}(I - D_{do}C_c)]x(k)$$
(3.18)

Using the values of  $A_{do}$ ,  $B_{do}$ ,  $C_{do}$ , and  $D_{do}$  from Table 3.1, we rewrite (3.18) for each of the three discretization methods.

#### Forward Difference Method:

$$\eta(k+1) = A_{do}\eta(k) + \frac{1}{\epsilon^{r-1}}D[x(k+1) - x(k) - TA_cx(k)]$$
 (3.19)

**Backward Difference Method:** 

$$\eta(k+1) = A_{do}\eta(k) + \frac{1}{\epsilon^{r-1}}A_{do}D[x(k+1) - x(k) - TA_{c}x(k+1)]$$
 (3.20)

**Bilinear Transformation Method:** 

$$\eta(k+1) = \bar{A}_{do}\eta(k) + \frac{1}{\epsilon^{r-1}}M_2D\{[x(k+1) - x(k)] - \frac{T}{2}A_c[x(k+1) + x(k)]\} \quad (3.21)$$

where  $\bar{A}_{do} = M_2 A_{do} M_2^{-1}$ .

For the nonlinear HGO,  $\eta(k)$  satisfies the equation

$$\eta(k+1) = A_{do}\eta(k) + \frac{1}{\epsilon^{r-1}}D[x(k+1) - x(k) - TA_cx(k)] 
-TB_c\phi_o(x(k) - N\eta(k), \zeta(k), u(k))$$
(3.22)

where  $N = \epsilon^{r-1}D^{-1}$ ;  $N(\epsilon)$  is an analytic function of  $\epsilon$ . The estimate  $\hat{x}(k)$  is given by

$$\hat{x}_i(k) = x_i(k) - \epsilon^{r-i} \eta_i(k), \quad 1 \le i \le r$$

## 3.3.3 The Discrete-time Singularly Perturbed Form

The closed-loop sampled-data system can be represented at the sampling points by a discrete-time model in the singularly perturbed form:

$$\chi(k+1) = \chi(k) + \epsilon \Psi(\chi(k), u(k), \epsilon)$$
 (3.23)

$$\xi(k+1) = A_f \xi(k) + \epsilon \Gamma(\chi(k), u(k), \hat{x}(k), \epsilon)$$
 (3.24)

$$u(k) = \gamma(\hat{x}(k), \zeta(k)) \tag{3.25}$$

$$\hat{x}(k) = x(k) - N(\epsilon)\xi(k) + \epsilon \mathcal{W}(x(k), \xi(k), \epsilon)$$
 (3.26)

where  $W(x(k), \xi(k), \epsilon)$  is a continuous function of  $\epsilon$  at  $\epsilon = 0$ , and  $A_f$  is independent of  $\epsilon$  and its eigenvalues satisfy  $|\lambda| < 1$ . The fast variable  $\xi$  replaces  $\eta$  through a change of variables. To illustrate the idea of arriving at (3.23) and (3.24), let us note that substitution of x(k+1) using (3.17) in (3.19), (3.20), (3.21), or (3.22) yields an equation of the form

$$\eta(k+1) = A_f \eta(k) + \epsilon h(\chi(k), u(k), \epsilon) - \epsilon \alpha B_c \phi_o(\hat{x}(k), \zeta(k), u(k)) 
+ \sum_{j=2}^{r-1} \frac{1}{\epsilon^{r-1-j}} H_j D A_c^j x(k)$$
(3.27)

where the function  $h(\cdot)$  and the matrix  $A_f$  depend on the observer equation; that is, equations (3.19), (3.20), (3.21), or (3.22) yield different h,  $A_f$ , and  $H'_f s$ , and  $\phi_o = 0$  for linear observers. For some values of r, equation (3.27) is in the form (3.24). In particular, for  $r \leq 2$ , the summation term on the right-hand side of (3.27) does not exist. Therefore, the equation takes the form (3.24), and (3.26) simplifies to  $\hat{x}(k) = x(k) - N\eta(k)$ . In the case of a linear HGO discretized using the bilinear transformation method (3.21), the summation term on the right-hand side of (3.27) takes the form  $\sum_{j=3}^{r-1} (\cdot) = O(\epsilon)$  which can be grouped with  $h(\cdot)$ . In this case, (3.27) takes the form (3.24) for  $r \leq 3$  and (3.26) simplifies to  $\hat{x}(k) = x(k) - N\eta(k)$ .

In the more general case where r > 2 (or r > 3 in the bilinear case), (3.27) is not in the form (3.24) since the summation term is of the order  $1/\epsilon^{r-3}$  ( $1/\epsilon^{r-4}$  respectively). We can perform a change of variables to weaken the x-input to the  $\eta$ -equation. Using the fact that, for sufficiently small  $\epsilon$ ,  $\chi$  is much slower than  $\eta$ , we consider the quasi-steady-state value of  $\eta$  given, up to an  $O(\epsilon)$  error, by

$$\eta = A_f \eta + \sum_{i=2}^{r-1} \frac{1}{\epsilon^{r-1-j}} H_j D A_c^j x$$

or

$$\eta = (I - A_f)^{-1} \sum_{i=2}^{r-1} \frac{1}{\epsilon^{r-1-j}} H_j D A_c^j x$$

The change of variables

$$\xi = \eta - (I - A_f)^{-1} \sum_{j=2}^{r-1} \frac{1}{\epsilon^{r-1-j}} H_j D A_c^j x$$
 (3.28)

transforms (3.27) into

$$\xi(k+1) = A_f \xi(k) + \epsilon \tilde{h}(\chi(k), u(k), \epsilon) - \epsilon \alpha B_c \phi_o(\hat{x}(k), \zeta(k), u(k))$$

$$+ \sum_{j=3}^{r-1} \frac{1}{\epsilon^{r-1-j}} \tilde{H}_j D A_c^j x(k)$$
(3.29)

Inspection of (3.27) and (3.29) shows that (3.29) has the same form as (3.27) except that the summation term is of order  $1/\epsilon^{r-4}$  compared with  $1/\epsilon^{r-3}$  in (3.27). Repeated application of this transformation yields (3.24). Noting that in the change of variables (3.28) the coefficient of x has negative powers of  $\epsilon$ , it is not obvious why on the right-hand side of (3.26) x appears as  $x+\epsilon \mathcal{W}(x,\xi,\epsilon)$  where  $\mathcal{W}(x,\xi,\epsilon)$  has only nonnegative powers of  $\epsilon$ . This crucial fact can be verified by tedious calculations which can be found in Appendix A.

# 3.4 Performance Recovery

Now we show that the output feedback sampled-data controller

$$u(k) = \gamma(\hat{x}(k), \zeta(k))$$

recovers the performance of the state feedback controller (3.5) for sufficiently small  $\epsilon$ . The performance recovery manifests itself in three points. First, the origin

 $(x=0,\ z=0,\ u=0,\ \hat{x}=0)$  of the closed-loop system under the sampled-data output feedback controller is asymptotically stable. Second, the sampled-data output feedback controller recovers the region of attraction of the continuous-time state feedback controller in the sense that if  $\mathcal{R}$  is the region of attraction under state feedback, then for any compact set  $\mathcal{S}$  in the interior of  $\mathcal{R}$  and any compact set  $\mathcal{Q} \subset \mathcal{R}^r$ , the set  $\mathcal{S} \times \mathcal{Q}$  is included in the region of attraction under sampled-data output feedback control. Third, the trajectory of (x,z,u) under sampled-data output feedback control approaches the trajectory under continuous-time state feedback control as  $\epsilon \to 0$ .

The closed-loop sampled-data system is represented in the singularly perturbed form

$$\chi(k+1) = \chi(k) + \epsilon \mathcal{F}(\chi(k), \xi(k), \epsilon)$$
 (3.30)

$$\xi(k+1) = A_f \xi(k) + \epsilon \mathcal{G}(\chi(k), \xi(k), \epsilon)$$
 (3.31)

where

$$\mathcal{F}(\chi, \xi, \epsilon) = \Psi(\chi, u, \epsilon), \quad \mathcal{G}(\chi, \xi, \epsilon) = \Gamma(\chi, u, \hat{x}, \epsilon)$$

and u and  $\hat{x}$  are given by (3.25) and (3.26), respectively. The functions  $\mathcal{F}(\cdot)$  and  $\mathcal{G}(\cdot)$  are continuously differentiable functions of their arguments and globally bounded functions of  $\xi$ . At  $\epsilon = 0$ , (3.31) reduces to

$$\xi(k+1) = A_f \xi(k)$$

whose steady-state solution is  $\xi = 0$ . Substitution of  $\xi = 0$  in (3.30) results in the reduced system

$$\chi(k+1) = \chi(k) + \epsilon \mathcal{F}(\chi(k), 0, \epsilon)$$
 (3.32)

From (3.12), we see that  $\Psi(\chi, u, \epsilon)$  can be written as

$$\Psi(\chi, u, \epsilon) = F(\chi, u) + \epsilon \Phi(\chi, u, \epsilon)$$
(3.33)

where  $\Phi(\chi, u, \epsilon)$  is a continuously differentiable function of its arguments such that  $\Phi(0, 0, \epsilon) = 0$ . Moreover, from (3.26) we see that

$$\hat{x}|_{\xi=0} = x + \epsilon \mathcal{W}(x, 0, \epsilon) \tag{3.34}$$

Using (3.33) and (3.34) we can rewrite the reduced system (3.32) as

$$\chi(k+1) = \chi(k) + \epsilon F(\chi(k), \gamma(\chi(k), \zeta(k))) + \epsilon^2 \Phi(\chi(k), \gamma(\chi(k), \zeta(k)), \epsilon)$$
 (3.35)

where  $\Phi$  is a continuously differentiable function of its arguments and

$$\|\Phi(\chi,\gamma(\chi,\zeta),\epsilon)\| \leq \|\chi\|$$

#### 3.4.1 Boundedness and Ultimate Boundedness

The boundedness and ultimate boundedness of trajectories are established in the following theorem, where we show that trajectories of equations (3.30) and (3.31) starting in  $S \times Q$  come arbitrarily close to the origin as time progress.

Theorem 3.1 Let Assumptions 3.1 to 3.3 hold; then there exists  $\epsilon_1^* > 0$  such that for every  $0 < \epsilon \le \epsilon_1^*$ , the trajectories  $(\chi(k), \xi(k))$  of the system (3.30)-(3.31) starting at  $\chi(0) \in S$  and  $\hat{x}(0) \in Q$  are bounded for all  $k \ge 0$ . Moreover, the trajectory  $\chi(t)$  is bounded for all  $t \ge 0$ . In addition, given any  $\tau > 0$ , there exist  $\epsilon_2^*, T_1$  and an integer

 $k^*$  (all dependent on  $\tau$ ) such that, for every  $0<\epsilon\leq\epsilon_2^*$ , we have

$$\|\xi(k)\| \leq \tau, \ \forall \ k \geq k^*, \quad \|\chi(t)\| \leq \tau, \ \forall \ t \geq T_1$$

**Proof:** We divided the prove to two parts.

#### **Proof of Boundedness**

We start by proving boundedness of  $(\chi(k), \xi(k))$  at the sampling points, then we prove boundedness of  $\chi(t)$  for all t. Boundedness at the sampling points can be shown in two steps:

First: we show the positive invariance of an appropriately chosen set  $\Lambda$ , which is arbitrarily small in the direction of the fast variable  $\xi$ .

Second: we show that any closed-loop trajectory, starting in the compact set  $S \times Q$ , enters the positively invariant set  $\Lambda$  in finite time.

We know that the equilibrium point of the continuous-time system under state feedback is asymptotically stable with a region of attraction  $\mathcal{R}$ . By the converse Lyapunov theorem of Kurzweil [39] there is a continuously differentiable Lyapunov function  $V(\chi)$  and three positive definite functions  $U_1(\chi)$ ,  $U_2(\chi)$  and  $U_3(\chi)$ , all defined and continuous on  $\mathcal{R}$ , such that

$$U_1(\chi) \leq V(\chi) \leq U_2(\chi)$$

$$\lim_{\chi \to \partial \mathcal{R}} U_1(\chi) = \infty$$

$$\frac{\partial V}{\partial \chi} F(\chi, \gamma(x, \zeta)) \leq -U_3(\chi)$$

Writing the forward difference of the Lyapunov function and using the mean value

theorem we have

$$\Delta V(\chi(k)) \stackrel{\triangle}{=} V(\chi(k+1)) - V(\chi(k)) = \frac{\partial V}{\partial \chi}(\kappa(k))[\chi(k+1) - \chi(k)]$$

where  $\kappa(k)$  is a point on the line segment joining  $\chi(k)$  and  $\chi(k+1)$ . The properness of  $V(\chi)$  in  $\mathcal{R}$  guarantees that with any finite  $c_o > \max_{\chi \in \mathcal{S}} V(\chi)$ , the set  $\Omega = \{\chi \in \mathcal{R} : V(\chi) \leq c_o\}$  is a compact subset of  $\mathcal{R}$ , and  $\mathcal{S}$  is in the interior of  $\Omega$ .

Due to assumptions 3.1 to 3.3, we have for all  $(\chi, \xi) \in \Omega \times \mathbb{R}^r$ 

$$\|\mathcal{F}(\chi,\xi,\epsilon)\| \le K_1, \|\Phi(\chi,\gamma(\chi(k),\zeta(k)),\epsilon)\| \le K_2, \|\mathcal{G}(\chi,\xi,\epsilon)\| \le K_3$$

where  $K_1$ ,  $K_2$ , and  $K_3$  are positive constants independent of  $\epsilon$ . For  $c_2 > c_o$  and  $c_3 > 0$ , let

$$\tilde{\Omega} = \{ \chi \in \mathcal{R} : V(\chi) \le c_2 \}, \quad \Lambda = \tilde{\Omega} \times \{ W(\xi) \le c_3 \epsilon^2 \}$$

For any  $0 < \tilde{\epsilon} < 1$ , there is  $L_1$ , independent of  $\epsilon$ , such that for all  $(\chi, \xi) \in \Lambda$  and every  $0 < \epsilon < \tilde{\epsilon}$  we have

$$\|\mathcal{F}(\chi,\xi,\epsilon) - \mathcal{F}(\chi,0,\epsilon)\| \leq L_1 \|\xi\|$$

For the boundary-layer system, we define the Lyapunov function  $W(\xi) = \xi^T P \xi$ , where P is the positive definite solution of the Lyapunov equation  $A_f^T P A_f - P = -I$ . This function satisfies

$$\lambda_{min}(P) \|\xi\|^2 \le W(\xi) \le \|P\| \|\xi\|^2$$

where ||P|| > 1.

We start by showing that there exist positive constants  $c_3$  and  $\epsilon_1$  (dependent on

 $c_3$ ) such that the compact set  $\Lambda$  is positively invariant for  $0 < \epsilon < \epsilon_1$ .

$$\Delta V(\chi(k)) = \frac{\partial V}{\partial \chi}(\kappa(k))[\chi(k+1) - \chi(k)] 
= \frac{\partial V}{\partial \chi}(\chi(k))[\chi(k+1) - \chi(k)] + \left[\frac{\partial V}{\partial \chi}(\kappa(k)) - \frac{\partial V}{\partial \chi}(\chi(k))\right][\chi(k+1) - \chi(k)] 
\leq \frac{\partial V}{\partial \chi}(\chi(k))(\epsilon \mathcal{F}(\chi(k), \xi(k), \epsilon)) + L_2 \|\chi(k+1) - \chi(k)\|^2 
\leq -\epsilon U_3(\chi(k)) + \epsilon \left\|\frac{\partial V}{\partial \chi}(\chi(k))\right\| \|\mathcal{F}(\chi(k), \xi(k), \epsilon) - \mathcal{F}(\chi(k), 0, \epsilon)\| 
+ \epsilon^2 \left\|\frac{\partial V}{\partial \chi}(\chi(k))\right\| \|\Phi(\chi(k), \gamma(x(k), \zeta(k)), \epsilon)\| + L_2 \|\chi(k+1) - \chi(k)\|^2 
\leq -\epsilon U_3(\chi(k)) + \epsilon L_2 L_1 \|\xi(k)\| + \epsilon^2 L_2 K_1^2 + \epsilon^2 L_2 K_2$$

where  $\|[\partial V/\partial \chi](\chi)\| \leq L_2$  in  $\Omega$ . In  $\Lambda$ , we have

$$\lambda_{min}(P)\|\xi\|^2 \le W(\xi) \le c_3 \epsilon^2$$

Thus

$$\|\xi\| \leq \sqrt{\frac{c_3}{\lambda_{min}(P)}} \ \epsilon$$

and

$$\Delta V(\chi(k)) \le \epsilon [-U_3(\chi(k)) + \epsilon K_4] \tag{3.36}$$

where  $K_4 = L_1 L_2 \sqrt{c_3/\lambda_{min}(P)} + L_2(K_1^2 + K_2)$ .

For any positive constant  $\tilde{c}_o < c_2$ , trajectories starting inside  $\{V(\chi) \leq \tilde{c}_o\}$  cannot leave  $\{V(\chi) \leq c_2\}$  provided  $\epsilon$  is sufficiently small. This is seen from

$$V(\chi(k+1)) \leq V(\chi(k)) - \epsilon U_3(\chi(k)) + \epsilon^2 K_4 \leq \tilde{c}_a + \epsilon^2 K_4 < c_2$$
 (3.37)

whenever  $\epsilon^2 < \epsilon_1^2 \stackrel{\text{def}}{=} (c_2 - \tilde{c}_o)/K_4$ . Trajectories starting inside  $\{V(\chi) \leq c_2\}$  but

outside  $\{V(\chi) \leq \tilde{c}_o\}$  remains inside  $\{V(\chi) \leq c_2\}$ , provided  $\epsilon$  is sufficiently small. This is seen from

$$V(\chi(k+1)) \leq V(\chi(k)) - \epsilon U_3(\chi(k)) + \epsilon^2 K_4$$
  
$$\leq c_2 - \epsilon \rho_1 + \epsilon^2 K_4 < c_2$$
 (3.38)

whenever  $\epsilon < \epsilon_2 \stackrel{\text{def}}{=} \rho_1/K_4$ , where  $\rho_1 = min_{\tilde{c}_0 \leq V(\chi) \leq c_2} U_3(\chi)$ .

Thus, we conclude that for  $\epsilon_3 \leq min\{\epsilon_1, \epsilon_2\}$ , the set  $\{\chi \in V(\chi) \leq c_2\}$  is positively invariant for  $0 < \epsilon < \epsilon_3$ .

On the other hand, from (3.31) we have

$$\Delta W(\xi(k)) = \xi^{T}(k+1)P\xi(k+1) - \xi^{T}(k)P\xi(k)$$

$$\leq \xi^{T}(k)[A_{f}^{T}PA_{f} - P]\xi(k) + 2\epsilon \|\xi(k)\| \|A_{f}\| \|P\| \|\mathcal{G}(\chi(k), \xi(k), \epsilon)\|$$

$$+ \epsilon^{2} \|\mathcal{G}(\chi(k), \xi(k), \epsilon)\|^{2} \|P\|$$

$$\leq -\|\xi(k)\|^{2} + \epsilon \left(2\|\xi(k)\| \|A_{f}\| \|P\| K_{3} + \epsilon K_{3}^{2} \|P\|\right)$$

Hence

$$W(\xi(k+1)) \le \left(1 - \frac{1}{\|P\|}\right) W(\xi(k)) + \epsilon K_3 \|P\| (2\|\xi(k)\| \|A_f\| + \epsilon K_3)$$
 (3.39)

Since  $\xi(k) \in \{W(\xi) \le c_3 \epsilon^2\}$ , we have

$$W(\xi(k+1)) \leq \left(1 - \frac{1}{\|P\|}\right) c_3 \epsilon^2 + 2\epsilon^2 K_3 \|P\| \|A_f\| \sqrt{\frac{c_3}{\lambda_{min}(P)}} + \epsilon^2 K_3^2 \|P\|$$

Choosing  $c_3$  large enough ensures that

$$W(\xi(k+1)) \le \epsilon^2 c_3 \tag{3.40}$$

We conclude from (3.37), (3.38) and (3.40) that the set  $\Lambda$  is positively invariant.

Now we consider the initial state  $(\chi(0), \hat{x}(0)) \in \mathcal{S} \times \mathcal{Q}$ . It can be verified that the corresponding initial state  $\xi(0)$  satisfies  $||\xi(0)|| \leq l/\epsilon^{r-1}$ , where l depends on S and Q. Using the fact that  $\chi(0)$  is in the interior of  $\Omega$ , it can be shown from (3.30) that

$$\|\chi(k) - \chi(0)\| = \epsilon \left\| \sum_{i=0}^{k-1} \mathcal{F}(\chi(i), \xi(i), \epsilon) \right\| \le \epsilon k K_1$$

as long as  $\chi(k) \in \Omega$ . Therefore, there exists a positive constant  $K_5$ , independent of  $\epsilon$ , such that  $\chi(k) \in \Omega \quad \forall k \leq K_5/\epsilon$ . Let  $\tilde{k}_o$  be the first time  $\xi(k)$  enters the set  $\{W(\xi) \leq c_3 \epsilon^2\}$  and take  $\bar{k}_o \leq min\{\tilde{k}_o - 1, \frac{K_b}{\epsilon}\}$ . During the time interval  $[0, \bar{k}_o]$ , we have

$$\xi \notin \{W(\xi) \le c_3 \epsilon^2\}$$
 and  $\chi(k) \in \Omega$ .

Since  $\chi(k) \in \Omega$ , inequality (3.39) is satisfied. We rewrite (3.39) as

$$W(\xi(k+1)) \leq \left[ -\frac{1}{2\|P\|} W(\xi(k)) + \epsilon K_3 \|P\| \left( 2\|A_f\| \sqrt{\frac{W(\xi(k))}{\lambda_{min}(P)}} + \epsilon K_3 \right) \right] + \left( 1 - \frac{1}{2\|P\|} \right) W(\xi(k))$$
(3.41)

where we used the fact that  $\|\xi\|^2 \leq W(\xi)/\lambda_{min}(P)$ . Choosing  $c_3$  large enough ensures that, for  $W(\xi(k)) \geq c_3 \epsilon^2$ , the bracketed term on the right-hand side of (3.41) is non-positive. Hence

$$W(\xi(k+1)) \le \lambda W(\xi(k))$$

where  $0 < \lambda = [1 - 1/(2||P||)] < 1$ . Therefore  $W(\xi(k)) \le \lambda^k W(\xi(0))$ . Recalling that  $W(\xi) \le ||P|| ||\xi(k)||^2$  and  $||\xi(0)|| \le l/\epsilon^{r-1}$ , we obtain

$$W(\xi(k)) \le \lambda^k ||P|| \frac{l^2}{\epsilon^{2r-2}}$$
 (3.42)

which shows that  $\lim_{k\to\infty} W(\xi(k)) = 0$ . Hence,  $\xi(k)$  must enter the set  $\{W(\xi) \le \epsilon^2 c_3\}$  in finite time. From

$$\lambda^k \|P\| \frac{l^2}{\epsilon^{2r-2}} \le \epsilon^2 c_3$$

we see that  $\xi(k)$  will be inside  $\{W(\xi) \le \epsilon^2 c_3\}$  for k satisfying

$$k \ge \frac{\ln\left(\frac{K_6}{\epsilon^{2r}}\right)}{\ln\left(\frac{1}{\lambda}\right)}$$

where  $K_6 = l^2 ||P||/c_3$ . To ensure that  $\xi(k)$  enters  $\{W(\xi) \le \epsilon^2 c_3\}$  before  $\chi(k)$  leaves  $\Omega$ , we choose  $\epsilon_4$  small enough that for  $0 < \epsilon \le \epsilon_4$ 

$$\frac{\ln\left(\frac{K_6}{\epsilon^{2r}}\right)}{\ln\left(\frac{1}{\lambda}\right)} < \frac{K_5}{\epsilon} - 1$$

or equivalently

$$\epsilon \ln \left(\frac{1}{\lambda}\right) + \epsilon \ln \left(\frac{K_6}{\epsilon^{2r}}\right) < K_5 \ln \left(\frac{1}{\lambda}\right)$$
(3.43)

Such a choice of  $\epsilon_4$  is possible since the left-hand side of (3.43) tends to zero as  $\epsilon$  tends to zero.

Taking  $\epsilon_1^* = min(\tilde{\epsilon}, \epsilon_1, \epsilon_4, \epsilon_3)$  guarantees that for every  $0 < \epsilon \le \epsilon_1^*$ , the trajectory  $(\chi(k), \xi(k))$  enters  $\Lambda$  during the interval  $[0, \Delta(\epsilon)]$  and remains inside thereafter, where  $\Delta(\epsilon)$  is the integer part of  $K_5/\epsilon$ . Thus the trajectory is bounded for all  $k \ge \Delta(\epsilon)$  and it is bounded for  $k \in [0, \Delta(\epsilon)]$  by virtue of

$$\|\chi(k) - \chi(0)\| \le \epsilon k K_1$$

and (3.42).

Now we show the boundedness of  $\chi(t)$  for all t. The continuous time system (3.11) can be represented by

$$\chi(t) = \chi(k) + \int_{kT}^{t} F(\chi(\tau), u(k)) d\tau$$
 (3.44)

for  $kT \leq t \leq T(k+1)$ . Add and subtract  $\int_{kT}^{t} F(\chi(k), u(k)) d\tau$  to (3.44), to obtain

$$\chi(t) = \chi(k) + \int_{kT}^{t} F(\chi(k), u(k)) d\tau + \int_{kT}^{t} \left[ F(\chi(\tau), u(k)) - F(\chi(k), u(k)) \right] d\tau$$
 (3.45)

From the Lipschitz property of  $F(\chi, u)$  we have

$$||F(\chi(t), u(k) - F(\chi(k), u(k))|| \le L_3 ||\chi(t) - \chi(k)||$$

Using this inequality in (3.45) yields

$$\|\chi(t) - \chi(k)\| \le T \|F(\chi(k), u(k))\| + \int_{kT}^{t} L_3 \|\chi(\tau) - \chi(k)\| d\tau$$

Apply Gronwall Lemma to obtain

$$\|\chi(\tau) - \chi(k)\| \le Te^{L_3T} \|F(\chi(k), u(k))\|$$

Let  $F(\chi, u) \triangleq \mathcal{M}(\chi, \xi)$ . Since  $F(\cdot, \cdot)$  is continuous and F(0, 0) = 0,  $\mathcal{M}(\cdot, \cdot)$  is continuous and  $\mathcal{M}(0, 0) = 0$ . Therefore

$$\|\chi(t) - \chi(k)\| \le TK_7 \|\mathcal{M}(\chi(k), \xi(k))\|$$
 (3.46)

where  $K_7 > 0$ . Thus, boundedness of  $\chi(k)$  and  $\xi(k)$  implies boundedness of  $\chi(t)$  for all  $t \ge 0$ .

#### **Proof of Ultimate Boundedness**

Next we show that trajectories of equations (3.30) and (3.31) starting in  $\mathcal{S} \times \mathcal{Q}$  come arbitrarily close to the origin as time progress. We know that for every  $0 < \epsilon \le \epsilon_1^*$  the trajectories of the closed loop system, starting from  $(\chi(k), \xi(k)) \in \mathcal{S} \times \mathcal{Q}$  are inside the set  $\Lambda$  for all  $k \ge \tilde{k}$ . Thus, we can find  $\epsilon_5 = \epsilon_5(\tau) \le \epsilon_1^*$  such that for every  $0 < \epsilon \le \epsilon_5$  we have  $\|\xi(k)\| \le \tau$ ,  $\forall k \ge \tilde{k}$ . Since  $\Omega$  is bounded, there is  $r_o > 0$  such that  $\Omega \subset B(0, r_o) \cap \mathcal{R}$ .

To prove ultimate boundedness we need to show the following steps

First: Trajectories starting inside the set

$$\Lambda = \{V(\chi(k)) \le c_2\} \cap \{W(\xi(k)) \le c_3 \epsilon^2\}$$

reach the set

$$\tilde{\Lambda} = \{V(\chi(k)) \le c_5(\epsilon)\} \cap \{W(\xi(k)) < c_3\epsilon^2\}$$

in a finite number of steps  $k = k^*$ , where  $\lim_{\epsilon \to 0} c_5(\epsilon) = 0$ .

Second: There exists a positive constant  $c_4 > c_5$  (dependent on  $\epsilon$  with  $\lim_{\epsilon \to 0} c_4(\epsilon) = 0$ ) such that trajectories lying in  $\tilde{\Lambda}$  at time  $k = k^*$  must belong to the set

$$\bar{\Lambda} = \{V(\chi(k)) \le c_4(\epsilon)\} \cap \{W(\xi(k)) \le c_3 \epsilon^2\}$$

for all  $k \ge k^* + 1$ .

Using (3.36), it can be shown that for all  $(\chi, \xi) \in \Lambda$  we have

$$V(\chi(k+1)) \le V(\chi(k)) - \frac{\epsilon}{2} U_3(\chi(k)) - \epsilon \left[ \frac{1}{2} U_3(\chi(k)) - \epsilon K_4 \right]$$
 (3.47)

Since  $U_3(\chi)$  is positive definite and continuous, the set  $\{U_3(\chi) \leq 2\epsilon K_4\}$  is a compact

set for sufficiently small  $\epsilon$ . Let  $c_5(\epsilon) = \max_{U_3(\chi) \leq 2\epsilon K_4} V(\chi)$ . Whenever  $V(\chi(k)) > c_5(\epsilon)$  we have  $U_3(\chi(k)) > 2\epsilon K_4$ , and

$$V(\chi(k+1)) \le V(\chi(k)) - \frac{\epsilon}{2} U_3(\chi(k)) \tag{3.48}$$

Starting with  $V(\chi(0)) > c_5$  it can be seen from (3.48) and mathematical induction that as long as  $V(\chi(k)) > c_5(\epsilon)$ 

$$V(\chi(k+1)) \leq V(\chi(0)) - \frac{\epsilon}{2} \sum_{i=0}^{k} U_3(\chi(i))$$

$$< V(\chi(0)) - \frac{\epsilon}{2} \sum_{i=0}^{k} 2\epsilon K_4 = V(\chi(0)) - \epsilon^2 K_4(1+k)$$

This inequality shows that there is a finite time  $k^*$  such that  $V(\chi(k^*)) \leq c_5(\epsilon)$ . From now on we can use  $k^*$  as our starting point. It follows from (3.47) that if  $U_3(\chi(k^*)) \leq 2\epsilon K_4$  then

$$V(\chi(k^*+1)) \le V(\chi(k^*)) + \epsilon^2 K_4 \le c_5(\epsilon) + \epsilon^2 K_4 \stackrel{\triangle}{=} c_4(\epsilon)$$

Else if  $U_3(\chi(k^*)) > 2\epsilon K_4$ , then

$$V(\chi(k^*+1)) \leq V(\chi(k^*)) - \frac{\epsilon}{2}U_3(\chi(k^*)) \leq c_5(\epsilon)$$

In general, if  $U_3(\chi(k)) \geq 2\epsilon K_4$  for all  $k^* \leq k \leq k^* + j$ , then from (3.47)

$$V(\chi(k^{\bullet}+j+1)) \leq V(\chi(k^{\bullet}+j)) - \epsilon \left[\frac{1}{2}U_{3}(\chi(k^{\bullet}+j)) - \epsilon K_{4}\right]$$

$$\leq V(\chi(k^{\bullet})) - \epsilon \sum_{i=0}^{j} \left[\frac{1}{2}U_{3}(\chi(k^{\bullet}+i)) - \epsilon K_{4}\right]$$

$$\leq V(\chi(k^{\bullet})) \leq c_{5}(\epsilon)$$

In the second and complementary case  $U_3(\chi(k)) > 2\epsilon K_4$  for all  $0 < k^* \le k \le k^* + j - 1$ , but  $U_3(\chi(k^* + j)) \le 2\epsilon K_4$ , it follows from (3.47) that

$$V(\chi(k^* + j + 1)) \leq V(\chi(k^* + j)) - \epsilon \left[ \frac{1}{2} U_3(\chi(k^* + j)) - \epsilon K_4 \right]$$

$$\leq V(\chi(k^*)) - \epsilon \sum_{i=0}^{j-1} \left[ \frac{1}{2} U_3(\chi(k^* + i)) - \epsilon K_4 \right]$$

$$-\epsilon \left[ \frac{1}{2} U_3(\chi(k^* + j)) - \epsilon K_4 \right]$$

$$\leq V(\chi(k^*)) - \epsilon \left[ \frac{1}{2} U_3(\chi(k^* + j)) - \epsilon K_4 \right]$$

$$\leq c_5(\epsilon) + \epsilon^2 K_4$$

Thus,

$$V(\chi(k+1)) \leq c_4(\epsilon), \quad \forall k \geq k^*$$

From now on, if  $c_5(\epsilon) < V(\chi(k)) \le c_4(\epsilon)$  we have  $U_3(\chi(k)) > 2\epsilon K_4$  which implies that the Lyapunov function as seen in (3.47) is decreasing and for  $V(\chi(k)) \le c_5(\epsilon)$  where  $U_3(\chi(k)) \le 2\epsilon K_4$  the Lyapunov function may increase but  $V(\chi(k+1)) \le c_4(\epsilon)$  for all  $k > k^*$ . From (3.46) and the fact that  $\lim_{\epsilon \to 0} c_4(\epsilon) = 0$ , we conclude that there is a finite time  $T_1$  such that, for sufficiently small  $\epsilon$ ,  $||\chi(t)|| \le \tau$  for all  $t \ge T_1$ .

# 3.4.2 Exponential Stability of The Origin and Trajectory Convergence

At this stage of the analysis we assume that the origin  $\chi=0$  of the continuous time system

$$\dot{\chi} = F(\chi, \gamma(x, \zeta)) \stackrel{\text{def}}{=} F_c(\chi) \tag{3.49}$$

is exponentially stable and place ourselves in small ball of radius  $\tau > 0$  around the origin; the value of  $\tau$  will be determined later on. Theorem 3.1 guarantees that trajectories of the system (3.30)-(3.31), starting in  $\mathcal{S} \times \mathcal{Q}$ , enter this ball in finite time

and stay thereafter. This result allows us to study the trajectory convergence. Let  $\chi_r(t)$  be the solution of the continuous-time closed-loop system under state feedback, starting at  $\chi_r(0) = \chi(0)$ , *i.e.*,

$$\dot{\chi}_r = F_c(\chi_r), \quad \chi_r(0) = \chi(0)$$

The following theorem shows that the origin is exponentially stable and  $\chi(t) = \chi(t, \epsilon)$ , the solution of the sampled-data closed-loop system under output feedback, converges to  $\chi_r(t)$  as  $\epsilon \to 0$ , uniformly in t, for all  $t \ge 0$ .

**Theorem 3.2** Let Assumptions 3.1 to 3.3 hold and the vector field  $F_c(\chi_r)$  be continuously differentiable around the origin. Moreover, assume the origin of the closed-loop system under state feedback is exponentially stable. Then, there exists  $\epsilon_3^* > 0$  such that for every  $0 < \epsilon \le \epsilon_3^*$ , the origin of the system (3.30)-(3.31) is exponentially stable. Furthermore, given any  $\tau > 0$ , there exists  $\epsilon_4^* > 0$  such that for every  $0 < \epsilon \le \epsilon_4^*$ , we have

$$\|\chi(t) - \chi_r(t)\| < \tau, \quad \forall \quad t \ge 0$$

**Proof:** The proof consist of two parts. First, we show exponential stability of the origin. Second, we show trajectory convergence.

# **Proof of Exponential Stability of The Origin**

Theorem 3.1 guarantees that trajectories of the system (3.30)-(3.31), starting in  $S \times Q$ , enter this ball after a finite time and stay thereafter. Due to exponential stability of (3.49), there exists a continuously differentiable Lyapunov function  $V(\chi)$  [34] defined over  $B(0, r_2) \subset \mathcal{R}$  for some  $r_2 > 0$ , and four constants  $\alpha_1, \alpha_2, \alpha_3$  and  $\alpha_4$  such that for all  $\chi \in B(0, r_2)$  we have

$$\alpha_1 \|\chi\|^2 \le V(\chi) \le \alpha_2 \|\chi\|^2$$
 (3.50)

$$\frac{\partial V}{\partial \chi} F_c(\chi) \leq -\alpha_3 \|\chi\|^2 \tag{3.51}$$

$$\left\|\frac{\partial V}{\partial \chi}\right\| \leq \alpha_4 \|\chi\| \tag{3.52}$$

For the fast variables  $\xi(k)$ , we use the Lyapunov function  $W(\xi(k)) = \xi^T(k)P\xi(k)$ . The composite Lyapunov function  $\nu = V + W$  satisfies

$$\Delta \nu = \Delta V + \Delta W$$

$$\leq -\frac{1}{2} \epsilon \alpha_3 ||\chi(k)||^2 - \frac{1}{2} ||\xi(k)||^2 - \epsilon \tilde{\Psi}^T \Lambda_3 \tilde{\Psi}$$

where

$$\Lambda_{3} = \begin{bmatrix} \frac{1}{2}\alpha_{3} - \epsilon\beta_{1} & -\beta_{2} - \epsilon\beta_{3} \\ -\beta_{2} - \epsilon\beta_{3} & +\frac{1}{2\epsilon} - \beta_{4} - \epsilon\beta_{5} \end{bmatrix}, \tilde{\Psi} = \begin{bmatrix} \|\chi(k)\| \\ \|\xi(k)\| \end{bmatrix}$$

for some nonnegative constant  $\beta_i$ . Hence

$$\Delta \nu \leq -\frac{\epsilon}{2}\alpha_3 \|\chi(k)\|^2 - \frac{1}{2} \|\xi\|^2$$

for sufficiently small  $\epsilon$ . Then, there exists  $\epsilon_3^* > 0$  such that for every  $0 < \epsilon \le \epsilon_3^*$ , the origin of the system (3.30)-(3.31) is exponentially stable.

# **Proof of Trajectory Convergence**

The outline of the proof goes as follows. Let  $\bar{\chi}_r(k)$  be the solution of

$$\bar{\chi}_r(k+1) = \bar{\chi}_r(k) + TF_c(\bar{\chi}_r(k)), \quad \bar{\chi}_r(0) = \chi(0)$$

and show that for  $kT \leq t \leq (k+1)T$ ,  $\|\chi_r(t) - \bar{\chi}_r(k)\| < \tau/2$ . Argue that for any  $\tau > 0$ ,  $\exists \ \epsilon_3^* > 0$  such that  $\|\chi(k) - \bar{\chi}_r(k)\| < \tau/4 \ \forall \ k \geq 0$  and  $0 < \epsilon \leq \epsilon_3^*$ . Using (3.46) argue that  $\|\chi(t) - \chi(k)\| = O(\epsilon) < \tau/4$ . Finally, show that  $\|\chi(t) - \chi_r(t)\| < \tau$ .

We proceed to prove the first part. The solution of the reduced system under state feedback is given by

$$\chi_r(t) = \chi_r(k) + \int_{T_k}^t F_c(\chi_r(\tau)) d\tau, \quad \chi_r(0) = \chi(0)$$
 (3.53)

where  $t \in [Tk, T(k+1)]$ . By adding and subtracting  $F_c(\chi_r(k))$  to the integral in (3.53), we have

$$\chi_r(k+1) = \chi_r(k) + TF_c(\chi_r(k)) + T^2g(\chi_r(k))$$
 (3.54)

where  $||g(\chi_r(k))|| \leq K_8$ . The  $O(T^2)$  approximation of (3.54) is

$$\bar{\chi}_r(k+1) = \bar{\chi}_r(k) + TF_c(\bar{\chi}_r(k)), \quad \bar{\chi}_r(0) = \chi(0)$$
 (3.55)

Define  $e = \chi_r - \bar{\chi}_r$ , where e(0) = 0. Then

$$e(k+1) = e(k) + TF_c(e(k)) + T\Delta F_c(\chi_r(k), e(k)) + T^2g(\chi_r(k))$$

where  $\Delta F_c(\chi_r, e) = F_c(\chi_r) - F_c(\chi_r - e) - F_c(e)$ . Using the mean value theorem with the scalar function  $\Delta F_{c_i}(\chi_r, e)$ , we get

$$\Delta F_{c_i}(\chi_r, e) = \left[ \frac{\partial F_{c_i}}{\partial \chi_r} (\varrho \chi_r + (1 - \varrho)e) - \frac{\partial F_{c_i}}{\partial \chi_r} (\rho e) \right] e$$

where  $0 < \rho < 1$  and  $0 < \rho < 1$ . Therefore

$$||\Delta F_c(\chi_r, e)|| \le \varrho L_7 ||\chi_r|| ||e|| + L_7 |1 - \varrho - \rho|||e||^2$$

$$\|\Delta F_c(\chi_r, e)\|^2 \le \delta_1 \|\chi_r\|^4 + \delta_2 \|e\|^4$$

$$||F_c(e)|| \leq L_8||e||$$

$$\|e(k+1) - e(k)\|^2 \le T^2 \delta_3 \left[ \|F_c(e(k))\|^2 + \|\Delta F_c(\chi_r(k), e(k))\|^2 + T^2 K_8^2 \right]$$

The Lyapunov function V(e) satisfies inequalities similar to (3.50)-(3.52) in e in the neighborhood of e = 0. Then

$$\Delta V = V(e(k+1)) - V(e(k)) = \frac{\partial V}{\partial e}(\kappa_1(k)) \left[ e(k+1) - e(k) \right]$$

$$= \frac{\partial V}{\partial e}(e(k)) \left[ e(k+1) - e(k) \right] + \left[ \frac{\partial V}{\partial e}(\kappa_1(k)) - \frac{\partial V}{\partial e}(e(k)) \right] \left[ e(k+1) - e(k) \right]$$

$$\leq -T \left[ \frac{\alpha_3}{2} - \alpha_4 \varrho L_7 \|\chi(k)\| \right] \|e(k)\|^2 + T\mathcal{B}(\cdot)$$
(3.56)

where

$$\mathcal{B}(\cdot) = \left[ -\frac{\alpha_3}{2} + \alpha_4 L_7 |1 - \varrho - \rho| \|e(k)\| \right] \|e(k)\|^2$$

$$+ T \left[ \alpha_4 K_8 + T L_9 \delta_3 L_8^2 \|e(k)\| + T L_9 \delta_3 \delta_2 \|e(k)\|^2 \right] \|e(k)\|$$

$$+ T \left[ L_9 \delta_3 \delta_1 \|\chi_r(k)\|^4 + T^2 L_9 \delta_3 K_8^2 \right]$$

Using the fact that the solution of the nominal system decays to zero exponentially fast, we have  $\|\chi_r(k)\| \leq \mu e^{-\alpha_3 T k}$ . Also for all  $\|e\| \leq r_1 < r_o$ , with  $0 < r_1 \leq \alpha_3/[2\alpha_4 L_7|1-\varrho-\rho|]$ , we obtain  $\|\mathcal{B}(\cdot)\| \leq T\delta_4$ . Then from (3.56) we obtain

$$V(e(k+1)) \leq V(e(k)) - T\left[\frac{\alpha_3}{2} - \alpha_4 \varrho L_7 \|\chi(k)\|\right] \|e(k)\|^2 + T^2 \delta_4$$

$$= \left[1 - T\frac{\alpha_3}{2} + T\alpha_4 \varrho L_{10} \|\chi(k)\|\right] V(e(k)) + T^2 \delta_4 \qquad (3.57)$$

We can relate to the initial condition as follows:

$$V(e(k+1)) \leq \prod_{i=i+1}^{k} \left[1 - T\frac{\alpha_3}{2} + T\alpha_4 \varrho L_{10} \|\chi(i)\|\right] V(e(0))$$

$$+T^{2}\delta_{4}\left[1+\sum_{i=0}^{k}\prod_{j=i+1}^{k}\left[1-T\frac{lpha_{3}}{2}+Ta_{2}||\chi(k)||
ight]
ight]$$

From e(0) = 0 and due to the exponentially decaying bound on  $||\chi||$ , there is a number of samples p such that for

• 
$$i < p$$
,  $\alpha_4 \varrho L_{10} \mu e^{-\alpha_3 T i} \ge \frac{\alpha_3}{2}$ ,  $1 < 1 - T \frac{\alpha_3}{2} + T \alpha_4 \varrho L_{10} \mu e^{-\alpha_3 T i} \le \delta_5$ 

$$\bullet \ i>p, \ \alpha_4 \varrho L_{10} \mu e^{-\alpha_3 Ti} < \tfrac{\alpha_3}{2}, \ 0<1-T\tfrac{\alpha_3}{2} + T\alpha_4 \varrho L_{10} \mu e^{-\alpha_3 Ti} \leq \lambda_1 < 1$$

Then

$$V(e(k+1)) \le T^2 \delta_4 \left[ 1 + \sum_{i=0}^k \delta_5^p \lambda_1^{k-p} \right] = T^2 \delta_4 \left[ 1 + \delta_6 \lambda_1^{k-p} \right]$$

and we have

$$||e(k+1)||^2 \le \frac{1}{\alpha_1} V(e(k+1)) \le T^2 \delta_4 \left[ 1 + \delta_6 \lambda_1^{k-p} \right]$$

$$||e(k+1)|| \le T \sqrt{\frac{\delta_4 (1 + \delta_6 \lambda_1^{k-p})}{\alpha_1}} < \frac{\tau}{4}$$

for sufficiently small T. Thus,

$$\|\chi_r(k) - \bar{\chi}_r(k)\| < \frac{\tau}{4}$$

Consider now the difference  $\chi_r(t) - \chi_r(k)$ .

$$\|\chi_r(t) - \chi_r(k)\| \le T \|F_c(\chi_r(k))\| + \int_{kT}^t L_{10} \|\chi_r(\tau) - \chi_r(k)\| d\tau$$

Using Gronwall lemma for  $t \in [kT, (k+1)T]$ , we obtain

$$\|\chi_r(t) - \chi_r(k)\| \le Te^{L_{10}T} \|F_c(\chi_r(k))\| \le TK_9$$

Thus,

$$\|\chi_r(t) - \bar{\chi}_r(k)\| = \|\chi_r(t) - \chi_r(k) + \chi_r(k) - \bar{\chi}_r(k)\| < \frac{\tau}{2}$$

In the second step we show that  $\|\chi(k) - \bar{\chi}_r(k)\| < \tau/4$ . We partition the time interval  $[0, \infty)$  into two intervals  $[0, \Delta(\epsilon)]$  and  $[\Delta(\epsilon), \infty)$ , where  $\Delta(\epsilon)$  is the number of samples needed to get the estimation error  $\xi(k)$  to  $O(\epsilon)$ , as defined after (3.43). In the first interval  $[0, \Delta(\epsilon)]$ ,

$$\chi(k) = \chi(0) + \epsilon \sum_{i=0}^{k-1} \mathcal{F}(\chi(i), \xi(i), \epsilon)$$

$$\|\chi(k) - \chi(0)\| \le \epsilon \sum_{i=0}^{k-1} K_1 = \epsilon k K_1$$

where  $\|\mathcal{F}(\chi, \xi, \epsilon)\| \leq K_1 \ \forall \chi \in \tilde{\Omega}$ . Hence

$$\|\chi(k) - \chi(0)\| \le \epsilon \Delta(\epsilon) K_1 \quad \forall \ k \in [0, \Delta(\epsilon)]$$

The same can be done for  $\bar{\chi}_r$  and we conclude that

$$\|\bar{\chi}_r(k) - \bar{\chi}_r(0)\| \le \epsilon \Delta(\epsilon) K_9$$

where  $F_c(\chi) \leq K_{10}$ . Therefore

$$\|\chi(k) - \bar{\chi}_r(k)\| \leq 2\epsilon \Delta(\epsilon)(K_1 + K_{10}) < \frac{\tau}{4} \quad \forall \ k \in [0, \Delta(\epsilon)]$$

for sufficiently small  $\epsilon$ . Notice that the effect of the estimated error  $\xi$  does not appear in the picture because of the saturation of the control in  $\mathcal{F}(\cdot)$ . At the end of this period, as in Theorem 3.1, we have  $\|\xi(\tilde{k})\| \leq \sqrt{\frac{c_3}{\lambda_{\min}(P)}}\epsilon = \sigma T$ ; also  $\|\chi(k) - \bar{\chi}_r(k)\| < \tau$  and  $\|\chi(k)\| < \tau \quad \forall k \in [0, \Delta(\epsilon)]$ .

In the second time interval  $[\Delta(\epsilon), \infty)$ , we need to study the difference  $\chi(k) - \bar{\chi}_r(k)$ . Since

$$\chi(k+1) = \chi(k) + T\mathcal{F}(\chi(k), \xi(k), \epsilon), \quad \chi(0) = \chi_0$$
 (3.58)

where  $\mathcal{F}(\chi, \xi, \epsilon) = \mathcal{M}(\chi, \xi) + T\Phi(\chi, \gamma(x, \zeta), \epsilon)$  and  $\mathcal{M}(\chi, \xi) = F(\chi, u)$ , let us consider (3.58) as a perturbation of (3.55) and define the difference  $\tilde{e} = \chi - \bar{\chi}_r$  where  $\|\tilde{e}(\Delta(\epsilon))\| < \tau/4$  at the end of the first interval.

$$\tilde{e}(k+1) = \tilde{e}(k) + TF_c(\tilde{e}(k)) + T\mathcal{E}(\chi(k), \xi(k), \tilde{e}(k)) + T^2\Phi(\chi(k), \gamma(x(k), \zeta(k)), \epsilon)$$

where  $\mathcal{E}(\chi, \xi, \tilde{e}) = \mathcal{M}(\chi, \xi) - F_c(\bar{\chi}_r) - F_c(\tilde{e})$ . By adding and subtracting  $F_c(\chi(k))$  to  $\mathcal{E}(\cdot)$  we rewrite it as

$$\mathcal{E}(\chi, \xi, \tilde{e}) = \mathcal{M}(\chi, \xi) - F_c(\chi) + \Delta \mathcal{M}(\chi, \tilde{e})$$

where  $\Delta \mathcal{M}(\chi, \tilde{e})$  has the same structure of  $\Delta F_c(\chi, e)$ . Repeating with  $\tilde{e}$  the same argument used with e, we can show that  $\|\tilde{e}(k)\| \leq \tau/4 \quad \forall k \geq \Delta(\epsilon)$ . Using (3.46), we obtain

$$\|\chi(t)-\chi(k)\|\leq TK_7\|\mathcal{M}(\chi(k),\xi(k))\|\leq \frac{\tau}{4},\ \forall k\geq 0$$

for sufficiently small T. Then

$$\|\chi(t) - \bar{\chi}_r(k)\| \le \|\chi(t) - \chi(k)\| + \|\chi(k) - \bar{\chi}_r(k)\| < \frac{\tau}{2}$$

Finally,

$$\|\chi(t) - \chi_r(t)\| \le \|\chi(t) - \bar{\chi}_r(k)\| + \|\chi_r(t) - \bar{\chi}_r(k)\|$$
  
  $\le \frac{\tau}{2} + \frac{\tau}{2} = \tau$ 

which completes the proof.

# 3.5 Example on the Recovery of the Region of Attraction

We apply the developed technique to show how we recover the region of attraction as  $\epsilon$  tends to zero.

### Example 3.1 Consider the second order system

$$\dot{x}_1 = x_2 \tag{3.59}$$

$$\dot{x}_2 = 2x_1 + 10 \tanh(u) \tag{3.60}$$

$$y = x_1 \tag{3.61}$$

which has an exponentially unstable mode. The bounded state feedback control  $u = -\tanh(x_1 + x_2)$  stabilizes the origin and results in a finite region of attraction. To implement the sampled-data controller, we consider the discrete-time linear full-order HGO (discretized by the bilinear transformation method)

$$q(k+1) = A_{do}q(k) + B_{do}y(k)$$
$$\hat{x}(k) = C_{do}q(k) + D_{do}y(k)$$

where

$$A_{do} = rac{1}{det(\cdot)} \left[ egin{array}{ccc} 1 - lpha_1 - lpha_2 & 1 \ -2lpha_2 & 1 + lpha_1 - lpha_2 \end{array} 
ight], \quad B_{do} = rac{2}{det(\cdot)} \left[ egin{array}{c} lpha_1 + lpha_2 \ lpha_2 \end{array} 
ight]$$

$$C_{do} = rac{1}{det(\cdot)} \left[ egin{array}{cc} 1 & 1 \ -rac{lpha_2}{\epsilon} & rac{1+lpha_1}{\epsilon} \end{array} 
ight], \quad D_{do} = rac{2}{det(\cdot)} \left[ egin{array}{cc} lpha_1 + lpha_2 \ rac{lpha_2}{\epsilon} \end{array} 
ight]$$

and  $det(\cdot) = 1 + \alpha_1 + \alpha_2$ . We take the observer initial conditions as  $\hat{x}(k=0) = 0$ .

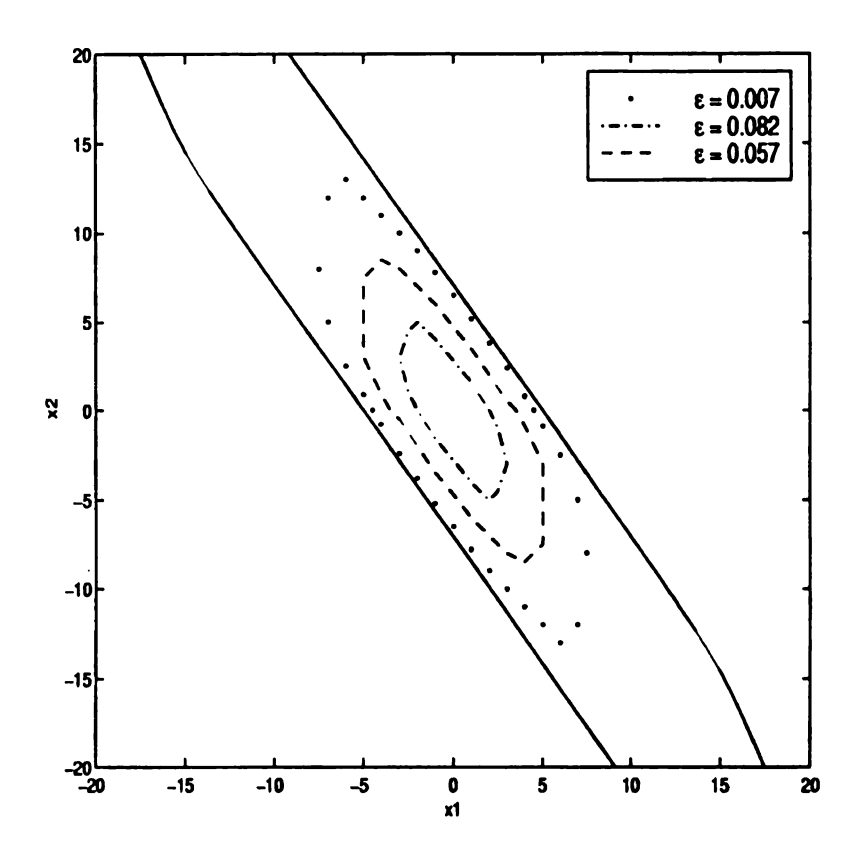


Figure 3.1. Recovery of region of attraction:  $\epsilon^* = 0$  (solid),  $\epsilon^* = 0.007$  (dotted),  $\epsilon^* = 0.057$  (dashed), and  $\epsilon^* = 0.082$  (dash-dotted)

The observer parameter  $\epsilon = 0.5T$  and the observer poles are real due to the choice  $\alpha_1 = 2$ ,  $\alpha_2 = 1$ . This example shows how the sampled-data output feedback recovers the region of attraction achieved under state feedback.

Figure 3.1 shows the region of attraction under state feedback control (the solid line), and three compact subsets that are recovered using the output feedback sampled-data controller. For each specified compact subset there is a design parameter  $\epsilon^*$  such that for every  $\epsilon \leq \epsilon^*$  the sampled-data output feedback controller is able to recover the given subset. The upper bound  $\epsilon^*$  is tight in the sense that for  $\epsilon > \epsilon^*$  a part of the set is not included in the region of attraction. The bounds  $\epsilon^* = 0.082$ , 0.057, and 0.007 correspond to the three sets, from smallest to the

largest. This show that as  $\epsilon$  gets smaller we recover the region of attraction under state feedback control.

# 3.6 Conclusion

In this Chapter we study sampled-data control of nonlinear systems using high-gain observers. The observer is designed in continuous time, then discretized using three different discretization methods. To perform the closed-loop analysis we represent the interconnected system in a singularly perturbed form. The reduction of the negative power of  $\epsilon$  is done in number of steps to reach the singularly perturbed form. Closed-loop analysis shows that the sampled-data controller recovers the performance of the continuous-time controller as the sampling frequency and the observer gain become sufficiently large. Performance recovery is shown in two steps. First we show boundedness of trajectories which come arbitrarily close to the origin as time progress. Second, we assume that the origin of the continuous time system is exponentially stable and show that trajectories enter some ball in the neighborhood of the origin in finite time and stay thereafter.

# CHAPTER 4

# Application to the Pendubot

# 4.1 Introduction

One of the usual concerns with high-gain observers is how they function in the presence of noise. This can be addressed either by performing additional analysis to study the effect of noise or by carrying out simulations and experiments. In Chapter 2 we used simulations to study the effect of noise. In this chapter, we study the behavior of a closed-loop system by performing experiments. The performance of the closed-loop system will reveal the effect of noise and the choice of the sampling rates.

This chapter applies the high-gain observer in the control of the Pendubot, an electro-mechanical system consisting of two rigid links interconnected by revolute joints. The pendulum motion is controlled by actuation of the first link. We perform experiments to confirm the open-loop conclusions of Chapter 2. The experimental results confirm all the conclusions of that chapter. Moreover, we perform experiments to confirm the closed-loop results of Chapter 3 regarding ultimate boundedness and trajectory convergence. We use the experiment to compare the use of high-gain observers as a tool for calculating velocities from position sensors with the engineering practice of using Euler's formula (difference method). The algorithm provided by the

manufacturer of the pendubot use Euler's formula. The chapter starts by introducing the pendubot in Section 4.2. The mathematical model and the equilibrium manifold are described in Sections 4.3 and 4.4, respectively. Because of the nature of the pendubot, the control algorithm is divided into swing up and balancing controls. Detailed description of that is given in Section 4.5. The hardware description and the experimental results are in Sections 4.6 and 4.7.

# 4.2 What Is The Pendubot?

The pendubot (Pendulum Robot) is an electro-mechanical system consisting of two rigid links interconnected by revolute joints. The first joint is actuated by a DC-motor while the second joint is unactuated as a simple pendulum.

The Pendubot is, in some ways, similar to the inverted pendulum on a cart, where the linear motion of the cart is used to balance the pendulum. The Pendulum uses instead the rotational motion of the first link to balance the second (pendulum) link. In this regard, the Pendubot is also similar to the more recent rotational inverted pendulum, pioneered by Professor Furuta of The Tokyo Institute of Technology [22]. In the rotational inverted pendulum, the axis of rotation of the pendulum is perpendicular to the axis of rotation of the first link. The Pendubot has both joint axes parallel, which results in some additional rotational coupling between the degrees of freedom. This additional coupling, which is not found in either the linear inverted pendulum or the rotational inverted pendulum makes the Pendubot more interesting and more challenging from both a kinematic and a dynamic standpoints. For example, in both the linear inverted pendulum and the rotational inverted pendulum, the Taylor series linearization computed around any operating point results in a controllable linear system. Moreover, the linearized model (A,B,C) is the same at all operating points. With the Pendubot, the linearization is operating point dependent;

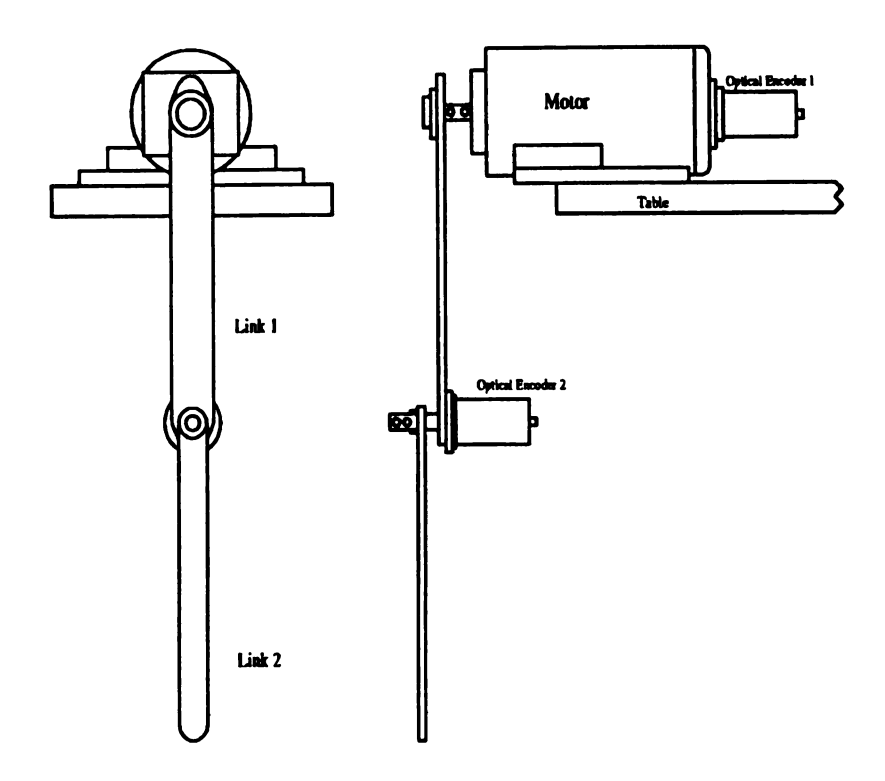


Figure 4.1. Front and side view drawing of the pendubot

in other words, the linearization (A,B,C) changes at each configuration and there are even special configurations where the linearization is uncontrollable.

The Pendubot possesses many attractive features for control research and education. It can be used to investigate system identification, linear control, nonlinear control, optimal control, learning control, robust and adaptive control, fuzzy logic control, intelligent control, hybrid and switching control, gain scheduling, and other control paradigms. One can program the Pendubot for swing up control, balancing, regulation, tracking, identification, gain scheduling, disturbance rejection, and friction compensation to name just a few of the applications. Some of these applications are described in [59, 60, 58]. The maker of the Pendubot is Mechatronic Systems, Inc. Figure 4.1 shows front and side view of the pendubot.

# 4.3 Mathematical Model

The pendubot is a two link robot with one actuator. The (Euler-Lagrange) equation of motion is [61]

$$D(q)\ddot{q} + C(q,\dot{q})\dot{q} + g(q) = \tilde{\tau}$$
(4.1)

where

$$D(q) = \begin{bmatrix} d_{11} & d_{12} \\ d_{21} & d_{22} \end{bmatrix}, \quad C(q, \dot{q})\dot{q} = \begin{bmatrix} h\dot{q}_{2} & h\dot{q}_{2} + h\dot{q}_{1} \\ -h\dot{q}_{1} & 0 \end{bmatrix} \begin{bmatrix} \dot{q}_{1} \\ \dot{q}_{2} \end{bmatrix} = \begin{bmatrix} h_{1} \\ h_{2} \end{bmatrix}$$

$$g(q) = \left[ egin{array}{c} \phi_1 \ \phi_2 \end{array} 
ight], \quad ilde{ au} = \left[ egin{array}{c} au \ 0 \end{array} 
ight]$$

$$d_{11} = m_1 l_{c1}^2 + m_2 \left( l_1^2 + l_{c2}^2 + 2 l_1 l_{c2} \cos(q_2) \right) + I_1 + I_2$$

$$d_{22} = m_2 l_{c2}^2 + I_2$$

$$d_{12} = d_{21} = m_2 (l_{c2}^2 + l_1 l_{c2} \cos(q_2)) + I_2$$

$$h = -m_2 l_1 l_{c2} \sin(q_2)$$

$$h_1 = -m_2 l_1 l_{c2} \sin(q_2) \dot{q}_2^2 - 2m_2 l_1 l_{c2} \sin(q_2) \dot{q}_2 \dot{q}_1$$

$$h_2 = m_2 l_1 l_{c2} \sin(q_2) \dot{q}_1^2$$

$$\phi_1 = (m_1 l_{c1} + m_2 l_1) g \cos(q_1) + m_2 l_{c2} g \cos(q_1 + q_2)$$

$$\phi_2 = m_2 l_{c2} g \cos(q_1 + q_2)$$

au: Torque applied to the first link by the DC-motor

 $m_1(m_2)$ : Total mass of link one (two)

 $l_1$ : Length of link one

 $l_{c1}(l_{c2})$ : Distance from base of the link to the center of mass of link one (two)

 $I_1$  ( $I_2$ ): Moment of inertia of link one (two) to its centroid

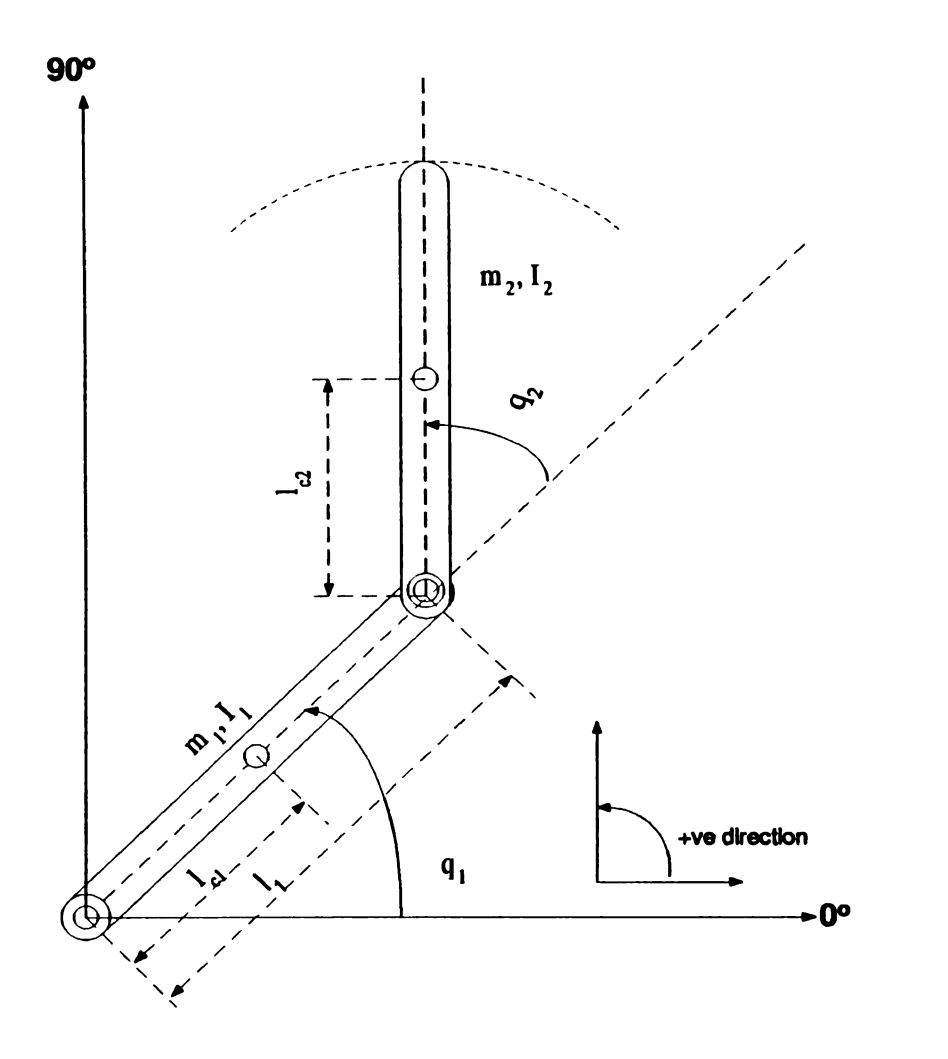


Figure 4.2. The Pendubot model parameters are shown on a pendubot schematic.

# g : Acceleration of gravity

Figure 4.2 shows the parameters of the pendubot model. It also shows the direction of increasing the angles. For simplicity let us define the parameters

$$\theta_1 = m_1 l_{c1}^2 + m_2 l_1^2 + I_1$$

$$\theta_2 = m_2 l_{c2}^2 + I_2$$

$$\theta_3 = m_2 l_1 l_{c2}$$

$$\theta_4 = m_1 l_{c1} + m_2 l_1$$

$$\theta_5 = m_2 l_{c2}$$

We can rewrite D(q),  $C(q, \dot{q})$  and g(q) as

$$D(q) = \begin{bmatrix} \theta_1 + \theta_2 + 2\theta_3 \cos(q_2) & \theta_2 + \theta_3 \cos(q_2) \\ \theta_2 + \theta_3 \cos(q_2) & \theta_2 \end{bmatrix}$$

$$C(q,\dot{q}) = \left[ egin{array}{ccc} - heta_3 \sin(q_2) \dot{q}_2 & - heta_3 \sin(q_2) (\dot{q}_2 + \dot{q}_1) \\ heta_3 \sin(q_2) \dot{q}_1 & 0 \end{array} 
ight]$$

$$g(q) = \left[ egin{array}{l} heta_4 g \cos(q_1) + heta_5 g \cos(q_1 + q_2) \ heta_5 g \cos(q_1 + q_2) \end{array} 
ight]$$

Finally using the fact that the matrix D(q) is invertible, the equation of motion is given by

$$\ddot{q} = D(q)^{-1} \left[ \tilde{\tau} - C(q, \dot{q}) \dot{q} - g(q) \right]$$

# 4.4 The Equilibrium Manifold

If the pendubot is mounted so that the joint axes are perpendicular to gravity, then there will be a continuum of equilibrium configurations, each corresponding to a constant value of  $\tau$ . Since at equilibrium  $\ddot{q}_1 = \dot{q}_1 = \ddot{q}_2 = \dot{q}_2 = 0$ , we have

$$\theta_4 g \cos(q_1) + \theta_5 g \cos(q_1 + q_2) = \tau$$
  
$$\theta_5 g \cos(q_1 + q_2) = 0$$

Then, the pendubot will balance at

$$q_1 = \cos^{-1}\left(\frac{\tau}{\theta_4 g}\right)$$

$$q_2 = n\frac{\pi}{2} - q_1; \quad n = 1, 3$$

such that  $(\tau/(\theta_4 g)) \leq 1$ .

# 4.5 Controlling The Pendubot

The pendubot control strategy developed in [60, 58] is divided into two parts: a balancing control which balances the pendubot about one of its equilibrium configurations and a swinging control that swings the pendubot up from the downward configuration to the inverted configuration.

### **Balancing Control**

The balancing problem may be solved by linearizing the equation of motion about an operating point using a Taylor series expansion and designing a linear state feedback controller. As we saw before, the pendubot has an equilibrium manifold which is a continuum of balancing positions. The linearized system becomes uncontrollable at  $q_1 = 0$ ,  $\pi$  as illustrated in Figure 4.3 which shows controllable and uncontrollable positions of the arms. Notice that the reference position for  $q_1$  is the horizontal axis.

### **Swing Up Control**

The problem of swinging the pendubot up from the downward position to the inverted position is an interesting and challenging nonlinear control problem. This problem illustrates the nonlinear control ideas of nonlinear relative degree, partial feedback

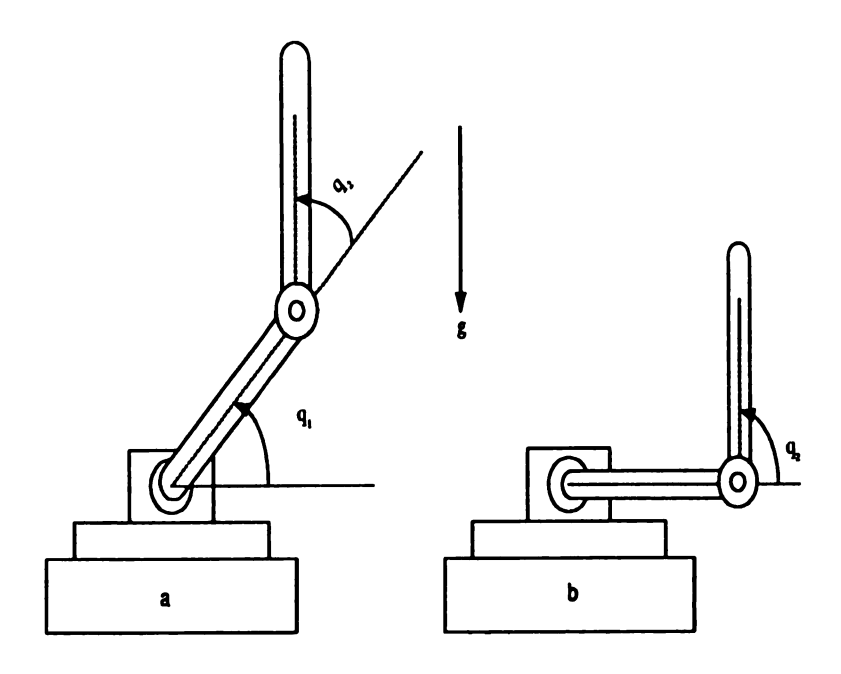


Figure 4.3. The pendubot arm at a: controllable position, b: uncontrollable position

linearization and zero dynamics.

#### **Partial Feedback Linearization**

We take the point  $(q_1 = -\pi/2, q_2 = \pi)$  on the equilibrium manifold  $q_1 + q_2 = \pm \pi/2$  as our desired equilibrium position and linearize the equation of motion about it. Let us consider

$$d_{11}\ddot{q}_1 + d_{12}\ddot{q}_2 + h_1 + \phi_1 = \tau \tag{4.2}$$

$$d_{21}\ddot{q}_1 + d_{22}\ddot{q}_2 + h_2 + \phi_2 = 0 (4.3)$$

Solving for  $\ddot{q}_2$  from (4.3) and substituting it in (4.2), we obtain

$$\ddot{q}_1\left(d_{11}-\frac{d_{12}d_{21}}{d_{22}}\right)+\left(h_1-\frac{d_{12}h_2}{d_{22}}\right)+\left(\phi_1-\frac{d_{12}\phi_2}{d_{22}}\right)=\tau$$

Taking the control variable  $\tau$  as

$$\tau = \left(d_{11} - \frac{d_{12}d_{21}}{d_{22}}\right)v_1 + \left(h_1 - \frac{d_{12}h_2}{d_{22}}\right) + \left(\phi_1 - \frac{d_{12}\phi_2}{d_{22}}\right)$$

results in

$$\ddot{q}_1 = v_1$$

$$d_{22}\ddot{q}_2 + h_2 + \phi_2 = -d_{21}v_1$$

To track some reference signal (reference position)  $r = q_1^d$  and  $\dot{r} = \dot{q}_1^d = 0$ , the control variable  $v_1$  can be designed as

$$v_1 = k_p(q_1^d - q_1) + k_d(\dot{q}_1^d - \dot{q}_1)$$

where the positive constant  $k_p$  and  $k_d$  are the control gains. Now we can define the tracking error as our new states

$$e_1 = q_1 - q_1^d$$
 ,  $e_2 = \dot{q}_1 - \dot{q}_1^d = \dot{q}_1$   $\eta_1 = q_2$  ,  $\eta_2 = \dot{q}_2$ 

and rewrite the system as

$$\dot{e}_1 = e_2$$

$$\dot{e}_2 = -k_p e_1 - k_d e_2$$

$$\dot{\eta}_1 = \eta_2 
\dot{\eta}_2 = -\frac{1}{d_{22}}(h_2 + \phi_2) - \frac{d_{12}}{d_{22}}\left(k_p(q_1^d - q_1) + k_d(\dot{q}_1^d - \dot{q}_1)\right) 
y = e_1$$

The surface  $e = [e_1 \quad e_2]^T = [0 \quad 0]^T$  in the state space defines an invariant manifold for the system. The tracking error part can be written as

$$\dot{e} = \begin{bmatrix} 0 & 1 \\ -k_p & -k_d \end{bmatrix} e = Ae$$

Choose  $k_p$  and  $k_d$  such that A is Hurwitz. On the sliding surface e = 0, the dynamics are given by

$$\dot{\eta}_1 = \eta_2 \tag{4.4}$$

$$\dot{\eta}_2 = -\frac{1}{d_{22}}\phi_2 - \frac{h_2}{d_{22}} \tag{4.5}$$

where

$$h_2 = m_2 l_1 l_{c2} \sin(q_2) \dot{q}_1^2 = 0$$

$$\phi_2 = m_2 l_{c2} g \cos(q_1^d + \eta_1)$$

$$d_{22} = m_2 l_{c2}^2 + I_2$$

which represent the zero dynamics with respect to the output  $y = e_1$ . We see from (4.4)-(4.5) that the zero dynamics are just the dynamics of the unactuated arm, which has a periodic orbit. While the error e(t) converges to zero, the steady state behavior for the first link converges exponentially to  $q_1 = -\pi/2$  for the middle position (the first link downward and the second link upward) or  $q_1 = \pi/2$  for the upper position (both links are upward), and the second link oscillates about the

equilibrium  $(+\pi,0)$  for the middle position or  $(-\pi,0)$  for the upper position. The swing up control job then is to excite the zero dynamics sufficiently by the motion of link 1 such that the pendulum swings close to its unstable equilibrium. When the pendulum is close enough to the desired equilibrium position, we switch from the partial feedback linearization controller to the linear balancing control in order to balance the pendulum about the middle or upper position.

# 4.6 Hardware Description

The pendubot consists of two rigid aluminum links of lengths 14 in. and 8 in. Link one is directly coupled to the shaft of a 90 V permanent magnet DC motor mounted to the end of a table. The motor mount and bearings support the entire system. Link one includes the bearing housing for joint two. The shaft extends out in both directions of the housing, allowing coupling to the second link and to an optical encoder mounted on link one. The design gives both links full 360° of rotational motion. Link two is constructed of a  $\frac{1}{4}$  inch thick length of aluminum with coupling that attaches to the shaft of joint two. The optical encoder resolution is  $1250 \ pulse/rev$ .

All the control computations are performed in Pentium PC with a D/A card and encoder interface card. Using the software routines supplied with the pendubot, the control algorithms are programed in C. Figure 4.4 shows a pictorial description of the interface between the pendubot and the controller.

# 4.7 Experimental Results

Because we only measure the positions of the pendubot links, i.e., the angles  $q_1$  and  $q_2$ , by optical encoders, we estimate the speeds  $\dot{q}_1$  and  $\dot{q}_2$ . With  $x_1 = q_1, x_2 = \dot{q}_1, x_3 = q_2$ 

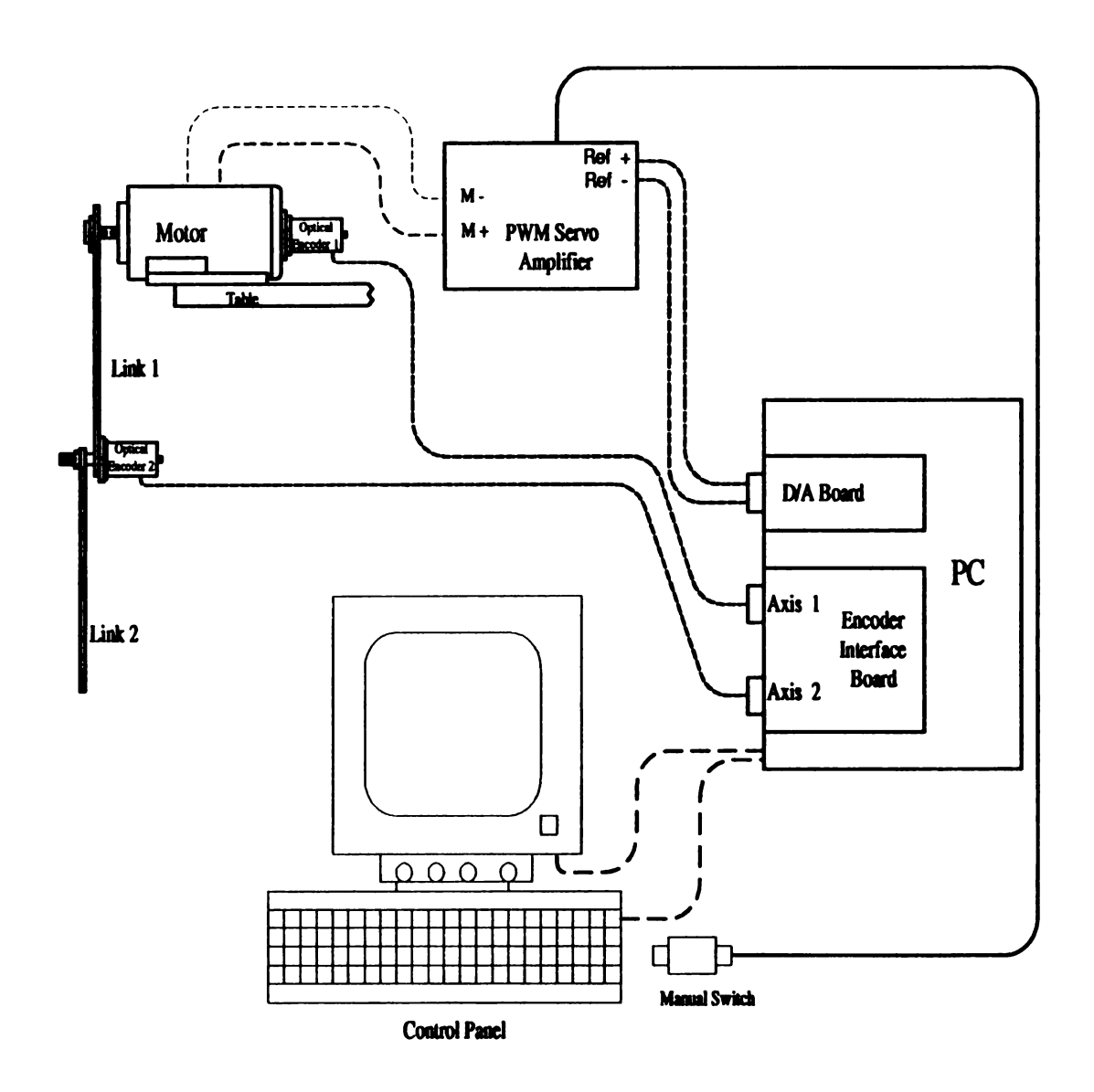


Figure 4.4. Pictorial description of the Pendubot's interface with its controller

and  $x_4 = \dot{q}_2$  as state variables, the states space model is given by

$$\begin{array}{rcl} \dot{x}_1 & = & x_2 \\ \dot{x}_2 & = & \ddot{q}_1 \\ \dot{x}_3 & = & x_4 \\ \dot{x}_4 & = & \ddot{q}_2 \end{array}$$

We use a high-gain observer to estimate the states. The nonlinearity of the system is dependent on all states. If it is known exactly we can include it in the observer design resulting in the nonlinear full-order HGO

$$\dot{\hat{x}} = A_c \hat{x} + B_c \phi_o(x, \hat{x}) + L(y - C_c \hat{x})$$

where

$$A_{c} = \begin{bmatrix} 0 & 1 & 0 & 0 \\ 0 & 0 & 0 & 0 \\ 0 & 0 & 0 & 1 \\ 0 & 0 & 0 & 0 \end{bmatrix}, \quad B_{c} = \begin{bmatrix} 0 & 0 \\ 1 & 0 \\ 0 & 0 \\ 0 & 1 \end{bmatrix}, \quad C_{c} = \begin{bmatrix} 1 & 0 & 0 & 0 \\ 0 & 0 & 1 & 0 \end{bmatrix}$$

The observer gains are designed as

$$L = \begin{bmatrix} \frac{2}{\epsilon} & 0 \\ \frac{1}{\epsilon^2} & 0 \\ 0 & \frac{2}{\epsilon} \\ 0 & \frac{1}{\epsilon^2} \end{bmatrix}$$

where  $\epsilon > 0$  is small parameter to be chosen. In the case of a linear observer,  $\phi_o = 0$ ; hence, no knowledge of the nonlinearity is included in the observer design. The discretization of the observer can be implemented by any one of the methods described in Chapter 2. We use the same state feedback control parameters for output feedback. The system parameters are

$$\theta^T = [0.0308 \quad 0.0106 \quad 0.0095 \quad 0.2087 \quad 0.063]$$

The HGO will be discretized with sampling period T and the observer parameters are as in L. We relate T to  $\epsilon$  by  $\alpha = T/\epsilon$ . The parameter  $\epsilon$  can be made small by either fixing T and increasing  $\alpha$ , or fixing  $\alpha$  and decreasing T.

The optical encoder resolution will add noise to the links positions. The noise depends on the number of pulses per revolution; the higher the number of pulses the smaller the noise. In our case, the optical encoder resolution is 1250 pulse/revelution which means the maximum deviation for each link is  $360/1250 = 0.288^{\circ}$ . The actual deviation depends on the synchronization between the sampling points and the optical encoder pulses.

The pendubot starts at its only stable equilibrium point p  $(q_1 = -\frac{\pi}{2}, q_2 = 0)$  as shown in figure 4.1. The state estimates can start from the same initial conditions of the pendubot, which are known in this case, or with the default zero initial conditions. Choosing the initial conditions of the observer at the default values brings in peaking during the transient period. This phenomenon could derive the pendubot to instability and saturation is used to limit the effect of peaking. The physical saturation of the system by the manufacturer is  $\pm 10$  volts. We had to reduce the saturation level in the case of peaking to be able to balance the pendubot. The saturation level depends on the sampling period T in such way that if T is large the default saturation level is enough; otherwise we need to reduce the saturation level.

# 4.7.1 Confirmation of the Open-Loop Study

In Chapter 2 we arrived at various conclusions regarding the discretization of the high-gain observer. The simulation-based study of Chapter 2 addressed the following issues:

- 1. the discretization method,
- 2. the order of the observer,
- 3. the effect of the ratio  $T/\epsilon$ ,
- 4. the assignment of the observer poles, and
- 5. the comparison with other numerical differentiators.

We use the pendubot experiment to address these issues. We need to balance the robot arm at an unstable equilibrium point. Since we have two links, we use two optical encoders to measure their positions and then use the high-gain observer to estimate their speeds. The Sampling period range for the pendubot is limited. The minimum sampling period we can get is  $T_{min} = 0.0016$  sec. The pendubot initial conditions are  $x = \begin{bmatrix} -\pi/2 & 0 & 0 \end{bmatrix}^T$ . The second link angle is zero along with the extension of the first link, as illustrated in Figure 4.2.

For large sampling periods the peaking phenomena is not that significant because the system is only second order. When the sampling period decreases, the need for saturation increases rapidly to be able to balance the pendubot. Experimentally, we see the importance of using saturation, especially when the high-gain observer starts from zero initial conditions. The control input is limited to |u| < 10 volts.

#### Comparison of the Discretization Methods

In this part we compare three discretization methods (Bilinear, Backward Difference and Forward Difference) for the linear high-gain observer, with T = 0.003 sec.

Bilinear Trans.	$\alpha =$	1.0	1.5	2.0	2.5
Backward Diff.	$\alpha =$	1.2	1.5	2.0	2.5
Forward Diff.	$\alpha =$	0.8	0.9	1.0	1.1

Table 4.1. The values of  $\alpha = T/\epsilon$  for the different discretization methods.

 $\alpha = T/\epsilon$  taken as shown in Table 4.1.

The choices for the bilinear and backward difference (BD) method were made to check Figure 2.2 of Chapter 2, where we found that for the highest derivative of the output, the bilinear method has less r.m.s. error than the BD method. This will explain why we could not balance the pendubot arm by using BD method when  $\alpha = 1.0$  while we were able to do it with a larger  $\alpha$ . Figure 4.5 (for T = 0.003 and  $\alpha = 2.5$ ) shows the position and the speed for both links when the steady state position is  $(\theta_1 = -\pi/2, \theta_2 = +\pi)$ . The speed of both links goes to zero at steady state but, because of the optical encoder resolution, we notice some chattering.

On other hand, the forward difference (FD) method will map the eigenvalues of the HGO inside the unit circle. But if  $\alpha$  increases while keeping T fixed, then the eigenvalues will start to map outside the unit circle which will bring instability, especially if  $\alpha > 1.6$ . This is the reason why in Figure 2.2 of Chapter 2 the HGO discretized by FD method at  $\alpha \geq 1.5$  was unstable for T = 0.01. For T = 0.003, the poles will go outside the unit-circle for  $\alpha > 1.1$ . But the FD method will have less r.m.s. error for smaller  $\alpha$  as in Figure 2.2 of Chapter 2.

Figures 4.6, 4.7 and 4.8 for the bilinear, BD and FD methods confirm that as  $\alpha$  increases the steady state error decreases and the transient period includes oscillation. The chattering effect we see at steady state is due to the resolution of the optical encoder. The installed optical encoders have a resolution of 1250 pulse/revolution,

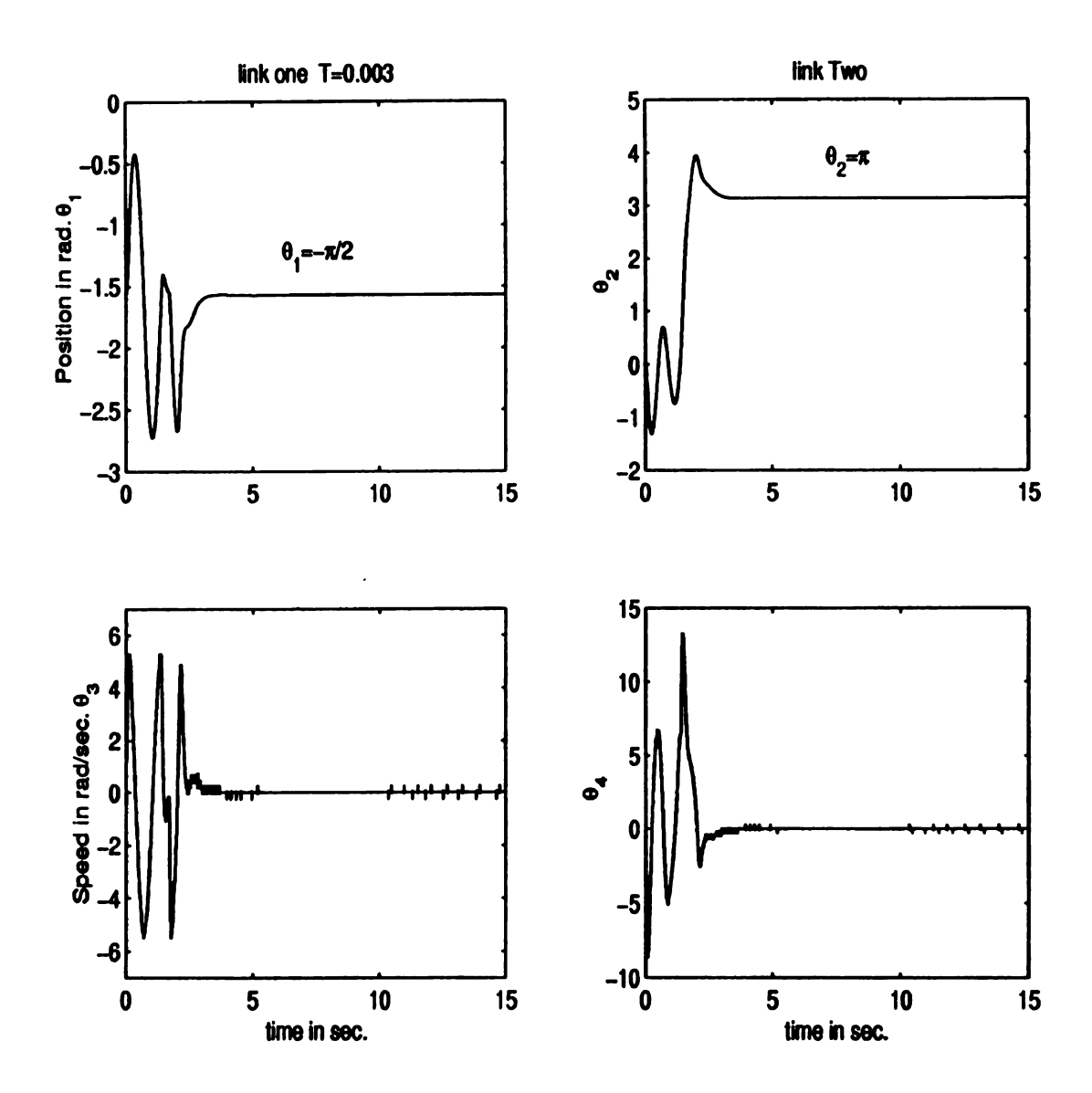


Figure 4.5. The output signals for both links and their derivatives, T=0.003 and  $\alpha=2.5$ 

which results in an error of  $360^{\circ}/1250 = 0.288^{\circ}$ . Increasing  $\alpha$  when T is fixed reduces the transient time.

If we consider the range of the operation for increasing  $\alpha$  while fixing T and the transient period, we find that the bilinear transformation method is the proper choice, which is in agreement with our earlier conclusion in Chapter 2.

#### **Bilinear Implementation**

On the basis of the foregoing comparative study, we adopt the bilinear transformation as our discretization method. Let us study the design of the high-gain observer with the bilinear implementation. The design parameters are the sampling period T, the observer parameter  $\epsilon$  and the  $\alpha_i$  coefficients which assign the roots of the characteristic equation.

Regarding the choice of poles, we note that the bilinear HGO can be made an FIR (finite impulse response) filter or an IIR (infinite impulse response) filter. Figure 4.9 shows that with complex poles the transient response is oscillatory and the transient period is longer than the case of real poles, especially for  $60^{\circ} \geq \theta \geq 40^{\circ}$ . If  $\theta > 60^{\circ}$  the oscillation prevents the pendubot from balancing at the required position. Since there is no advantage for using complex poles, we use real poles as we did in Chapter 2.

Another degree of freedom is the choice of the order of the observer. For example, we use reduced (first), full (second) and extended (third) order observers to estimate the speed of both links of the pendubot. Figure 4.10 shows that the extended-order observer has less transient oscillations and fast convergence of the tracking error to zero; in this figure T = 0.01 and  $\alpha = 2.1$ . The same figure show also that the control magnitude for the extended-order observer is less than the other two observers.

The parameter  $\alpha$  determines the bandwidth of the discrete-time observer, the bandwidth increases with  $\alpha$ . Increasing  $\alpha$  while fixing T makes the peaking more

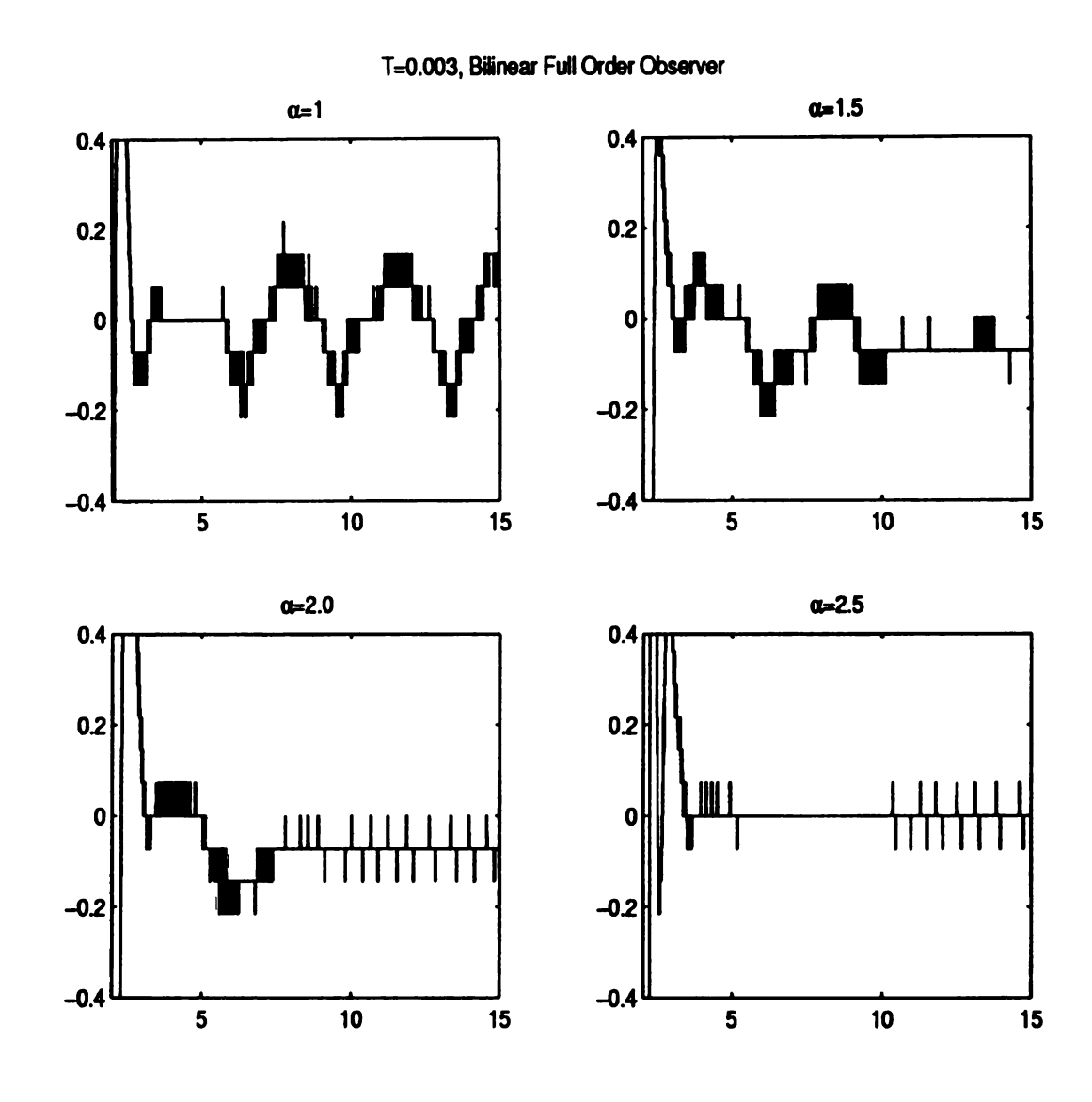


Figure 4.6. Using the bilinear transformation to calculate the steady state tracking error  $e_{ss} = x_1 + x_3 - \pi/2$ , where T = 0.003sec. and  $\alpha = 1.0$ , 1.5, 2.0, 2.5 respectively.

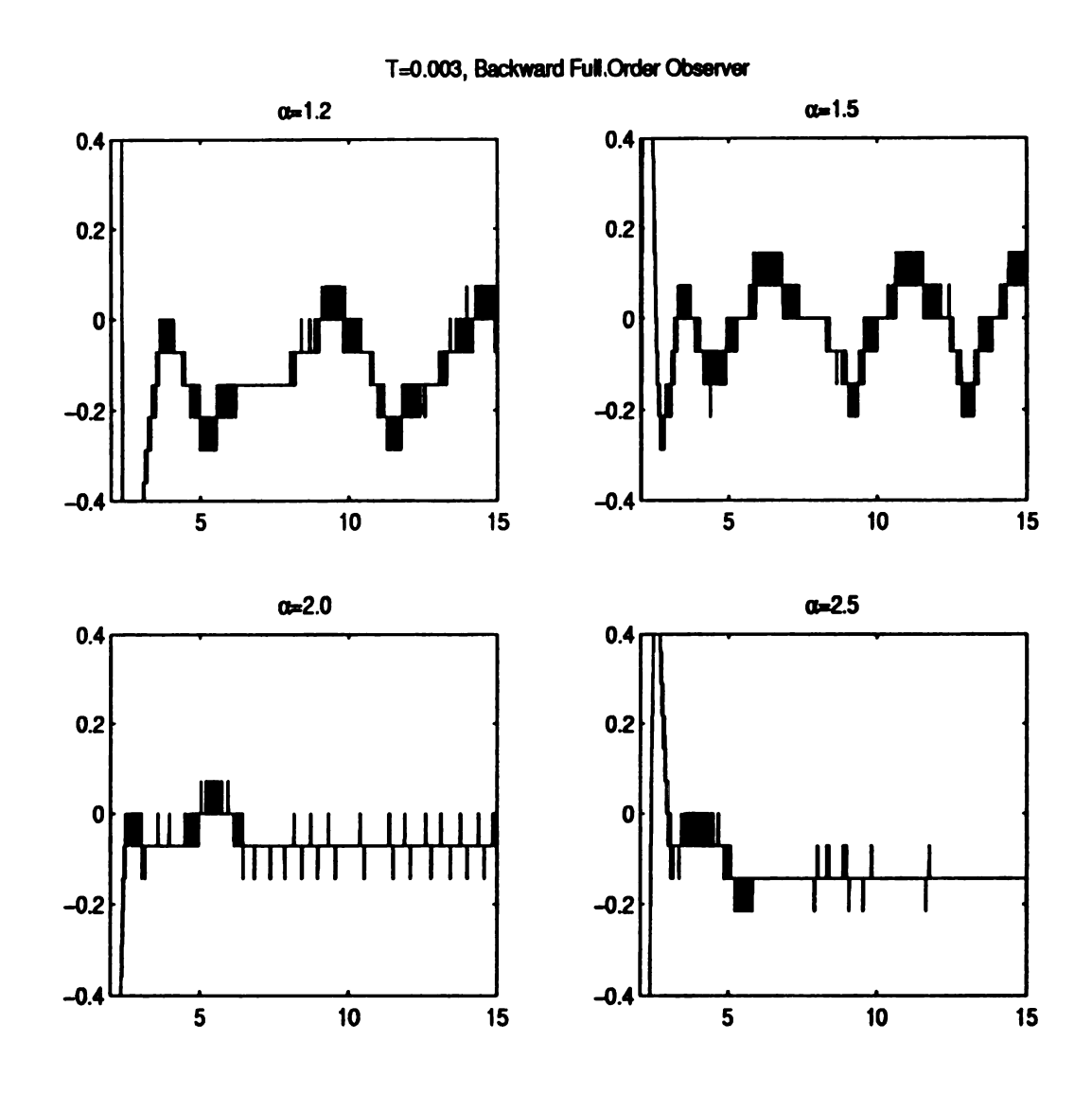


Figure 4.7. Using the backward difference method to calculate the steady state tracking error  $e_{ss}$ , where T=0.003sec. and  $\alpha=1.2,\ 1.5,\ 2.0,\ 2.5$  respectively.

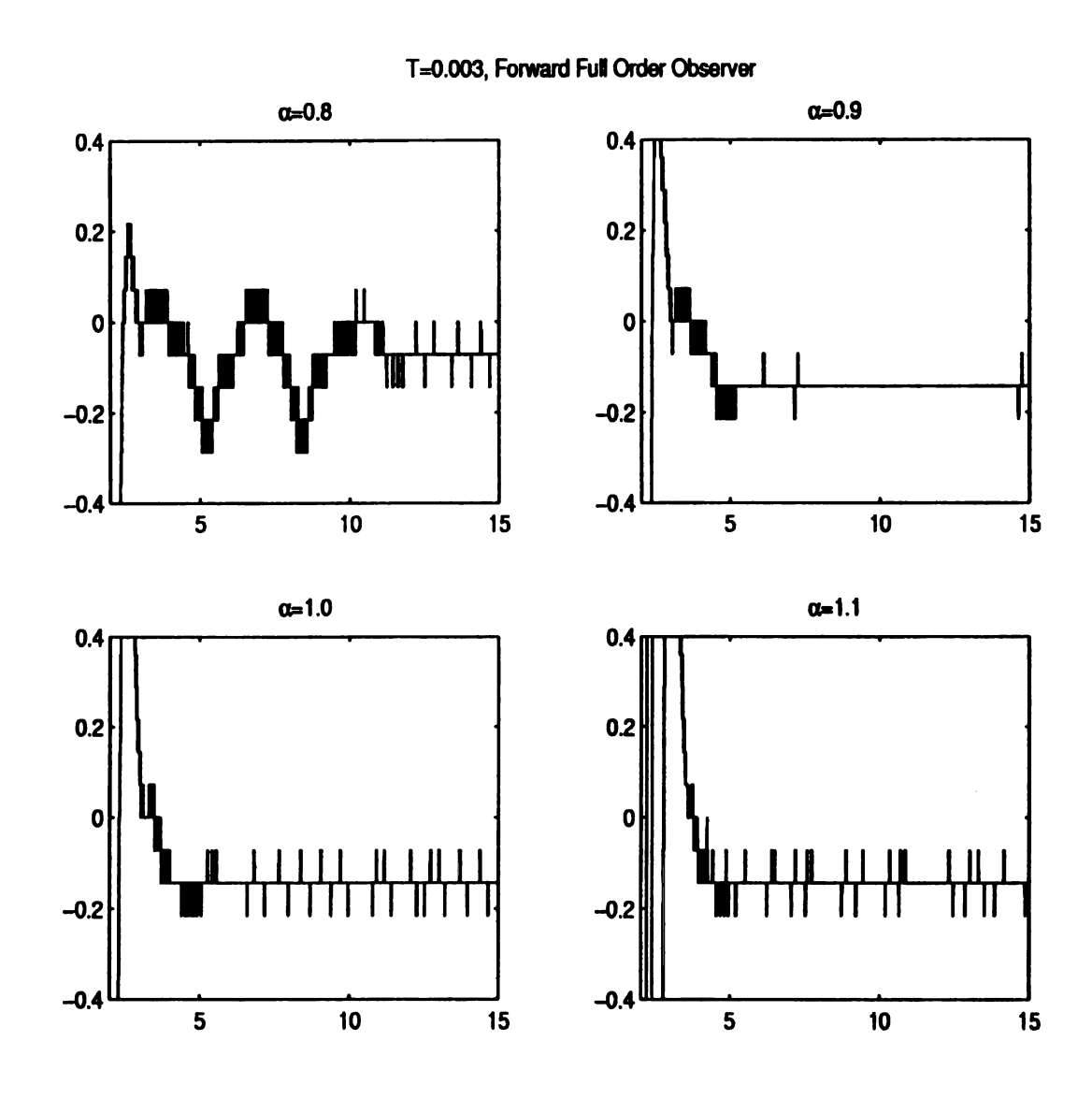


Figure 4.8. Using the forward difference method to calculate the steady state tracking error  $e_{ss}$ , where T=0.003sec. and  $\alpha=0.8,\ 0.9,\ 1.0,\ 1.1$  respectively.

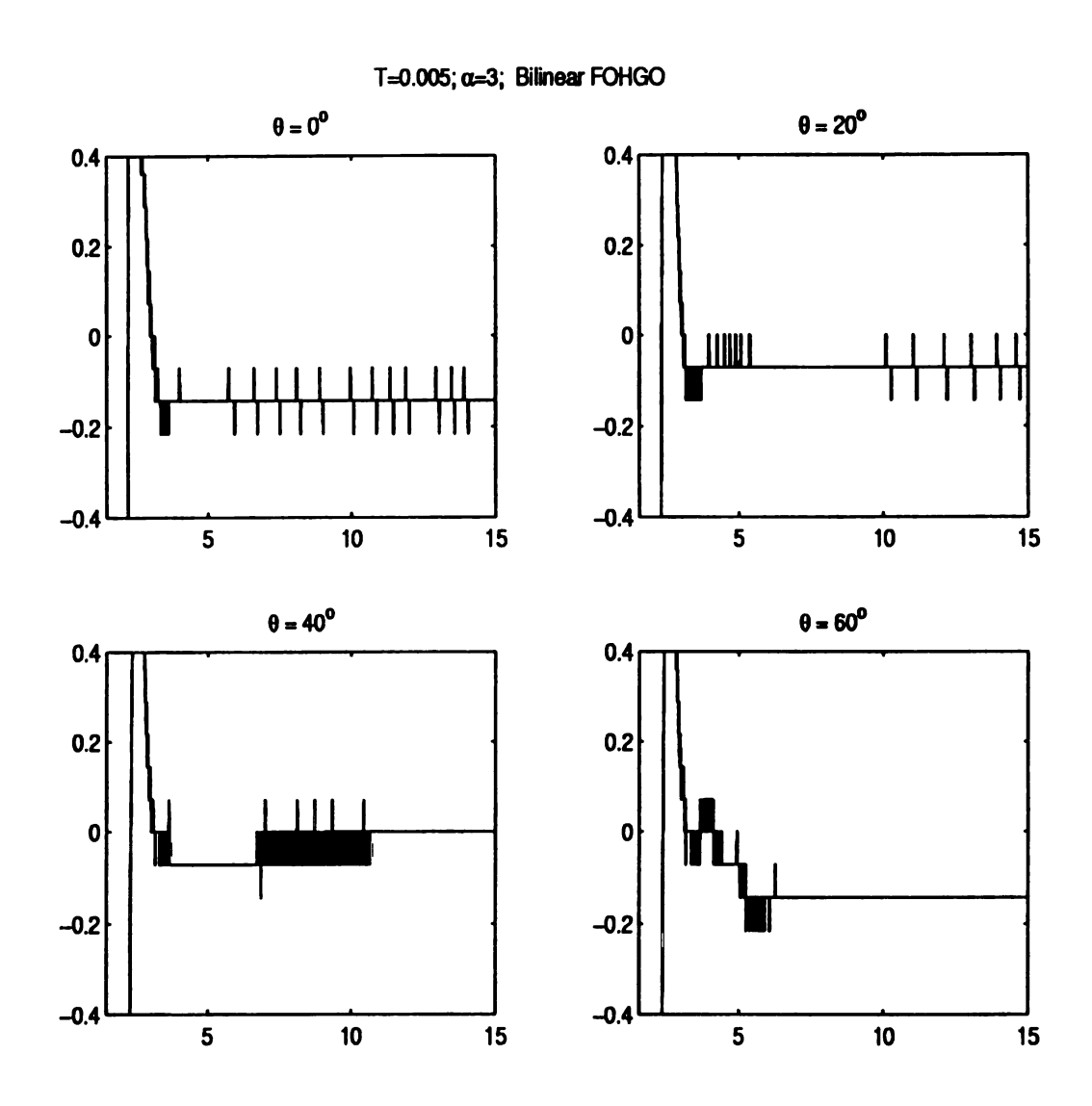


Figure 4.9. The effect of different choices of poles real and complex on the transient response, T = 0.005 and  $\alpha = 3.0$  discretized by the bilinear transformation.

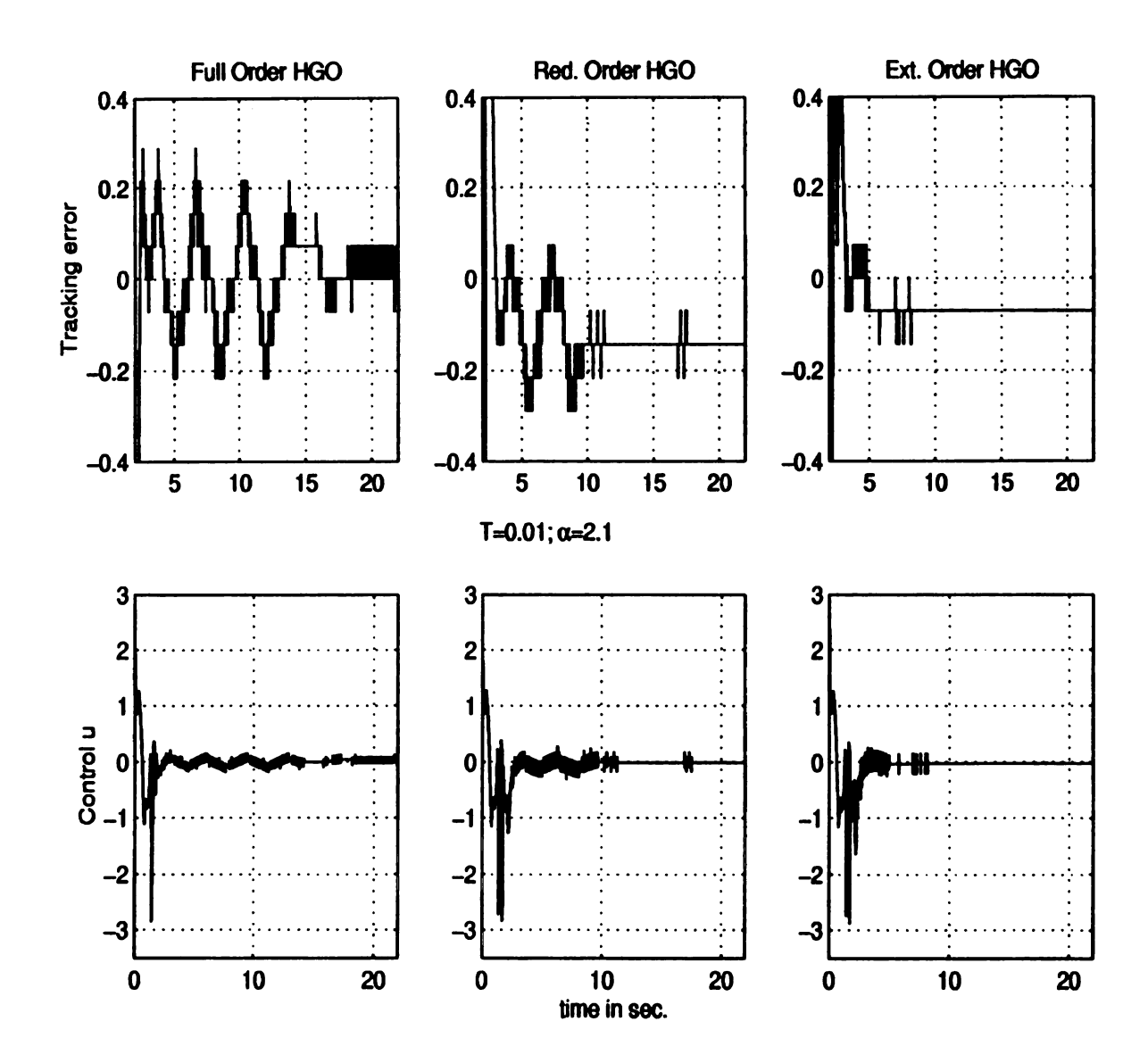


Figure 4.10. Tracking error e and control signal for the full, reduced and extended order HGO using the bilinear transformation, T = 0.01 and  $\alpha = 2.1$ .

aggressive, and we need to lower the saturation level. Moreover, peaking saturates the controller, which disturbs the swing up control and the controller fails to balance the arm. So, we study the effect of increasing  $\alpha$  while the sampling period is fairly large, such as fixing T at 0.01 sec. For  $\alpha \leq 2$   $\epsilon$  is not sufficiently small. For  $\alpha = 2.1$  the high-gain observer (discretized by the bilinear transformation method) gives good estimates of the speed and the controller balances the pendubot arms. Increasing  $\alpha$  improves the performance by decreasing the estimation error. Figure 4.11 confirms the results of Chapter 2. It is important to draw attention to the need of lower saturation levels, for  $\alpha > 3.0$ . We find out that we need to saturate the outer-loop control  $v_1$  such that  $-130 \leq v_1 \leq 120$  only for the swing up period. For  $\alpha > 6$  peaking makes it difficult even with saturation to make the swing up successful.

#### 4.7.2 Confirmation of the Closed-Loop Study

The high-gain observer poles are located at  $s = -1/\epsilon$ . We use the bilinear transformation method for the discretization of the HGO. We are going to discuss the following points:

- 1. saturation as a tool to overcome peaking;
- 2. effect of decreasing  $\epsilon$  on the steady state error;
- 3. linear vs. nonlinear HGO; and
- 4. how large the sampling period can be.

#### **Peaking and Saturation**

As the observer parameter  $\epsilon$  decreases, the peaking effect increases. Since this reduction of  $\epsilon$  can be done by more than one method, the study is divided into two parts.

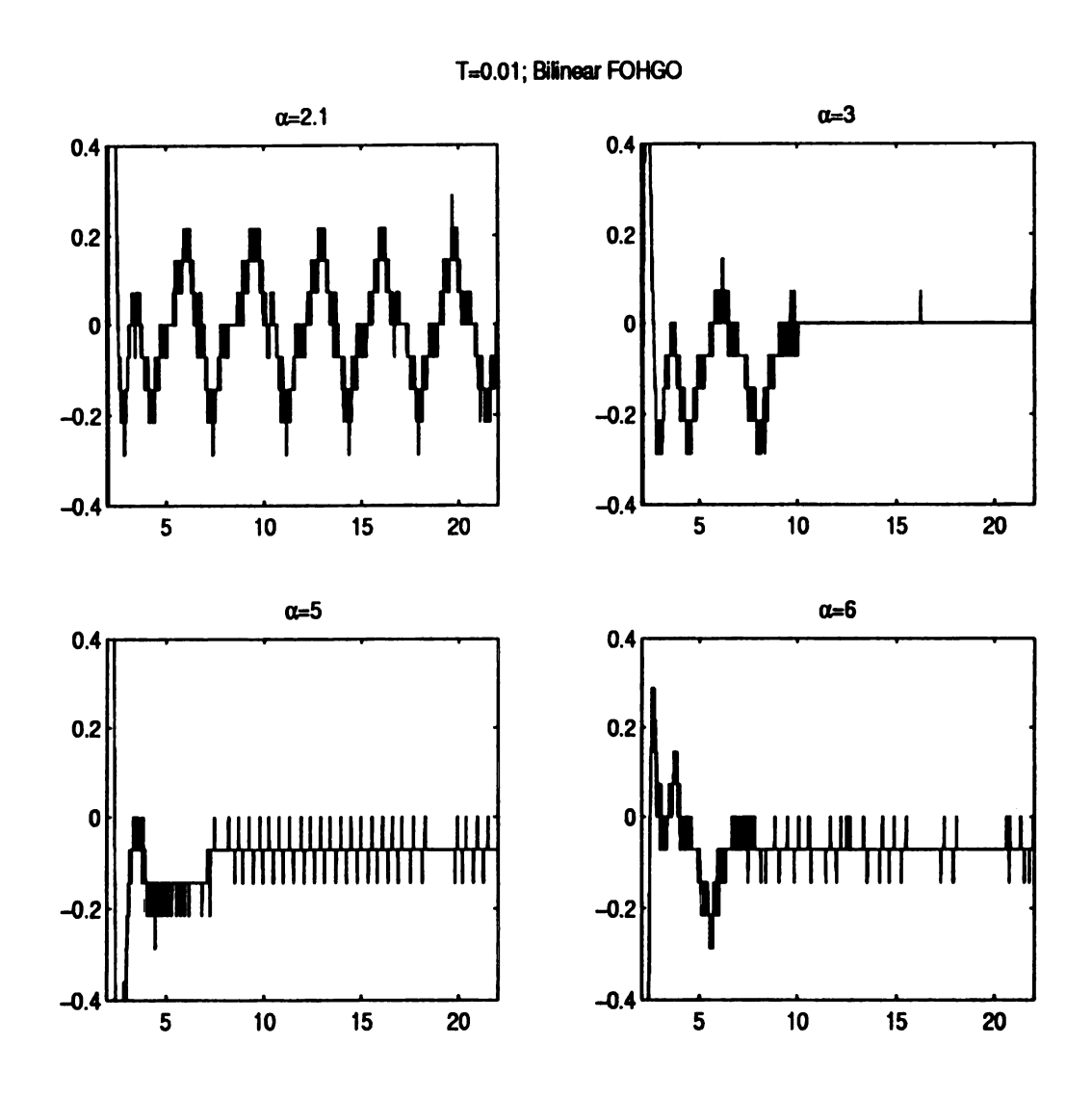


Figure 4.11. Effect of increasing the ratio  $\alpha=T/\epsilon$  on the full order HGO with real poles at  $s=-1/\epsilon$ , T=0.01 and  $\alpha=2.1$ , 3.0, 5.0, ,6.0 respectively.

First, the sampling time T is fixed and  $\epsilon$  is decreased through increasing  $\alpha = T/\epsilon$ . Second,  $\alpha$  is fixed and T is decreased.

Let us start by taking the initial conditions of the observer to be the same as the system  $(\hat{x}(0) = x(0))$ . This is a case of no peaking since peaking is induced by the difference  $\hat{x}(0) - x(0)$ . Figure 4.12 represents the first case (T is fixed) where we can see that increasing  $\alpha$  doesn't change the starting level of  $x_2$ . Figure 4.13 shows the control magnitude which, in all cases, is less than 3 volts at the starting point.

For the second case as we decrease T and keep  $\alpha=2.5$  fixed. The speed estimate for link one has the same starting point as T decreases but reaches steady-state faster as shown in Figure 4.14. The same thing happens for the control as shown in Figure 4.15.

Now let us initiate the observer at  $\hat{x}(0) = 0$ , which is different than the system initial condition x(0). Figure 4.16 represents the first case where we can see that increasing  $\alpha$  increases the peaking level in  $x_2$ . This affects the control magnitude by bringing more oscillation during the transient period as shown in Figure 4.17. Notice that the control is saturated at the device limit, *i.e.*,  $|u| \leq 10$  volts, while in the no-peaking case the control signal is  $|u| \leq 3$  volts.

For the second case as we decrease T and keep  $\alpha=2.5$  fixed, the speed estimate for link has more peaking as T decreases, but reaches steady-state faster as shown in Figure 4.18. The same thing happens for the control as shown in Figure 4.19. With large peaking, the balancing control fails to bring the pendulum arm to the balancing region. This puts a limit on how small  $\epsilon$  could be , i.e, how small T when  $\alpha$  is fixed or how large  $\alpha$  when T is fixed. For example, if  $\alpha=4$  we cannot reduce T beyond 0.006 sec. This is contrasted with the no peaking case (when  $\hat{x}(0)=x(0)$ ) where T can be reduced to 0.003 sec. Smaller values of  $\epsilon$  result in smaller steady-state errors.

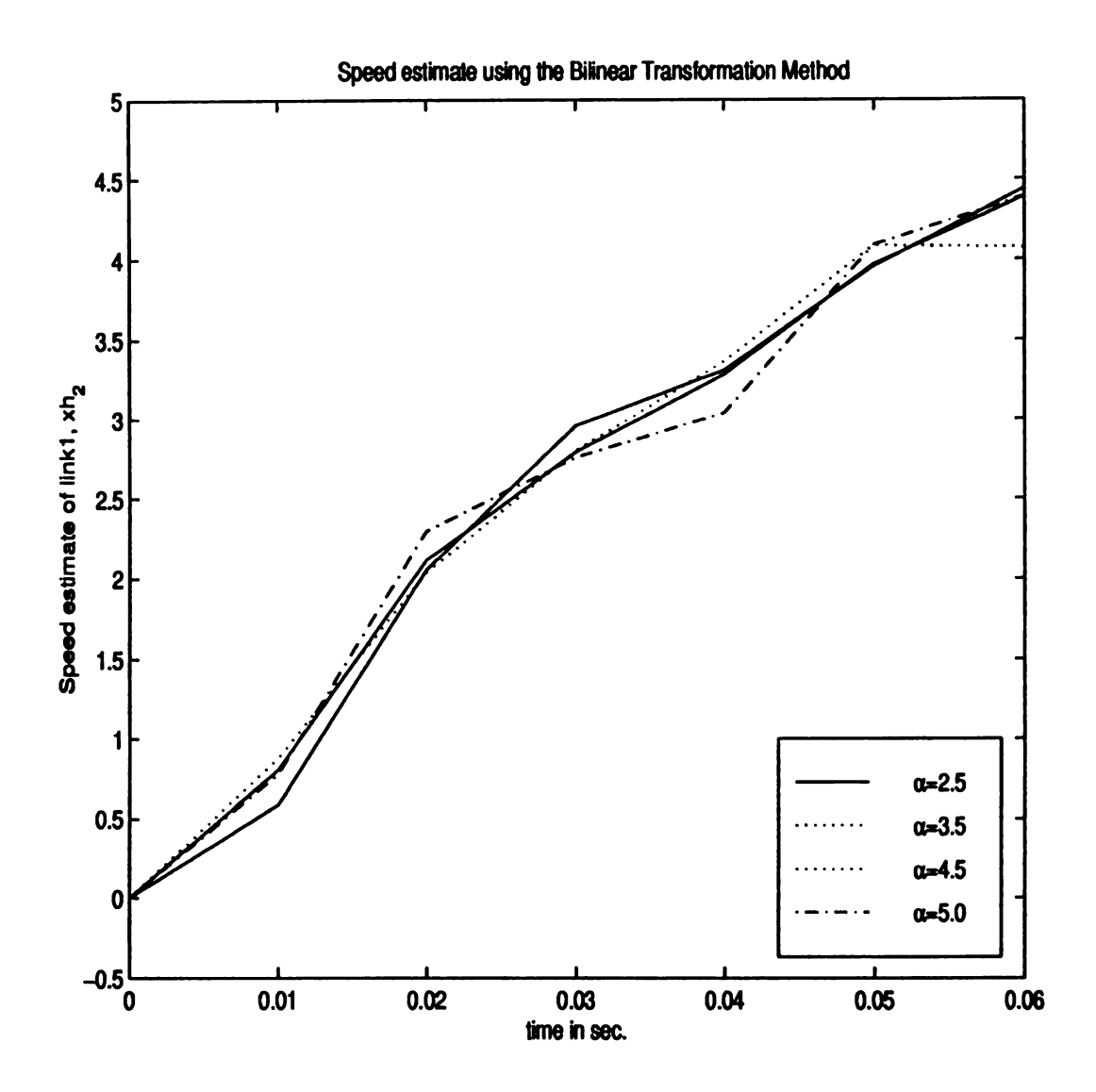


Figure 4.12. The transient of estimating speed of the first link as  $\alpha$  increases while T=0.01

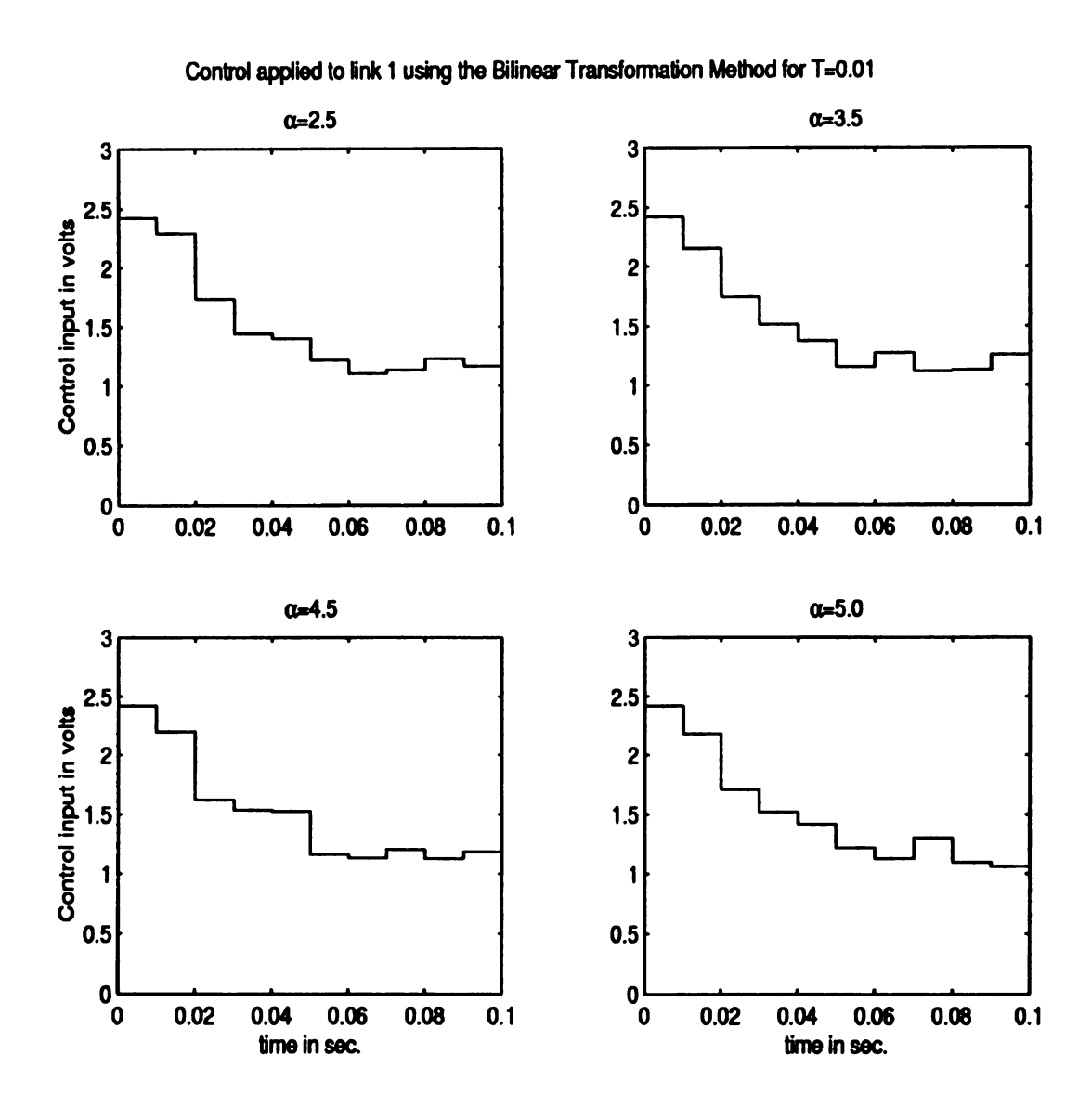


Figure 4.13. The control during the transient period as  $\alpha$  increases while T=0.01

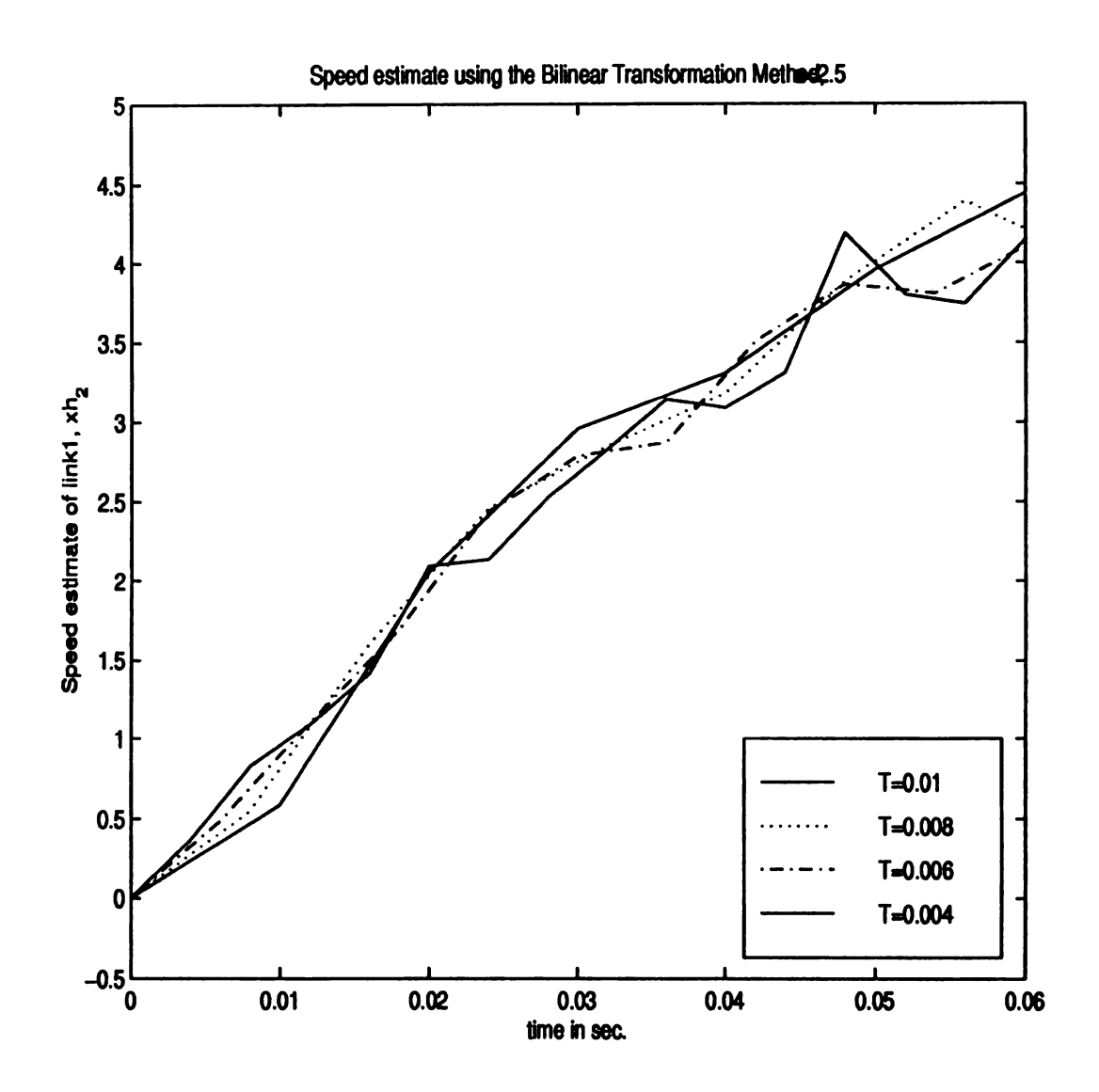


Figure 4.14. The transient speed of link one while T decreases

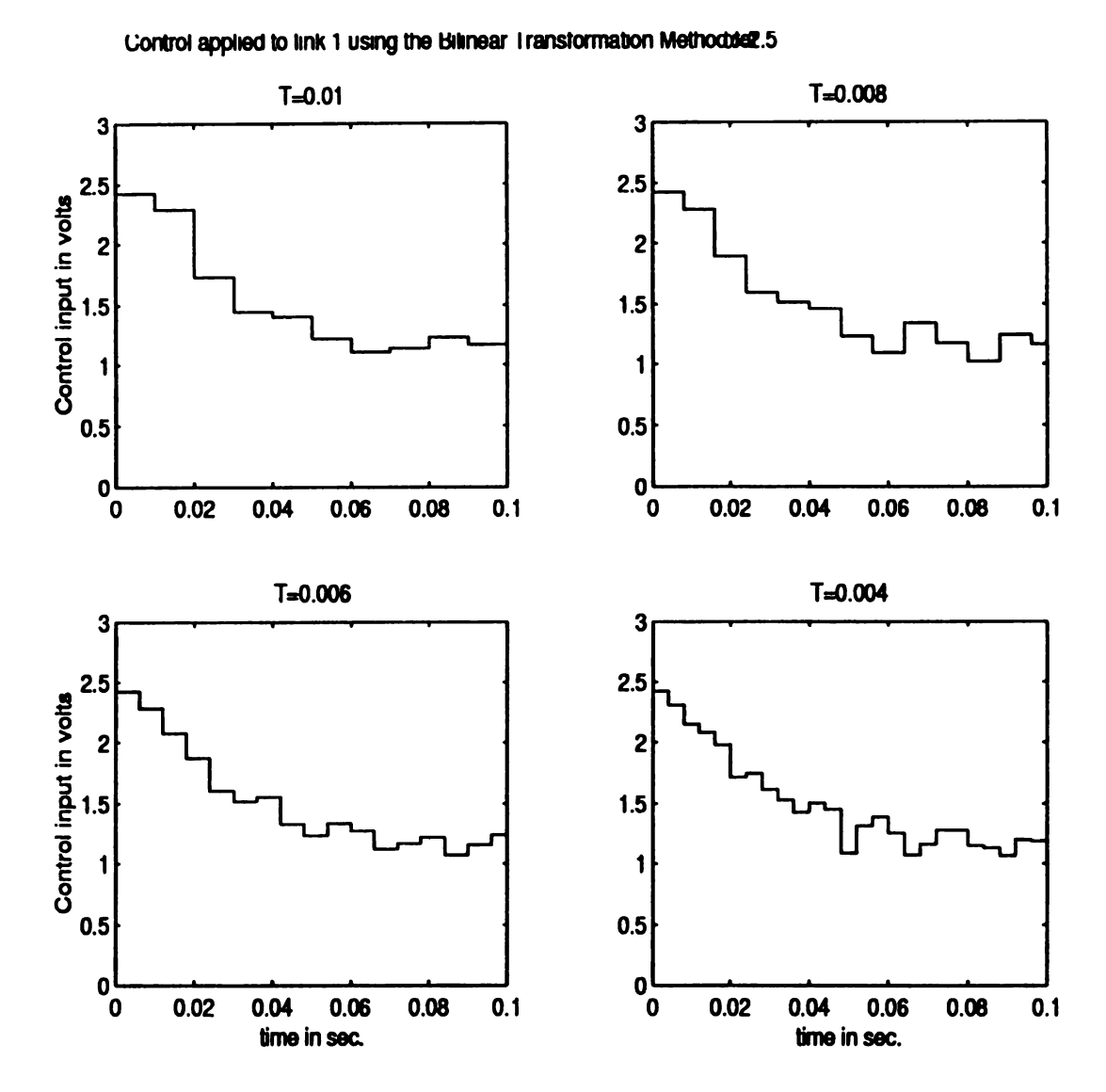


Figure 4.15. The control during the transient period as T decreases

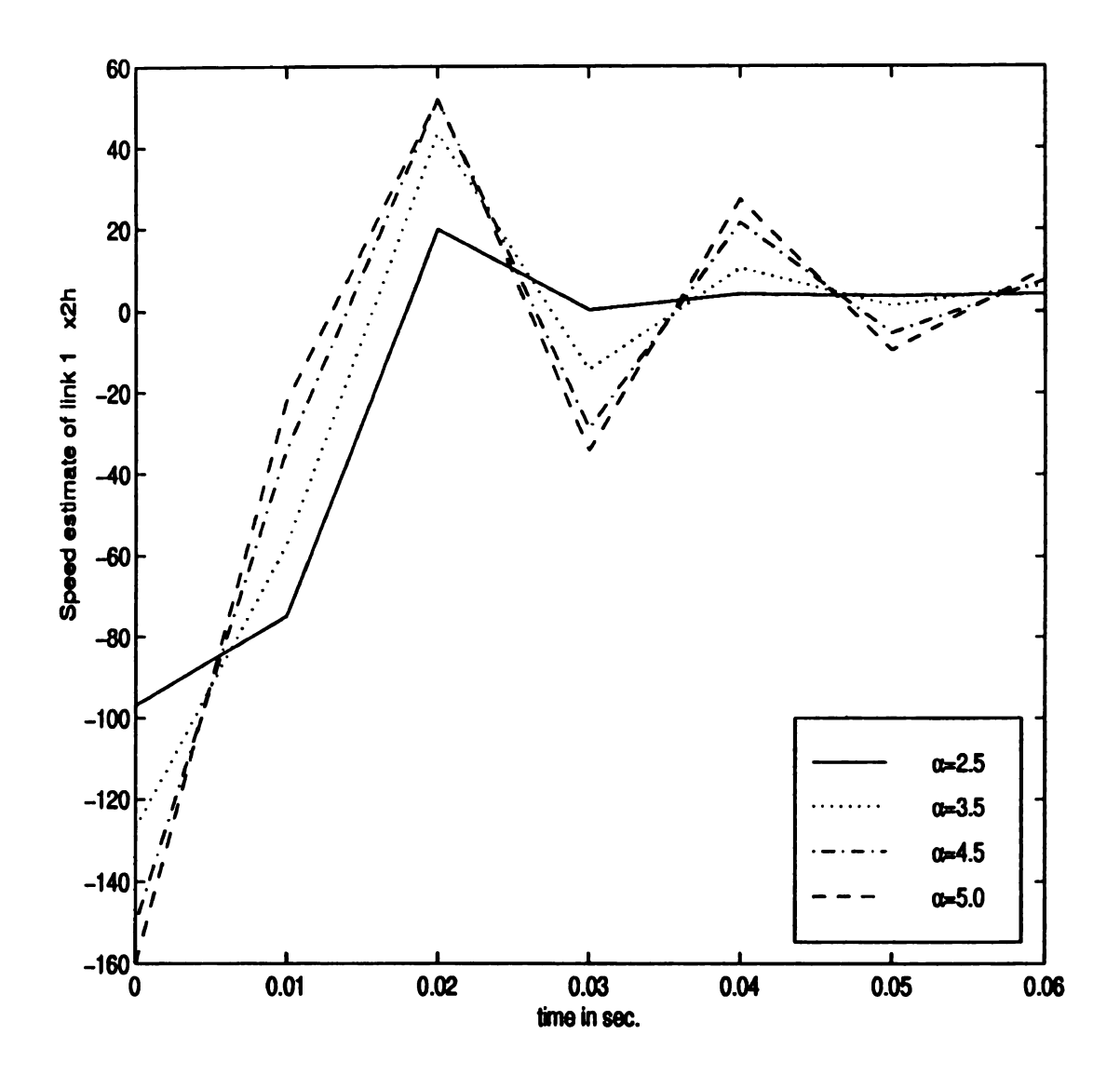


Figure 4.16. Peaking in the transient of estimating speed of the first link as  $\alpha$  increases while T=0.01

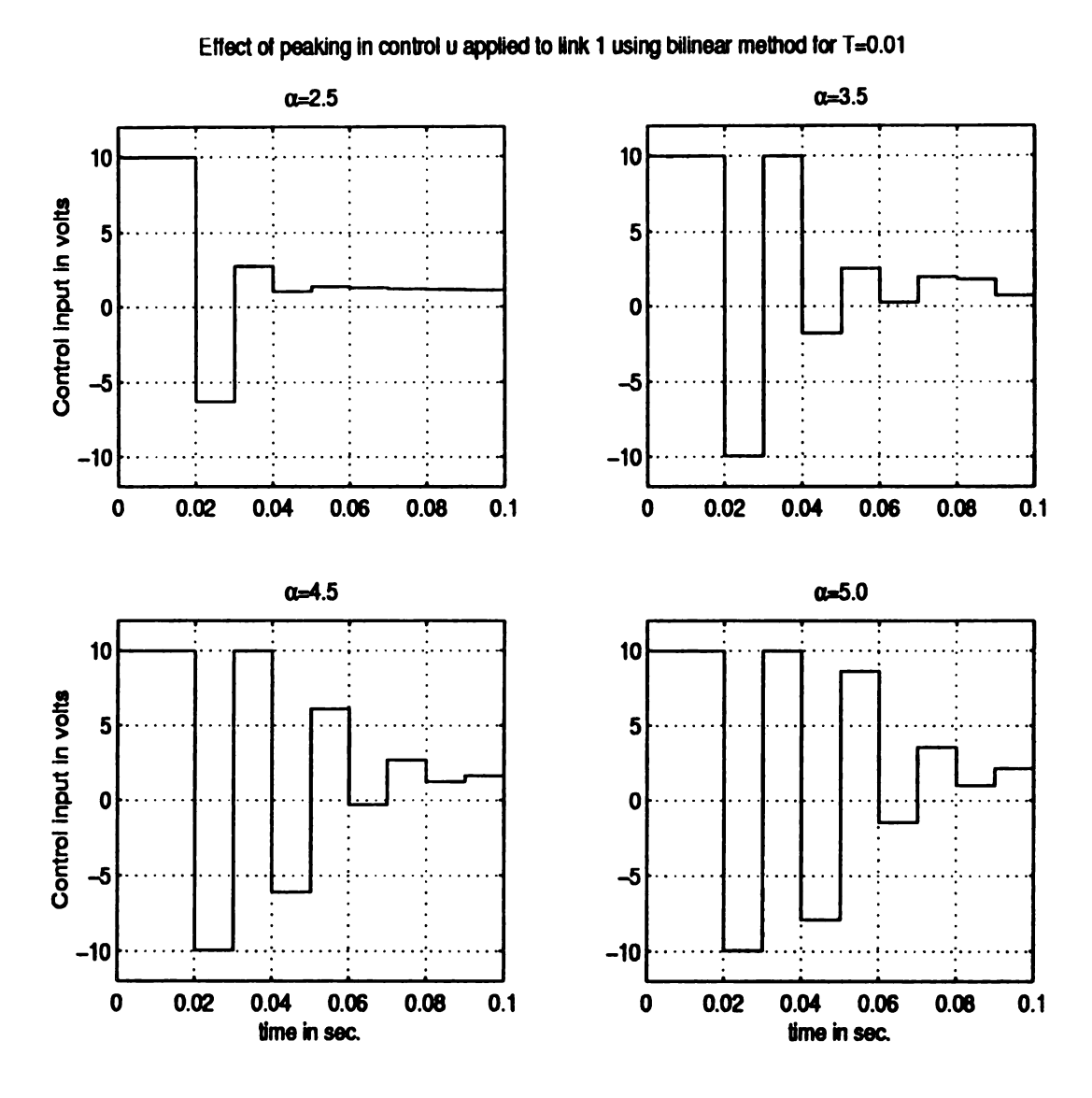


Figure 4.17. The effect of the peaking on the control during the transient period as  $\alpha$  increases while T=0.01

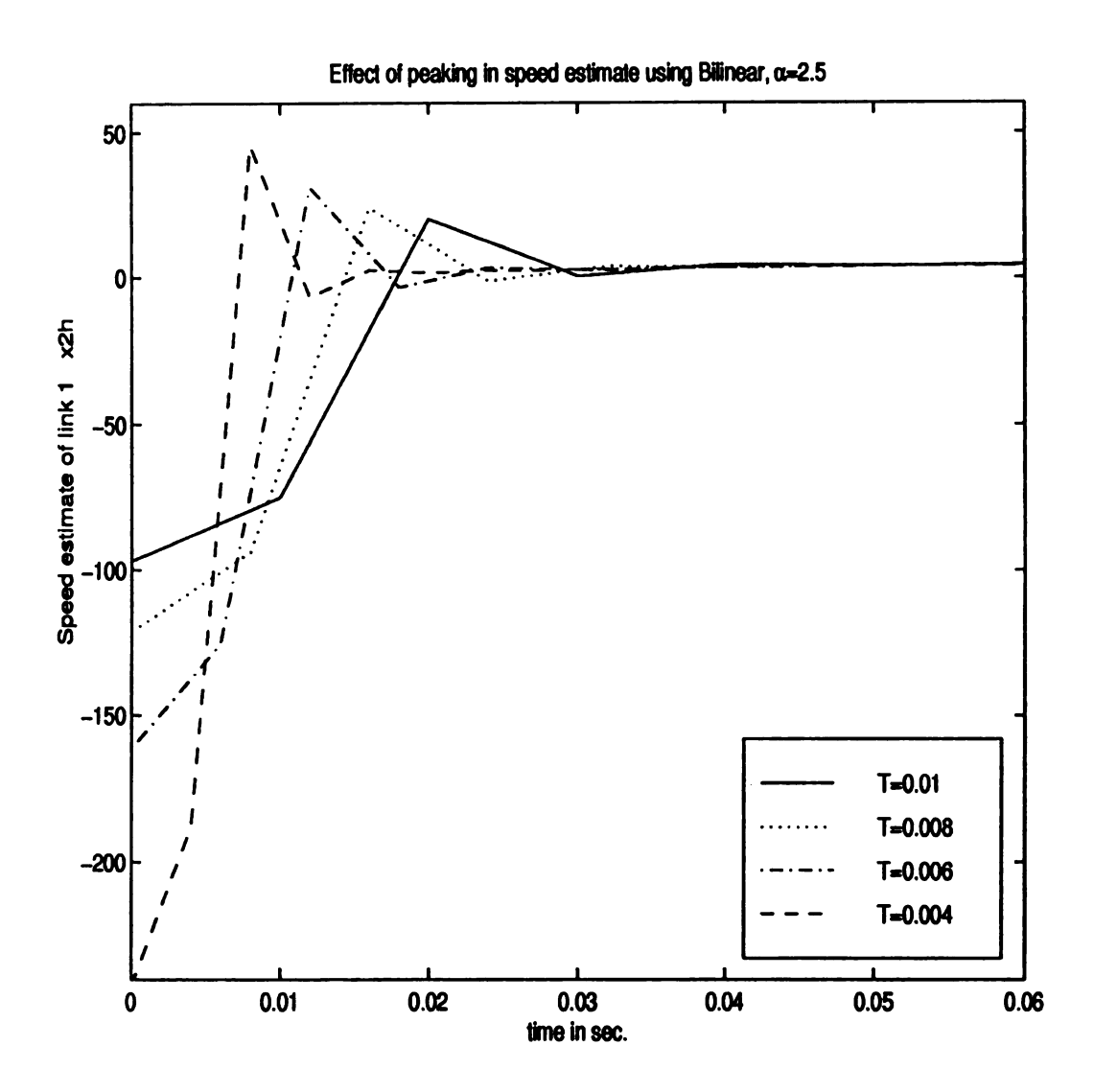


Figure 4.18. Peaking in the transient speed of link one while T decreases

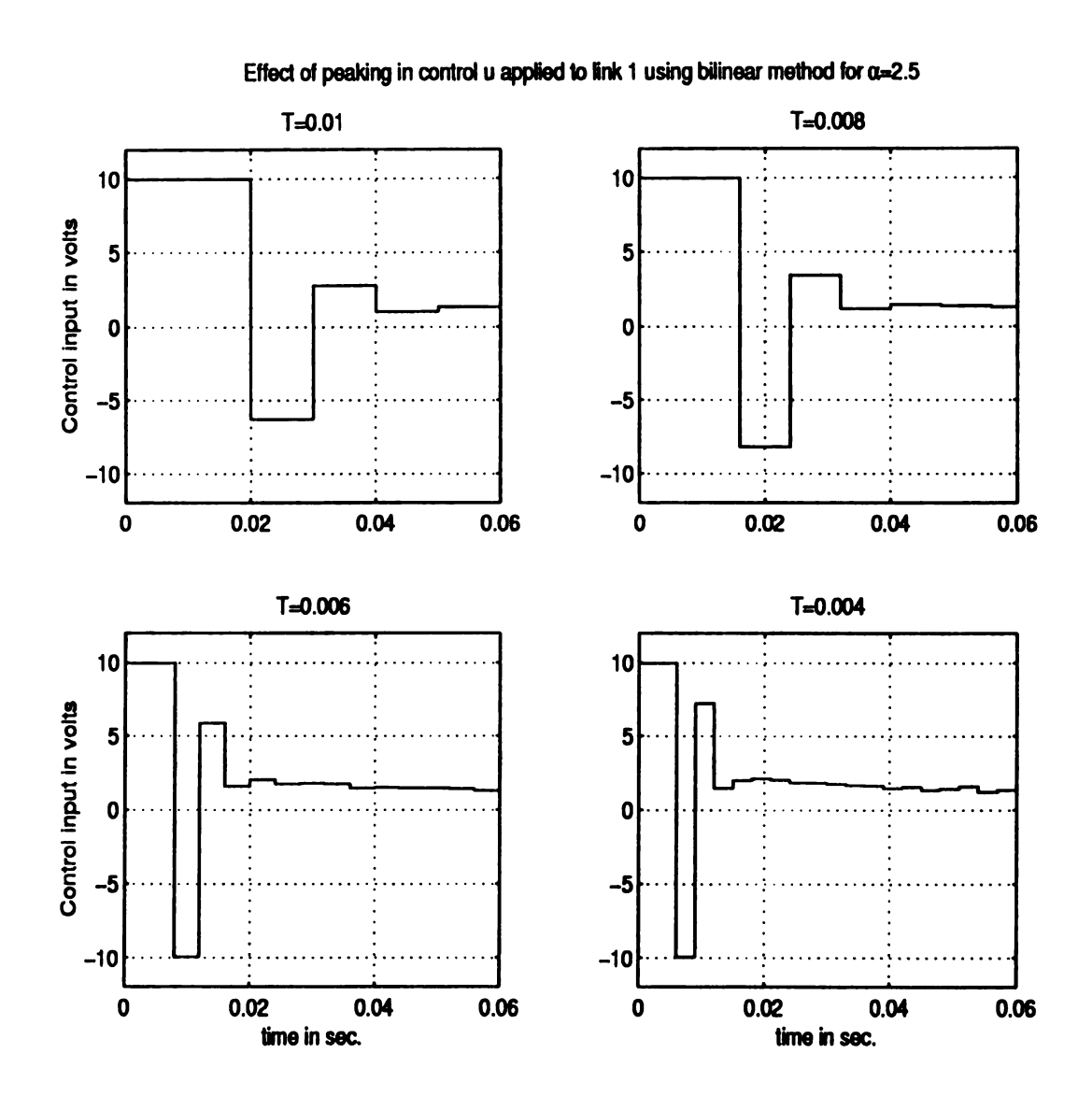


Figure 4.19. The effect of the peaking on the control during the transient period as T decreases

#### **Steady-State Tracking**

In this part of the experiment we study the effect of decreasing  $\epsilon$  on the steady state tracking error. The parameter  $\epsilon$  can be decreased as long as the linear observer poles remain inside the unit circle. In the bilinear transformation and backward difference methods the poles are always inside the unit circle. In the presence of noise, increasing  $\alpha$  increases the bandwidth of the HGO which leads to complete or partial distortion of the estimates, depending on the signal to noise ratio. Figure 4.20 shows the effect of increasing  $\alpha$  when T=0.003 sec.. Increasing  $\alpha$  reduces the transient time. We can obtain the same result by fixing  $\alpha=3.0$  and decreasing T as shown in Figure 4.21. These two results confirm Theorem 3.1.

#### Linear versus Nonlinear HGO

In this part we study the use of linear versus nonlinear high-gain observers to estimate the pendubot states. Many runs were made to detect if there was any difference between the two observers. We did not find noticeable differences between the two observers. Figure 4.22 shows the steady-state error in one run of the experiment for both observers, while Figure 4.23 shows another run. The two observers act almost the same and this could be because of uncertainty in the model parameters. Paper [8] reports an improvement with the nonlinear observer when the model is known.

#### Comparison between HGO and Euler method

It is shown in Section 2.5 that the Euler method (the most common method for estimating speed from optical encoder) is a special case of a reduced-order high-gain observer discretized using the forward difference method with  $T/\epsilon = 1$ . This is just one of many options we have when we address the problem as a high-gain observer design. We can choose between reduced-order and full-order observers. Within each

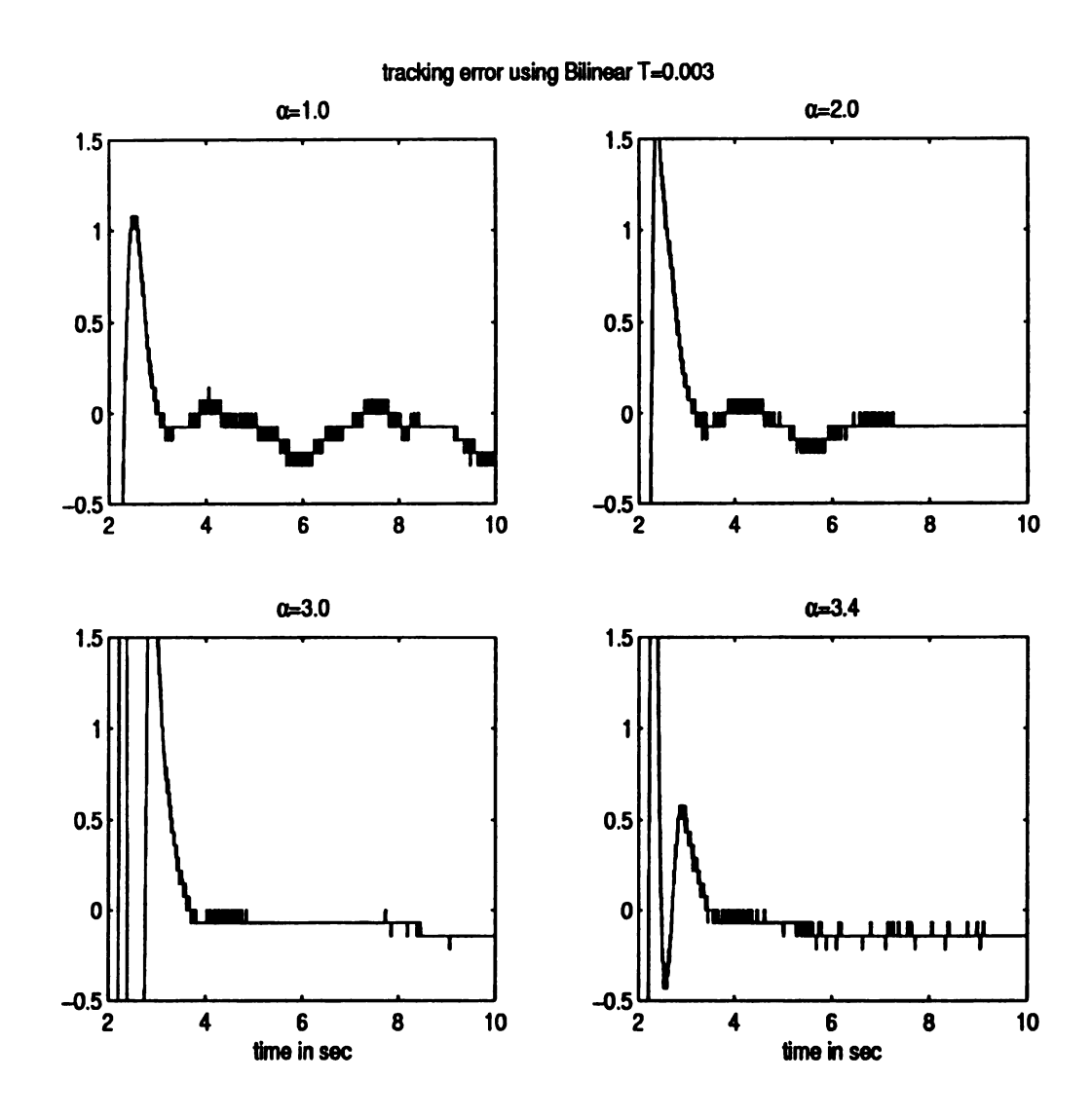


Figure 4.20. The sampling time T=0.003 is fixed while  $\alpha$  is increased

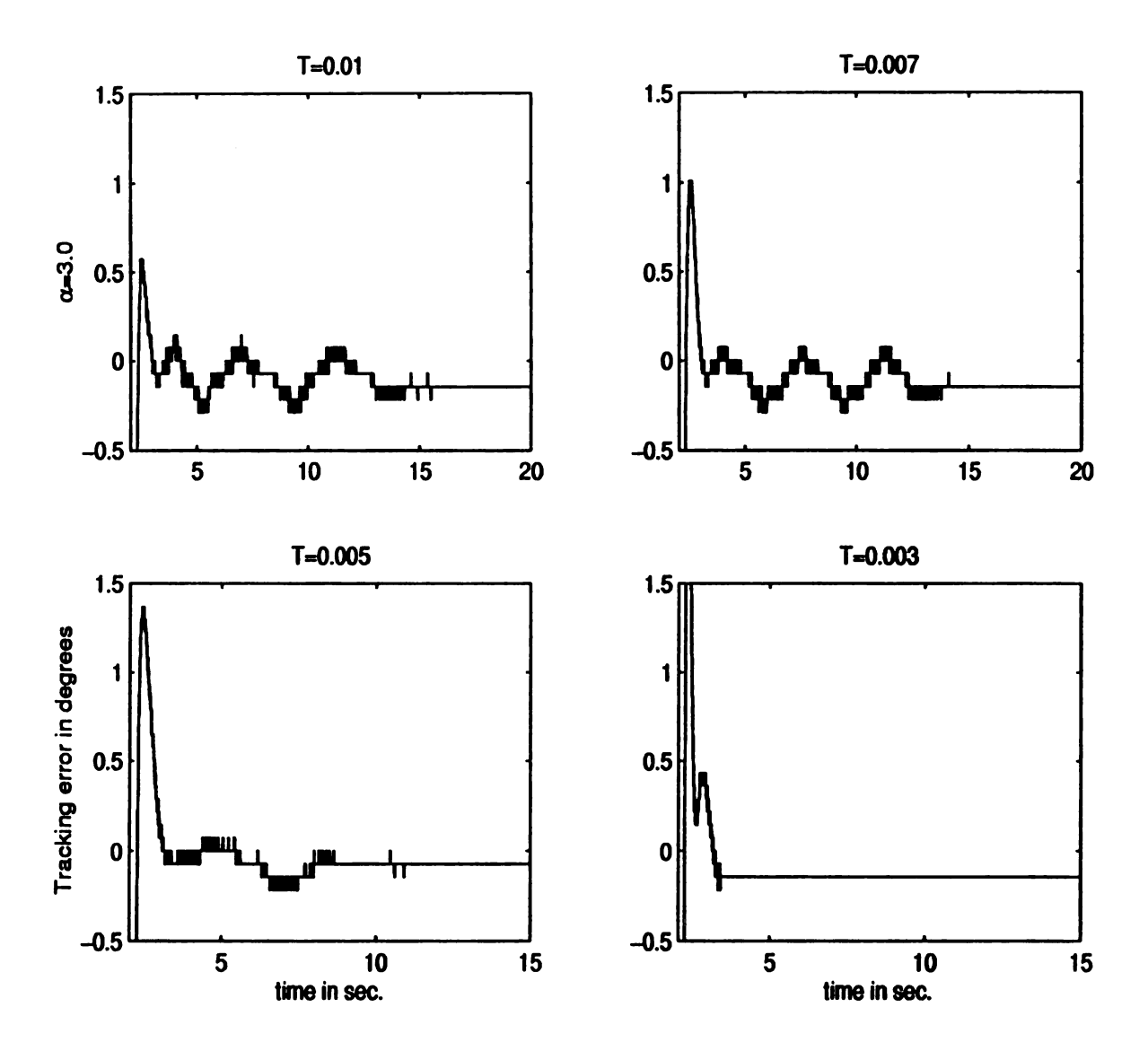


Figure 4.21. Fixing  $\alpha = 3.0$  and decreasing the sampling time T

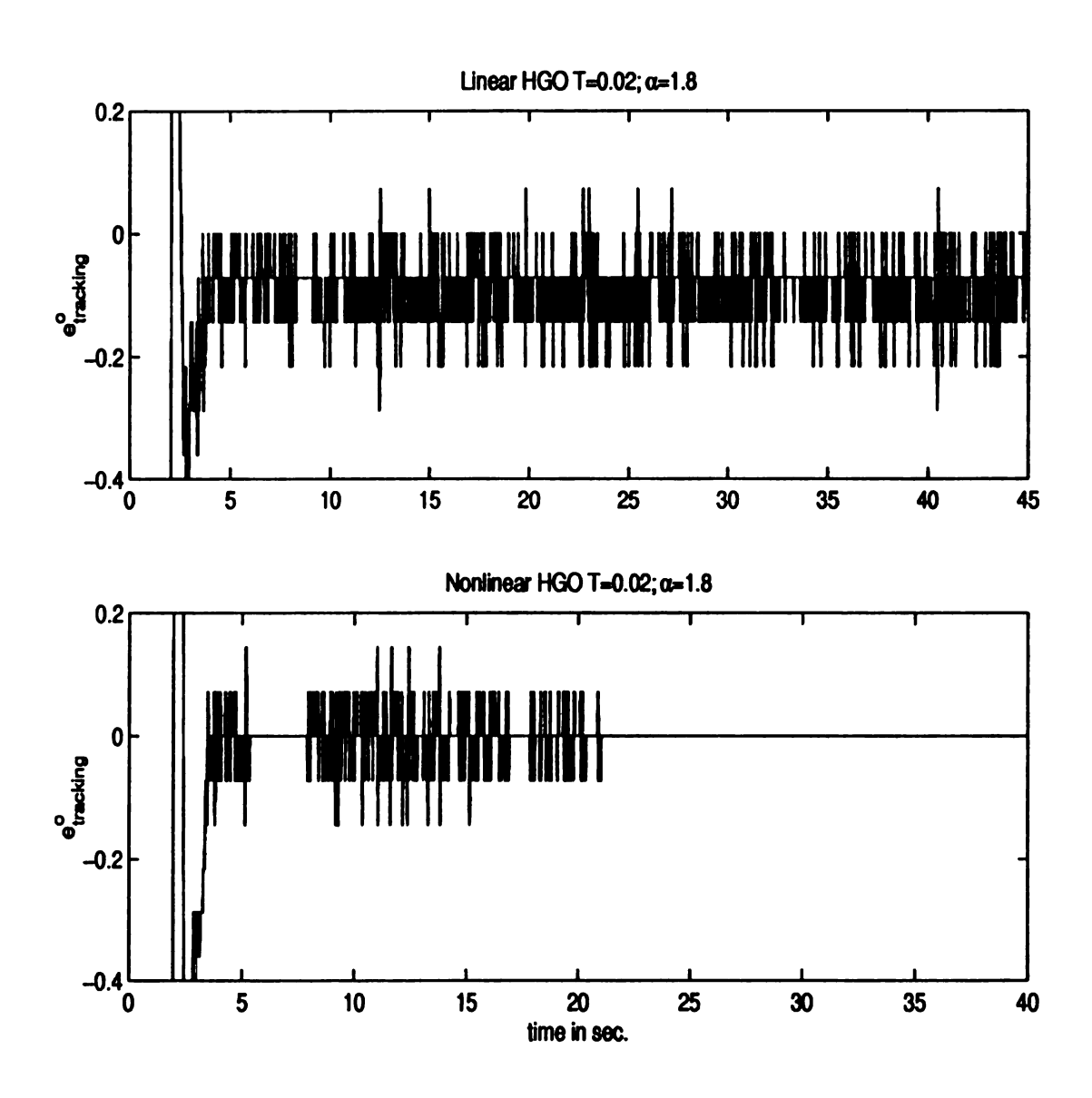


Figure 4.22. Tracking error at steady-state using linear and nonlinear HGO.

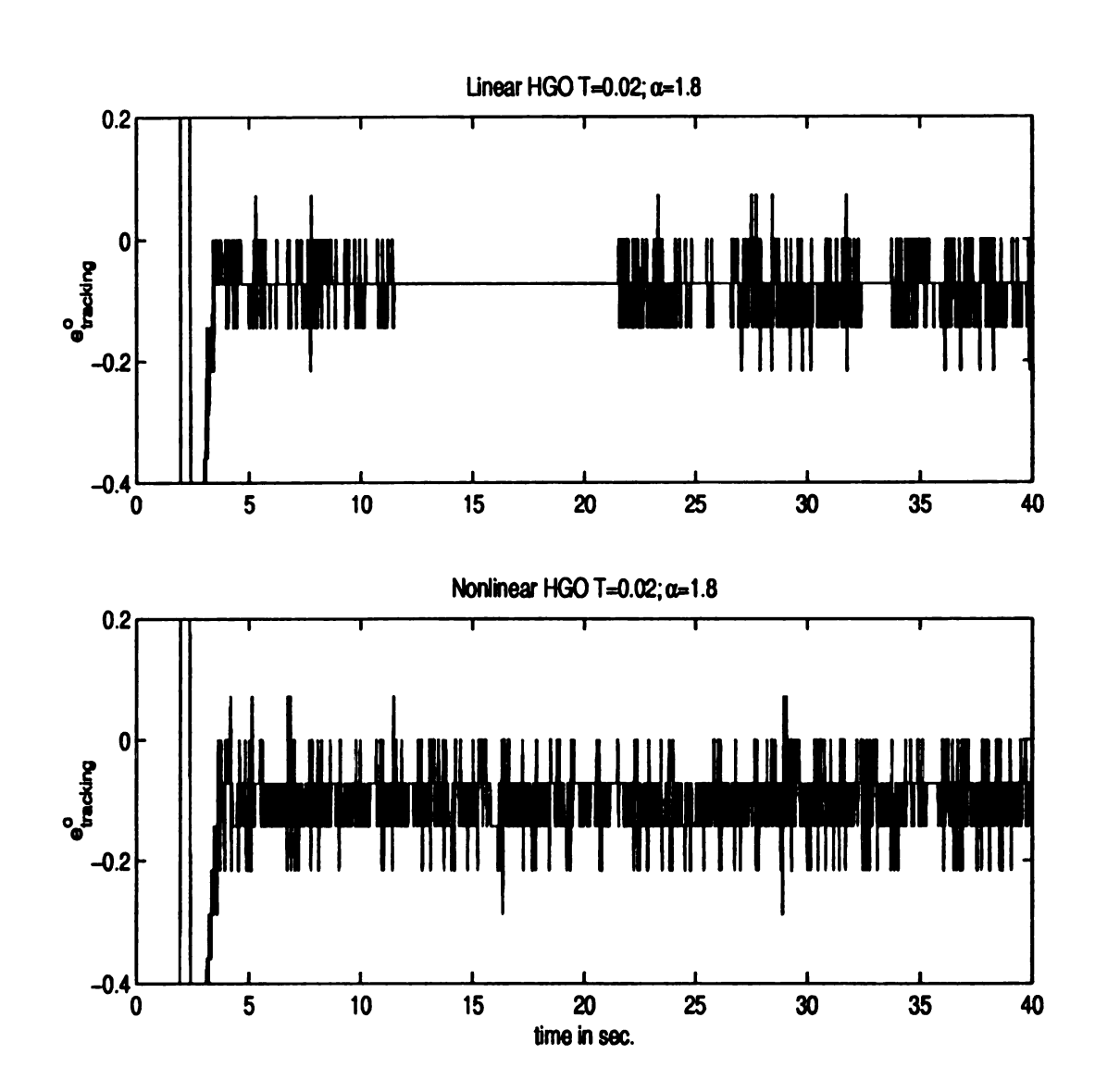


Figure 4.23. Tracking error at the steady-state using the linear and nonlinear in another run

type, we have the flexibility of choosing several design parameters, most important of which is the ratio  $T/\epsilon$ . We also have the freedom to use different discretization methods. We have explored many of these options in Section 2.5. In this section we explore some of these options, as applied to the pendubot, and compare the results with those obtained using the Euler method and a variant of it.

The pendubot manufacturer provided an averaged Euler formula to estimate the links, speed, where the sum of the last three calculated speeds by the Euler formula was divided by 3. Notice that, for this method to work it needs very small sampling period. Figure 4.24 compares the operation range for the different discretization methods of the high-gain observers and the Euler method, with and without averaging. By operation range we mean how large the sampling period can be before the controller fails to balance the pendulum. This figure shows that the use of the reduced order high-gain observer can guarantee larger operation range (larger sampling period). The Euler formula fails for T > 0.04 sec. Figure 4.25 shows that for larger sampling periods the high-gain observer outperforms the Euler method for the same sampling period T = 0.04 sec. Even if we discretize the high-gain observer with T = 0.06 and compare its performance with the Euler formula when T = 0.04, the reduced order HGO outperforms the Euler formula. Figure 4.24 shows also that the Euler method with averaging can not work for T > 0.01.

### 4.8 Conclusion

The experimental results confirm our earlier simulation and analytical results. Comparison of the three discretization methods (forward, backward and bilinear transformation methods) showed that the bilinear transformation method provides a larger range of operation when  $\alpha$  increases while T is fixed. This feature helps in reducing the transient time. After adapting the bilinear transformation as the discretization

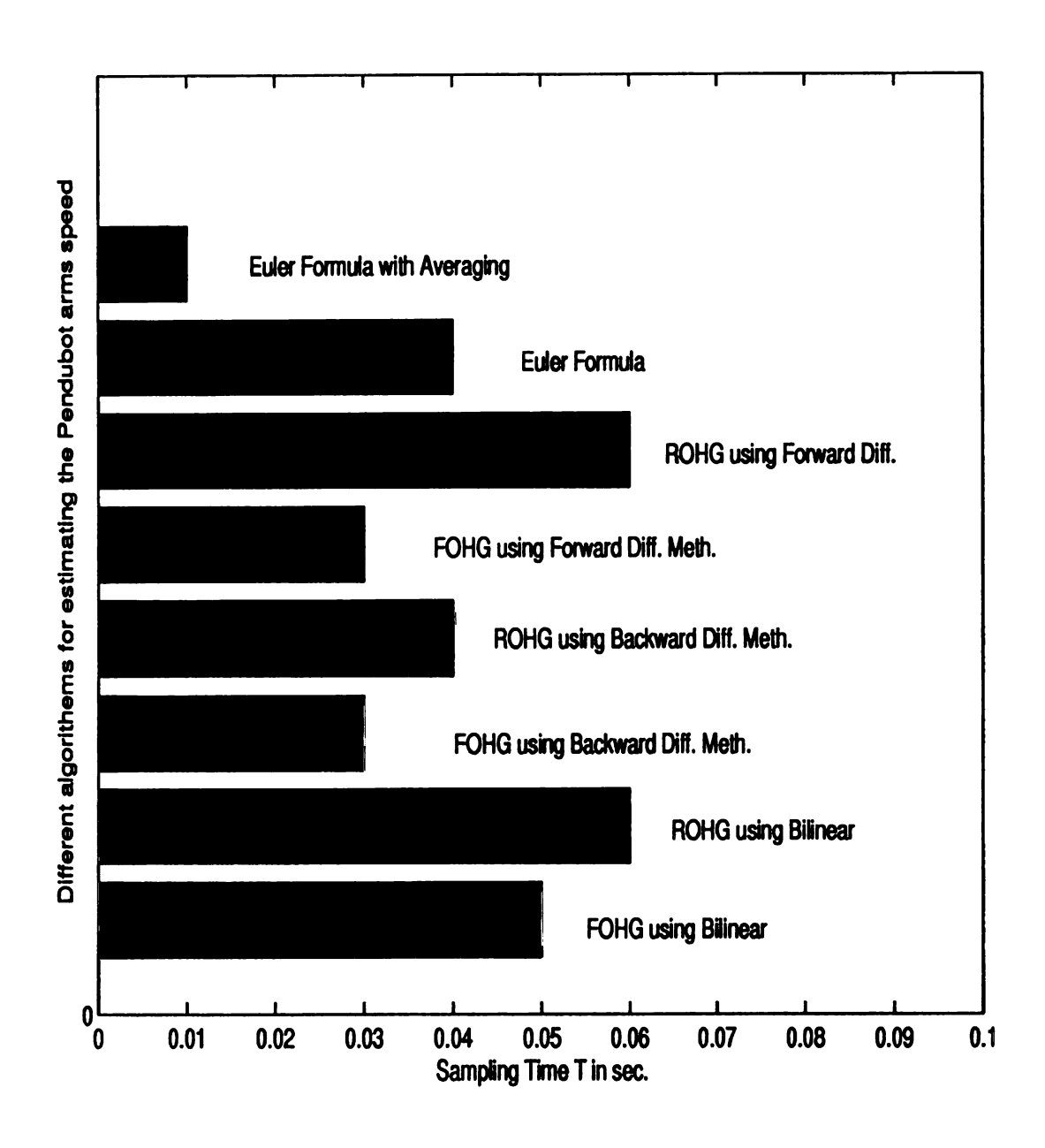


Figure 4.24. Comparison of the different discretization methods of the full order (FOHG) and reduced order (ROHG) with the Euler formula with and without averaging

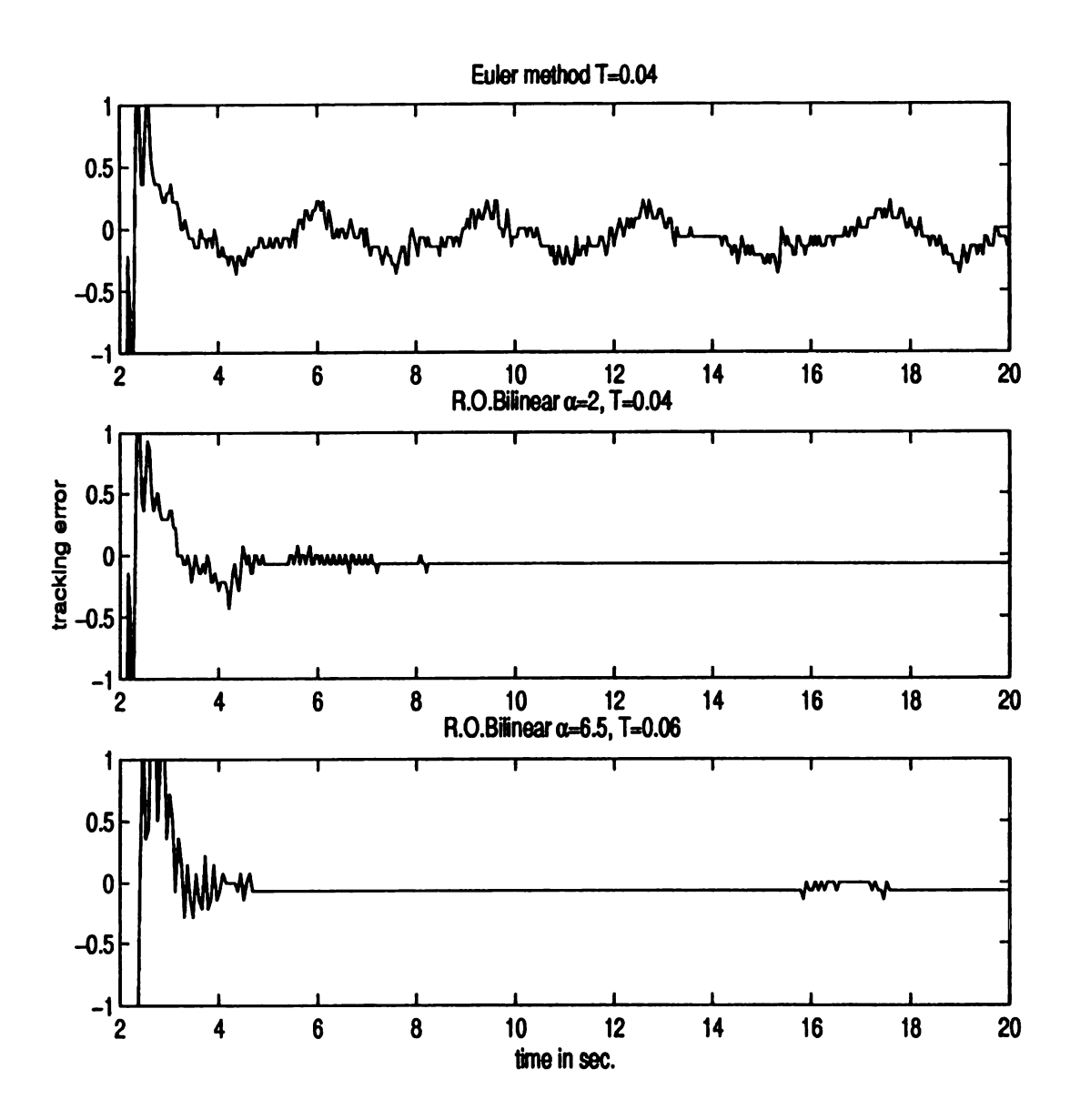


Figure 4.25. Comparing the performance of the reduced order HGO discretized by bilinear method for  $\alpha=2$  and T=0.04 and  $\alpha=6.5$  and T=0.06 with the Euler method when T=0.04 sec.

method we confirmed all the results of Chapter 2.

The closed-loop study targeted different issues, such as the effect of peaking and how the global saturation of the control will preserve stability of the closed-loop system. Regarding the effect of decreasing  $\epsilon$  on the steady-state tracking error, it was shown how the steady-state error improves as  $\epsilon$  becomes sufficiently small, which confirms Theorems 3.1 and 3.2. Comparison of the linear and nonlinear high-gain observers showed no advantage for one over the other. Comparison of the performance of the high-gain observer versus the Euler method showed that there is a definite advantage for approaching the problem as a digital high-gain observer design rather than simply using the Euler method. This advantage can be seen in two ways. First, the high-gain observer can work for a larger range of sampling periods compared with the Euler method. Second, for the same sampling period, the high-gain observer produces better performance with less oscillation at steady state.

## CHAPTER 5

## Conclusions and Future Work

#### 5.1 Conclusions

This thesis presents a separation principle for sampled-data control of a class of nonlinear systems. The basic ingredients of this technique are: a continuous-time high-gain observer that robustly estimates the derivatives of the output, a global bounded state feedback control, and a discrete-time implementation of the high-gain observer. For sufficiently small sampling period and sufficiently high observer gain, the sampled-data controller recovers the performance of the continuous-time state feedback controller. The high-gain observer is discretized using different discretization methods to achieve the best discretization algorithm and parameters choice.

Chapter 2 provides answers to a number of important questions such as: what is the best discretization method? what are the best choices for the observer parameters  $\alpha_i's$  and  $\epsilon$  and how do they relate to the sampling period T? and what is the effect of the order of the observer on the estimation of the output derivatives. This is done for noisy as well as noise-free measurements. We also show how other numerical differentiators are special cases of the high-gain observer discretized by the bilinear discretization method. The study can be extended to multi-input multi-output systems. From the simulation-based study of Chapter 2 we move into closed-

loop analysis of Chapter 3. We study sampled-data controllers which use discretized high-gain observers. The closed-loop analysis shows that the sampled-data output feedback controller recovers the performance of the continuous-time state feedback controller as the sampling frequency and the observer gain become sufficiently large. Performance recovery is shown in two steps. First we show boundedness of trajectories which come arbitrarily close to the origin as time progress. Second, we assume that the origin of the continuous time system is exponentially stable and show that trajectories converge to the origin.

In Chapter 4, we take the theoretical results one step farther by experimentally testing the use of the discretized high-gain observer in controlling the pendubot. We show how saturation is used to overcome peaking and the effect of decreasing  $\epsilon$  on the steady-state error. The experimental results agree with and confirm all conclusions of Chapters 2 and 3. Moreover, we show that the discretized high-gain observer outperforms the Euler formula as a means for calculating velocities from optical encoder.

#### 5.2 Future Work

There are two lines for future work: one is extending the scope of studies done in the thesis and the other is using the developed tools and techniques to study sample-data control of nonlinear systems even when no high-gain observer is used.

# 5.2.1 Extending the Scope of the Sampled-Data Observer-Based Control

The assumptions used in achieving the results of this thesis are based on exponential stability of the equilibrium point and the use of static feedback control for stabilization. These assumptions were used in the early work on the continuous-time case,

but later on the work was extended to cover more cases. There is room for extending our discrete-time results to include the following:

- the use of dynamic controllers as in the work of Atassi and Khalil [8];
- replacing exponential stability with asymptotic stability;
- developing the results for other control problems such as tracking, adaptive control, and servomechanisms, in the spirit of [4, 33, 32, 42, 43, 27, 63, 15].
- experimentally applying the discrete-time high-gain observer to applications
  where higher derivatives of the output are needed such as the induction motor
  controller of [31] which requires both velocity and acceleration estimates.

#### 5.2.2 Sampled-Data Control

Using the tools and techniques developed in the thesis, we can address other sampled-data control problems. In particular, we can address the question of what we can prove about the behavior of sampled-data control under fast sampling. Some researchers address this question either by obtaining local results using linearization [11] or nonlocal results using some sophisticated techniques as the work of Teel at el [65] which models the zero-order hold as a time delay element. The techniques developed in the thesis can be used to provide some nonlocal results for sampled-data control of nonlinear systems with fast sampling, in a way that could be much simpler than [65].

# **APPENDICES**

## APPENDIX A

# **Appendix**

# A.1 Developing The Singularly Perturbed Form For The Forward Difference Method

The state equations of the closed-loop system are

$$\chi(k+1) = \chi(k) + \epsilon \Psi(\chi(k), u(k), \epsilon) 
\eta(k+1) = A_f \eta(k) + \frac{1}{\epsilon^{r-1}} D\left[x(k+1) - x(k) - TA_c x(k)\right] 
x(k+1) = x(k) + \sum_{l=1}^{r-1} \frac{T^l}{l!} A_c^l x(k) + \sum_{l=1}^r \frac{T^l}{l!} A_c^{l-1} B_c G_l(\chi(k), u(k)) 
+ T^{r+1} R_x(\chi(k), u(k), T)$$

The negative power of  $\epsilon$  appear in the term

$$\begin{split} &\frac{1}{\epsilon^{r-1}}D\left[x(k+1)-x(k)-TA_{c}x(k)\right] \\ &= \frac{1}{\epsilon^{r-1}}D\left[\sum_{l=2}^{r-1}\frac{T^{l}}{l!}A_{c}^{l}x(k)+\sum_{l=1}^{r}\frac{T^{l}}{l!}A_{c}^{l-1}B_{c}G_{l}(\cdot)+T^{r+1}R_{x}(\cdot)\right] \\ &= \sum_{l=2}^{r-1}\frac{\alpha^{l}}{l!\epsilon^{r-l-1}}DA_{c}^{l}x(k)+\frac{1}{\epsilon^{r-2}}\sum_{l=1}^{r}\frac{\alpha^{l}}{l!}A_{c}^{l-1}DB_{c}G_{l}(\cdot)+\alpha^{r-1}T^{2}DR_{x}(\cdot) \\ &= \sum_{l=2}^{r-1}\frac{\alpha^{l}}{l!\epsilon^{r-l-1}}DA_{c}^{l}x(k)+T\sum_{l=1}^{r}\frac{\alpha^{l-1}}{l!}A_{c}^{l-1}B_{c}G_{l}(\cdot)+T^{2}\alpha^{r-1}DR_{x}(\cdot) \end{split}$$

where we used  $DB_c = \epsilon^{r-1}B_c$ . Notice that all the summation terms will be limited to r-1 or r because  $A_c^r = 0$ . Rewriting  $\eta(k+1)$  we obtain

$$\eta(k+1) = A_f \eta(k) + \sum_{l=2}^{r-1} \frac{\alpha^l}{l! \epsilon^{r-l-1}} DA_c^l x(k) + T \left[ \sum_{l=1}^r \frac{\alpha^{l-1}}{l!} A_c^{l-1} B_c G_l(\cdot) + T \alpha^{r-1} DR_x(\cdot) \right]$$

Let  $H_l = \frac{\alpha^l}{l!}$  and

$$h(\chi(k), u(k), \epsilon) = \alpha \left[ \sum_{l=1}^{r} \frac{\alpha^{l-1}}{l!} A_c^{l-1} B_c G_l(\cdot) + T \alpha^{r-1} D R_x(\cdot) \right]$$

to obtain

$$\eta(k+1) = A_f \eta(k) + \sum_{j=2}^{r-1} \frac{1}{\epsilon^{r-j-1}} H_j D A_c^j x(k) + \epsilon h(\chi(k), u(k), \epsilon)$$

which represents (27), when  $\phi_o(\cdot) = 0$ , i.e., for the linear observer. It is clear that the negative power of  $\epsilon$  is limited to the summation part. We need to apply a change of variables in a number of steps to reduce the negative power of  $\epsilon$  by one in each step. At quasi steady state  $\eta(k+1) = \eta(k)$ , which can be written as

$$\eta(k) = A_f \eta_o(k) + \sum_{l=2}^{r-1} \epsilon^{l+1-r} H_l D A_c^l x(k) + \epsilon h(\chi(k), u(k), \epsilon)$$

$$\eta(k) = (I - A_f)^{-1} \left[ \sum_{l=2}^{r-1} \epsilon^{l+1-r} H_l D A_c^l x(k) + \epsilon h(\chi(k), u(k), \epsilon) \right]$$

Define  $\eta_1(k)$  as

$$\eta_1(k) = \eta(k) - (I - A_f)^{-1} \left[ \sum_{l=2}^{r-1} \epsilon^{l+1-r} H_l D A_c^l x(k) + \epsilon h(\chi(k), u(k), \epsilon) \right]$$

Then

$$\eta_1(k+1) = \eta(k+1) - (I - A_f)^{-1} \left[ \sum_{l=2}^{r-1} \epsilon^{l+1-r} H_l D A_c^l x(k+1) \right] + (I - A_f)^{-1} \left[ \epsilon h(\chi(k+1), u(k+1), \epsilon) \right]$$

We have expressions for  $\eta(k+1)$  and x(k+1), but we need to find an expression for  $h(\chi(k+1), u(k+1), \epsilon)$ . Since the control is globally bounded, u(k) and u(k+1) have the same order of magnitude, and so are  $\chi(k+1)$  and  $\chi(k)$ . This mean that the difference between  $h(\chi(k), u(k), \epsilon)$  and  $h(\chi(k+1), u(k+1), \epsilon)$  has the same order of magnitude. Substitute for  $\eta(k+1)$  and  $\chi(k+1)$ , and let  $\varrho = (I - A_f)^{-1}$ . The new state  $\eta_1(k+1)$  satisfies follow

$$\begin{split} \eta_{1}(k+1) &= A_{f}\eta_{1}(k) \\ &+ A_{f}\varrho \left[ \frac{1}{\epsilon^{r-1}} \sum_{j=2}^{r-1} \epsilon^{j} H_{j} D A_{c}^{j} x(k) + \epsilon h(\chi(k), u(k), \epsilon) \right] \\ &+ (I - A_{f})\varrho \left[ \frac{1}{\epsilon^{r-1}} \sum_{j=2}^{r-1} \epsilon^{j} H_{j} D A_{c}^{j} x(k) + \epsilon h(\chi(k), u(k), \epsilon) \right] \\ &- \varrho \left[ \frac{1}{\epsilon^{r-1}} \sum_{j=2}^{r-1} \epsilon^{j} H_{j} D A_{c}^{j} x(k) + \frac{1}{\epsilon^{r-1}} \sum_{j=2}^{r-1} \sum_{l=1}^{r-1} \frac{\alpha^{j} \epsilon^{j+l}}{l!} H_{j} D A_{c}^{j+l} x(k) \right] \\ &- \varrho \left[ \frac{1}{\epsilon^{r-1}} \sum_{j=2}^{r-1} \sum_{l=1}^{r} \frac{\alpha^{l} \epsilon^{j+l}}{l!} H_{j} D A_{c}^{j+l-1} B_{c} G_{l}(\chi(k), u(k)) \right] \\ &- \epsilon \varrho \left[ \alpha^{r+1} \sum_{j=2}^{r-1} \epsilon^{j+1} H_{j} D A_{c}^{j} R_{x}(\chi(k), u(k), \epsilon) + h(\chi(k+1), u(k+1), \epsilon) \right] \end{split}$$

We did multiply one of the brackets by  $(I - A_f)\varrho = I$  to help in canceling some of the terms and simplify the whole expression. Further simplification results in

$$\eta_{1}(k+1) = A_{f}\eta_{1}(k) - \varrho \sum_{j=2}^{r-1} \sum_{l=1}^{r-1} \frac{\alpha^{l}}{l! \epsilon^{r-1-j-l}} H_{j} D A_{c}^{j+l} x(k) 
- \varrho \sum_{j=2}^{r-1} \sum_{l=1}^{r} \frac{\alpha^{l}}{l! \epsilon^{r-1-j-l}} H_{j} D A_{c}^{j+l-1} B_{c} G_{l}(\chi(k), u(k))$$

$$-\varrho \sum_{j=2}^{r-1} \alpha^{r+1} \epsilon^{j+2} H_j D A_c^j R_x(\chi(k), u(k), \epsilon) \\ -\epsilon \varrho h(\chi(k+1), u(k+1), \epsilon) - \epsilon h(\chi(k), u(k), \epsilon)$$

The double summation terms can be written as

$$\sum_{j=2}^{r-1} \sum_{l=1}^{r-1} \frac{\alpha^{l}}{l! \epsilon^{r-1-j-l}} H_{j} D A_{c}^{j+l} x(k) = \frac{1}{\epsilon^{r-1}} \sum_{j=3}^{r-1} a_{j1} \epsilon^{j} D A_{c}^{j} x(k)$$

$$\sum_{j=2}^{r-1} \sum_{l=1}^{r} \frac{\alpha^{l}}{l! \epsilon^{r-1-j-l}} H_{j} D A_{c}^{j+l-1} B_{c} G_{l}(\cdot) = \epsilon \sum_{j=2}^{r-1} b_{j1} A_{c}^{j} B_{c} G_{l}(\cdot)$$

$$\sum_{j=2}^{r-1} \alpha^{r+1} \epsilon^{j+2} H_{j} D A_{c}^{j} R_{x}(\cdot) = \epsilon^{2} \sum_{j=2}^{r-1} \epsilon^{j} c_{j1} D A_{c}^{j} R_{x}(\cdot)$$

Define  $h_1(\cdot)$  as

$$h_1(\chi(k), u(k), \epsilon) = h(\chi(k+1), u(k+1), \epsilon) - h(\chi(k), u(k), \epsilon)$$

$$+ \sum_{i=2}^{r-1} b_{i1} A_c^i B_c G_i(\cdot) + \epsilon \sum_{j=2}^{r-1} \epsilon^j c_{j1} D A_c^j R_x(\cdot)$$

Then

$$\eta_{1}(k+1) = A_{f}\eta_{1}(k) - \varrho \left[ \frac{1}{\epsilon^{r-4}} \sum_{j=3}^{r-1} a_{j1} \epsilon^{j-3} D A_{c}^{j} x(k) + \epsilon h_{1}(\chi(k), u(k), \epsilon) \right]$$

Repeating the transformation to the ith step, we obtain

$$\eta_{i}(k+1) = A_{f}\eta_{i}(k) + (-1)^{i} \varrho^{i} \left[ \sum_{j=i+2}^{r-1} a_{ji} \frac{1}{\epsilon^{r-j-1}} DA_{c}^{j} x(k) + \epsilon h_{i}(\chi(k), u(k), \epsilon) \right]$$

The quasi steady state  $\eta_i(k+1) = \eta_i(k)$  of this equation is

$$\eta_{i}(k) = (-1)^{i} \varrho^{i+1} \left[ \sum_{j=i+2}^{r-1} a_{ji} \frac{1}{\epsilon^{r-j-1}} DA_{c}^{j} x(k) + \epsilon h_{i}(\chi(k), u(k), \epsilon) \right]$$

Hence, the change of variables is taken as

$$\eta_{i+1}(k) = \eta_{i}(k) + (-1)^{i+1} \varrho^{i+1} \left[ \sum_{j=i+2}^{r-1} a_{ji} \frac{1}{\epsilon^{r-j-1}} DA_{c}^{j} x(k) + \epsilon h_{i}(\chi(k), u(k), \epsilon) \right]$$

and the new variable satisfies

$$\eta_{i+1}(k+1) = \eta_{i}(k+1) + (-1)^{i+1} \varrho^{i+1} \left[ \sum_{j=i+2}^{r-1} a_{j} \frac{1}{\epsilon^{r-j-1}} DA_{c}^{j} x(k+1) \right] + (-1)^{i+1} \varrho^{i+1} \epsilon h_{i}(\chi(k+1), u(k+1), \epsilon)$$

Substitute for  $\eta_i(k+1)$  and  $\chi(k+1)$  to obtain

$$\eta_{i+1}(k+1) = A_f \eta_{i+1}(k) + (-1)^{i+1} \varrho^{i+1} \left[ \sum_{j=i+3}^{r-1} a_{ji+1} \frac{1}{\epsilon^{r-j-1}} DA_c^j x(k) + \epsilon h_{i+1}(\chi(k), u(k), \epsilon) \right]$$

where

$$\begin{array}{lcl} h_{i+1}(\chi(k),u(k),\epsilon) & = & h_{i}(\chi(k+1),u(k+1),\epsilon) - h_{i}(\chi(k),u(k),\epsilon) \\ \\ & + \sum_{j=i+2}^{r-1} b_{ji+1} A_{c}^{j} B_{c} G_{j}(\chi(k),u(k)) \\ \\ & + \epsilon \sum_{j=i+2}^{r-1} \epsilon^{j} c_{ji+1} D A_{c}^{j} R_{x}(\chi(k),u(k),\epsilon) \end{array}$$

If  $i \ge r - 3$  then  $A_c^r = 0$  which eliminates the negative power of  $\epsilon$  and the change of variables reach its end

$$\eta_{i+1}(k+1) = A_f \eta_{i+1}(k) + (-1)^{i+1} \varrho^{i+1} [0 + \epsilon h_{i+1}(\chi(k), u(k), \epsilon)]$$

Let  $\eta_{i+1} \stackrel{\text{def}}{=} \xi$ , then

$$\xi(k+1) = A_f \xi(k) + \epsilon(-1)^{i+1} \left( (I - A_f)^{-1} \right)^{i+1} h_{i+1}(\chi(k), u(k), \epsilon)$$

Which can be rewritten as

$$\xi(k+1) = A_f \xi(k) + \epsilon \Gamma(\chi(k), u(k), \hat{x}(k), \epsilon)$$

where

$$\Gamma(\chi(k), u(k), \hat{x}(k), \epsilon) = (-1)^{i+1} \left( (I - A_f)^{-1} \right)^{i+1} h_{i+1}(\chi(k), u(k), \epsilon)$$

From this we can see that as  $\epsilon \to 0$ , the system stability depends only on the eigenvalues of  $A_f$  which lie inside the unit circle.

To Show (3.26), we need to write  $\eta$  in terms of  $\xi$ . This can be achieved by listing all the transformations and write them in one step. Let  $N(\epsilon) = \epsilon^{r-1}D^{-1}$  and  $N(\epsilon)^{-1} = \frac{1}{\epsilon^{r-1}}D$  then

$$\xi(k) = \eta_{i}(k) + (-1)^{i+1} \varrho^{i+1} \left[ \sum_{j=i+2}^{r-1} a_{ji} \epsilon^{j} N^{-1}(\epsilon) A_{c}^{j} x(k) + \epsilon h_{i}(\chi(k), u(k), \epsilon) \right]$$

$$\eta_{i}(k) = \eta_{i-1}(k) + (-1)^{i} \varrho^{i} \left[ \sum_{j=i+1}^{r-1} a_{ji-1} \epsilon^{j} N^{-1}(\epsilon) A_{c}^{j} x(k) + \epsilon h_{i-1}(\chi(k), u(k), \epsilon) \right]$$

$$\vdots$$

$$\eta_{2}(k) = \eta_{1}(k) + (-1)^{2} \varrho^{2} \left[ \sum_{j=3}^{r-1} a_{j1} \epsilon^{j} N^{-1}(\epsilon) A_{c}^{j} x(k) + \epsilon h_{1}(\chi(k), u(k), \epsilon) \right]$$

$$\eta_{1}(k) = \eta(k) + (-1) \varrho \left[ \sum_{j=2}^{r-1} a_{j0} \epsilon^{j} N^{-1}(\epsilon) A_{c}^{j} x(k) + \epsilon h_{0}(\chi(k), u(k), \epsilon) \right]$$

Now we write  $\eta(k)$  equations with respect to  $\xi(k)$ 

$$\eta(k) = \varrho \left[ \sum_{j=2}^{r-1} a_{j0} \epsilon^{j} N^{-1}(\epsilon) A_{c}^{j} x(k) + \epsilon h_{0}(\chi(k), u(k), \epsilon) \right] \\
+ (-1) \varrho^{2} \left[ \sum_{j=3}^{r-1} a_{j1} \epsilon^{j} N^{-1}(\epsilon) A_{c}^{j} x(k) + \epsilon h_{1}(\chi(k), u(k), \epsilon) \right] \\
\vdots \\
+ (-1)^{i-1} \varrho^{i} \left[ \sum_{j=i+1}^{r-1} a_{ji-1} \epsilon^{j} N^{-1}(\epsilon) A_{c}^{j} x(k) + \epsilon h_{i-1}(\chi(k), u(k), \epsilon) \right] \\
+ (-1)^{i} \varrho^{i+1} \left[ \sum_{j=i+2}^{r-1} a_{ji} \epsilon^{j} N^{-1}(\epsilon) A_{c}^{j} x(k) + \epsilon h_{i}(\chi(k), u(k), \epsilon) \right] + \xi(k)$$

$$\eta(k) = \xi(k) + \sum_{l=1}^{i+1} (-1)^{l-1} \varrho^{l} \left[ \sum_{j=l+1}^{r-1} a_{jl} \epsilon^{j} N(\epsilon)^{-1} A_{c}^{j} x(k) + \epsilon h_{l-1}(\chi(k), u(k), \epsilon) \right]$$

From

$$\hat{x}(k) = x(k) - N(\epsilon)\eta(k)$$

$$= \left[I + \epsilon \sum_{l=1}^{i+1} (-1)^{l} N(\epsilon) \varrho^{l} N(\epsilon)^{-1} \left[ \sum_{j=l+1}^{r-1} a_{j} \epsilon^{j-1} A_{c}^{j} \right] \right] x(k)$$

$$-N(\epsilon) \xi(k) + \epsilon \sum_{l=1}^{i+1} (-1)^{l-1} N(\epsilon) \varrho^{l} \left[ h_{l-1}(\chi(k), u(k), \epsilon) \right]$$

$$= \left[I + \epsilon M(\epsilon)\right] x(k) - N(\epsilon) \xi(k) + \epsilon \mathcal{Z}(x(k), \xi(k), \epsilon)$$

$$= x(k) - N(\epsilon) \xi(k) + \epsilon \mathcal{W}(x(k), \xi(k), \epsilon)$$

where

$$M(\epsilon) = \sum_{l=1}^{i+1} (-1)^l N(\epsilon) \varrho^l N(\epsilon)^{-1} \left[ \sum_{j=l+1}^{r-1} a_j \epsilon^{j-1} A_c^j \right]$$

$$\mathcal{Z}(x(k), \xi(k), \epsilon) = \sum_{l=1}^{i+1} (-1)^{l-1} N(\epsilon) \varrho^l h_{l-1}(\chi(k), u(k), \epsilon)$$

$$\mathcal{W}(x(k), \xi(k), \epsilon) = M(\epsilon) x(k) + \mathcal{Z}(x(k), \xi(k), \epsilon)$$

# A.2 The Transformation Steps To The Singularly perturbed Form For The Other Discretization methods

We need to study

$$\frac{1}{\epsilon^{r-1}}D\Omega(\cdot) = \frac{1}{\epsilon^{r-1}}D\left[x(k+1) - x(k) - TA_{c}x(k+1)\right]$$

$$\frac{1}{\epsilon^{r-1}}D\bar{\Omega}(\cdot) = \frac{1}{\epsilon^{r-1}}D\left[x(k+1) - x(k) - \frac{T}{2}A_c(x(k+1) + x(k))\right]$$

for the backward difference method and bilinear transformation method respectively. Other calculation will follow the same as we did in the forward difference method. Notice that this need to be done in each step to show the true order of the error term to get the singularly perturbed form.

### A.2.1 Using Backward Difference Method

$$x(k+1) = x(k) + \sum_{l=1}^{r-1} \frac{T^l}{l!} A_c^l x(k) + \sum_{l=1}^{r} \frac{T^l}{l!} A_c^{l-1} B_c G_l(\cdot) + T^{r+1} R_x(\cdot)$$

Let 
$$\Omega(\cdot) = x(k+1) - x(k) - TA_cx(k+1)$$
, then

$$\Omega = \sum_{l=1}^{r-1} A_c^l x(k) + \sum_{l=1}^r \frac{T^l}{l!} A_c^{l-1} B_c G_l(\cdot) 
+ T^{r+1} R_x(\cdot) - T A_c x(k) - \sum_{l=1}^{r-1} \frac{T^{l+1}}{l!} A_c^{l+1} x(k) 
- \sum_{l=1}^r \frac{T^{l+1}}{l!} A_c^l B_c G_l(\cdot) - T^{r+2} A_c R_x(\cdot)$$

$$= \sum_{l=2}^{r-1} \frac{(1-l)T^{l}}{l!} A_{c}^{l} x(k) + T B_{c} G_{l}(\cdot)$$

$$T^{r+1} (I - T A_{c}) R_{x}(\cdot) + \sum_{l=2}^{r} \frac{T^{l}}{l!} A_{c}^{l-1} B_{c} [G_{l}(\cdot) - l G_{l-1}(\cdot)]$$

$$= T [B_{c} G_{l}(\cdot) + T^{r} (I - T A_{c}) R_{x}(\cdot)]$$

$$+ \sum_{l=2}^{r-1} \frac{(1-l)T^{l}}{l!} A_{c}^{l} x(k) + \sum_{l=2}^{r} \frac{T^{l}}{l!} A_{c}^{l-1} B_{c} \bar{G}_{l}(\cdot)$$

Where

$$\bar{G}_0(\cdot) = 0$$

$$\bar{G}_1(\cdot) = G_1(\cdot)$$

$$\bar{G}_l(\cdot) = G_l(\cdot) - lG_{l-1}(\cdot)$$

Then

$$\Omega(\cdot) = T \left[ B_c G_l(\cdot) + T^r (I - T A_c) R_x(\cdot) \right] 
+ \sum_{l=2}^{r-1} \frac{(1-l)T^l}{l!} A_c^l x(k) + \sum_{l=2}^r \frac{T^l}{l!} A_c^{l-1} B_c \bar{G}_l(\cdot) \right]$$

Now multiply both side by  $\frac{1}{\epsilon^{r-1}}D$ . Also notice that

$$DB_{c} = \epsilon^{r-1}B_{c}$$

$$DA_c^l = \frac{1}{\epsilon^{r-l-1}} A_c^l D$$

We get

$$\begin{split} \frac{1}{\epsilon^{r-1}}D\Omega(\cdot) &= T\left[B_{c}G_{l}(\cdot) + \alpha^{r-1}TD(I - TA_{c})R_{x}(\cdot)\right] \\ &+ \sum_{l=2}^{r-1} \frac{(1-l)\alpha^{l}}{l!\epsilon^{r-l-1}}DA_{c}^{l}x(k) + T\sum_{l=2}^{r} \frac{\alpha^{l-1}}{l!}A_{c}^{l-1}B_{c}\bar{G}_{l}(\cdot) \end{split}$$

$$= T \left[ \sum_{l=1}^{r} \frac{\alpha^{l-1}}{l!} A_c^{l-1} B_c \bar{G}_l(\cdot) + T \alpha^{r-1} D(I - T A_c) R_x(\cdot) \right]$$

$$+ \sum_{l=2}^{r-1} \frac{(1-l)\alpha^l}{l! \epsilon^{r-l-1}} DA_c^l x(k)$$

The order of

$$\frac{1}{\epsilon^{r-1}}D\Omega(\cdot) = O\left(\sum_{l=2}^{r-1} \frac{(1-l)\alpha^l}{l!\epsilon^{r-l-1}} DA_c^l x(k)\right)$$

Let  $H_l\alpha^l/l!$ , then

$$\frac{1}{\epsilon^{r-1}}D\Omega(\cdot) = O\left(\frac{1}{\epsilon^{r-3}}\sum_{l=2}^{r-1}(1-l)\epsilon^{l-2}H_lDA_c^lx(k)\right)$$

which is equivalent to  $O\left(\frac{1}{\epsilon^{r-3}}\right)$ .

#### A.2.2 Using Bilinear Transformation

Starting from the difference equation in ??. Let

$$\bar{\Omega}(\cdot) = x(k+1) - x(k) - \frac{T}{2}A_c(x(k+1) + x(k))$$

$$\begin{split} \bar{\Omega}(\cdot) &= \sum_{l=2}^{r-1} \frac{T^{l}}{l!} A_{c}^{l} x(k) + \sum_{l=1}^{r} \frac{T^{l}}{l!} A_{c}^{l-1} B_{c} G_{l}(\cdot) + T^{r+1} R_{x}(\cdot) \\ &- \sum_{l=1}^{r-1} \frac{T^{l+1}}{2(l!)} A_{c}^{l+1} x(k) - \sum_{l=1}^{r} \frac{T^{l+1}}{2(l!)} A_{c}^{l} B_{c} G_{l}(\cdot) - \frac{T^{r+2}}{2} A_{c} R_{x}(\cdot) \\ &= \sum_{l=2}^{r-1} \frac{(2-l)T^{l}}{2(l!)} A_{c}^{l} x(k) + T \left[ B_{c} G_{l}(\cdot) + T^{r} (I - \frac{T}{2} A_{c}) R_{x}(\cdot) \right] \\ &+ \sum_{l=2}^{r} \frac{T^{l}}{l!} A_{c}^{l-1} B_{c} \left[ G_{l}(\cdot) - \frac{l}{2} G_{l-1}(\cdot) \right] \\ &= T \left[ B_{c} G_{l}(\cdot) + T^{r} (I - \frac{T}{2} A_{c}) R_{x}(\cdot) \right] \\ &+ \sum_{l=2}^{r-1} \frac{(2-l)T^{l}}{2(l!)} A_{c}^{l} x(k) + \sum_{l=2}^{r} \frac{T^{l}}{l!} A_{c}^{l-1} B_{c} \tilde{G}_{l}(\cdot) \end{split}$$

Where

$$\tilde{G}_0(\cdot) = 0$$

$$\tilde{G}_1(\cdot) = G_1(\cdot)$$

$$\tilde{G}_l(\cdot) = G_l(\cdot) - \frac{l}{2}G_{l-1}(\cdot)$$

Then

$$\bar{\Omega}(\cdot) = T \left[ B_c G_l(\cdot) + T^r (I - \frac{T}{2} A_c) R_x(\cdot) \right] 
+ \sum_{l=3}^{r-1} \frac{(1 - l/2) T^l}{l!} A_c^l x(k) + \sum_{l=2}^r \frac{T^l}{l!} A_c^{l-1} B_c \tilde{G}_l(\cdot) \right]$$

Now multiply both side by  $\frac{1}{\epsilon^{r-1}}D$ , we get

$$\begin{split} \frac{1}{\epsilon^{r-1}}D\bar{\Omega}(\cdot) &= T\left[B_{c}G_{l}(\cdot) + \alpha^{r-1}TD(I - \frac{T}{2}A_{c})R_{x}(\cdot)\right] \\ &+ \sum_{l=3}^{r-1} \frac{(1 - l/2)\alpha^{l}}{l!\epsilon^{r-l-1}}DA_{c}^{l}x(k) + T\sum_{l=2}^{r} \frac{\alpha^{l-1}}{l!}A_{c}^{l-1}B_{c}\tilde{G}_{l}(\cdot) \\ &= T\left[\sum_{l=1}^{r} \frac{\alpha^{l-1}}{l!}A_{c}^{l-1}B_{c}\tilde{G}_{l}(\cdot) + T\alpha^{r-1}D(I - \frac{T}{2}A_{c})R_{x}(\cdot)\right] \\ &+ \sum_{l=3}^{r-1} \frac{(1 - l/2)\alpha^{l}}{l!\epsilon^{r-l-1}}DA_{c}^{l}x(k) \end{split}$$

The order of

$$\begin{split} \frac{1}{\epsilon^{r-1}}D\bar{\Omega}(\cdot) &= O\left(\sum_{l=3}^{r-1} \frac{(1-l/2)\alpha^l}{l!\epsilon^{r-l-1}} DA_c^l x(k)\right) \\ &= O\left(\frac{1}{\epsilon^{r-4}} \sum_{l=3}^{r-1} (1-l/2)\epsilon^{l-3} H_l DA_c^l x(k)\right) \end{split}$$

which is equivalent to  $O\left(\frac{1}{\epsilon^{r-4}}\right)$ .

From this point on we can apply the change of variables the same way described for the forward difference method.

## **BIBLIOGRAPHY**

#### BIBLIOGRAPHY

- [1] M. Al-Alaoui. Novel digital integrator and differentiator. Elect Lett, 29, 1993.
- [2] M. Al-Alaoui. Novel iir differentiator from the simpson integration rule. 41, 1994.
- [3] M. Al-Alaoui. A class of second-order integrators and low-pass differentiators. *IEEE Trans CS*, 42, 1995.
- [4] B. Aloliwi and H.K. Khalil. Adaptive output feedback regulation of a class of nonlinear systems: convergence and robustness. *IEEE Trans. Automat. Contr.*, 42, 1997.
- [5] B. Aloliwi and H.K. Khalil. Robust adaptive output feedback control of nonlinear systems without persistence of excitations. *Automatica*, 33, 1997.
- [6] A.N. Atassi and H.K.Khalil. A separation principle for the control of a class of nonlinear systems. In Proc. IEEE Conf. on Decision and Control, 1998.
- [7] A.N. Atassi and H.K. Khalil. Separation results for the stabilization of nonlinear systems using different high-gain observer designs. 1998.
- [8] A.N. Atassi and H.K. Khalil. A seperation principle for the stabilization of a class of nonlinear systems. *IEEE Trans. Automat. Contr.*, 44(9):1672 1687, 1999.
- [9] J. Le Bihan. Novel class of digital integrators and differentiators. *Elect Lett*, 29, 1993.
- [10] K. Busawon, M. Saif, and M. Farza. A discrete-time observer for a class of nonlinear systems. Proc. Conf. on Decision and Control, 1997.
- [11] T. Chen and B.A. Francis. Input-output stability of sampled-data systems. *IEEE Trans. Automat. Contr.*, 36, 1991.

- [12] S.T. Chung and J.W. Grizzle. Observer error linearization for sampled-data systems. *Automatica*, 26(6):997 1007, 1990.
- [13] J.C. Doyle and G. Stein. Robustness with observers. *IEEE Trans. Automat. Contr.*, (4):607 611, 1979.
- [14] F. Esfandiari and H.K. Khalil. Observer-based design of uncertain systems: recovering state feedback robustness under matching conditions. In Proc. Allerton Conf., 1987.
- [15] F. Esfandiari and H.K. Khalil. Observer-based design of uncertain systems: recovering state feedback robustness under matching conditions. *Proc. Allerton Conf.*, Monticello, IL., 1992.
- [16] F. Esfandiari and H.K. Khalil. Output feedback stabilization of fully linearizable systems. *Int. J. Contr.*, 56, 1992.
- [17] S. Diop et al. Interpolation and numerical differentiation for observer design. ACC, 1994.
- [18] T. Boukhobza et al. Nonlinear sliding observer for systems in output and output derivative injection form. preprint of the 13th IFAC Congress, 1996.
- [19] W. Su et al. Variable structure observer and their applications to control systems. Internal Report. Dept. of Elect. Engineering Ohio State University.
- [20] M. Farza, S. Othman, H. Hammouri, and M. Fick. Discrete-time nonlinear observer-based estimators for the on-line estimation of the kinetic rates in bioreactors. *Bioprocess Engineering*, 17, 1997.
- [21] G.F. Franklin, D. Powell, and M.L. Workman. *Digital Control of Dynamic Systems*. Addison Wesley, 1990.
- [22] K. Furuta and M. Yamakita. Swing up control of inverted pendulum. IECON'91, 1991.
- [23] J.P. Gauthier, H. Hammouri, and S. Othman. A simple observer for nonlinear systems application to bioreactors. *IEEE Trans. Automat. Contr.*, 37(6):875 – 880, 1992.
- [24] R. Gurumoorthy and S.R. Sanders. Controlling non-minimum phase nonlinear systems - the inverted pendulum on a cart exampl. Proc. of the Amer. Control Conf., 1993.

- [25] J. Hauser, S. Saatry, and P. Kokotovic. Nonlinear control via approximate input-output linearization: the ball and beam example. *IEEE Trans. Automat.* Contr., 37(3):392 – 398, 1992.
- [26] A. Isidori. Nonlinear Control Systems. Springer-Verlag, 1995.
- [27] A. Isidori. A remark on the problem of semiglobal nonlinear output regulation. *IEEE Trans. Automatic Control*, 42(12):1734 1738, 1997.
- [28] A. Isidori and C.I. Byrnes. Output regulation of nonlinear output regulation. *IEEE Trans. Automat. Contr.*, 35, 1990.
- [29] M. Jankovic. Adaptive output feedback control of nonlinear feedback linearizable systems. Int. J. Adaptive Control and Signal Processing, 10, 1996.
- [30] Z.P. Jiang, D.J. Hill, and Y. Guo. Semiglobal output feedback stabilization for the nonlinear benchmark example. Proc. of the Europ. Contr. Conf., Brussels, Belgium, 1997.
- [31] H.K. Khaili and E. Strangas. Robust speed control of induction motors using position and current measurements. *IEEE Trans Autom. Cont.*, 1996.
- [32] H.K. Khalil. Robust servomechanism output feedback controller for a class of feedback linearizable systems. *Automatica*, 30(10):1587 1599, 1994.
- [33] H.K. Khalil. Adaptive output feedback control of nonlinear systems represented by input-output models. *IEEE Trans. Automat. Contr.*, 41(2):177 188, 1996.
- [34] H.K. Khalil. Nonlinear Systems. Prentice Hall, second edition edition, 1996.
- [35] H.K. Khalil. Universal regulators for minimum phase nonlinear systems. In Proc. American Control Conf., 1998.
- [36] H.K. Khalil and F. Esfandiari. Semiglobal stabilization of a class of nonlinear systems using output feedback. *IEEE Trans. Automat. Contr.*, 41(8):1216 – 1220, 1996.
- [37] A. Krener and A. Isidori. Linearization by output injection and nonlinear observers. Systems & Control Lett., 3, 1983.
- [38] B. Kumar and S.C. Dutta-Roy. Design of digital differentiators for low frequencies. Proc. IEEE, 76, 1988.

- [39] J. Kurzweil. On the inversion of lyapunov's second theorem on stability of motion. Amer. Math. Soc. Transl., 24, 1956.
- [40] Z. Lin and A. Saberi. Robust semi-global stabilization of minimum-phase input-output linearizable systems via partial state and output feedback. *IEEE Trans.*Automatic Control, 40(6):1029 1041, 1995.
- [41] Z. Lin, A. Saberi, M. Gutmann, and Y.A. Shamash. Linear controller for an inverted pendulum having restricted interval: a high-gain approach. *Automatica*, 32(6):933 – 937, 1996.
- [42] N.A. Mahmoud and H.K. Khalil. Asymptotic regulation of minimum phase nonlinear systems using output feedback. *IEEE Trans. Automat. Contr.*, 41(10):1402 - 1412, 1996.
- [43] N.A. Mahmoud and H.K. Khalil. Robust control for a nonlinear servomechanism problem. *Int. J. Contr.*, 66(6):779 802, 1997.
- [44] S. Monaco and D. Normand-Cyrot. Invariant distributions under sampling. Proc. of Conf. on Mathematical Theory of Networks and Systems, Stockholm, 19.
- [45] S. Monaco and D. Normand-Cyrot. On the sampling of a linear analytic control system. *Proc. Conf. on Decision and Control*, 1985.
- [46] S. Monaco and D. Normand-Cyrot. On the sampling of a linear analytic system. Proc. 24th IEEE Conf. on Decision and Control, Ft. Lauderdale, FL., 1985.
- [47] P. Moral and J.W. Grizzle. Observer design for nonlinear systems with discrete-time measurements. *IEEE Trans. Automatic Control*, 40(3):395 404, 1995.
- [48] S. Nicosia and P. Tomei. Nonlinear observer and output feedback attitude control of space craft. *IEEE Trans Aerospace and Electronic Systems*, 28, 1992.
- [49] S. Oh and H.K. Khalil. Output feedback stabilization using variable structure control. Int. J. Contr., 62, 1995.
- [50] I.R. Petersen and C.V. Holot. High-gain observers applied to problems in disturbance attenuation, h-infinity optimization and the stabilization of uncertain linear systems. In Proc. American Control Conf., 1988.
- [51] Z. Qu. Robust control of nonlinear uncertain system. John Wiley and Sons, 1998.

- [52] L.R. Rabiner and K. Steiglitz. The design of wide band recursive and nonrecursive digital differentiators. IEEE Trans AU, (18):204 209, 1970.
- [53] A. Saberi, B. Chen, and P. Sannuti. Loop Transfer Recovery: Analysis and Design. Springer-Verlag, 1993.
- [54] A. Saberi and P. Sannuti. Observer design for loop transfer recovery and for uncertain dynamical systems. *IEEE Trans. Automat. Contr.*, 35, 1990.
- [55] Y. Song and J. Grizzle. The extended kalman filter as a local asymptotic observer for nonlinear discrete-time systems. in Proc. of ACC Chicago, 1992.
- [56] E. Sontag. A concept of local observability. System & Control Lett., 5, 1984.
- [57] E. Sontag and H. Sussmann. Accessibility under sampling. Proc. Conf. on Decision and Control, 1982.
- [58] M. Spong. Energy based control of a class of underactuated mechanical systems. IFAC World Congress, 1996.
- [59] M. Spong and D. Block. The pendubot: A mechatronic system for control research and education. *IEEE Conf. on Decision and Control*, 1995.
- [60] M. Spong and L. Praly. Control of underactuated mechanical systems using switching and saturation. *Proc. of the Block Island Workshop on Control Using Logic Based Switching, Springer-Verlag,* 1996.
- [61] M.W. Spong and M. Vidyasagar. Robot dynamics and control. John Wiley and Sons, Inc., New York, 1989.
- [62] A. Teel and L. Praly. Global stabilizability and observability imply semi-global stabilizability by output feedback. Systems & Control Lett., 22, 1994.
- [63] A. Teel and L. Praly. Tools for semiglobal stabilization by partial state and output feedback. SIAM J. Control & Optimization, 33, 1995.
- [64] A.R. Teel. Semi-global stabilization of the ball and beam using output feedback. Proc. of the Amer. Conf., 1993.
- [65] A.R. Teel, D. Nesic, and P.V. Kokotovic. A note on input-to-state stability of sampled-data nonlinear systems. Proc. of the 37th IEEE Conf. on Decision and Control, 1998.

[66] A. Tornambe. Output feedback stabilization of a class of non-minimum phase nonlinear systems. System & Control Lett., 1992.